Theoretical Astroparticle Physics

Contents

1. Topics

- Electron-positron plasma
  - Relativistic degeneracy in nonequilibrium electron-positron plasma
- Thermal emission from relativistic plasma and GRBs
  - Transparency of an instantaneously created electron-positron-photon plasma
  - Spreading of ultrarelativistically expanding shell
  - Relativistic spotlight effect
  - Interaction of the GRB ejecta with circumburst medium
  - Thermal emission in early afterglow from the GRB-SNR interaction
- Neutrinos in cosmology
- Self-gravitating systems as Dark Matter in galaxies
  - The distribution of dark matter in galaxies based quantum treatments
  - A novel core-halo distribution of dark matter in galaxies
  - Critical configurations for a system of semidegenerate fermions
  - Super massive black holes and dark matter halos in big elliptical galaxies
  - Dark Einstein clusters within the S2 orbit in SgrA*
  - Dark matter and baryons in dwarf galaxies

2. Participants

2.1. ICRANet participants

- Carlo Luciano Bianco
- Jorge Rueda
- Remo Ruffini
- Gregory Vereshchagin
- She-Sheng Xue

2.2. Past collaborators

- Marco Valerio Arbolino (DUNE s.r.l., Italy)
- Andrea Bianconi (INFN Pavia, Italy)
- Neta A. Bahcall (Princeton University, USA)
- Micol Benetti (Observatório Nacional, Rio de Janeiro, Brazil)
- Daniella Calzetti (University of Massachusets, USA)
- Valeri Chechetkin (Keldysh Institute, Russia)
- Gustavo de Barros (former IRAP PhD, Brazil)
- Jaan Einasto (Tartu Observatory, Estonia)
- Roberto Fabbri (University of Firenze, Italy)
- Long-Long Feng (University of Science and Technology of China, China)

- Jiang Gong Gao (Xinjiang Institute of Technology, China)
- Andrea Geralico (ICRA, Rome, Italy)
- Mauro Giavalisco (University of Massachusets, USA)
- Gabriele Ingrosso (INFN, University of Lecce, Italy)
- Yi-peng Jing (Shanghai Astronomical Observatory, China)
- Wien Biao Han (Shanghai Astronomical Observatory, Chinese Academy of Science, China)
- Massimiliano Lattanzi (University of Ferrara, Italy)
- Hyung-Won Lee (Inje University, South Korea)
- Alessandro Melchiorri (Univ. "Sapienza" di Roma, Italy)
- Marco Merafina (University of Rome "Sapienza", Italy)
- Houjun Mo (University of Massachusetts, USA)
- Enn Saar (Tartu Observatory, Estonia)
- Jay D. Salmonson (Livermore Lab, USA)
- Luis Alberto Sanchez (National University Medellin, Colombia)
- Costantino Sigismondi (ICRA and University of Rome "La Sapienza", Italy)
- Doo Jong Song (Korea Astronomy Observatory, South Korea)
- Luigi Stella (Astronomical Observatory of Rome, Italy)
- William Stoeger (Vatican Observatory, University of Arizona USA)
- Sergio Taraglio (ENEA, Italy)
- Gerda Wiedenmann (MPE Garching, Germany)
- Jim Wilson (Livermore Lab, USA)
- Urbano França (Instituto de Física Corpuscular, Valencia, Spain)

- Julien Lesgourgues (CERN, Theory Division, Geneva, Switzerland)
- Lidia Pieri (Institute d'Astrophysique, Paris, France)
- Sergio Pastor (Instituto de Física Corpuscolar, Valencia, Spain)
- Joseph Silk (Oxford University, UK)
- Roustam Zalaletdinov (Tashkent University, Uzbekistan)

2.3. Ongoing collaborations

- Alexey Aksenov (ICAD, RAS, Russia)
- Alberto Benedetti (Max Planck Institute for Nuclear Physics, Heidelberg)
- Bernardo Fraga (ICRANet, Rome, Italy)
- Nikolaos Mavromatos (King's College London, University of London, UK)
- Ivan Siutsou (ICRANet-Rio, Brazil)

2.4. Students

- Carlos Arguelles (IRAP PhD, Argentina)
- Damien Begue (Erasmus Mundus IRAP PhD, France)
- Wang Yu (IRAP PhD, China)

3. Brief description

Astroparticle physics is a new field of research emerging at the intersection of particle physics, astrophysics and cosmology. Theoretical development in these fields is mainly triggered by the growing amount of experimental data of unprecedented accuracy, coming both from the ground based laboratories and from the dedicated space missions.

3.1. Electron-positron plasma

Electron-positron plasma is of interest in many fields of physics and astrophysics, e.g. in the early universe, active galactic nuclei, the center of our Galaxy, compact astrophysical objects such as hypothetical quark stars, neutron stars and gamma-ray bursts sources. It is also relevant for the physics of ultraintense lasers and thermonuclear reactions. We study physical properties of dense and hot electron-positron plasmas. In particular, we are interested in the issues of its creation and relaxation, its kinetic properties and hydrodynamic description, baryon loading and radiation from such plasmas.

Two different states exist for electron-positron plasma: optically thin and optically thick. Optically thin pair plasma may exist in active galactic nuclei and in X-ray binaries. The theory of relativistic optically thin nonmagnetic plasma and especially its equilibrium configurations was established in the 80s by Svensson, Lightman, Gould and others. It was shown that relaxation of the plasma to some equilibrium state is determined by a dominant reaction, e.g. Compton scattering or bremsstrahlung.

Developments in the theory of gamma ray bursts from one side, and observational data from the other side, unambiguously point out on existence of optically thick pair dominated non-steady phase in the beginning of formation of GRBs. The spectrum of radiation from optically thick plasma is usually assumed to be thermal.

These months we have been focusing on two topics: electron-positron plasma and thermal emission from relativistic plasma and GRBs. In the first

topic we focused on effects of relativistic degeneracy. In doing so we have generalized the numerical schemes for solution of Boltzmann equations for pairs and photons, used in previous works. As the outcome, we have developed a computer code.

Then, in a broader context, we consider the appearance of thermal emission from relativistic plasma, focusing on several topics.

In what follows all this work is discussed in details, while in Appendix all relevant papers can be found.

3.1.1. Relativistic degeneracy in the pair plasma

It is well known that at relativistic temperatures plasma becomes degenerate Landau and Lifshitz (1980). In order to study relativistic degeneracy we have introduced the Bose enhancement and Pauli blocking factors in the Boltzmann equation that allows us to follow the relaxation of the pair plasma to Planck spectrum of photons and Fermi-Dirac distribution of electrons and positrons. This improvement allows us to study higher energy densities with respect to those treated before in Aksenov et al. (2007, 2009). However, for such high energy densities the assumption adopted in these works, namely that three-particle interactions operate on longer timescale with respect to two-particle ones, does not hold any longer. For this reason we had to introduce the collisional integrals for three-particle interactions based on the exact QED matrix elements, in full analogy with previously treated two-particle interactions.

Thus in this work we consider relaxation of nonequilibrium optically thick pair plasma to complete thermal equilibrium by integrating numerically relativistic Boltzmann equations with collisional integrals computed from the first principles, namely from the QED matrix elements both for two-particle and three-particle interactions.

We point out that unlike classical Boltzmann equation for binary interactions such as scattering, more general interactions are typically described by four collisional integrals for each particle that appears both among incoming and outgoing particles.

Our numerical results indicate that the rates of three-particle interactions become comparable to those of two-particle ones for temperatures exceeding the electron rest-mass energy. Thus three particle interactions such as relativistic bremsstrahlung, double Compton scattering and radiative pair cre-

ation become essential not only for establishment of thermal equilibrium, but also for correct evaluation of interaction rates, energy losses etc. Our results on this topic are reported in Appendix A.

3.2. Thermal emission from relativistic plasma and GRBs

Emission from optically thick stationary plasma is an important topic in astrophysics. Such plasma confined by the gravitational field constitutes stars, accretion disks and other objects. The light from these systems is coming from the so called photosphere defined as a region where the optical depth computed from the interior of the optically thick plasma outwards reaches unity.

There are also dynamical sources where bulk velocities of plasma reach ultrarelativistic values such as microquasars, active galactic nuclei and gamma-ray bursts (GRBs). While in the former two objects there is clear evidence for jets which contain optically thin plasma, in the latter objects the issue of jets is controversial, and the source is required to be optically thick. This observational fact poses a new problem: the emission from (spherically) expanding plasma which initially is optically thick. Such plasma eventually becomes optically thin during its expansion, and initially trapped photons should be released.

Recently, thermal components were found in spectra of GRBs not only in the prompt emission, but also in the early afterglow. This motivated us to extend the study of thermal emission previously focused on ultrarelativistic photosphere into a more broad context of thermal emission from relativistic plasma in GRBs.

3.2.1. Transparency of an instantaneously created electron-positron-photon plasma

We focused in the problem of the expansion of a relativistic plasma generated when a large amount of energy is released in a small volume, which has been considered previously by many authors, including Fermi and Landau. We use the approximate analytical solution of hydrodynamic equations by Bisnovatyi-Kogan and Murzina for the spherically symmetric relativistic ex-

pansion. We obtain the light curves and the spectra from transparency of an electron–positron–photon plasma by virtue of the recently developed method by one of us (G.V.) together with I.A. Siutsou and R. Ruffini of approximate solution of the radiative transfer equation. We compare our results with the work of Goodman and found that our spectrum is wider than Goodman's due to our explicit account for dynamical character of the relativistic photosphere. Our results are reported in Appendix B.

3.2.2. Spreading of ultrarelativistically expanding shell

Optically thick energy dominated plasma created in the source of Gamma-Ray Bursts (GRBs) expands radially with acceleration and forms a shell with constant width measured in the laboratory frame. When strong Lorentz factor gradients are present within the shell it is supposed to spread at sufficiently large radii. There are two possible mechanisms of spreading: hydrodynamical and thermal ones. We consider both mechanisms evaluating the amount of spreading that occurs during expansion up to the moment when the expanding shell becomes transparent for photons. We compute the hydrodynamical spreading of an ultrarelativistically expanding shell. In the case of thermal spreading we compute the velocity spread as a function of two parameters: comoving temperature and bulk Lorentz factor of relativistic Maxwellian distribution. Based on this result we determine the value of thermal spreading of relativistically expanding shell. We found that thermal spreading is negligible for typical GRB parameters. Instead hydrodynamical spreading appears to be significant, with the shell width reaching $\sim 10^{10}$ cm for total energy 10^{54} erg and baryonic loading $B = 10^{-2}$. Within the fireshell model such spreading will result in the duration of Proper Gamma-Ray Bursts up to several seconds. For details see Appendix C.

3.2.3. Relativistic spotlight

Relativistic motion gives rise to a large number of interesting and sometimes counterintuitive effects. In this work we consider an example of such effects, which we term relativistic spotlight. When an isotropic source of soft photons with proper intensity I_0 is placed at rest between a distant observer and photosphere of relativistic wind, its intensity as seen by the observer gets enhanced up to $\sim \Gamma^4 I_0$, where Γ is bulk Lorentz factor of the wind. In addition,

these photons may extract a large part of the wind kinetic energy. We speculate that such effect may be relevant for the physics of GRBs. For details see Appendix D.

3.2.4. Interaction of the GRB ejecta with circumburst medium

We study the physical properties of filamentary structure of overdensities in circumburst medium near the GRB sources and identify main characteristics of this structure: density, physical dimension, opacity. We obtain observational constraints on these quantities, and present consistent treatment of the interaction of relativistic shell originating from the GRB source and this filamentary structure. We also discuss high energy emission originating from this interaction. For details see Appendix E.

3.2.5. Thermal emission in early afterglow from the GRB-SNR interaction

The interaction between the GRB ejecta and a baryonic shell is considered in the context of the binary driven hypernova model of GRBs. The kinematic and observational properties of the shell after the interaction are derived. In particular, the temperature and the duration of the thermal emission are obtained. The model is then applied to GRB 090618 and other sources, and the observed characteristics of the thermal component are reproduced. For details see Appendix F.

3.3. Relativistic kinetic theory and its applications

We pay particular attention to presenting our results in relativistic kinetic theory in a systematic and pedagogic manner. This approach resulted in a lecture course created by G.V. Vereshchagin for the students of the IRAP PhD Erasmus Mundus Joint Doctorate program. This lecture course was also delivered at the XV Brazilian School of Cosmology and Gravitation in Mangaratiba, Brazil in 2012. The lecture notes summarizing this course are presented in Appendix G.

3.4. Neutrinos in cosmology

Many observational facts make it clear that luminous matter alone cannot account for the whole matter content of the Universe. Among them there is the cosmic background radiation anisotropy spectrum, that is well fitted by a cosmological model in which just a small fraction of the total density is supported by baryons.

In particular, the best fit to the observed spectrum is given by a flat ΛCDM model, namely a model in which the main contribution to the energy density of the Universe comes from vacuum energy and cold dark matter. This result is confirmed by other observational data, like the power spectrum of large scale structures.

Another strong evidence for the presence of dark matter is given by the rotation curves of galaxies. In fact, if we assume a spherical or ellipsoidal mass distribution inside the galaxy, the orbital velocity at a radius r is given by Newton's equation of motion. The peculiar velocity of stars beyond the visible edge of the galaxy should then decrease as $1/r$. What is instead observed is that the velocity stays nearly constant with r. This requires a halo of invisible, dark, matter to be present outside the edge. Galactic size should then be extended beyond the visible edge. From observations is follows that the halo radius is at least 10 times larger than the radius of visible part of the galaxy. Then it follows that a halo is at least 10 times more massive than all stars in a galaxy.

Neutrinos were considered as the best candidate for dark matter about twenty years ago. Indeed, it was shown that if these particles have a small mass $m_\nu \sim 30\,\mathrm{eV}$, they provide a large energy density contribution up to critical density. Tremaine and Gunn (1979) have claimed, however, that massive neutrinos cannot be considered as dark matter. Their paper was very influential and turned most of cosmologists away from neutrinos as cosmologically important particles.

Tremaine and Gunn paper was based on estimation of lower and upper bounds for neutrino mass; when contradiction with these bounds was found, the conclusion was made that neutrinos cannot supply dark matter. The upper bound was given by cosmological considerations, but compared with the energy density of clustered matter. It is possible, however, that a fraction of neutrinos lays outside galaxies.

Moreover, their lower bound was found on the basis of considerations of galactic halos and derived on the ground of the classical Maxwell-Boltzmann

statistics. Gao and Ruffini (1980) established a lower limit on the neutrino mass by the assumption that galactic halos are composed by degenerate neutrinos. Subsequent development of their approach Arbolino and Ruffini (1988) has shown that contradiction with two limits can be avoided.

At the same time, in 1977 the paper by Lee and Weinberg (1977) appeared, in which authors turned their attention to massive neutrinos with $m_\nu >> 2\,\mathrm{GeV}$. Such particles could also provide a large contribution into the energy density of the Universe, in spite of much smaller value of number density.

Recent experimental results from laboratory (see Dolgov (2002) for a review) rule out massive neutrinos with $m_\nu > 2\,\mathrm{GeV}$. However, the paper by Lee and Weinberg was among the first where very massive particles were considered as candidates for dark matter. This can be considered as the first of cold dark matter models.

Today the interest toward neutrinos as a candidate for dark matter came down, since from one side, the laboratory limit on its mass do not allow for significant contribution to the density of the Universe, and from other side, conventional neutrino dominated models have problems with formation of structure on small scales. However, in these scenarios the role of the chemical potential of neutrinos was overlooked, while it could help solving both problems.

3.4.1. Massive neutrino and structure formation

Lattanzi et al. (2003) have studied the possible role of massive neutrinos in the large scale structure formation. Although now it is clear, that massive light neutrinos cannot be the dominant part of the dark matter, their influence on the large scale structure formation should not be underestimated. In particular, large lepton asymmetry, still allowed by observations, can affect cosmological constraints on neutrino mass.

3.4.2. Cellular structure of the Universe

One of the interesting possibilities, from a conceptual point of view, is the change from the description of the physical properties by a continuous function, to a new picture by introducing a self-similar fractal structure. This approach has been relevant, since the concept of homogeneity and isotropy formerly apply to any geometrical point in space and leads to the concept

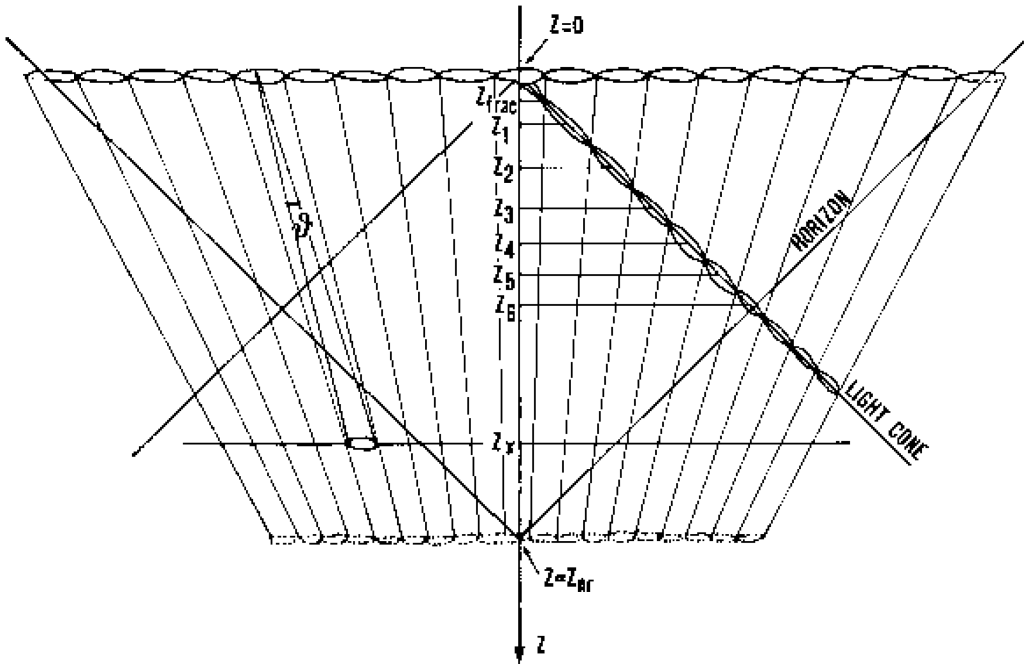

Figure 3.1.: Cellular structure of the Universe.

of a Universe observer-homogeneous (Ruffini (1989)). Calzetti et al. (1987), Giavalisco (1992), Calzetti et al. (1988) have defined the correlation length of a fractal

$$r_0 = \left(1 - \frac{\gamma}{3}\right)^{1/\gamma} R_S, \tag{3.4.1}$$

where R_S is the sample size, $\gamma = 3 - D$, and D is the Hausdorff dimension of the fractal. Most challenging was the merging of the concepts of fractal, Jeans mass of dark matter and the cellular structure in the Universe, advanced by Ruffini et al. (1988). The cellular structure emerging from this study is represented in Figure 3.1. There the upper cutoff in the fractal structure $R_{\text{cutoff}} \approx 100$ Mpc, was associated to the Jeans mass of the "ino" $M_{\text{cell}} = \left(\frac{m_{pl}}{m_{ino}}\right)^2 m_{pl}$.

3.4.3. Lepton asymmetry of the Universe

Lattanzi et al. (2005), Lattanzi et al. (2006) studied how the cosmological constraints on neutrino mass are affected by the presence of a lepton asymmetry. The main conclusion is that while constraints on neutrino mass do not change by the inclusion into the cosmological model the dimensional chemical potential of neutrino, as an additional parameter, the value of lepton asymmetry allowed by the present cosmological data is surprisingly large, being

$$L = \sum_{\nu} \frac{n_{\nu} - n_{\bar{\nu}}}{n_{\gamma}} \lesssim 0.9. \tag{3.4.2}$$

Therefore, large lepton asymmetry is not ruled out by the current cosmological data.

3.5. Self-gravitating systems of Dark Matter particles

A general study of Dark Matter (DM) within the particle DM paradigm requires the interconnection between particle Physics (Standard Model (SM) and beyond SM Physics), together with a fully general relativistic treatment. The study of the Physics must be always guided by the many different known astrophysical scenarios where DM plays certainly a role, i.e.: the interaction nature within the primordial plasma in the early universe, leptogenesis, baryogenesis, the large structure of the Universe, structure formation, gravitational lensing in clusters of galaxies, galaxy rotation curves and the overall galaxy density profiles. The current attention of research within our group is focused in the Physics and astrophysics of DM particles in the early Universe, its effects in the mass and neutrino species number constraints, and mainly, the role of DM in galaxies at all scales.

The study of all these issues are in part a natural continuation of the pioneering works developed in the past by former members of the ICRA group and collaborators, all headed by the director of the institute, Prof. R. Ruffini (see Ruffini et al. (1983), Ruffini et al. (1988), Ruffini and Stella (1983), Arbolino and Ruffini (1988), Merafina and Ruffini (1989), Gao et al. (1990), Ingrosso et al. (1992), Bisnovatyj-Kogan et al. (1993a), Bisnovatyi-Kogan et al. (1998)).

The nature of the DM particle interactions for the recently proposed sterile neutrino in the context of the so called neutrino Minimal Standard Model (νMSM, see Boyarsky et al. (2009b) and references therein), in compatibility with the early cosmology and further constrained with data coming form the center of the galaxies, is being studied by the Ph.D student C. R. Argüelles under the tutorship of the Prof. J. A. Rueda and Prof. R. Ruffini, in collaboration with N. Mavromatos. Some correlated aspects of the role of sterile ν in the early Universe, as neutrino species number constraints is currently being studied by the Ph.D student B. Fraga, guided by the professors J. A. Rueda and Prof. R. Ruffini.

The actual main topic of research respecting the role of fermionic DM particles in halos as well as in the centers of the galaxies together with its possible interaction regime is studied by the Ph.D students C. R. Argüelles and B. Fraga, with the collaboration of the ICRANet colleagues I. Siutsou, J. A. Rueda, and the external collaboration of the Prof. N. Mavromatos, headed by Prof. R. Ruffini.

Below we present an introduction for each topic of research together with a more detailed description through the links to actual results and ongoing papers.

The problem of the distribution of DM in galaxies as generally studied in the literature, is mainly focused in the halo regions and associated with the galactic rotation curves, where the major amount of data is available. The most common actual mathematical techniques used to deal with this problem are phenomenological fits (See e.g. Burkert (1995)) as well as best fits resulting from numerical N-body simulations centered in the ΛCDM paradigm (See Navarro et al. (1997), Navarro et al. (2004a)).

We propose here a new approach for this problem based on the following main assumptions:

1) that the problem of the galactic core and the halo have to be addressed unitarily;

2) for definiteness we study the simplest problem of 'bare' neutrinos in thermodynamic equilibrium fulfilling only the Fermi Dirac statistical distribution

$$f = \frac{1}{\exp\frac{\epsilon-\mu}{kT}+1} = \frac{1}{\exp\left(\frac{\epsilon}{\beta mc^2}-\theta\right)+1}, \tag{3.5.1}$$

where ϵ is kinetic energy of the particles, μ is chemical potential, T is the temperature, k is Boltzmann constant, m is the mass of 'ino', c is the speed of light,

$\beta = kT/mc^2$, $\theta = \mu/kT$, without consider either Fermi weak interactions or alternative interactions;

3) we consider zero total angular momentum and also we neglect any effect of Baryonic matter.

The equilibrium configurations of a self-gravitating semi-degenerate system of fermions were first studied in Newtonian gravity by Ruffini and Stella (1983) and then generalized in general relativity by Gao et al. (1990). It is shown that in any such system the density at large radii scales as r^{-2} quite independently of the values of the central density, always providing a flat rotation curve. These solutions were extended to an energy and angular momentum cut-off in the distribution function Ingrosso et al. (1992).

A typical mass density profile solution from the model, contrasted with a Navarro-Frenk-White (NFW) profile Navarro et al. (1997), as well as a Boltzmannian Isothermal sphere model is shown in Fig. 3.2,

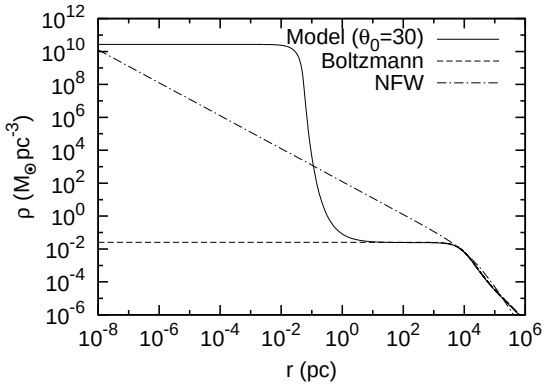

Figure 3.2.: The cored behaviour of the dark matter density profiles from our model is contrasted with the cuspy NFW density profile. The free parameters of the model are fixed as $\beta_0 = 1.251 \times 10^{-7}$, $\theta_0 = 30$ and $m = 10.54\text{keV}/c^2$, while the corresponding free parameters in the NFW formula $\rho_{NFW}(r) = \rho_0 r_0/(r(1+r/r_0)^2)$ are chosen as $\rho_0 = 5 \times 10^{-3} M_\odot \text{pc}^{-3}$ and $r_0 = 25$ Kpc (i.e. typical of spiral galaxies according to de Blok et al. (2008)).

It is interesting that the quantum and relativistic treatment of the configurations considered here are characterized by the presence of central cored structures unlike the typical cuspy configurations obtained from a classic non-relativistic approximation, such as the ones of numerical N-body simulations in Navarro et al. (1997). This naturally leads to a possible solution to

the well-known core-cusp discrepancy de Blok et al. (2001b).

We have recently returned to the Gao et. al. work, and propose a completely different way for solving the boundary condition problem for the system of non-linear first order differential equations, in order to fulfill the observationally inferred values of typical dark matter halos in spiral galaxies as given in de Blok et al. (2008). Namely, for a given initial condition for the total mass $M(0) = 0$ (consistent with no singularity at the center), arbitrary fixed θ_0 (depending on the chosen central degeneracy), and defining the halo radius r_h at the onset of the flat rotation curve, we solve an eigenvalue problem for the central temperature parameter β_0, until the *observed* halo circular velocity v_h is obtained. After this, we solve a second eigenvalue problem for the particle mass m until the *observed* halo mass M_h is reached at the radius r_h.

The quest has been to use all these information in order to put a novel lower constraints on the mass of the 'ino' in galactic halos by introducing the above mentioned observational properties. This bound is for typical spiral galaxies:

$$m \geq 0.42 keV/c^2. \tag{3.5.2}$$

The novel density profile solutions as well as the rotation curves in agreement with the *observed* halo properties are plotted in Fig. K.2 for different values of the central degeneracy parameter θ_0 in correspondence with the particle mass m,

Another relevant observational aspect on galactic halos is the so called *Universality laws*. Donato et al. (2009), fitting DM halos with Burkert profiles, found out that the surface density $\mu_{0D} = r_B \rho_0$ of galaxy dark matter halos, where r_B and ρ_0 are the burkert radius and central halo density, is nearly constant for a wide number of galaxies with different total masses and absolute magnitudes. This further implies a constant acceleration due to DM at the Burkert radius $a_{DM} G M_B / r_B^2 = 3.2 \times 10^{-9}$ cm/s^2. The fact that from our model we obtain scaling formulas for the magnitudes r_B and M_B with respect the free parameters of the model m, β_0 and θ_0, it allow us to show that always exist a definite range of the θ_0 as well as β_0 parameter for a given particle mass above the limit found in (3.5.2), which is in agreement with the observational universal result.

In these months the group was focused on the following issues.

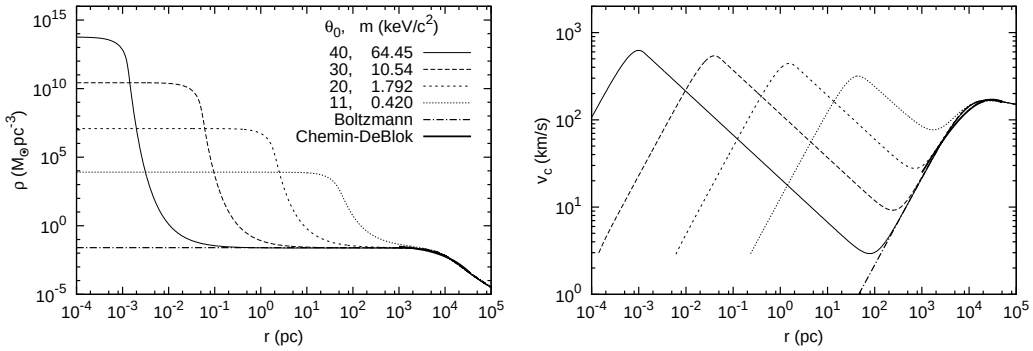

Figure 3.3.: Mass density profiles and rotation curves for specific ino masses m and central degeneracies θ_0 fulfilling the observational constraints $M_h = 1.6 \times 10^{11} M_\odot$ at $r_h = 25$ Kpc. All the quantum configurations have a dark matter halo circular velocity $v_h = 168$ km/s in correspondence with $\beta_0 = 1.251 \times 10^{-7}$. These solutions are contrasted with a Boltzmannian isothermal sphere and the observationally inferred dark matter profile of typical spirals (see Chemin et al. (2011), de Blok et al. (2008)).

3.6. The distribution of dark matter in galaxies based quantum treatments

The problem of modeling the distribution of dark matter in galaxies in terms of equilibrium configurations of collisionless self-gravitating quantum particles is considered. We first summarize the pioneering model of a Newtonian self-gravitating Fermi gas in thermodynamic equilibrium developed by Ruffini and Stella (1983), which is shown to be a generalization of the King model for fermions. We further review the extension of the former model developed by Gao, Merafina and Ruffini (1990), done for any degree of fermion degeneracy at the center (θ_0), within general relativity. Finally, we present here for the first time the solutions of the density profiles and rotation curves corresponding to the model of Gao et al. Those solutions have a definite mass M_h and a circular velocity v_h at the halo radius r_h of the configurations, which are typical of spiral galaxies. This treatment allows us to determine a novel core-halo morphology for the dark-matter profiles, as well as a novel bound on the particle mass associated with those profiles. For details see Appendix H.

3.7. A novel core-halo distribution of dark matter in galaxies

We investigate the distribution of dark matter in galaxies by solving the equations of equilibrium of a self-gravitating system of massive fermions ('inos') at selected temperatures and degeneracy parameters within general relativity. The most general solutions present, as a function of the radius, a segregation of three physical regimes: 1) an inner core of almost constant density governed by degenerate quantum statistics; 2) an intermediate region with a sharply decreasing density distribution followed by an extended plateau, implying quantum corrections; 3) a decreasing density distribution $\rho \propto r^{-2}$ leading to flat rotation curves fulfilling the classical Boltzmann statistics. The mass of the inos is determined as an eigenfunction of the mass of the inner quantum cores. We compare and contrast this mass value with the lower limit on the particle mass by Tremaine and Gunn (1979), and show that the latter is approached for the less degenerate quantum cores in agreement with the fixed halo observables. Consequences of this alternative approach to the massive core in SgrA* and to dwarf galaxies are outlined. For details see Appendix I.

3.8. Critical configurations for a system of semidegenerate fermions

We study an isothermal system of semidegenerate self-gravitating fermions in general relativity. Such systems present mass density solutions with a central degenerate core, a plateau and a tail, this last following a power law behavior r^{-2}. The different solutions are governed by the free parameters of the model: the degeneracy and the temperature parameters at the center and the particle mass m. We then analyze in detail the free parameter space for a fixed m in the keV region, by studying the one-parameter sequences of equilibrium configurations up to the critical point, which is represented by the maximum in a central density (ρ_0) vs. core mass (M_c) diagram. We show that for fully degenerate cores, the known expression for the critical core mass $M_c^{cr} \propto m_{pl}^3/m^2$ is obtained, while for low degenerate cores, the critical core mass increases, showing temperature effects in a nonlinear way. The main result of this work is that when applying this theory to model the distribu-

tion of dark matter in galaxies from the very center to the outer halos, we do not find any critical core-halo configuration of self-gravitating fermions that would be able to explain the super-massive dark object in their centers and the outer halo simultaneously. For details see Appendix J.

3.9. Super massive black holes and dark matter halos in big elliptical galaxies

Big elliptical and early-type galaxies, most of them containing super massive dark objects at their centers, present no definitive evidence for the existence of DM halos. The low surface brightness beyond R_e makes it a hard task to obtain reliable spectra to determine dispersion velocities. Among the several methods available to prove the mass distribution beyond R_e in elliptical galaxies, such as integrated stellar light spectrum, globular cluster and planetary nebulae kinematics, diffuse X-ray observation or weak gravitational lensing; no evidence for DM halos has been found even out to few R_e in many ellipticals by the use of kinematical methods as shown by Gebhardt et. al. (2001). Meanwhile, by using X-ray observations in an small sample of nearby ellipticals, a clear evidence for considerable amounts of DM at radii $r \sim 10R_e$ was given in Humphrey et. al. (2006). In any case, the more interesting constraints on DM in early-type galaxies are restricted to the more massive systems, which are placed near the center of group or clusters. This implies to be a difficult task to confirm whether the existence of extensive halos is an inherent property of the galaxy itself, or corresponds to the DM content at the group-scale. We thus propose to use the critical configurations of semi-degenerate self-gravitating fermions in General Relativity (GR) to model the distribution of dark matter in big elliptical galaxies from miliparsec distance-scales up to 10^2 Kpc. As a partial conclusion we do not find any critical core-halo configuration of self-gravitating fermions, able to explain both the most super-massive dark object at their center together with the DM halo simultaneously. While an interesting discussion in relation with observations of the most super massive dark compact objects and formation history at different cosmological redshift z is given. For details see Appendix K.

3.10. Dark Einstein clusters within the S2 orbit in SgrA*

We use the Einstein Cluster model in order to provide an alternative to the massive black hole thought to be hosted at the center of SgrA*. For this we model the central sub-miliparsec region of our galaxy in terms of a constant density Einstein cluster composed by dark matter particles of mass m, regardless of its nature. We analyze its stability conditions by two different methods considered in the literature, and explicitly show through the total mass (M)versus radius(R) relation, up to which point an Einstein cluster of constant particle number can be contracted, without losing its global stability. Finally, we compare the uppermost constant density constraints of stable clusters, with the lowest limit in the mass density of SgrA* as imposed by modern VLBI mm radio observations. For details see Appendix L.

3.11. Dark matter and baryons in dwarf galaxies

A generalization of the Jeans equations in the context of galactic dynamics is developed for a multi-component self-gravitating system composed of dark matter particles and stars. In addition to the luminous profile, an underlying fermionic phase-space density for the dark component is assumed. Under the ansatz of isotropy, spherical symmetry and constant dispersion velocities, this approach is applied to typical well resolved nucleated dwarf galaxies, to obtain novel dark matter density profiles showing central mass concentrations at pc distance-scales. Narrow constraints on the mass of the dark matter candidate of $m \sim 1$ keV are obtained. For details see Appendix M.

4. Publications

4.1. Publications before 2005

1. R. Ruffini, D. J. Song, and L. Stella, "On the statistical distribution of massive fermions and bosons in a Friedmann universe" Astronomy and Astrophysics, Vol. 125, (1983) pp. 265-270.

   The distribution function of massive Fermi and Bose particles in an expanding universe is considered as well as some associated thermodynamic quantities, pressure and energy density. These considerations are then applied to cosmological neutrinos. A new limit is derived for the degeneracy of a cosmological gas of massive neutrinos.

2. R. Ruffini and D. J. Song, "On the Jeans mass of weakly interacting neutral massive leptons", in Gamow cosmology, eds. F. Melchiorri and R. Ruffini, (1986) pp. 370–385.

   The cosmological limits on the abundances and masses of weakly interacting neutral particles are strongly affected by the nonzero chemical potentials of these leptons. For heavy leptons ($m_x >$ GeV), the value of the chemical potential must be much smaller than unity in order not to give very high values of the cosmological density parameter and the mass of heavy leptons, or they will be unstable. The Jeans' mass of weakly interacting neutral particles could give the scale of cosmological structure and the masses of astrophysical objects. For a mass of the order 10 eV, the Jeans' mass could give the scenario of galaxy formation, the supercluster forming first and then the smaller scales, such as clusters and galaxies, could form inside the large supercluster.

3. D. Calzetti, M. Giavalisco, R. Ruffini, J. Einasto, and E. Saar, "The correlation function of galaxies in the direction of the Coma cluster", Astrophysics and Space Science, Vol. 137 (1987) pp. 101-106.

   Data obtained by Einasto et al. (1986) on the amplitude of the correlation function of galaxies in the direction of the Coma cluster are compared with theo-

retical predictions of a model derived for a self-similar observer-homogeneous structure. The observational samples can be approximated by cones of angular width alpha of about 77 deg. Eliminating sources of large observational error, and by making a specified correction, the observational data are found to agree very well with the theoretical predictions of Calzetti et al. (1987).

4. R. Ruffini, D. J. Song, and S. Taraglio, "The 'ino' mass and the cellular large-scale structure of the universe", Astronomy and Astrophysics, Vol. 190, (1988) pp. 1-9.

   Within the theoretical framework of a Gamow cosmology with massive "inos", the authors show how the observed correlation functions between galaxies and between clusters of galaxies naturally lead to a "cellular" structure for the Universe. From the size of the "elementary cells" they derive constraints on the value of the masses and chemical potentials of the cosmological "inos". They outline a procedure to estimate the "effective" average mass density of the Universe. They also predict the angular size of the inhomogeneities to be expected in the cosmological black body radiation as remnants of this cellular structure. A possible relationship between the model and a fractal structure is indicated.

5. D. Calzetti, M. Giavalisco, and R. Ruffini, "The normalization of the correlation functions for extragalactic structures", Astronomy and Astrophysics, Vol. 198 (1988), pp. 1-15.

   It is shown that the spatial two-point correlation functions for galaxies, clusters and superclusters depend explicitly on the spatial volume of the statistical sample considered. Rules for the normalization of the correlation functions are given and the traditional classification of galaxies into field galaxies, clusters and superclusters is replaced by the introduction of a single fractal structure, with a lower cut-off at galactic scales. The roles played by random and stochastic fractal components in the galaxy distribution are discussed in detail.

6. M. V. Arbolino and R. Ruffini, "The ratio between the mass of the halo and visible matter in spiral galaxies and limits on the neutrino mass", Astronomy and Astrophysics, Vol. 192, (1988) pp. 107-116.

   Observed rotation curves for galaxies with values of the visible mass ranging over three orders of magnitude together with considerations involving equilibrium configurations of massive neutrinos, impose constraints on the ratio between the masses of visible and dark halo comporents in spiral galaxies.

Upper and lower limits are derived for the mass of the particles making up the dark matter.

7. A. Bianconi, H. W. Lee, and R. Ruffini, "Limits from cosmological nucleosynthesis on the leptonic numbers of the universe", Astronomy and Astrophysics, Vol. 241 (1991) pp. 343-357.

   Constraints on chemical potentials and masses of 'inos' are calculated using cosmological standard nucleosynthesis processes. It is shown that the electron neutrino chemical potential (ENCP) should not be greater than a value of the order of 1, and that the possible effective chemical potential of the other neutrino species should be about 10 times the ENCP in order not to conflict with observational data. The allowed region (consistent with the He-4 abundance observations) is insensitive to the baryon to proton ratio η, while those imposed by other light elements strongly depend on η.

8. R. Ruffini, J. D. Salmonson, J. R. Wilson, and S.-S. Xue, "On the pair electromagnetic pulse of a black hole with electromagnetic structure", Astronomy and Astrophysics, Vol. 350 (1999) pp. 334-343.

   We study the relativistically expanding electron-positron pair plasma formed by the process of vacuum polarization around an electromagnetic black hole (EMBH). Such processes can occur for EMBH's with mass all the way up to $6 \cdot 10^5 M_\odot$. Beginning with a idealized model of a Reissner-Nordstrom EMBH with charge to mass ratio $\xi = 0.1$, numerical hydrodynamic calculations are made to model the expansion of the pair-electromagnetic pulse (PEM pulse) to the point that the system is transparent to photons. Three idealized special relativistic models have been compared and contrasted with the results of the numerically integrated general relativistic hydrodynamic equations. One of the three models has been validated: a PEM pulse of constant thickness in the laboratory frame is shown to be in excellent agreement with results of the general relativistic hydrodynamic code. It is remarkable that this precise model, starting from the fundamental parameters of the EMBH, leads uniquely to the explicit evaluation of the parameters of the PEM pulse, including the energy spectrum and the astrophysically unprecedented large Lorentz factors (up to $6 \cdot 10^3$ for a 10^3 $M_\odot$ EMBH). The observed photon energy at the peak of the photon spectrum at the moment of photon decoupling is shown to range from 0.1 MeV to 4 MeV as a function of the EMBH mass. Correspondingly the total energy in photons is in the range of 10^{52} to 10^{54} ergs, consistent with observed

gamma-ray bursts. In these computations we neglect the presence of baryonic matter which will be the subject of forthcoming publications.

9. R. Ruffini, J. D. Salmonson, J. R. Wilson, and S.-S. Xue, "On the pair-electromagnetic pulse from an electromagnetic black hole surrounded by a baryonic remnant", Astronomy and Astrophysics, Vol. 359 (2000) pp. 855-864.

   The interaction of an expanding Pair-Electromagnetic pulse (PEM pulse) with a shell of baryonic matter surrounding a Black Hole with electromagnetic structure (EMBH) is analyzed for selected values of the baryonic mass at selected distances well outside the dyadosphere of an EMBH. The dyadosphere, the region in which a super critical field exists for the creation of e^+e^- pairs, is here considered in the special case of a Reissner-Nordstrom geometry. The interaction of the PEM pulse with the baryonic matter is described using a simplified model of a slab of constant thickness in the laboratory frame (constant-thickness approximation) as well as performing the integration of the general relativistic hydrodynamical equations. Te validation of the constant-thickness approximation, already presented in a previous paper Ruffini et al. (1999) for a PEM pulse in vacuum, is here generalized to the presence of baryonic matter. It is found that for a baryonic shell of mass-energy less than 1% of the total energy of the dyadosphere, the constant-thickness approximation is in excellent agreement with full general relativistic computations. The approximation breaks down for larger values of the baryonic shell mass, however such cases are of less interest for observed Gamma Ray Bursts (GRBs). On the basis of numerical computations of the slab model for PEM pulses, we describe (i) the properties of relativistic evolution of a PEM pulse colliding with a baryonic shell; (ii) the details of the expected emission energy and observed temperature of the associated GRBs for a given value of the EMBH mass; $10^3 M_\odot$, and for baryonic mass-energies in the range 10^{-8} to 10^{-2} the total energy of the dyadosphere.

10. M. Lattanzi, R. Ruffini, and G. Vereshchagin, "On the possible role of massive neutrinos in cosmological structure formation", in Cosmology and Gravitation, eds. M. Novello and S. E. Perez Bergliaffa, Vol. 668 of AIP Conference Series, (2003) pp. 263–287.

    In addition to the problem of galaxy formation, one of the greatest open questions of cosmology is represented by the existence of an asymmetry between matter and antimatter in the baryonic component of the Universe. We believe

that a net lepton number for the three neutrino species can be used to understand this asymmetry. This also implies an asymmetry in the matter-antimatter component of the leptons. The existence of a nonnull lepton number for the neutrinos can easily explain a cosmological abundance of neutrinos consistent with the one needed to explain both the rotation curves of galaxies and the flatness of the Universe. Some propedeutic results are presented in order to attack this problem.

4.2. Publications (2005 – 2013)

1. A. Benedetti, R. Ruffini and G.V. Vereshchagin, "Evolution of the pair plasma generated by a strong electric field", Physics Letters A, Volume 377 (2013), Issue 3-4, p. 206-215.

   We study the process of energy conversion from overcritical electric field into electron-positron-photon plasma. We solve numerically Vlasov-Boltzmann equations for pairs and photons assuming the system to be homogeneous and anisotropic. All the 2-particle QED interactions between pairs and photons are described by collision terms. We evidence several epochs of this energy conversion, each of them associated to a specific physical process. Firstly pair creation occurs, secondly back reaction results in plasma oscillations. Thirdly photons are produced by electron-positron annihilation. Finally particle interactions lead to completely equilibrated thermal electron-positron-photon plasma.

2. D. Begue, I. A. Siutsou and G. V. Vereshchagin, "Monte Carlo simulations of the photospheric emission in GRBs", the Astrophysical Journal Volume 767 (2013), Issue 2, article id. 139.

   We studied the decoupling of photons from ultra-relativistic spherically symmetric outflows expanding with constant velocity by means of Monte Carlo simulations. For outflows with finite widths we confirm the existence of two regimes: photon-thick and photon-thin, introduced recently by Ruffini et al. (RSV). The probability density function of the last scattering of photons is shown to be very different in these two cases. We also obtained spectra as well as light curves. In the photon-thick case, the time-integrated spectrum is much broader than the Planck function and its shape is well described by the fuzzy photosphere approximation introduced by RSV. In the photon-thin case, we confirm the crucial role of photon diffusion, hence the probability

density of decoupling has a maximum near the diffusion radius well below the photosphere. The time-integrated spectrum of the photon-thin case has a Band shape that is produced when the outflow is optically thick and its peak is formed at the diffusion radius.

3. R. Ruffni, I. A. Siutsou and G. V. Vereshchagin, "Theory of photospheric emission from relativistic outflows" , the Astrophysical Journal, Vol. 772, Issue 1 (2013) article id. 11.

   We derive the optical depth and photospheric radius of relativistic outflow using the model of relativistic wind with finite duration. We also discuss the role of radiative diffusion in such outflow. We solve numerically radiative transfer equation and obtain light curves and observed spectra of photospheric emission. The obtained spectra are nonthermal and in some cases have Band shape.

4. R. Ruffini and G.V. Vereshchagin, "Electron-positron plasma in GRBs and in cosmology", Il Nuovo Cimento C 36 (2013) 255.

   Electron-positron plasma is believed to play imporant role both in the early Universe and in sources of Gamma-Ray Bursts (GRBs). We focus on analogy and difference between physical conditions of electron-positron plasma in the early Universe and in sources of GRBs. We discuss a) dynamical differences, namely thermal acceleration of the outflow in GRB sources vs cosmological deceleration; b) nuclear composition differences as synthesis of light elements in the early Universe and possible destruction of heavy elements in GRB plasma; c) different physical conditions during last scattering of photons by electrons. Only during the acceleration phase of the optically thick electron-positron plasma comoving observer may find it similar to the early Universe. This similarity breaks down during the coasting phase. Reprocessing of nuclear abundances may likely take place in GRB sources. Heavy nuclear elements are then destroyed, resulting mainly in protons with small admixture of helium. Unlike the primordial plasma which recombines to form neutral hydrogen, and emits the Cosmic Microwave Background Radiation, GRB plasma does not cool down enough to recombine.

5. A.G. Aksenov, R. Ruffni and G. V. Vereshchagin, "Comptonization of photons near the photosphere of relativistic outflows", MNRAS Letters, Vol. 436, Issue 1 (2013) pp. L54-L58.

We consider the formation of photon spectrum at the photosphere of ultra-relativistically expanding outflow. We use the Fokker–Planck approximation to the Boltzmann equation, and obtain the generalized Kompaneets equation which takes into account anisotropic distribution of photons developed near the photosphere. This equation is solved numerically for relativistic steady wind and the observed spectrum is found in agreement with previous studies. We also study the photospheric emission for different temperature dependences on radius in such outflows. In particular, we found that for $T \propto r^{-2}$ the Band low-energy photon index of the observed spectrum is $\simeq -1$, as typically observed in Gamma-Ray Bursts.

6. R. Ruffini, C. R. Argüelles, B. M. O. Fraga, A. Geralico, H. Quevedo, J. A. Rueda, I. Siutsou, "Black Holes in Gamma Ray Bursts and Galactic Nuclei", IJMPD 22 No. 11, 1360008, 2013.

   Current research marks a clear success in identifying the moment of formation of a Black Hole of $10M_{\odot}$, with the emission of a Gamma Ray Burst. This explains in terms of the 'Blackholic Energy' the source of the energy of these astrophysical systems. Their energetics up to 10^{54} erg, make them detectable all over our Universe. Concurrently a new problematic has been arising related to: (a) The evidence of Dark Matter in galactic halos; (b) The origin of the Super Massive Black Holes in active galactic nuclei and Quasars and (c) The purported existence of a Black Hole in the Center of our Galaxy. These three aspects of this new problematic have been traditionally approached independently. We propose an unified approach to all three of them based on a system of massive self-gravitating neutrinos in General Relativity. Perspectives of future research are presented.

7. C. R. Argüelles, I. Siutsou, R. Ruffini, J. A. Rueda, B. Machado, "On the core-halo constituents of a semi-degenerate gas of massive fermions" AAS, Probes of Dark Matter on Galaxy Scales, 45, 30204, 2013.

   We propose a model of self-gravitating bare fermions at finite temperature in General Relativity to describe the dark matter (DM) in galaxies. We obtain a universal density profile composed by a flat and fully degenerate core for small radii, a low-degenerate plateau and a Newtonian tail that scales with r^{-2} for the outer halo region. The free parameters of the model are fitted using galactic observables such as the constant rotation velocity, mass of the central object and the halo radius, concluding that the particle mass should be in the

keV range. We further show that thighter constraints of a few keV for the mass of the fermions are obtained when using typical smallest dwarf galaxies.

8. B. M. O. Fraga, C. R. Argüelles, R. Ruffini, "Self-Gravitating System of Semidegenerated Fermions as Central Objects and Dark Matter Halos in Galaxies", IJMPS 23, 357-362, 2013.

   We propose a unified model for dark matter haloes and central galactic objects as a self-gravitating system of semidegenerated fermions in thermal equilibrium. We consider spherical symmetry and then we solve the equations of gravitational equilibrium using the Fermi integrals in a dimensionless manner, obtaining the density profile and velocity curve. We also obtain scaling laws for the observables of the system and show that, for a wide range of our parameters, our model is consistent with the so called universality of the surface density of dark matter.

9. Micol Benetti, S. Pandolfi, M. Lattanzi, M.Martinelli, A. Melchiorri. "Featuring the primordial power spectrum: new constraints on interrupted slow-roll from CMB and LRG data ", Physical Review D (2013) vol. 87, Issue 2, id. 023519

   Using the most recent data from the WMAP, ACT and SPT experiments, we update the constraints on models with oscillatory features in the primordial power spectrum of scalar perturbations. This kind of features can appear in models of inflation where slow-roll is interrupted, like multifield models. We also derive constraints for the case in which, in addition to cosmic microwave observations, we also consider the data on the spectrum of luminous red galaxies from the 7th SDSS catalog, and the SNIa Union Compilation 2 data. We have found that: (i) considering a model with features in the primordial power spectrum increases the agreement with data with the respect of the featureless "vanilla" ΛCDM model by $\Delta\chi^2 \simeq 7$; (ii) the uncertainty on the determination of the standard parameters is not degraded when features are included; (iii) the best fit for the features model locates the step in the primordial spectrum at a scale $k \simeq 0.005$ Mpc^{-1}, corresponding to the scale where the outliers in the WMAP7 data at $\ell = 22$ and $\ell = 40$ are located.; (iv) a distinct, albeit less statistically significant peak is present in the likelihood at smaller scales, with a $\Delta\chi^2 \simeq 3.5$, whose presence might be related to the WMAP7 preference for a negative value of the running of the scalar spectral index parameter; (v) the inclusion of the LRG-7 data do not change significantly the best fit model, but allows to better constrain the amplitude of the oscillations.

10. M. Benetti, M. Gerbino, W. H. Kinney, E. W. Kolb, M. Lattanzi, A. Melchiorri, L. Pagano, A. Riotto. "Cosmological data and indications for new physics", Journal of Cosmology and Astroparticle Physics, 10 (2013) 030.

    Data from the Atacama Cosmology Telescope (ACT) and the South Pole Telescope (SPT), combined with the nine-year data release from the WMAP satellite, provide very precise measurements of the cosmic microwave background (CMB) angular anisotropies down to very small angular scales. Augmented with measurements from Baryonic Acoustic Oscillations surveys and determinations of the Hubble constant, we investigate whether there are indications for new physics beyond a Harrison-Zel'dovich model for primordial perturbations and the standard number of relativistic degrees of freedom at primordial recombination. All combinations of datasets point to physics beyond the minimal Harrison-Zel'dovich model in the form of either a scalar spectral index different from unity or additional relativistic degrees of freedom at recombination (e.g., additional light neutrinos). Beyond that, the extended datasets including either ACT or SPT provide very different indications: while the extended-ACT (eACT) dataset is perfectly consistent with the predictions of standard slow-roll inflation, the extended-SPT (eSPT) dataset prefers a non-power-law scalar spectral index with a very large variation with scale of the spectral index. Both eACT and eSPT favor additional light degrees of freedom. eACT is consistent with zero neutrino masses, while eSPT favors nonzero neutrino masses at more than 95% confidence.

11. M. Benetti. "Updating constraints by Planck data on inlationary features model", Physical Review D 88 (2013) 087302.

    We present new constraints on possible features in the primordial inflationary density perturbations power spectrum in light of the recent Cosmic Microwave Background Anisotropies measurements from the Planck satellite. We found that the Planck data hints for the presence of features in two different ranges of angular scales, corresponding to multipoles $10 < l < 60$ and $150 < l < 300$, with a decrease in the best fit χ^2 value with respect to the featureless "vanilla" LCDM model of $\Delta\chi^2$ around 9 in both cases.

12. B. Patricelli, M.G. Bernardini, C.L. Bianco, L. Caito, G. de Barros, L. Izzo, R. Ruffini and G.V. Vereshchagin, "Analysis of GRB 080319B and GRB 050904 within the Fireshell Model: Evidence for a Broader Spectral

Energy Distribution", The Astrophysical Journal, Volume 756, Issue 1, article id. 16 (2012).

The observation of GRB 080319B, with an isotropic energy $E_{iso}= 1.32 \cdot 10^{54}$ erg, and GRB 050904, with $E_{iso}= 1.04 \cdot 10^{54}$ erg, offers the possibility of studying the spectral properties of the prompt radiation of two of the most energetic gamma-ray bursts (GRBs). This allows us to probe the validity of the fireshell model for GRBs beyond 10^{54} erg, well outside the energy range where it has been successfully tested up to now (10^{49}-10^{53}erg). We find that in the low-energy region, the prompt emission spectra observed by Swift Burst Alert Telescope (BAT) reveals more power than theoretically predicted. The opportunities offered by these observations to improve the fireshell model are outlined in this paper. One of the distinguishing features of the fireshell model is that it relates the observed GRB spectra to the spectrum in the comoving frame of the fireshell. Originally, a fully radiative condition and a comoving thermal spectrum were adopted. An additional power law in the comoving thermal spectrum is required due to the discrepancy of the theoretical and observed light curves and spectra in the fireshell model for GRBs 080319B and 050904. A new phenomenological parameter α is correspondingly introduced in the model. We perform numerical simulations of the prompt emission in the Swift BAT bandpass by assuming different values of within the fireshell model. We compare them with the GRB 080319B and GRB 050904 observed time-resolved spectra, as well as with their time-integrated spectra and light curves. Although GRB 080319B and GRB 050904 are at very different redshifts ($z = 0.937$ and $z = 6.29$, respectively), a value of $\alpha = -1.8$ for both of them leads to a good agreement between the numerical simulations and the observed BAT light curves, time-resolved and time-integrated spectra. Such a modified spectrum is also consistent with the observations of previously analyzed less energetic GRBs and reasons for this additional agreement are given. Perspectives for future low-energy missions are outlined.

13. A.G. Aksenov, R. Ruffni, I. A. Siutsou and G. V. Vereshchagin, "Dynamics and emission of mildly relativistic plasma", International Journal of Modern Physics: Conference Series, Vol. 12, Issue 01, (2012) pp. 1-9.

Initially optically thick (with $\tau = 3 \cdot 10^7$) spherically symmetric outflow consisting of electron-positron pairs and photons is considered. We do not assume thermal equilibrium, and include the two-body processes that occur in such plasma: Moller and Bhaba scattering of pairs, Compton scattering, two-

photon pair annihilation, two-photon pair production, together with their radiative three-body variants: bremsstrahlung, double Compton scattering, and three-photon pair annihilation, with their inverse processes. We solve numerically the relativistic Boltzmann equations in spherically symmetric case for distribution functions of pairs and photons. Three epochs are considered in details: a) the thermalization, which brings initially nonequilibrium plasma to thermal equilibrium; b) the self-accelerated expansion, which we find in agreement with previous hydrodynamic studies and c) decoupling of photons from the expanding electron-positron plasma. Photon spectra are computed, and appear to be non thermal near the peak of the luminosity. In particular, the low energy part of the spectrum contain more power with respect to the black body one.

14. A. Benedetti, W.-B. Han, R. Ruffini and G.V. Vereshchagin, "On the frequency of oscillations in the pair plasma generated by a strong electric field", Physics Letters B, Vol. 698 (2011) 75-79.

    We study the frequency of the plasma oscillations of electron-positron pairs created by the vacuum polarization in a uniform electric field with strength E in the range $0.2E_c < E < 10E_c$. Following the approach adopted in Ruffini et al. (2007) we work out one second order ordinary differential equation for a variable related to the velocity from which we can recover the classical plasma oscillation equation when E$\rightarrow$0. Thereby, we focus our attention on its evolution in time studying how this oscillation frequency approaches the plasma frequency. The time-scale needed to approach to the plasma frequency and the power spectrum of these oscillations are computed. The characteristic frequency of the power spectrum is determined uniquely from the initial value of the electric field strength. The effects of plasma degeneracy and pair annihilation are discussed.

15. B. Patricelli, M.G. Bernardini, C.L. Bianco, L. Caito, L. Izzo, R. Ruffini and G.V. Vereshchagin, "A New Spectral Energy Distribution of Photons in the Fireshell Model of GRBs", International Journal of Modern Physics D, Vol. 20 (2011) 1983-1987.

    The analysis of various Gamma-Ray Bursts (GRBs) having a low energetics within the fireshell model has shown how the N(E) spectrum of their prompt emission can be reproduced in a satisfactory way by a convolution of thermal spectra. Nevertheless, from the study of very energetic bursts such as,

for example, GRB 080319B, some discrepancies between the numerical simulations and the observational data have been observed. We investigate a different spectrum of photons in the comoving frame of the fireshell in order to better reproduce the spectral properties of GRB prompt emission within the fireshell model. We introduce a phenomenologically modified thermal spectrum: a thermal spectrum characterized by a different asymptotic power-law index in the low energy region. Such an index depends on a free parameter α, so that the pure thermal spectrum corresponds to the case $\alpha = 0$. We test this spectrum by comparing the numerical simulations with the observed prompt emission spectra of various GRBs. From this analysis it has emerged that the observational data can be correctly reproduced by assuming a modified thermal spectrum with $\alpha = -1.8$.

16. Elena Giusarma, Martina Corsi, Maria Archidiacono, Roland de Putter, Alessandro Melchiorri, Olga Mena, Stefania Pandolfi. "Constraints on massive sterile neutrino species from current and future cosmological data", Phys.Rev. D83, 115023 (2011)

    Sterile massive neutrinos are a natural extension of the standard model of elementary particles. The energy density of the extra sterile massive states affects cosmological measurements in an analogous way to that of active neutrino species. We perform here an analysis of current cosmological data and derive bounds on the masses of the active and the sterile neutrino states, as well as on the number of sterile states. The so-called (3+2) models, with three sub-eV active massive neutrinos plus two sub-eV massive sterile species, is well within the 95% CL allowed regions when considering cosmological data only. If the two extra sterile states have thermal abundances at decoupling, big bang nucleosynthesis bounds compromise the viability of (3+2) models. Forecasts from future cosmological data on the active and sterile neutrino parameters are also presented. Independent measurements of the neutrino mass from tritium beta-decay experiments and of the Hubble constant could shed light on sub-eV massive sterile neutrino scenarios.

17. M. Archidiacono, A. Melchiorri, S. Pandolfi, "The impact of Reionization modelling on CMB Neutrino Mass Bounds", Nuclear Physics B, Proceedings Supplements, Volume 217, Issue 1, p. 65-67. (2011)

    We investigate the bounds on the neutrino mass in a general reionization scenario based on a principal component approach. We found the constraint on

the sum of the neutrino masses from CMB data can be relaxed by a ~ 40 % in a generalized reionization scenario.

18. Erminia Calabrese, Eloisa Menegoni, C. J. A. P. Martins, Alessandro Melchiorri, and Graca Rocha, "Constraining variations in the fine structure constant in the presence of early dark energy", Phys.Rev. D84 (2011) 023518.

    We discuss present and future cosmological constraints on variations of the fine structure constant α induced by an early dark energy component having the simplest allowed (linear) coupling to electromagnetism. We find that current cosmological data show no variation of the fine structure constant at recombination respect to the present-day value, with $\alpha/\alpha_0 = 0.975 \pm 0.020$ at 95% c.l., constraining the energy density in early dark energy to $\Omega_e < 0.060$ at 95% c.l. Moreover, we consider constraints on the parameter quantifying the strength of the coupling by the scalar field. We find that current cosmological constraints on the coupling are about 20 times weaker than those obtainable locally (which come from Equivalence Principle tests). However forthcoming or future missions, such as Planck Surveyor and CMBPol, can match and possibly even surpass the sensitivity of current local tests.

19. Micol Benetti, Massimiliano Lattanzi, Erminia Calabrese, Alessandro Melchiorri, "Features in the primordial spectrum: new constraints from WMAP7+ACT data and prospects for Planck", Phys. Rev. D 84, 063509 (2011)

    We update the constraints on possible features in the primordial inflationary density perturbation spectrum by using the latest data from the WMAP7 and ACT Cosmic Microwave Background experiments. The inclusion of new data significantly improves the constraints with respect to older work, especially to smaller angular scales. While we found no clear statistical evidence in the data for extensions to the simplest, featureless, inflationary model, models with a step provide a significantly better fit than standard featureless power-law spectra. We show that the possibility of a step in the inflationary potential like the one preferred by current data will soon be tested by the forthcoming temperature and polarization data from the Planck satellite mission.

20. Stefania Pandolfi, Elena Giusarma, Edward W. Kolb, Massimiliano Lattanzi, Alessandro Melchiorri, Olga Mena, Manuel Pena, Asantha

Cooray, Paolo Serra, "Impact of general reionization scenarios on extraction of inflationary parameters", Phys.Rev. D82, 123527, (2010).

Determination of whether the Harrison–Zel'dovich spectrum for primordial scalar perturbations is consistent with observations is sensitive to assumptions about the reionization scenario. In light of this result, we revisit constraints on inflationary models using more general reionization scenarios. While the bounds on the tensor-to-scalar ratio are largely unmodified, when different reionization schemes are addressed, hybrid models are back into the inflationary game. In the general reionization picture, we reconstruct both the shape and amplitude of the inflaton potential. We find a broader spectrum of potential shapes when relaxing the simple reionization restriction. An upper limit of 10^{16} GeV to the amplitude of the potential is found, regardless of the assumptions on the reionization history.

21. A.G. Aksenov, R. Ruffini and G.V. Vereshchagin, "Pair plasma relaxation time scales", Physical Review E, Vol. 81 (2010) 046401.

    By numerically solving the relativistic Boltzmann equations, we compute the time scale for relaxation to thermal equilibrium for an optically thick electron-positron plasma with baryon loading. We focus on the time scales of electromagnetic interactions. The collisional integrals are obtained directly from the corresponding QED matrix elements. Thermalization time scales are computed for a wide range of values of both the total energy density (over 10 orders of magnitude) and of the baryonic loading parameter (over 6 orders of magnitude). This also allows us to study such interesting limiting cases as the almost purely electron-positron plasma or electron-proton plasma as well as intermediate cases. These results appear to be important both for laboratory experiments aimed at generating optically thick pair plasmas as well as for astrophysical models in which electron-positron pair plasmas play a relevant role.

22. R. Ruffini, G.V. Vereshchagin and S.-S. Xue, "Electron-positron pairs in physics and astrophysics: from heavy nuclei to black holes" Physics Reports, Vol. 487 (2010) No 1-4, pp. 1-140.

    From the interaction of physics and astrophysics we are witnessing in these years a splendid synthesis of theoretical, experimental and observational results originating from three fundametal physical processes. They were originally proposed by Dirac, by Breit and Wheeler and by Sauter, Heisenberg, Euler and Schwinger. For almost seventy years they have all three been followed

by a continued effort of experimental verification on Earth-based experiments. The Dirac process, $e^+e^- \to 2\gamma$, has been by far the most successful. It has obtained extremely accurate experimental verification and has led as well to an enormous number of new physics in possibly one of the most fruitful experimental avenue by introduction of storage rings in Frascati and followed by the largest accelerators worldwide: DESY, SLAC etc. The Breit-Wheeler process, $2\gamma \to e^+e^-$, although conceptually simple, being the inverse process of the Dirac one, has been by far one of the most difficult to be verified experimentally. Only recently, through the technology based on free electron X-ray laser and its numerous applications in Earth-based experiments, some first indications of its possible verification have been reached. The vacuum polarization process in strong electromagnetic field, pioneered by Sauter, Heisenberg, Euler and Schwinger, introduced the concept of critical electric field $E_c = m_e^2c^3/e\hbar$. It has been searched without success for more than forty years by heavy-ion collisions in many of the leading particle accelerators worldwide. The novel situation today is that these same processes can be studied on a much more grandiose scale during the gravitational collapse leading to the formation of a black hole being observed in Gamma Ray Bursts (GRBs). This report is dedicated to the scientific race in act. The theoretical and experimental work developed in Earth-based laboratories is confronted with the theoretical interpretation of space-based observations of phenomena originating on cosmological scales. What has become clear in the last ten years is that all the three above mentioned processes, duly extended in the general relativistic framework, are necessary for the understanding of the physics of the gravitational collapse to a black hole. Vice versa, the natural arena where these processes can be observed in mutual interaction and on an unprecedented scale, is indeed the realm of relativistic astrophysics. We systematically analyze the conceptual developments which have followed the basic work of Dirac and Breit-Wheeler. We also recall how the seminal work of Born and Infeld inspired the work by Sauter, Heisenberg and Euler on effective Lagrangian leading to the estimate of the rate for the process of electron-positron production in a constant electric field. In addition of reviewing the intuitive semi-classical treatment of quantum mechanical tunneling for describing the process of electron-positron production, we recall the calculations in *Quantum Electro-Dynamics* of the Schwinger rate and effective Lagrangian for constant electromagnetic fields. We also review the electron-positron production in both time-alternating electromagnetic fields, studied by Brezin, Itzykson, Popov, Nikishov and Narozhny, and the corresponding processes relevant for pair production at the focus of coherent laser

beams as well as electron beam-laser collision. We finally report some current developments based on the general JWKB approach which allows to compute the Schwinger rate in spatially varying and time varying electromagnetic fields. We also recall the pioneering work of Landau and Lifshitz, and Racah on the collision of charged particles as well as experimental success of AdA and ADONE in the production of electron-positron pairs. We then turn to the possible experimental verification of these phenomena. We review: A) the experimental verification of the $e^+e^- \rightarrow 2\gamma$ process studied by Dirac. We also briefly recall the very successful experiments of e^+e^- annihilation to hadronic channels, in addition to the Dirac electromagnetic channel; B) ongoing Earth based experiments to detect electron-positron production in strong fields by focusing coherent laser beams and by electron beam-laser collisions; and C) the multiyear attempts to detect electron-positron production in Coulomb fields for a large atomic number $Z > 137$ in heavy ion collisions. These attempts follow the classical theoretical work of Popov and Zeldovich, and Greiner and their schools. We then turn to astrophysics. We first review the basic work on the energetics and electrodynamical properties of an electromagnetic black hole and the application of the Schwinger formula around Kerr-Newman black holes as pioneered by Damour and Ruffini. We only focus on black hole masses larger than the critical mass of neutron stars, for convenience assumed to coincide with the Rhoades and Ruffini upper limit of $3.2M_{\odot}$. In this case the electron Compton wavelength is much smaller than the spacetime curvature and all previous results invariantly expressed can be applied following well established rules of the equivalence principle. We derive the corresponding rate of electron-positron pair production and the introduction of the concept of Dyadosphere. We review recent progress in describing the evolution of optically thick electron-positron plasma in presence of supercritical electric field, which is relevant both in astrophysics as well as ongoing laser beam experiments. In particular we review recent progress based on the Vlasov-Boltzmann-Maxwell equations to study the feedback of the created electron-positron pairs on the original constant electric field. We evidence the existence of plasma oscillations and its interaction with photons leading to energy and number equipartition of photons, electrons and positrons. We finally review the recent progress obtained by using the Boltzmann equations to study the evolution of an electron-positron-photon plasma towards thermal equilibrium and determination of its characteristic timescales. The crucial difference introduced by the correct evaluation of the role of two and three body collisions, direct and inverse, is especially evidenced. We then present some general conclusions. The results

reviewed in this report are going to be submitted to decisive tests in the forthcoming years both in physics and astrophysics. To mention only a few of the fundamental steps in testing in physics we recall the starting of experimental facilities at the National Ignition Facility at the Lawrence Livermore National Laboratory as well as corresponding French Laser the Mega Joule project. In astrophysics these results will be tested in galactic and extragalactic black holes observed in binary X-ray sources, active galactic nuclei, microquasars and in the process of gravitational collapse to a neutron star and also of two neutron stars to a black hole giving origin to GRBs. The astrophysical description of the stellar precursors and the initial physical conditions leading to a gravitational collapse process will be the subject of a forthcoming report. As of today no theoretical description has yet been found to explain either the emission of the remnant for supernova or the formation of a charged black hole for GRBs. Important current progress toward the understanding of such phenomena as well as of the electrodynamical structure of neutron stars, the supernova explosion and the theories of GRBs will be discussed in the above mentioned forthcoming report. What is important to recall at this stage is only that both the supernovae and GRBs processes are among the most energetic and transient phenomena ever observed in the Universe: a supernova can reach energy of $\tilde{}10^{54}$ ergs on a time scale of a few months and GRBs can have emission of up to $\tilde{}10^{54}$ ergs in a time scale as short as of a few seconds. The central role of neutron stars in the description of supernovae, as well as of black holes and the electron-positron plasma, in the description of GRBs, pioneered by one of us (rr) in 1975, are widely recognized. Only the theoretical basis to address these topics are discussed in the present report.

23. A. G. Aksenov, R. Ruffini, and G. V. Vereshchagin, "Kinetics of the Mildly Relativistic Plasma and GRBs" in the Proceedings of "The Sun, the stars, the Universe and General Relativity" meeting in honor of 95th Anniversary of Ya. B. Zeldovich in Minsk, AIP Conference Proceedings 1205 (2010) 11-16.

    We consider optically thick photon-pair-proton plasma in the framework of Boltzmann equations. For the sake of simplicity we consider the uniform and isotropic plasma. It has been shown that arbitrary initial distribution functions evolve to the thermal equilibrium state through so called kinetic equilibrium state with common temperature of all particles and nonzero chemical potentials. For the plasma temperature $0.1 - 10$ MeV relevant for GRB (Gamma-Ray Burst) sources we evaluate the thermalization time scale as function of total

energy density and baryonic loading parameter.

24. E. Menegoni, S. Pandolfi, S. Galli, M. Lattanzi, A. Melchiorri "Constraints on the dark energy equation of state in presence of a varying fine structure constant" in Int. J. Mod. Phys D19, 507 (2010).

    We discuss the cosmological constraints on the dark energy equation of state in the pres- ence of primordial variations in the fine structure constant. We find that the constraints from CMB data alone on w and the Hubble constant are much weaker when variations in the fine structure constant are permitted. Vice versa, constraints on the fine struc- ture constant are relaxed by more than 50% when dark energy models different from a cosmological constant are considered.

25. C.J.A.P. Martins, E. Menegoni, S. Galli and A. Melchiorri, "Varying couplings in the early universe: correlated variations of α and G, Physical Review D 82 023532 (2010)

    The cosmic microwave background anisotropies provide a unique opportunity to constrain simultaneous variations of the fine-structure constant α and Newton's gravitational constant G. Those correlated variations are possible in a wide class of theoretical models. In this brief paper we show that the current data, assuming that particle masses are constant, give no clear indication for such variations, but already prefer that any relative variations in α should be of the same sign of those of G for variations of 1%. We also show that a cosmic complementarity is present with big bang nucleosynthesis and that a combination of current CMB and big bang nucleosynthesis data strongly constraints simultaneous variations in α and G. We finally discuss the future bounds achievable by the Planck satellite mission.

26. E. Menegoni, "New Constraints on Variations of Fine Structure Constant from Cosmic Microwave Background Anisotropies", GRAVITATIONAL PHYSICS: TESTING GRAVITY FROM SUBMILLIMETER TO COSMIC: Proceedings of the VIII Mexican School on Gravitation and Mathematical Physics. AIP Conference Proceedings, Volume 1256, pp. 288-292 (2010).

    The recent measurements of Cosmic Microwave Background temperature and polarization anisotropy made by the ACBAR, QUAD and BICEP experiments substantially improve the cosmological constraints on possible variations of the fine structure constant in the early universe. In this work I analyze this

recent data obtaining the constraint $\alpha/\alpha 0$ = 0.987+/-0.012 at 68% c.l.. The inclusion of the new HST constraints on the Hubble constant further increases the bound to $\alpha/\alpha 0$ = 1.001+/-0.007 at 68% c.l., bringing possible deviations from the current value below the 1% level.

27. A. Melchiorri, F. De Bernardis, E. Menegoni, "Limits on the neutrino mass from cosmology". GRAVITATIONAL PHYSICS: TESTING GRAVITY FROM SUBMILLIMETER TO COSMIC: Proceedings of the VIII Mexican School on Gravitation and Mathematical Physics. AIP Conference Proceedings, Volume 1256, pp. 96-106 (2010).

    We use measurements of luminosity-dependent galaxy bias at several different redshifts, SDSS at z = 0.05, DEEP2 at z = 1 and LBGs at z = 3.8, combined with WMAP five-year cosmic microwave background anisotropy data and SDSS Red Luminous Galaxy survey three-dimensional clustering power spectrum to put constraints on cosmological parameters.

28. A.G. Aksenov, R. Ruffini and G.V. Vereshchagin, "Thermalization of the mildly relativistic plasma", Physical Review D, Vol. 79 (2009) 043008.

    In the recent Letter Aksenov et al. (2007) we considered the approach of nonequilibrium pair plasma towards thermal equilibrium state adopting a kinetic treatment and solving numerically the relativistic Boltzmann equations. It was shown that plasma in the energy range 0.1-10 MeV first reaches kinetic equilibrium, on a timescale $t_{\rm k} \lesssim 10^{-14}$ sec, with detailed balance between binary interactions such as Compton, Bhabha and Møller scattering, and pair production and annihilation. Later the electron-positron-photon plasma approaches thermal equilibrium on a timescale $t_{\rm th} \lesssim 10^{-12}$ sec, with detailed balance for all direct and inverse reactions. In the present paper we systematically present details of the computational scheme used in Aksenov et al. (2007), as well as generalize our treatment, considering proton loading of the pair plasma. When proton loading is large, protons thermalize first by proton-proton scattering, and then with the electron-positron-photon plasma by proton-electron scattering. In the opposite case of small proton loading proton-electron scattering dominates over proton-proton one. Thus in all cases the plasma, even with proton admixture, reaches thermal equilibrium configuration on a timescale $t_{\rm th} \lesssim 10^{-11}$ sec. We show that it is crucial to account for not only binary but also triple direct and inverse interactions between electrons, positrons, photons and protons. Several explicit examples are given and

the corresponding timescales for reaching kinetic and thermal equilibria are determined.

29. A. G. Aksenov, R. Ruffini, and G. V. Vereshchagin, "Thermalization of pair plasma with proton loading" in the Proceedings of "PROBING STELLAR POPULATIONS OUT TO THE DISTANT UNIVERSE" meeting, AIP Conference Proceedings 1111 (2009) 344-350.

    We study kinetic evolution of nonequilibrium optically thick electron-positron plasma towards thermal equilibrium solving numerically relativistic Boltzmann equations with energy per particle ranging from 0.1 to 10 MeV. We generalize our results presented in Aksenov et al. (2007), considering proton loading of the pair plasma. Proton loading introduces new characteristic timescales essentially due to proton-proton and proton-electron Coulomb collisions. Taking into account not only binary but also triple direct and inverse interactions between electrons, positrons, photons and protons we show that thermal equilibrium is reached on a timescale $t_{\rm th} \simeq 10^{-11}$ sec.

30. A.G. Aksenov, R. Ruffini and G.V. Vereshchagin, "Thermalization of nonequilibrium electron-positron-photon plasmas", Physical Review Letters, Vol. 99 (2007) No 12, 125003.

    Starting from a nonequilibrium configuration we analyze the role of the direct and the inverse binary and triple interactions in reaching thermal equilibrium in a homogeneous isotropic pair plasma. We focus on energies in the range $0.1 - 10$ MeV. We numerically integrate the relativistic Boltzmann equation with the exact QED collisional integrals taking into account all binary and triple interactions. We show that first, when a detailed balance is reached for all binary interactions on a time scale $t_k < 10^{-14}$ sec, photons and electron-positron pairs establish kinetic equilibrium. Subsequently, when triple interactions satisfy the detailed balance on a time scale $t_{eq} < 10^{-12}$ sec, the plasma reaches thermal equilibrium. It is shown that neglecting the inverse triple interactions prevents reaching thermal equilibrium. Our results obtained in the theoretical physics domain also find application in astrophysics and cosmology.

31. C.L. Bianco, R. Ruffini, G.V. Vereshchagin and S.-S. Xue, "Equations of Motion and Initial and Boundary Conditions for Gamma-ray Burst", Journal of the Korean Physical Society, Vol. 49 (2006) No. 2, pp. 722-731.

We compare and contrast the different approaches to the optically thick adiabatic phase of GRB all the way to the transparency. Special attention is given to the role of the rate equation to be self consistently solved with the relativistic hydrodynamic equations. The works of Shemi and Piran (1990), Piran, Shemi and Narayan (1993), Meszaros, Laguna and Rees (1993) and Ruffini, Salmonson, Wilson and Xue (1999,2000) are compared and contrasted. The role of the baryonic loading in these three treatments is pointed out. Constraints on initial conditions for the fireball produced by electro-magnetic black hole are obtained.

32. P. Singh, K. Vandersloot and G.V. Vereshchagin, "Nonsingular bouncing universes in loop quantum cosmology", Physical Review D, Vol. 74 (2006) 043510.

    Nonperturbative quantum geometric effects in loop quantum cosmology (LQC) predict a ρ^2 modification to the Friedmann equation at high energies. The quadratic term is negative definite and can lead to generic bounces when the matter energy density becomes equal to a critical value of the order of the Planck density. The nonsingular bounce is achieved for arbitrary matter without violation of positive energy conditions. By performing a qualitative analysis we explore the nature of the bounce for inflationary and cyclic model potentials. For the former we show that inflationary trajectories are attractors of the dynamics after the bounce implying that inflation can be harmoniously embedded in LQC. For the latter difficulties associated with singularities in cyclic models can be overcome. We show that nonsingular cyclic models can be constructed with a small variation in the original cyclic model potential by making it slightly positive in the regime where scalar field is negative.

33. M. Lattanzi, R. Ruffini and G.V. Vereshchagin, "Joint constraints on the lepton asymmetry of the Universe and neutrino mass from the Wilkinson Microwave Anisotropy Probe", Physical Review D, Vol. 72 (2005) 063003.

    We use the Wilkinson Microwave Anisotropy Probe (WMAP) data on the spectrum of cosmic microwave background anisotropies to put constraints on the present amount of lepton asymmetry L, parametrized by the dimensionless chemical potential (also called degeneracy parameter) xi and on the effective number of relativistic particle species. We assume a flat cosmological model with three thermally distributed neutrino species having all the same mass

and chemical potential, plus an additional amount of effectively massless exotic particle species. The extra energy density associated to these species is parametrized through an effective number of additional species $\Delta N_{others}{}^{eff}$. We find that $0 < |\xi| < 1.1$ and correspondingly $0 < |L| < 0.9$ at 2σ, so that WMAP data alone cannot firmly rule out scenarios with a large lepton number; moreover, a small preference for this kind of scenarios is actually found. We also discuss the effect of the asymmetry on the estimation of other parameters and, in particular, of the neutrino mass. In the case of perfect lepton symmetry, we obtain the standard results. When the amount of asymmetry is left free, we find at 2sigma. Finally we study how the determination of $|L|$ is affected by the assumptions on ΔN^{eff}_{others}. We find that lower values of the extra energy density allow for larger values of the lepton asymmetry, effectively ruling out, at 2sigma level, lepton symmetric models with $\Delta N^{eff}_{others} \simeq 0$.

34. G.V. Vereshchagin, "Gauge Theories of Gravity with the Scalar Field in Cosmology", in "Frontiers in Field Theory", edited by O. Kovras, Nova Science Publishers, New York, (2005), pp. 213-255 (ISBN: 1-59454-127-2).

Brief introduction into gauge theories of gravity is presented. The most general gravitational lagrangian including quadratic on curvature, torsion and nonmetricity invariants for metric-affine gravity is given. Cosmological implications of gauge gravity are considered. The problem of cosmological singularity is discussed within the framework of general relativity as well as gauge theories of gravity. We consider the role of scalar field in connection to this problem. Initial conditions for nonsingular homogeneous isotropic Universe filled by single scalar field are discussed within the framework of gauge theories of gravity. Homogeneous isotropic cosmological models including ultrarelativistic matter and scalar field with gravitational coupling are investigated. We consider different symmetry states of effective potential of the scalar field, in particular restored symmetry at high temperatures and broken symmetry. Obtained bouncing solutions can be divided in two groups, namely nonsingular inflationary and
oscillating solutions. It is shown that inflationary solutions exist for quite general initial conditions like in the case of general relativity. However, the phase space of the dynamical system, corresponding to the cosmological equations is bounded. Violation of the uniqueness of solutions on the boundaries of the phase space takes place. As a result, it is impossible to define either the past

or the future for a given solution. However, definitely there are singular solutions and therefore the problem of cosmological singularity cannot be solved in models with the scalar field within gauge theories of gravity.

35. R. Ruffini, M. G. Bernardini, C. L. Bianco, L. Caito, P. Chardonnet, M. G. Dainotti, F. Fraschetti, R. Guida, M. Rotondo, G. Vereshchagin, L. Vitagliano, S.-S. Xue,
"The Blackholic energy and the canonical Gamma-Ray Burst" in Cosmology and Gravitation: XIIth Brazilian School of Cosmology and Gravitation, edited by M. Novello and S.E. Perez Bergliaffa, AIP Conference Proceedings, Vol. 910, Melville, New York, 2007, pp. 55-217.

Gamma-Ray Bursts (GRBs) represent very likely "the" most extensive computational, theoretical and observational effort ever carried out successfully in physics and astrophysics. The extensive campaign of observation from space based X-ray and γ-ray observatory, such as the Vela, CGRO, BeppoSAX, HETE-II, INTEGRAL, Swift, R-XTE, Chandra, XMM satellites, have been matched by complementary observations in the radio wavelength (e.g. by the VLA) and in the optical band (e.g. by VLT, Keck, ROSAT). The net result is unprecedented accuracy in the received data allowing the determination of the energetics, the time variability and the spectral properties of these GRB sources. The very fortunate situation occurs that these data can be confronted with a mature theoretical development. Theoretical interpretation of the above data allows progress in three different frontiers of knowledge: a) the ultrarelativistic regimes of a macroscopic source moving at Lorentz gamma factors up to ~ 400; b) the occurrence of vacuum polarization process verifying some of the yet untested regimes of ultrarelativistic quantum field theories; and c) the first evidence for extracting, during the process of gravitational collapse leading to the formation of a black hole, amounts of energies up to 10^{55} ergs of blackholic energy — a new form of energy in physics and astrophysics. We outline how this progress leads to the confirmation of three interpretation paradigms for GRBs proposed in July 2001. Thanks mainly to the observations by Swift and the optical observations by VLT, the outcome of this analysis points to the existence of a "canonical" GRB, originating from a variety of different initial astrophysical scenarios. The communality of these GRBs appears to be that they all are emitted in the process of formation of a black hole with a negligible value of its angular momentum. The following sequence of events appears to be canonical: the vacuum polarization process in the dyadosphere with the creation of the optically thick self accelerating

electron-positron plasma; the engulfment of baryonic mass during the plasma expansion; adiabatic expansion of the optically thick "fireshell" of electron-positron-baryon plasma up to the transparency; the interaction of the accelerated baryonic matter with the interstellar medium (ISM). This leads to the canonical GRB composed of a proper GRB (P-GRB), emitted at the moment of transparency, followed by an extended afterglow. The sole parameters in this scenario are the total energy of the dyadosphere E_{dya}, the fireshell baryon loading M_B defined by the dimensionless parameter $B = M_B c^2 / E_{dya}$, and the ISM filamentary distribution around the source. In the limit $B \longrightarrow 0$ the total energy is radiated in the P-GRB with a vanishing contribution in the afterglow. In this limit, the canonical GRBs explain as well the short GRBs. In these lecture notes we systematically outline the main results of our model comparing and contrasting them with the ones in the current literature. In both cases, we have limited ourselves to review already published results in refereed publications. We emphasize as well the role of GRBs in testing yet unexplored grounds in the foundations of general relativity and relativistic field theories.

36. M. Lattanzi, R. Ruffini and G.V. Vereshchagin, "Do WMAP data constraint the lepton asymmetry of the Universe to be zero?" in Albert Einstein Century International Conference, edited by J.-M. Alimi, and A. Füzfa, AIP Conference Proceedings, Vol. 861, Melville, New York, 2006, pp.912-919.

    It is shown that extended flat ΛCDM models with massive neutrinos, a sizeable lepton asymmetry and an additional contribution to the radiation content of the Universe, are not excluded by the Wilkinson Microwave Anisotropy Probe (WMAP) first year data. We assume a flat cosmological model with three thermally distributed neutrino species having all the same mass and chemical potential, plus an additional amount of effectively massless exotic particle species X. After maximizing over seven other cosmological parameters, we derive from WMAP first year data the following constraints for the lepton asymmetry L of the Universe (95% CL): $0 < |L| < 0.9$, so that WMAP data alone cannot firmly rule out scenarios with a large lepton number; moreover, a small preference for this kind of scenarios is actually found. We also find for the neutrino mass $m_\nu < 1.2eV$ and for the effective number of relativistic particle species $-0.45 < \Delta N^{eff} < 2.10$, both at 95% CL. The limit on ΔN^{eff} is more restrictive man others found in the literature, but we argue that this is due to our choice of priors.

37. R. Ruffini, C.L. Bianco, G.V. Vereshchagin, S.-S. Xue "Baryonic loading and e^+e^- rate equation in GRB sources" to appear in the proceedings of "Relativistic Astrophysics and Cosmology - Einstein's Legacy" Meeting, November 7-11, 2005, Munich, Germany.

    The expansion of the electron-positron plasma in the GRB phenomenon is compared and contrasted in the treatments of Meszaros, Laguna and Rees, of Shemi, Piran and Narayan, and of Ruffini et al. The role of the correct numerical integration of the hydrodynamical equations, as well as of the rate equation for the electron-positron plasma loaded with a baryonic mass, are outlined and confronted for crucial differences.

38. G.V. Vereshchagin, M. Lattanzi, H.W. Lee, R. Ruffini, "Cosmological massive neutrinos with nonzero chemical potential: I. Perturbations in cosmological models with neutrino in ideal fluid approximation", in proceedings of the Xth Marcel Grossmann Meeting on Recent Developments in Theoretical and Experimental General Relativity, World Scientific: Singapore, 2005, vol. 2, pp. 1246-1248.

    Recent constraints on neutrino mass and chemical potential are discussed with application to large scale structure formation. Power spectra in cosmological model with hot and cold dark matter, baryons and cosmological term are calculated in newtonian approximation using linear perturbation theory. All components are considered to be ideal fluids. Dissipative processes are taken into account by initial spectrum of perturbations so the problem is reduced to a simple system of equations. Our results are in good agreement with those obtained before using more complicated treatments.

39. M. Lattanzi, H.W. Lee, R. Ruffini, G.V. Vereshchagin, "Cosmological massive neutrinos with nonzero chemical potential: II. Effect on the estimation of cosmological parameters", in proceedings of the Xth Marcel Grossmann Meeting on Recent Developments in Theoretical and Experimental General Relativity, World Scientific: Singapore, 2005, vol. 2, pp. 1255-1257.

    The recent analysis of the cosmic microwave background data carried out by the WMAP team seems to show that the sum of the neutrino mass is ¡0.7 eV. However, this result is not model-independent, depending on precise assumptions on the cosmological model. We study how this result is modified when the assumption of perfect lepton symmetry is dropped out.

40. R. Ruffini, M. Lattanzi and G. Vereshchagin, "On the possible role of massive neutrinos in cosmological structure formation" in Cosmology and Gravitation: Xth Brazilian School of Cosmology and Gravitation, edited by M. Novello and S.E. Perez Bergliaffa, AIP Conference Proceedings, Vol. 668, Melville, New York, 2003, pp.263-287.

    In addition to the problem of galaxy formation, one of the greatest open questions of cosmology is represented by the existence of an asymmetry between matter and antimatter in the baryonic component of the Universe. We believe that a net lepton number for the three neutrino species can be used to understand this asymmetry. This also implies an asymmetry in the matter-antimatter component of the leptons. The existence of a nonnull lepton number for the neutrinos can easily explain a cosmological abundance of neutrinos consistent with the one needed to explain both the rotation curves of galaxies and the flatness of the Universe. Some propedeutic results are presented in order to attack this problem.

41. A.G. Aksenov, C.L. Bianco, R. Ruffini and G.V. Vereshchagin, "GRBs and the thermalization process of electron-positron plasmas" in the Proceedings of the "Gamma Ray Bursts 2007" meeting, AIP Conf.Proc. 1000 (2008) 309-312.

    We discuss temporal evolution of the pair plasma, created in Gamma-Ray Bursts sources. A particular attention is paid to the relaxation of plasma into thermal equilibrium. We also discuss the connection between the dynamics of expansion and spatial geometry of plasma. The role of the baryonic loading parameter is emphasized.

42. A. G. Aksenov, R. Ruffini, and G. V. Vereshchagin, "Thermalization of Electron-Positron-Photon Plasmas with an Application to GRB" in RELATIVISTIC ASTROPHYSICS: 4th Italian-Sino Workshop, AIP Conference Proceedings, Vol. 966, Melville, New York, 2008, pp. 191-196.

    The pair plasma with photon energies in the range $0.1 - 10$MeV is believed to play crucial role in cosmic Gamma-Ray Bursts. Starting from a nonequilibrium configuration we analyze the role of the direct and the inverse binary and triple interactions in reaching thermal equilibrium in a homogeneous isotropic pair plasma.We numerically integrate the relativistic Boltzmann equation with the exact QED collisional integrals taking into account all binary and triple interactions. We show that first, when a detailed balance is reached for all binary interactions on a time scale $t_k = 10^{-14}$sec , photons and electronpositron

pairs establish kinetic equilibrium. Subsequently, when triple interactions satisfy the detailed balance on a time scale $t_{eq}= 10^{-12}$sec , the plasma reaches thermal equilibrium. It is shown that neglecting the inverse triple interactions prevents reaching thermal equilibrium. Our results obtained in the theoretical physics domain also find application in astrophysics and cosmology.

43. R. Ruffini, G. V. Vereshchagin and S.-S. Xue, "Vacuum Polarization and Electron-Positron Plasma Oscillations" in RELATIVISTIC ASTROPHYSICS: 4th Italian-Sino Workshop, AIP Conference Proceedings, Vol. 966, Melville, New York, 2008, pp. 207-212.

    We study plasma oscillations of electrons-positron pairs created by the vacuum polarization in an uniform electric field. Our treatment, encompassing the case of $E > E_c$, shows also in the case $E < E_c$the existence of a maximum Lorentz factor acquired by electrons and positrons and allows determination of the a maximal length of oscillation. We quantitatively estimate how plasma oscillations reduce the rate of pair creation and increase the time scale of the pair production.

4.3. Publications (2014)

1. D. Begue and G.V. Vereshchagin, "Transparency of an instantaneously created electron-positron-photon plasma", MNRAS, Vol. 439 (2014), pp. 924-928.

    The problem of the expansion of a relativistic plasma generated when a large amount of energy is released in a small volume has been considered by many authors. We use the analytical solution of Bisnovatyi-Kogan and Murzina for the spherically symmetric relativistic expansion. The light curves and the spectra from transparency of an electron-positron-photon plasma are obtained. We compare our results with the work of Goodman.

2. I.A. Siutsou and G.V. Vereshchagin, "Relativistic spotlight ", Physics Letters B, Volume 730 (2014), pp. 190192.

    Relativistic motion gives rise to a large number of interesting and sometimes counterintuitive effects. In this work we consider an example of such effects, which we term relativistic spotlight. When an isotropic source of soft photons with proper intensity I_0 is placed at rest between a distant observer and photosphere of relativistic wind, its intensity as seen by the observer gets enhanced

up to $\sim \Gamma^4 I_0$, where Γ is bulk Lorentz factor of the wind. In addition, these photons may extract a large part of the wind kinetic energy. We speculate that such effect may be relevant for the physics of GRBs.

3. G.V. Vereshchagin, "Physics of non-dissipative ultrarelativistic photospheres ", International Journal of Modern Physics D Vol. 23, No. 1 (2014) 1430003.

   Recent observations, especially by the Fermi satellite, point out the importance of the thermal component in GRB spectra. This fact revives strong interest in photospheric emission from relativistic outflows. Early studies already suggested that the observed spectrum of photospheric emission from relativistically moving objects differs in shape from the Planck spectrum. However, this component appears to be subdominant in many GRBs and the origin of the dominant component is still unclear. One of the popular ideas is that energy dissipation near the photosphere may produce a nonthermal spectrum and account for such emission. Before considering such models, though, one has to determine precise spectral and timing characteristics of the photospheric emission in the simplest possible case. Hence this paper focuses on various physical effects which make the photospheric emission spectrum different from the black body spectrum and quantifies them.

4. I.A. Siutsou, R. Ruffini and G.V. Vereshchagin, "Spreading of ultrarelativistically expanding shell: an application to GRBs", New Astronomy, Vol. 27 (2014), pp. 30-33.

   Optically thick energy dominated plasma created in the source of Gamma-Ray Bursts (GRBs) expands radially with acceleration and forms a shell with constant width measured in the laboratory frame. When strong Lorentz factor gradients are present within the shell it is supposed to spread at sufficiently large radii. There are two possible mechanisms of spreading: hydrodynamical and thermal ones. We consider both mechanisms evaluating the amount of spreading that occurs during expansion up to the moment when the expanding shell becomes transparent for photons. We compute the hydrodynamical spreading of an ultrarelativistically expanding shell. In the case of thermal spreading we compute the velocity spread as a function of two parameters: comoving temperature and bulk Lorentz factor of relativistic Maxwellian distribution. Based on this result we determine the value of thermal spreading of relativistically expanding shell. We found that thermal spreading is negligible for typical GRB parameters. Instead hydrodynamical spreading appears

to be significant, with the shell width reaching $\sim 10^{10}$ cm for total energy $E = 10^{54}$ erg and baryonic loading $B = 10^{-2}$. Within the fireshell model such spreading will result in the duration of Proper Gamma-Ray Bursts up to several seconds.

5. G. V. Vereshchagin, "Relativistic kinetic theory and its applications in astrophysics and cosmology", Proceedings of XV Brazilian School of Cosmology and Gravitation, Mangaratiba - Rio de Janeiro – Brazil, August 19 - September 1, 2012, Cambridge Scientific Publishers, 2014, in press.

   A brief introduction into relativistic kinetic theory is given. Some applications of this theory in plasma physics, astrophysics and cosmology are reviewed.

6. A.G. Aksenov, R. Ruffni, I. A. Siutsou and G. V. Vereshchagin, "Relativistic degeneracy in the pair plasma ", in preparation (2014).

7. A. G. Aksenov, R. Ruffini, and G. V. Vereshchagin, "Radiative transfer in relativistic plasma outflows and comptonization of photons near the photosphere", Astronomy Reports, 2014, in press.

8. D. Begue and R. Ruffini and G.V. Vereshchagin, "On the filling factor of the circumburst medium and GRB emission ", in preparation (2014).

9. R. Ruffini G. V. Vereshchagin Yu Wang, "Thermal emission in early afterglow from the GRB-SNR interaction ", in preparation (2014).

10. R. Ruffini, C. R. Argüelles, and J. A. Rueda, "On the core-halo distribution of dark matter in galaxies", Submitted to PRL, arXiv:astro-ph/1409.7365, 2014.

    We investigate the distribution of dark matter in galaxies by solving the equations of equilibrium of a self-gravitating system of massive fermions ('inos') at selected temperatures and degeneracy parameters within general relativity. The most general solutions present, as a function of the radius, a segregation of three physical regimes: 1) an inner core of almost constant density governed by degenerate quantum statistics; 2) an intermediate region with a sharply decreasing density distribution followed by an extended plateau, implying quantum corrections; 3) a decreasing density distribution $\rho \propto r^{-2}$ leading to flat rotation curves fulfilling the classical Boltzmann statistics. The mass of the inos is determined as an eigenfunction of the mass of the inner quantum cores. We

compare and contrast this mass value with the lower limit on the particle mass by Tremaine and Gunn (1979), and show that the latter is approached for the less degenerate quantum cores in agreement with the fixed halo observables. Consequences of this alternative approach to the massive core in SgrA* and to dwarf galaxies are outlined.

11. C. R. Argüelles, R. Ruffini, I. Siutsou, and B. Fraga, "On the distribution of dark matter in galaxies: quantum treatments", JKPS 65: 801, 2014.

    The problem of modeling the distribution of dark matter in galaxies in terms of equilibrium configurations of collisionless self-gravitating quantum particles is considered. We first summarize the pioneering model of a Newtonian self-gravitating Fermi gas in thermodynamic equilibrium developed by Ruffini and Stella (1983), which is shown to be a generalization of the King model for fermions. We further review the extension of the former model developed by Gao, Merafina and Ruffini (1990), done for any degree of fermion degeneracy at the center (θ_0), within general relativity. Finally, we present here for the first time the solutions of the density profiles and rotation curves corresponding to the model of Gao et al. Those solutions have a definite mass M_h and a circular velocity v_h at the halo radius r_h of the configurations, which are typical of spiral galaxies. This treatment allows us to determine a novel core-halo morphology for the dark-matter profiles, as well as a novel bound on the particle mass associated with those profiles.

12. C. R. Argüelles, B. Fraga, and R. Ruffini, "Critical configurations for a system of semidegenerate fermions", JKPS 65: 809, arXiv:astro-ph/1402.1329, 2014.

    We study an isothermal system of semidegenerate self-gravitating fermions in general relativity. Such systems present mass density solutions with a central degenerate core, a plateau and a tail, this last following a power law behavior r^{-2}. The different solutions are governed by the free parameters of the model: the degeneracy and the temperature parameters at the center and the particle mass m. We then analyze in detail the free parameter space for a fixed m in the keV region, by studying the one-parameter sequences of equilibrium configurations up to the critical point, which is represented by the maximum in a central density (ρ_0) vs. core mass (M_c) diagram. We show that for fully degenerate cores, the known expression for the critical core mass $M_c^{cr} \propto m_{pl}^3/m^2$ is obtained, while for low degenerate cores, the critical core mass increases, showing temperature effects in a nonlinear way. The main result of this work

is that when applying this theory to model the distribution of dark matter in galaxies from the very center to the outer halos, we do not find any critical core-halo configuration of self-gravitating fermions that would be able to explain the super-massive dark object in their centers and the outer halo simultaneously.

13. C. R. Argüelles and R. Ruffini, "Are the most super-massive dark compact objects harbored at the center of dark matter halos?", Honorable mention by the Gravity Research Foundation 2014, IJMPD 23 No. 12, 1442020, arXiv:astro-ph/1405.7505, 2014.

    We study an isothermal system of semi-degenerate self-gravitating fermions in General Relativity (GR). The most general solutions present mass density profiles with a central degenerate compact core governed by quantum statistics followed by an extended plateau, and ending in a power law behaviour r^{-2}. By fixing the fermion mass m in the keV regime, the different solutions depending on the free parameters of the model: the degeneracy and temperature parameters at the center, are systematically constructed along the one-parameter sequences of equilibrium configurations up to the critical point, which is represented by the maximum in a central density (ρ_0) Vs. core mass (M_c) diagram. We show that for fully degenerate cores, the Oppenheimer-Volkoff (OV) mass limit $M_c^{cr} \propto M_{pl}^3/m^2$ is obtained, while instead for low degenerate cores, the critical core mass increases showing the temperature effects in a non linear way. The main result of this work is that when applying this theory to model the distribution of dark matter in big elliptical galaxies from miliparsec distance-scales up to 10^2 Kpc, we do not find any critical core-halo configuration of self-gravitating fermions, able to explain both the most super-massive dark object at their center together with the DM halo simultaneously.

14. C. R. Argüelles and R. Ruffini, "A regular and relativistic Einstein cluster within the S2 orbit centered in SgrA*", IJMPD in press, 2014.

    We use the Einstein Cluster model in order to provide an alternative to the massive black hole thought to be hosted at the center of SgrA*. For this we model the central sub-miliparsec region of our galaxy in terms of a constant density Einstein cluster composed by dark matter particles of mass m, regardless of its nature. We analyze its stability conditions by two different methods considered in the literature, and explicitly show through the total mass (M)versus radius(R) relation, up to which point an Einstein cluster of constant particle number can be contracted, without losing its global stability. Finally,

we compare the uppermost constant density constraints of stable clusters, with the lowest limit in the mass density of SgrA* as imposed by modern VLBI mm radio observations.

15. C. R. Argüelles, J. A. Rueda, and R. Ruffini, "Fermionic dark matter plus baryons in dwarf galaxies", Submitted to Nonlinear phenomena in complex systems, 2014.

    A generalization of the Jeans equations in the context of galactic dynamics is developed for a multi-component self-gravitating system composed of dark matter particles and stars. In addition to the luminous profile, an underlying fermionic phase-space density for the dark component is assumed. Under the ansatz of isotropy, spherical symmetry and constant dispersion velocities, this approach is applied to typical well resolved nucleated dwarf galaxies, to obtain novel dark matter density profiles showing central mass concentrations at pc distance-scales. Narrow constraints on the mass of the dark matter candidate of $m \sim 1$ keV are obtained.

4.4. Invited talks at international conferences

1. "Thermal emission in the early afterglow", 1st Scientific ICRANet Meeting in Armenia, Yerevan, Armenia, 30 June - 4 July 2014.

   (G.V. Vereshchagin)

2. "Photospheric emission from relativistic outflows", Zeldovich-100 International Conference, Space Research Institute (IKI), Moscow, Russia, 16-20 June, 2014

   (G.V. Vereshchagin)

3. "Dark matter massive fermions and Einasto profiles in galactic haloes "

   (Ivan Siutsou)

   Subatomic particles, Nucleons, Atoms, Universe: Processes and Structure International conference in honor of Ya. B. Zeldovich 100th Anniversary, March 10-14, 2014, Minsk, Belarus

4. "DM halos and super massive dark objects at sub-parsec scales:the nature of the DM particle "

(Carlos R. Argüelles)

Subatomic particles, Nucleons, Atoms, Universe: Processes and Structure International conference in honor of Ya. B. Zeldovich 100th Anniversary, March 10-14, 2014, Minsk, Belarus

5. "Physics of non-dissipative ultrarelativistic photospheres"

   (G.V. Vereshchagin)

   On recent developments in theoretical and experimental general relativity, gravitation and relativistic field theories: XIII Marcel Grossmann Meeting, Stockholm, 1-7 July 2012.

6. "Photon thick and photon thin relativistic outflows and GRBs"

   (I.A. Siutsou, R. Ruffini and G.V. Vereshchagin)

   On recent developments in theoretical and experimental general relativity, gravitation and relativistic field theories: XIII Marcel Grossmann Meeting, Stockholm, 1-7 July 2012.

7. "Monte Carlo simulations of the photospheric emission in GRBs"

   (D. Begue, I.A. Siutsou and G.V. Vereshchagin)

   On recent developments in theoretical and experimental general relativity, gravitation and relativistic field theories: XIII Marcel Grossmann Meeting, Stockholm, 1-7 July 2012.

8. "Phase space evolution of pairs created in strong electric fields" (A. Benedetti, R. Ruffini and G.V. Vereshchagin) On recent developments in theoretical and experimental general relativity, gravitation and relativistic field theories: XIII Marcel Grossmann Meeting, Stockholm, 1-7 July 2012.

9. "Applications of the Boltzmann equation: from an interacting plasma toward the photospheric emission of a GRB" (A. Benedetti, R. Ruffini and G.V. Vereshchagin) Erasmus Mundus School, Nice, France, 3rd – 19th September, 2012.

10. "Photospheric emission from thermally accelerated relativistic outflows"

GRBs, their progenitors and the role of thermal emission, Les Houches, France, 2-7 October, 2011

(G.V. Vereshchagin, R. Ruffini and I.A. Siutsou)

11. "Thermalization of the pair plasma"

    (G.V. Vereshchagin, A.G. Aksenov and R. Ruffini)

    From Nuclei to White Dwarfs and Neutron Stars, Les Houches, France, 3-8 April, 2011

12. "Photospheric emission from relativistic outflows: 1DHD"

    (G.V. Vereshchagin, R. Ruffini and I.A. Siutsou)

    Recent News from the MeV, GeV and TeV Gamma-Ray Domains, Pescara, Italy, 21-26 March, 2011

13. "Thermalization of degenerate electron-positron plasma"

    I.A. Siutsou, A.G. Aksenov, R. Ruffini and G.V. Vereshchagin

    IRAP Ph.D. Erasmus Mundus School—May 27, 2011, Nice, France

14. "Semidegenerate self-gravitating systems of fermions as central objects and dark matter halos in galaxies"

    (I. A. Siutsou, A. Geralico and R. Ruffini)

    Recent News from the MeV, GeV and TeV Gamma-Ray Domains, March 24, 2011, Pescara, Italy

15. "Thermalization of degenerate electron-positron plasma"

    (I.A. Siutsou, A.G. Aksenov, G.V. Vereshchagin and R. Ruffini)

    3rd Galileo-Xu Guangqi Meeting—October 12, 2011, Beijing, China

16. "Photospheric emission of relativistically expanding outflows"

    (I.A. Siutsou, G.V. Vereshchagin and R. Ruffini)

    12th Italian-Korean Symposium on Relativistic Astrophysics—July 5, 2011, Pescara, Italy

17. On the frequency of oscillations in the pair plasma generated by a strong electric field.

    (Alberto Benedetti, W.-B. Han, R. Ruffini, G.V. Vereshchagin)
    IRAP Ph.D. Erasmus Mundus Workshop, April 5, 2011, Pescara (Italy)

18. Oscillations in the pair plasma generated by a strong electric field

    (Alberto Benedetti, W.-B. Han, R. Ruffini, G.V. Vereshchagin)
    Italian-Korean Meeting, July 4-9, 2011, Pescara (Italy)

19. Electron-Positron plasma oscillations: hydro-electrodynamic and kinetic approaches

    (Alberto Benedetti, R. Ruffini, G.V. Vereshchagin)
    IRAP Ph.D. Erasmus Mundus School, September 7, 2011, Nice (France)

20. Boltzmann equation: from an interacting plasma toward the photospheric emission of a GRB

    (Alberto Benedetti, A. Aksenov, R. Ruffini, I. Siotsou, G.V. Vereshchagin)
    IRAP Ph.D. Erasmus Mundus Workshop, October 6, 2011, Les Houches (France)

21. Electron-Positron plasma oscillations: hydro-electrodynamic and kinetic approaches.

    (Alberto Benedetti, A. Aksenov, R. Ruffini, I. Siutsou, G.V. Vereshchagin)
    Galileo-Xu Guanqui Meeting, October 12, 2011, Beijing (China)

22. "Inflation in a general reionization scenario "

    (S. Pandolfi)

    Essential Cosmology for the Next Generation, Puerto Vallarta, Mexico, January 10-14, 2011

23. "Constraints on Inflation in extended cosmological scenarios "

    (S. Pandolfi)

    28 January 2011, Dark Cosmlogy Center, Copenhagen, Denmark.

24. “Theoretical Development toward the Planck mission ”

    (S. Pandolfi)

    IRAP PhD and Erasmus MundusWorkshop: Workshop on Recent News from the GeV and TeV Gamma-RayDomains: Results and Interpretations,21-26 March 2011, ICRANet (Pescara), Italy.

25. “Joint Astrophysical and Cosmological constrains on reionization ”

    (S. Pandolfi)

    DAVID WORKSHOP VI, Scuola Normale Superiore, Pisa, October 18-20 2011

26. “New constraints on features in the primordial spectrum ”

    (M. Benetti)

    3rd Galileo- Xu Guangqi meeting, Beijing (China), October 11-15, 2011.

27. “Thermalization of the pair plasma”

    (G.V. Vereshchagin with A.G. Aksenov and R. Ruffini)

    Korean Physical Society 2010 Fall Meeting, Pyeong-chang, Korea, 20-22 October, 2010.

28. “The spatial structure of expanding optically thick relativistic plasma and the onset of GRBs”

    (G.V. Vereshchagin with A.G. Aksenov, G. de Barros and R. Ruffini)

    GRB 2010 / Dall’eV al TeV tutti i colori dei GRB, Secondo Congresso Italiano sui Gamma-ray Burst, Cefalu’ 15-18 June 2010.

29. “From thermalization mechanisms to emission processes in GRBs”

    (G.V. Vereshchagin)

    XII Marcel Grossmann Meeting, Paris, 12-18 July 2009.

30. “Kinetics of the mildly relativistic plasma and GRBs”

    (A.G. Aksenov R. Ruffini, and G.V. Vereshchagin)

    “The Sun, the Stars, the Universe, and General Relativity” - International conference in honor of Ya. B. Zeldovich 95th Anniversary, Minsk, Belarus, April 19-23, 2009.

31. "Pair plasma around compact astrophysical sources: kinetics, electrodynamics and hydrodynamics"

    (G.V. Vereshchagin and R. Ruffini)

    Invited seminar at RMKI, Budapest, February 24, 2009.

32. "Thermalization of the pair plasma with proton loading"

    (G.V. Vereshchagin, R. Ruffini, and A.G. Aksenov)

    Probing Stellar Populations out to the Distant Universe, Cefalu', Italy, September 7-19, 2008.

33. "Thermalization of the pair plasma with proton loading"

    (G.V. Vereshchagin, R. Ruffini, and A.G. Aksenov)

    3rd Stueckelberg Workshop, Pescara, Italy, 8-18 July, 2008.

34. "Thermalization of the pair plasma"

    (G.V. Vereshchagin, R. Ruffini, and A.G. Aksenov)

35. "Non-singular solutions in Loop Quantum Cosmology"

    (G.V. Vereshchagin)

    2nd Stueckelberg Workshop, Pescara, Italy, 3-7 September, 2007.

36. "(From) massive neutrinos and inos and the upper cutoff to the fractal structure of the Universe (to recent progress in theoretical cosmology)"

    (G.V. Vereshchagin, M. Lattanzi and R. Ruffini)

    A Century of Cosmology, San Servolo, Venice, Italy, 27-31 August, 2007.

37. "Pair creation and plasma oscillations"

    (G.V. Vereshchagin, R. Ruffini, and S.-S. Xue)
    4th Italian-Sino Workshop on Relativistic Astrophysics, Pescara, Italy, 20-29 July, 2007.

38. "Thermalization of electron-positron plasma in GRB sources"

    (G.V. Vereshchagin, R. Ruffini, and A.G. Aksenov)
    Xth Italian-Korean Symposium on Relativistic Astrophysics, Pescara, Italy, 25-30 June, 2007.

39. "Kinetics and hydrodynamics of the pair plasma"

    (G.V. Vereshchagin, R. Ruffini, C.L. Bianco, A.G. Aksenov)

40. "Pair creation and plasma oscillations"

    (G.V. Vereshchagin, R. Ruffini and S.-S. Xue)
    Cesare Lattes Meeting on GRBs, Black Holes and Supernovae, Mangaratiba-Portobello, Brazil, 26 February - 3 March 2007.

41. "Cavallo-Rees classification revisited"

    (G.V. Vereshchagin, R.Ruffini and S.-S. Xue)

    On recent developments in theoretical and experimental general relativity, gravitation and relativistic field theories: XIth Marcel Grossmann Meeting, Berlin, Germany, 23-29 July, 2006.

42. "Kinetic and thermal equilibria in the pair plasma"

    (G.V. Vereshchagin)

    The 1st Bego scientific rencontre, Nice, 5-16 February 2006.

43. "From semi-classical LQC to Friedmann Universe"

    (G.V. Vereshchagin)

    Loops '05, Potsdam, Golm, Max-Plank Institut für Gravitationsphysik (Albert-Einstein-Institut), 10-14 October 2005.

44. "Equations of motion, initial and boundary conditions for GRBs"

    (G.V. Vereshchagin, R. Ruffini and S.-S. Xue)

    IXth Italian-Korean Symposium on Relativistic Astrophysics, Seoul, Mt. Kumgang, Korea, 19-24 July 2005.

45. "On the Cavallo-Rees classification and GRBs"

    (G.V. Vereshchagin, R. Ruffini and S.-S. Xue)

    II Italian-Sino Workshop on Relativistic Astrophysics, Pescara, Italy, 10-20 June, 2005.

46. "New constraints on features in the primordial spectrum "

    (M. Benetti)

Essential Cosmology for the Next Generation Ph.D School, January 16-21 2012, Cancun, Mexico

47. "New constraints on features in the primordial spectrum "

    (M. Benetti)

    XIth School of Cosmology, Gravitational Lenses: their impact in the study of galaxies and Cosmology, Ph.D School, September 17-22 2012, Cargese, France

48. "New Horizons for Observational Cosmology "

    (M. Benetti)

    Ph.D School, June 30th-July 6th 2013, Varenna, Italy

49. "BLACK HOLES IN GAMMA RAY-BURSTS AND GALACTIC NUCLEI "

    (R. Ruffini, C.R. Arguelles, B.M.O. Fraga, A. Geralico, H. Quevedo and J.A. Rueda, and I. Siutsou)

    3rd Galileo–Xuguangqi Meeting, Beijing, China, 11–15 October 2011

4.5. Lecture courses

1. "Relativistic kinetic theory and its applications in astrophysics and cosmology", 4 lectures

   (G.V. Vereshchagin)

   IRAP Ph.D. Erasmus Mundus September school, Nice, 2 – 20 September, 2013.

2. "Relativistic Boltzmann equations", 2 lectures

   (G.V. Vereshchagin)

   Second Bego Rencontre, IRAP Ph.D. Erasmus Mundus school, Nice, 16 – 31 May, 2013.

3. "First light from Gamma Ray Bursts", 3 lectures

   (G.V. Vereshchagin)

IRAP Ph.D. Erasmus Mundus September school, Nice, 3 – 21 September, 2012.

4. "Relativistic kinetic theory and its applications in astrophysics and cosmology", 5 lectures

   (G.V. Vereshchagin)

   XV Brazilian School of Cosmology and Gravitation, Mangaratiba - Rio de Janeiro – Brazil, August 19 - September 1, 2012.

5. "Pair plasma in GRBs and cosmology"

   (G.V. Vereshchagin)

   2 lectures, IRAP Ph.D. Erasmus Mundus September school, 12 – 23 September, 2011, University of Nice Sophia Antipolis, Nice, France.

6. "Relativistic kinetic theory and its applications in astrophysics and cosmology"

   (G.V. Vereshchagin)

   Lecture course for International Relativistic Astrophysics PhD, Erasmus Mundus Joint Doctorate Program from the

   European Commission, September 6-24, 2010, University of Nice Sophia Antipolis, Nice, France.

7. "Relativistic kinetic theory and its applications", IRAP Ph.D. lectures

   (G.V. Vereshchagin)

   February 1-19, 2010, Observatoire de la Cote d'Azur, Nice, France.

8. Inflationary Constraints and reionization

   (S. Pandolfi)

   IRAP Ph.D. Lectures in Nice, Observatoire de la Cote d'Azur, 12-16 February 2010

5. APPENDICES

A. Relativistic degeneracy in nonequilibrium electron-positron plasma

The description of processes involving electron-positron plasma is required in many phenomena in physics and astrophysics (Ruffini et al., 2010). The standard cosmological model includes lepton era with electron-positron plasma at high temperature and initially in thermal equilibrium, see e.g. Weinberg (2008). Strong electromagnetic fields are generated in laser experiments aiming at production of electron-positron pairs (Gerstner, 2010; Chen et al., 2009). When electromagnetic field invariants $\mathbf{E}^2 - \mathbf{H}^2$ and $\mathbf{E} \cdot \mathbf{H}$ approach critical value, vacuum breakdown is predicted (Schwinger, 1951) to lead to copious pair production, ultimately forming electron-positron plasma (Mustafa and Kämpfer, 2009). Strong electromagnetic fields are thought to occur in astrophysical conditions, near such compact objects as black holes (Damour and Ruffini, 1975), hypothetical strange stars (Alcock et al., 1986; Usov, 1998) and possibly neutron stars (Belvedere et al., 2012).

Pair production by vacuum breakdown or by laser beam interactions is in principle the out of equilibrium process. Relaxation of electron-positron plasma to thermal equilibrium has been considered in Aksenov et al. (2007, 2009). There relativistic Boltzmann equations with exact QED collision integrals taking into account all relevant two-particle (Bhabha scattering, Møller scattering, Compton scattering, pair creation and annihilation) and three-particle (relativistic bremsstrahlung, three photon annihilation, double Compton scattering, and radiative pair production) interactions were solved numerically. It was confirmed that a metastable state called *"kinetic equilibrium"* (Pilla and Shaham, 1997) exists in such plasma, which is characterized by the same temperature of all particles, but nonnull chemical potentials. Such state occurs when the detailed balance of all two-particle reactions is established. It was pointed out that direct and inverse three-particle inter-

actions become relevant when kinetic equilibrium has been reached. These three-particle interactions are shown to be essential (Aksenov et al., 2007) in bringing electron-positron plasma to thermal equilibrium, as they are particle non-conserving processes.

In Aksenov et al. (2010) relaxation timescales for optically thick electron-positron plasma in a wide range of temperatures and proton loadings were computed numerically using the kinetic code developed in Aksenov et al. (2007, 2009). These timescales were previously estimated in the literature by order of magnitude arguments using the reaction rates of the dominant processes (Gould, 1981; Stepney, 1983). It was shown that these numerically obtained timescales differ from previous estimations by several orders of magnitude. In the description of plasma Boltzmann statistics of particles was used in all these works. However, electrons, positrons and photons are quantum particles fulfilling Fermi-Dirac and Bose-Einstein statistics, respectively. This leads to change of reaction rates considered firstly in Uehling and Uhlenbeck (1933); Uehling (1934). The role of relativistic degeneracy in pair plasma in establishing thermal equilibrium has never been studied. In this Chapter we bridge this gap.

We generalize previous works on thermalization of uniform isotropic neutral pair plasma. In addition to collision integrals for two-particle interactions expressed through QED matrix elements we take into account also three-particle interactions in the same way. Plasma degeneracy is accounted for by quantum corrections to collision integrals with the corresponding Pauli blocking and Bose enhancement factors. In Sec. A.1 basic parameters of pair plasma are introduced. In Sec. A.2 concepts of kinetic and thermal equilibria and their relations to detailed balance conditions are recalled. In Sec. A.3 relativistic Boltzmann equation is introduced. In Sec. A.3.1 two-particle collision integrals are described. In Sec. A.3.2 three-particle collision integrals are introduced. In Sec. A.4 details of adopted numerical scheme are given. In Sec. A.6 our numerical results of integration of Boltzmann equations for several interesting cases are described. Conclusions follow in Sec. A.7.

A.1. Basic parameters

The qualitative character of processes in electron-positron plasma is determined by a number of parameters, which we recall below, for details see Aksenov et al. (2009).

The average energy per particle $\langle\varepsilon\rangle$ determines wether plasma is in relativistic or in non-relativistic domain. We consider mildly relativistic plasma with

$$0.01 \lesssim \frac{\langle\varepsilon\rangle}{m_e c^2} \lesssim 10, \tag{A.1.1}$$

where m_e is electron mass, c is the speed of light. This range contains both relativistic and non-relativistic domains. The upper limit is chosen to avoid thermal production of other particles such as neutrinos and muons, while the lower limit is required to have sufficient pair density (Aksenov et al., 2010).

The degeneracy parameter (Groot et al., 1980, p. 352) is defined as

$$D = \frac{1}{n\lambda_{th}^3}, \tag{A.1.2}$$

where n is number density of particles, $\lambda_{th} = \dfrac{c\hbar}{kT}$ is the thermal wave-length, k is Boltzmann constant, T is temperature, $\hbar = h/(2\pi)$, h is Planck constant. In Fig. A.1 on the number density–energy density diagram for relativistic electron-positron plasma we show nondegenerate ($D > 1$) and degenerate ($D < 1$) regions.

The plasma parameter $\mathfrak{g}$ is defined as

$$\mathfrak{g} = \frac{1}{n\lambda_D^3}, \tag{A.1.3}$$

where the Debye length (Groot et al., 1980, p. 351) is

$$\lambda_D = \begin{cases} \sqrt{\dfrac{kT}{4\pi e^2 n}}, & D > 1, \\ \sqrt{\dfrac{E_F}{4\pi e^2 n}}, & D < 1, \end{cases} \tag{A.1.4}$$

e is electron charge, and E_F is the Fermi energy. For $\mathfrak{g} \ll 1$ plasma is called ideal, and Boltzmann equation for one-particle distribution functions can be used for its description. This is indeed the case for relativistic plasma, as discussed in Groot et al. (1980, p. 352).

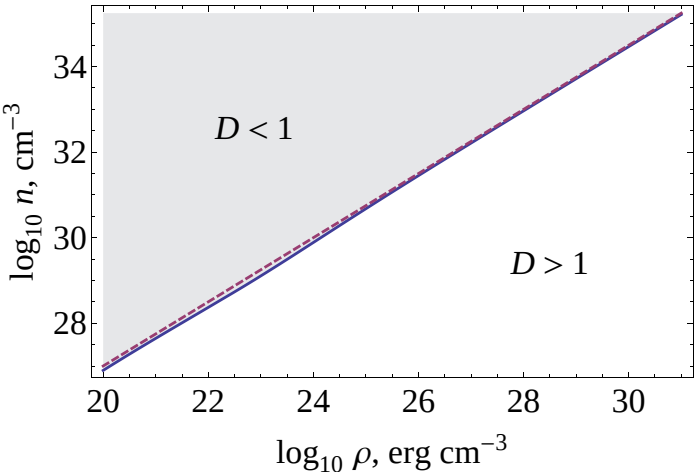

Figure A.1.: Number density-energy density diagram of relativistic electron-positron plasma. Solid curve shows critical particle density $n_{cr}(\rho)$, obtained from Eq. (A.2.1) with $\xi = 0$. Dashed line corresponds to transition from nondegenerate $D > 1$ to degenerate $D < 1$ plasma, where D is defined by Eq. (A.1.2).

The classicality parameter defined by

$$\kappa = \frac{e^2}{\hbar v_r} = \frac{\alpha}{\beta_r}, \tag{A.1.5}$$

where α is the fine-structure constant, $v_r = \beta_r c$ is mean relative velocity of the particles, determines the type of cross section to be used in charged particle collisions. In relativistic plasma $\kappa \ll 1$, which requires quantum description.

The Coulomb logarithm defined by

$$\Lambda = \frac{\mathcal{M}\lambda_D \Gamma_r v_r}{\hbar}, \tag{A.1.6}$$

where $\mathcal{M}$ is the reduced mass of charged particles, $\Gamma_r = (1 - \beta_r^2)^{-1/2}$, characterizes the strength of screening in Coulomb interactions.

Finally, *the optical depth* τ characterizes intensity of interactions between photons and other particles. We discuss the computation of this important parameter in details in the following Chapters. In static relativistic plasma, which is the case in this Chapter, the optical depth can be estimated as

$$\tau = \sigma n l, \tag{A.1.7}$$

where n is electron density, σ is Thompson cross section, and l is plasma linear dimension. In this Chapter we assume $\tau \gg 1$.

A.2. Kinetic and thermal equilibria

The concepts of kinetic and thermal equilibria play important role in description of relativistic plasma. They both are connected with conditions of detailed balance established for two-particles and three-particles interactions, respectively.

A.2.1. Two-particle interactions and kinetic equilibrium

Kinetic equilibrium (Rybicki and Lightman, 1979; Pilla and Shaham, 1997) is defined as the state with vanishing difference between the rates of direct and inverse interactions for each of the two-particle processes. Such state is characterized by two parameters: common temperature of all particles T

Table A.1.: Two-particle processes in electron-positron plasma and detailed balance conditions

Binary interactions	Conditions
Møller and Bhabha scattering	
$e_1^{\pm}e_2^{\pm} \longleftrightarrow e_1^{\pm\prime}e_2^{\pm\prime}$ $e^{\pm}e^{\mp} \longleftrightarrow e^{\pm\prime}e^{\mp\prime}$	$n_{\pm} = \dfrac{1}{\exp\frac{\epsilon_{\pm}-\mu_{\pm}}{kT_{\pm}}+1}$ $T_+ = T_-$
Compton scattering	
$e^{\pm}\gamma \longleftrightarrow e^{\pm}\gamma'$	$n_{\gamma} = \dfrac{1}{\exp\frac{\epsilon_{\gamma}-\mu_{\gamma}}{kT_{\gamma}}-1}$ $T_{\pm} = T_{\gamma}$
Pair production and annihilation	
$\gamma\gamma' \longleftrightarrow e^{\pm}e^{\mp}$	$2\mu_{\gamma} = \mu_+ + \mu_-$

and non-null chemical potential μ. Both these parameters can be found from given energy density ρ and number density n by the system of equations

$$\begin{cases} n = \dfrac{8\pi m_e^3 c^3}{h^3}\left(2\displaystyle\int_1^{\infty}\frac{\epsilon\sqrt{\epsilon^2-1}}{e^{\epsilon/\theta-\xi}+1}d\epsilon + \int_0^{\infty}\frac{\epsilon^2}{e^{\epsilon/\theta-\xi}-1}d\epsilon\right), \\ \rho = \dfrac{8\pi m_e^4 c^5}{h^3}\left(2\displaystyle\int_1^{\infty}\frac{\epsilon^2\sqrt{\epsilon^2-1}}{e^{\epsilon/\theta-\xi}+1}d\epsilon + \int_0^{\infty}\frac{\epsilon^3}{e^{\epsilon/\theta-\xi}-1}d\epsilon\right), \end{cases} \tag{A.2.1}$$

where $\epsilon = \dfrac{\varepsilon}{m_e c^2}$ is dimensionless energy, $\theta = \dfrac{kT}{m_e c^2}$ is dimensionless temperature and $\xi = \dfrac{\mu}{kT}$ is dimensionless chemical potential.

For instance, the detailed balance in electron-positron pair creation and annihilation process

$$e_1^+ + e_2^- \longleftrightarrow \gamma_3 + \gamma_4 \tag{A.2.2}$$

is described by the condition

$$f_+(\varepsilon_1)f_-(\varepsilon_2)\left[1+\frac{f_\gamma(\varepsilon_3)}{g_\gamma h^{-3}}\right]\left[1+\frac{f_\gamma(\varepsilon_4)}{g_\gamma h^{-3}}\right]= \\ = f_\gamma(\varepsilon_3)f_\gamma(\varepsilon_4)\left[1-\frac{f_+(\varepsilon_1)}{g_+ h^{-3}}\right]\left[1-\frac{f_-(\varepsilon_2)}{g_- h^{-3}}\right], \quad \text{(A.2.3)}$$

where $f_\alpha(\varepsilon)$ are distribution functions of particle species α, $g_\alpha = 2$ are spin weights of particles. Energies of interacting particles related by the conservation law $\varepsilon_1 + \varepsilon_2 = \varepsilon_3 + \varepsilon_4$. The distribution functions f_α are normalized as

$$n_\alpha(t) = \int f_\alpha(\vec{p}, t) d^3\vec{p}, \quad \text{(A.2.4)}$$

where n_α are the corresponding number densities. Similar conditions hold for the detailed balance conditions in all other two-particle interactions listed in Tab. A.1. Combining these conditions and requiring that distribution functions for electrons and positrons (photons) have Fermi-Dirac (Bose-Einstein) form we arrive to (Aksenov et al., 2009)

$$\theta = \theta_+ = \theta_- = \theta_\gamma, \qquad \xi = \xi_\gamma = \xi_+ = \xi_-. \quad \text{(A.2.5)}$$

In fact, the chemical potential in kinetic equilibrium is constrained by the condition $\xi \leq 0$. The equality in this relation implies that there is a critical number density n_{cr} given by Eq. (A.2.1) with $\xi = 0$. Since in two-particle processes the total number of particles (number density) is conserved, for $n > n_{cr}$ Bose condensation of photons is expected. However, in reality three-particle interactions do change the number of particles bringing the system to thermal equilibrium with $\xi = 0$ (Khatri et al., 2012).

A.2.2. Three-particle interactions and thermal equilibrium

Thermal equilibrium is defined as the state with vanishing difference between the rates of direct and inverse interactions of all processes. It was shown in Aksenov et al. (2007) that in electron-positron plasma two-particle processes are insufficient to bring the non-equilibrium system to thermal equilibrium. The necessary condition for reaching thermal equilibrium is detailed balance in three-particle processes.

For instance, the detailed balance in double Compton scattering

$$e_1^{\pm} + \gamma_2 \longleftrightarrow e_3^{\pm} + \gamma_4 + \gamma_5 \tag{A.2.6}$$

is described by the condition

$$\frac{f_{\pm}(\varepsilon_1)}{2h^{-3}} \frac{f_{\gamma}(\varepsilon_2)}{2h^{-3}} \left[1 - \frac{f_{\pm}(\varepsilon_3)}{2h^{-3}}\right] \left[1 + \frac{f_{\gamma}(\varepsilon_4)}{2h^{-3}}\right] \left[1 + \frac{f_{\gamma}(\varepsilon_5)}{2h^{-3}}\right] = \\ = \frac{f_{\pm}(\varepsilon_3)}{2h^{-3}} \frac{f_{\gamma}(\varepsilon_4)}{2h^{-3}} \frac{f_{\gamma}(\varepsilon_5)}{2h^{-3}} \left[1 - \frac{f_{\pm}(\varepsilon_1)}{2h^{-3}}\right] \left[1 + \frac{f_{\gamma}(\varepsilon_2)}{2h^{-3}}\right]. \tag{A.2.7}$$

Provided that kinetic equilibrium is established, this condition, as any of the corresponding conditions of all three-particle processes, constrains the chemical potential to vanish, $\xi = 0$.

A.3. Boltzmann equations

In uniform and isotropic electron-positron plasma relativistic Boltzmann equations for distribution functions f_α have the following form (Aksenov et al., 2007):

$$\frac{d}{dt} f_\alpha(\mathbf{p}, t) = \sum_q \left(\eta_\alpha^q - \chi_\alpha^q f_\alpha(\mathbf{p}, t)\right), \tag{A.3.1}$$

where the sum enumerated by index q is taken over all two- and three-particle processes q listed in Tab. A.2, η_α^q and χ_α^q are, respectively, emission and absorption coefficients.

A.3.1. Two-particle collision integrals

Consider interaction of two incoming particles of species I and II in quantum states 1 and 2, producing two outgoing particles of species III and IV in quantum states 3 and 4. Let initial particle momenta be $\vec{p}_1$ in a given range $d^3\vec{p}_1$ and $\vec{p}_2$ in $d^3\vec{p}_2$, and final particle momenta be $\vec{p}_3$ in $d^3\vec{p}_3$ and $\vec{p}_4$ in $d^3\vec{p}_4$, respectively. This process can be symbolically represented as follows

$$I_1 + II_2 \longrightarrow III_3 + IV_4. \tag{A.3.2}$$

Table A.2.: Particle interactions in the pair plasma.

Two-particle processes	Three-particle processes
Compton scattering	Double Compton
$e^{\pm}\gamma \longrightarrow e^{\pm\prime}\gamma'$	$e^{\pm}\gamma \longleftrightarrow e^{\pm\prime}\gamma'\gamma''$
Coulomb, Møller and Bhabha scattering	Bremmstrahlung
$e_1^{\pm}e_2^{\pm} \longrightarrow e_1^{\pm\prime}e_2^{\pm\prime}$ $e^+e^- \longrightarrow e^{+\prime}e^{-\prime}$	$e_1^{\pm}e_2^{\pm} \longleftrightarrow e_1^{\pm\prime}e_2^{\pm\prime}\gamma$ $e^+e^- \longleftrightarrow e^{+\prime}e^{-\prime}\gamma$
Creation/annihilation	Three-photon annihilation
$e^+e^- \longleftrightarrow \gamma_1\gamma_2$	$e^+e^- \longleftrightarrow \gamma_1\gamma_2\gamma_3$
	Pair creation/annihilation
	$\gamma_1\gamma_2 \longleftrightarrow e^+e^-\gamma'$ $e^{\pm}\gamma \longleftrightarrow e^{\pm\prime}e^+e^-$

The corresponding inverse process is thus

$$III_3 + IV_4 \longrightarrow I_1 + II_2. \tag{A.3.3}$$

Energy and momentum conservations read

$$\hat{\varepsilon} = \varepsilon_1 + \varepsilon_2 = \varepsilon_3 + \varepsilon_4, \qquad \hat{\vec{p}} = \vec{p}_1 + \vec{p}_2 = \vec{p}_3 + \vec{p}_4. \tag{A.3.4}$$

The number of collisions per unit time and volume is, see e.g. Landau and Lifshitz (1981, Eq. (2.1)),

$$\begin{aligned}\frac{dN}{dVdt} &= d^3\vec{p}_1 d^3\vec{p}_2 d^3\vec{p}_3 d^3\vec{p}_4 \times \\ &\times W_{(1,2|3,4)} f_I(\vec{p}_1,t) f_{II}(\vec{p}_2,t) \left(1 \pm \frac{f_{III}(\vec{p}_3,t)}{2h^{-3}}\right)\left(1 \pm \frac{f_{IV}(\vec{p}_4,t)}{2h^{-3}}\right),\end{aligned} \tag{A.3.5}$$

where W is the transition function, linked to QED matrix elements of the reaction M_{fi} as

$$W_{(1,2|3,4)} = \frac{\hbar^2 c^6}{(2\pi)^2}\frac{|M_{fi}|^2}{16\varepsilon_1\varepsilon_2\varepsilon_3\varepsilon_4}\delta(\varepsilon_1+\varepsilon_2-\varepsilon_3-\varepsilon_4)\delta^3(\vec{p}_1+\vec{p}_2-\vec{p}_3-\vec{p}_4), \tag{A.3.6}$$

δ is Dirac delta-function, and $\left[1 \pm f_\alpha(\vec{p},t)/(g_\alpha h^{-3})\right]$ are Bose enhancement (sign "+") and Pauli blocking (sign "−") factors. Matrix elements can be found, for example, in Berestetskii et al. (1982), Eqs. (86.6, 88.4, 81.7, 81.17).

Then collision integral for the particle I in the state 1 is

$$\eta_I(\vec{p}_1,t) - \chi_I(\vec{p}_1,t) f_I(\vec{p}_1,t) = \int d^3\vec{p}_2 d^3\vec{p}_3 d^3\vec{p}_4 \times$$
$$\times \left[W_{(3,4|1,2)} f_{III}(\vec{p}_3,t) f_{IV}(\vec{p}_4,t) \left(1 \pm \frac{f_I(\vec{p}_1,t)}{2h^{-3}}\right)\left(1 \pm \frac{f_{II}(\vec{p}_2,t)}{2h^{-3}}\right) - \right.$$
$$\left. - W_{(1,2|3,4)} f_I(\vec{p}_1,t) f_{II}(\vec{p}_2,t) \left(1 \pm \frac{f_{III}(\vec{p}_3,t)}{2h^{-3}}\right)\left(1 \pm \frac{f_{IV}(\vec{p}_4,t)}{2h^{-3}}\right)\right]. \quad \text{(A.3.7)}$$

Specifically, for a scattering with $I = III$ and $II = IV$ the inverse process is the same as the direct one since pairs of indices $(1,2)$ and $(3,4)$ can be interchanged. The relation $W_{(1,2|3,4)} = W_{(3,4|1,2)}$ holds for all processes listed in Tab. A.1. When incoming or outgoing particles coincide ($I = II$ and/or $III = IV$) quantum indistinguishability gives the term $\frac{1}{2}$ in front of the corresponding emission and absorption coefficients, see e.g. Ehlers (1973, p. 76), Groot et al. (1980, p. 18).

There are 4 delta-functions in Eq. (A.3.6) representing conservation of energy and momentum (A.3.4). Three integrations over momentum of particle III can be performed immediately

$$\int d\vec{p}_3 \delta^3(\vec{p}_1 + \vec{p}_2 - \vec{p}_3 - \vec{p}_4) \longrightarrow 1. \quad \text{(A.3.8)}$$

In the integration over energy ε_4 of particle IV it is necessary to take into account that ε_3 is now a function of energy and angles of particles I and II, as well as angles of particle IV, so we have

$$\int d\varepsilon_4 \delta(\varepsilon_1 + \varepsilon_2 - \varepsilon_3 - \varepsilon_4) \longrightarrow \frac{1}{1 - (\beta_3/\beta_4)\vec{n}_3 \cdot \vec{n}_4}, \quad \text{(A.3.9)}$$

where $\vec{n} = \vec{p}/p$ is the unit vector in the direction of particle momentum, $p = |\vec{p}| = \sqrt{(\varepsilon/c)^2 - m^2c^2}$ is the absolute value of particle momentum, $\beta = pc/\varepsilon$, and a dot denotes scalar product of 3-vectors. We use spherical coordinates in momentum space: $\{\varepsilon, \mu, \phi\}$, $\mu = \cos\vartheta$, where ε is the particle energy, and ϑ and ϕ are polar and azimuthal angles, respectively. Then energy and angles

of particle III and energy of particle IV follow from energy and momentum conservations (A.3.4) and relativistic energy-momentum relation, namely

$$\begin{gathered}\varepsilon_4 = c\sqrt{p_4^2 + m_{IV}^2 c^2}, \qquad \varepsilon_3 = \hat{\varepsilon} - \varepsilon_4, \qquad \vec{p}_3 = \hat{\vec{p}} - \vec{p}_4, \\ p_4 = \frac{AB \pm \sqrt{A^2 + 4m_{IV}^2 c^2 (B^2 - 1)}}{2(B^2 - 1)}, \\ A = \frac{c}{\hat{\varepsilon}}[\hat{p}^2 + (m_{III}^2 - m_{IV}^2)c^2] - \frac{\hat{\varepsilon}}{c}, \qquad B = \frac{c}{\hat{\varepsilon}}\vec{n}_4 \cdot \hat{\vec{p}}.\end{gathered} \tag{A.3.10}$$

Then we introduce these relations into collision integral (A.3.7). We also use spherical symmetry in momentum space to fix angles of the particle I: $\mu_1 = 1, \phi_1 = 0$, and to perform the integration over azimuthal angle of particle II: $\int d\phi_2 \longrightarrow 2\pi$, setting $\phi_2 = 0$ in the remaining integrals. Then final expression for collision integral is

$$\begin{aligned}&\eta_I(\varepsilon_1, t) - \chi_I(\varepsilon_1, t) f_I(\varepsilon_1, t) = \\ &\qquad = \frac{\hbar^2}{32\pi} \int d\varepsilon_2 d\mu_2\, d\mu_4 d\phi_4 \times \frac{p_2 p_4 |M_{fi}|^2}{\varepsilon_1 \varepsilon_3 \left[1 - (\beta_3/\beta_4)\vec{n}_3 \cdot \vec{n}_4\right]} \times \\ &\times \left[f_{III}(\varepsilon_3, t) f_{IV}(\varepsilon_4, t) \left(1 \pm \frac{f_I(\varepsilon_1, t)}{2h^{-3}}\right) \left(1 \pm \frac{f_{II}(\varepsilon_2, t)}{2h^{-3}}\right) - \right. \\ &\qquad - \left. f_I(\varepsilon_1, t) f_{II}(\varepsilon_2, t) \left(1 \pm \frac{f_{III}(\varepsilon_3, t)}{2h^{-3}}\right) \left(1 \pm \frac{f_{IV}(\varepsilon_4, t)}{2h^{-3}}\right) \right].\end{aligned} \tag{A.3.11}$$

For numerical integration, however, another expression is proved useful

$$\begin{aligned}\eta_I(\varepsilon,t)-\chi_I(\varepsilon,t)f_I(\varepsilon,t) &= \\ = \frac{\hbar^2}{32\pi}\Bigg[\int d\varepsilon_3\, d\varepsilon_4 d\mu_4\, d\mu_2 d\phi_2 \times \delta(\varepsilon_1-\varepsilon)\times \frac{p_2p_4|M_{fi}|^2}{\varepsilon_1\varepsilon_3\left[1-(\beta_1/\beta_2)\vec{n}_1\cdot\vec{n}_2\right]}\times \\ \times f_{III}(\varepsilon_3,t)f_{IV}(\varepsilon_4,t)\left(1\pm\frac{f_I(\varepsilon_1,t)}{2h^{-3}}\right)\left(1\pm\frac{f_{II}(\varepsilon_2,t)}{2h^{-3}}\right)- \\ -\int d\varepsilon_2 d\mu_2\, d\mu_4 d\phi_4 \times \frac{p_2p_4|M_{fi}|^2}{\varepsilon\varepsilon_3\left[1-(\beta_3/\beta_4)\vec{n}_3\cdot\vec{n}_4\right]}\times \\ \times \quad f_I(\varepsilon,t)f_{II}(\varepsilon_2,t)\left(1\pm\frac{f_{III}(\varepsilon_3,t)}{2h^{-3}}\right)\left(1\pm\frac{f_{IV}(\varepsilon_4,t)}{2h^{-3}}\right)\Bigg], \quad \text{(A.3.12)}\end{aligned}$$

where the first term, i.e. emission coefficient, is expressed in the form ready for replacement by the sum over incoming particles III and IV. In this term $\varepsilon_1, \mu_1, \phi_1, \varepsilon_2$ are given by relations (A.3.10) with indices exchange $1 \leftrightarrow 3$, $2 \leftrightarrow 4$, $I \leftrightarrow III$, $II \leftrightarrow IV$.

This collision integral of any of two-particle processes is a four-dimensional integral in momentum space. In Sec. A.4 we show how such integral is computed numerically on finite grid.

A.3.2. Three-particle collision integrals

Consider interaction of two incoming particles of species I and II in quantum states 1 and 2, producing three outgoing particles of species III, IV, and V in quantum states 3, 4, and 5. Let particle momenta be $\vec{p}_1$ and $\vec{p}_2$ before the interaction, and $\vec{p}_3$, $\vec{p}_4$, and $\vec{p}_5$ after interaction, respectively. This process can be represented as

$$I_1 + II_2 \longrightarrow III_3 + IV_4 + V_5. \quad \text{(A.3.13)}$$

The corresponding inverse process is

$$III_3 + IV_4 + V_5 \longrightarrow I_1 + II_2. \quad \text{(A.3.14)}$$

Energy and momentum conservations give

$$\varepsilon_1+\varepsilon_2=\varepsilon_3+\varepsilon_4+\varepsilon_5, \qquad \vec{p}_1+\vec{p}_2=\vec{p}_3+\vec{p}_4+\vec{p}_5. \quad \text{(A.3.15)}$$

The number of collisions of the direct process (A.3.13) per unit time and volume is

$$\frac{dN}{dVdt} = d^3\vec{p}_1 d^3\vec{p}_2 d^3\vec{p}_3 d^3\vec{p}_k d^3\vec{p}_5 \times W_{(1,2|3,4,5)} \times f_I(\vec{p}_1,t) f_{II}(\vec{p}_2,t) \times \\ \times \left(1 \pm \frac{f_{III}(\vec{p}_3,t)}{2h^{-3}}\right)\left(1 \pm \frac{f_{IV}(\vec{p}_4,t)}{2h^{-3}}\right)\left(1 \pm \frac{f_V(\vec{p}_5,t)}{2h^{-3}}\right). \quad \text{(A.3.16)}$$

For the inverse process (A.3.14) this number is

$$\frac{dN}{dVdt} = d^3\vec{p}_1 d^3\vec{p}_2 d^3\vec{p}_3 d^3\vec{p}_3 d^3\vec{p}_5 \times \\ \times W_{(3,4,5|1,2)} \times f_{III}(\vec{p}_3,t) f_{IV}(\vec{p}_4,t) f_V(\vec{p}_5,t) \times \\ \times \left(1 \pm \frac{f_I(\vec{p}_1,t)}{2h^{-3}}\right)\left(1 \pm \frac{f_{II}(\vec{p}_2,t)}{2h^{-3}}\right). \quad \text{(A.3.17)}$$

Then collision integral for particle I in the state 1 becomes

$$\eta_I(\vec{p}_1,t) - \chi_I(\vec{p}_1,t) f_I(\vec{p}_1,t) = \int d^3\vec{p}_2 d^3\vec{p}_3 d^3\vec{p}_4 d^3\vec{p}_5 \\ \times \Bigg[W_{(3,4,5|1,2)} \times f_{III}(\vec{p}_3,t) f_{IV}(\vec{p}_4,t) f_V(\vec{p}_5,t) \times \\ \times \left(1 \pm \frac{f_I(\vec{p}_1,t)}{2h^{-3}}\right)\left(1 \pm \frac{f_{II}(\vec{p}_2,t)}{2h^{-3}}\right) - \\ - W_{(1,2|3,4,5)} \times f_I(\vec{p}_1,t) f_{II}(\vec{p}_2,t) \times \\ \times \left(1 \pm \frac{f_{III}(\vec{p}_3,t)}{2h^{-3}}\right)\left(1 \pm \frac{f_{IV}(\vec{p}_4,t)}{2h^{-3}}\right)\left(1 \pm \frac{f_V(\vec{p}_5,t)}{2h^{-3}}\right)\Bigg], \quad \text{(A.3.18)}$$

where the first term in square parenthesis corresponds to emission of particle I in inverse process (A.3.14), while the second term corresponds to absorption of particle I in direct process (A.3.13). So far we considered the case when all incoming and outgoing particles are different. When the same particle is present among incoming and outgoing ones, the collision integral for this particle species becomes more complicated.

Consider, for instance, the case when $I = V$. This particle disappears from the quantum state 1 and appears in the quantum state 5 in the direct process (A.3.13). The same particle disappears from the quantum state 5 and appears

in the quantum state 1 in the inverse process (A.3.14). Consequently two terms in the collision integral on the RHS of Boltzmann equation (A.3.1) are ready to be written. These are the absorption coefficient $\chi_I(\vec{p}_1,t)f_I(\vec{p}_1,t)$ in the direct process (A.3.13) and the emission coefficient $\eta_I(\vec{p}_1,t)$ in the inverse process (A.3.14). Both these terms appear in Eq. (A.3.18). However, indices denoted with arabic numbers enumerate quantum particle states, which are arbitrary. Consequently, indices 1 and 5 can be interchanged both in direct (A.3.13) and inverse (A.3.14) processes. Then two new terms in collision integral for particle I in state 1 appear: emission coefficient $\eta_I(\vec{p}_1,t)$ in direct process $I_5 + II_2 \longrightarrow III_3 + IV_4 + I_1$, and absorption coefficient $\chi_I(\vec{p}_1,t)f_I(\vec{p}_1,t)$ in inverse process $III_3 + IV_4 + I_1 \longrightarrow I_5 + II_2$. Combining all four terms, the collision integral in this case becomes

$$\begin{aligned}
&\eta_I(\vec{p}_1,t) - \chi_I(\vec{p}_1,t)f_I(\vec{p}_1,t) = \int d^3\vec{p}_2 d^3\vec{p}_3 d^3\vec{p}_4 d^3\vec{p}_5 \times \\
&\times \Bigg[-W_{(1,2|3,4,5)} \times f_I(\vec{p}_1,t) f_{II}(\vec{p}_2,t) \times \\
&\qquad \times \left(1 \pm \frac{f_{III}(\vec{p}_3,t)}{2h^{-3}}\right)\left(1 \pm \frac{f_{IV}(\vec{p}_4,t)}{2h^{-3}}\right)\left(1 \pm \frac{f_I(\vec{p}_5,t)}{2h^{-3}}\right) + \\
&\quad + W_{(3,4,5|1,2)} \times f_{III}(\vec{p}_3,t) f_{IV}(\vec{p}_4,t) f_I(\vec{p}_5,t) \times \\
&\qquad \times \left(1 \pm \frac{f_I(\vec{p}_1,t)}{2h^{-3}}\right)\left(1 \pm \frac{f_{II}(\vec{p}_2,t)}{2h^{-3}}\right) - \\
&\quad + W_{(5,2|3,4,1)} \times f_I(\vec{p}_5,t) f_{II}(\vec{p}_2,t) \times \\
&\qquad \times \left(1 \pm \frac{f_{III}(\vec{p}_3,t)}{2h^{-3}}\right)\left(1 \pm \frac{f_{IV}(\vec{p}_4,t)}{2h^{-3}}\right)\left(1 \pm \frac{f_I(\vec{p}_1,t)}{2h^{-3}}\right) + \\
&\quad - W_{(3,4,1|5,2)} \times f_{III}(\vec{p}_3,t) f_{IV}(\vec{p}_4,t) f_I(\vec{p}_1,t) \times \\
&\qquad \times \left(1 \pm \frac{f_I(\vec{p}_5,t)}{2h^{-3}}\right)\left(1 \pm \frac{f_{II}(\vec{p}_2,t)}{2h^{-3}}\right)\Bigg]. \qquad \text{(A.3.19)}
\end{aligned}$$

Generally speaking, *such four terms should be present in collision integral of any reaction for a particle specie which is present both among incoming and outgoing particles, unless the process is a scattering.* This statement is valid for arbitrary number of incoming and outgoing particles. It is not limited to QED but applies to any quantum field theory in general.

All three-particle QED processes listed in Tab. A.2, with exception of three-photon annihilation, are indeed represented by four terms in collision integrals. Such four terms for double Compton scattering with corresponding symmetrization factors were considered by Chluba (2005). It should be noted, that the detailed balance conditions discussed in Sec. A.2.2 may be obtained (Lightman, 1981; Thorne, 1981) with only two terms in collision integrals, without interchanging the states 1 and 5. However, the structure of all four coefficients is different, and their presence in collision integral (A.3.19) is essential.

In three-particle processes transition function W can be expressed through the differential cross-section $d\sigma$. Using the definition of $d\sigma$ (Berestetskii et al., 1982, Eq. (64.18)) and its relation to number of collisions $\frac{dN}{dVdt}$ per unit time in unit volume (A.3.16), given by Eq. (12.7) in Landau and Lifshits (1994), we have

$$W_{(1,2|3,4,5)} d^3\vec{p}_3 d^3\vec{p}_4 d^3\vec{p}_5 = c \frac{\sqrt{[\varepsilon_1\varepsilon_2 - (\vec{p}_1\cdot\vec{p}_2)c^2]^2 - (m_I m_{II} c^4)^2}}{\varepsilon_1\varepsilon_2} d\sigma. \quad \text{(A.3.20)}$$

The differential cross section in turn can be expressed through dimensionless matrix element squared X, see Jauch and Rohrlich (1976, Eq. (11.31)). Then we obtain

$$W_{(1,2|3,4,5)} = \frac{\alpha r_e^2}{(4\pi)^2} \times \frac{c^7 X}{\varepsilon_1\varepsilon_2\varepsilon_3\varepsilon_4\varepsilon_5} \delta(\varepsilon_{initial} - \varepsilon_{final}) \delta^3(\mathbf{p}_{initial} - \mathbf{p}_{final}), \quad \text{(A.3.21)}$$

where $r_e = \frac{e^2}{m_e c^2}$ is the classical electron radius. For double Compton scattering X is given by Eqs. (3), (9), (10) of Mandl and Skyrme (1952). For relativistic bremsstrahlung $X = 16A$, where A is given by Eqs. in Appendix B of Haug and Nakel (2004).

Matrix elements for all other processes of Tab. A.2 can be obtained from the ones of double Compton scattering and of relativistic bremsstrahlung by the substitution law, given in Jauch and Rohrlich (1976, Sec. 8.5). For example, exchanging initial photon with the final electron or positron in double Compton scattering

$$e_1^- + \gamma_2 \longrightarrow e_3^- + \gamma_4 + \gamma_5, \quad \text{(A.3.22)}$$

we obtain three-photon annihilation process

$$e_1^- + e_3^+ \longrightarrow \gamma_2 + \gamma_4 + \gamma_5. \tag{A.3.23}$$

The matrix element squared of this process (A.3.23) can then be obtained from the one of double Compton process (A.3.22) with the following substitution law

$$\vec{p}_3 \longrightarrow -\vec{p}_3, \quad \varepsilon_3 \longrightarrow -\varepsilon_3, \quad \vec{p}_2 \longrightarrow -\vec{p}_2, \quad \varepsilon_2 \longrightarrow -\varepsilon_2. \tag{A.3.24}$$

The detailed balance condition for three-particle processes gives

$$h^3 W_{(1,2|3,4,5)} = 2W_{(3,4,5|1,2)}. \tag{A.3.25}$$

Following the same line of reasoning as in the derivation of Eq. (A.3.12), we arrive to the collision integral in the form

$$\begin{aligned}
&\eta_I(\varepsilon,t) - \chi_I(\varepsilon,t) f_I(\varepsilon,t) = \\
&\quad = \frac{\alpha r_e^2 c}{8\pi}\Bigg[\int d\varepsilon_3\, d\varepsilon_4 d\mu_4\, d\varepsilon_5 d\mu_5 d\phi_5\, d\mu_2 d\phi_2 \times \delta(\varepsilon_1 - \varepsilon)\times \\
&\qquad \times \frac{p_2 p_4 p_5 X}{\varepsilon_1 \varepsilon_3 \left[1 - (\beta_1/\beta_2)\vec{n}_1 \cdot \vec{n}_2\right]}\times \\
&\qquad \times f_{III}(\varepsilon_3,t) f_{IV}(\varepsilon_4,t) f_V(\varepsilon_5,t) \left(1 \pm \frac{f_I(\varepsilon_1,t)}{2h^{-3}}\right)\left(1 \pm \frac{f_{II}(\varepsilon_2,t)}{2h^{-3}}\right) - \\
&\qquad - \int d\varepsilon_2 d\mu_2\, d\mu_4 d\phi_4\, d\varepsilon_5 d\mu_5 d\phi_5 \times \frac{p_2 p_4 p_5\, X}{\varepsilon\varepsilon_3 \left[1 - (\beta_3/\beta_4)\vec{n}_3 \cdot \vec{n}_4\right]}\times \\
&\qquad \times f_I(\varepsilon,t) f_{II}(\varepsilon_2,t) \left(1 \pm \frac{f_{III}(\varepsilon_3,t)}{2h^{-3}}\right)\left(1 \pm \frac{f_{IV}(\varepsilon_4,t)}{2h^{-3}}\right)\left(1 \pm \frac{f_V(\varepsilon_5,t)}{2h^{-3}}\right)\Bigg],
\end{aligned} \tag{A.3.26}$$

where again the form of the first integral is ready to be substituted by corresponding sum over incoming particles III, IV, and V. In this first integral, i.e. in the emission coefficient, in order to find energy and angles of particle I and energy of particle II relations (A.3.10) should be used with indices

exchange $1 \leftrightarrow 3$, $2 \leftrightarrow 4$, $I \leftrightarrow III$, $II \leftrightarrow IV$, and

$$\hat{\varepsilon} = \varepsilon_3 + \varepsilon_4 + \varepsilon_5, \qquad \hat{\vec{p}} = \vec{p}_3 + \vec{p}_4 + \vec{p}_5. \tag{A.3.27}$$

In the absorption coefficient in order to find energy and angles of particle III and energy of particle IV from relation (A.3.10) instead of (A.3.4) the following relations must be used

$$\hat{\varepsilon} = \varepsilon_1 + \varepsilon_2 - \varepsilon_5, \qquad \hat{\vec{p}} = \vec{p}_1 + \vec{p}_2 - \vec{p}_5. \tag{A.3.28}$$

This collision integral (A.3.26) of any of three-particle processes is a seven-dimensional integral in momentum space. In the next Section we show how such integral is computed numerically on finite grid.

A.4. The numerical scheme

The main difficulty arising in computation of collision integrals in comparison with previous works (Aksenov et al., 2007, 2009, 2010) is that particle emission and absorbtion coefficients contain not only distribution functions of incoming particles, but also those of outgoing particles. Therefore we adopt a different approach which we refer to as "*reaction-oriented*" instead of "particle-oriented" one used earlier.

The phase space is divided in zones. The zone $\Omega^{\alpha}_{a,j,k}$ for particle specie α corresponds to energy ε_a, cosine of polar angle μ_j and azimuthal angle ϕ_k, where indices run in the following ranges $1 \leq a \leq a_{\max}$, $1 \leq j \leq j_{\max}$, and $1 \leq k \leq k_{\max}$. The zone boundaries are $\varepsilon_{a\mp1/2}$, $\mu_{j\mp1/2}$, $\phi_{k\mp1/2}$. The length of the a-th energy zone Ω^{α}_{a} is $\Delta\varepsilon_a \equiv \varepsilon_{a+1/2} - \varepsilon_{a-1/2}$. On finite grid f_α does not depend on μ and ϕ, and number density of particle α in zone a is

$$Y^{\alpha}_{a}(t) = 4\pi \int_{\varepsilon_{a-1/2}}^{\varepsilon_{a+1/2}} c^{-3}\varepsilon\sqrt{\varepsilon^2 - m^2_\alpha c^4} f_\alpha(\varepsilon, t) d\varepsilon = \\ = 4\pi c^{-3}\varepsilon_a\sqrt{\varepsilon^2_a - m^2_\alpha c^4} f_\alpha(\varepsilon_a, t)\Delta\varepsilon_a. \tag{A.4.1}$$

In this variables discretized Boltzmann equation for particle I and energy zone a reads

$$\frac{dY^{\alpha}_{a}(t)}{dt} = \sum \left[\eta^{I}_{a}(t) - \chi^{I}_{a}(t) Y^{I}_{a}(t)\right], \tag{A.4.2}$$

where the sum is taken over all processes involving particle I. Emission and absorption coefficients on the grid are obtained by integration of (A.3.12) for two-particle processes and of (A.3.26) for three-particle processes over the zone. The corresponding integrals are replaced by sums on the grid. For instance, absorption coefficient for incoming particle I in two-particle process (A.3.2) is

$$\chi_a^I(t)Y_a^I(t) = \frac{\hbar^2 c^4}{8(4\pi)^2} \sum_{b,j,s,k} \Delta\mu_j \Delta\mu_s \Delta\phi_k \times |M_{fi}|^2 \times \\ \times \frac{p_4}{\varepsilon_3[1-(\beta_3/\beta_4)\vec{n}_3\cdot\vec{n}_4]} \times \frac{Y_a^I(t)}{\varepsilon_a}\frac{Y_b^{II}(t)}{\varepsilon_b} \times \left[1 \pm \frac{Y_c^{III}(t)}{\bar{Y}_c^{III}}\right]\left[1 \pm \frac{Y_d^{IV}(t)}{\bar{Y}_d^{IV}}\right], \tag{A.4.3}$$

where index j denotes polar angle zone of incoming particle II, index s denotes polar angle zone of outgoing particle IV, index k denotes azimuthal angle zone of outgoing particle IV, and

$$\bar{Y}_a^\alpha = 4\pi \int_{\varepsilon_{a-1/2}}^{\varepsilon_{a+1/2}} c^{-3}\varepsilon\sqrt{\varepsilon^2 - m_\alpha^2 c^4}\, 2h^{-3} d\varepsilon = \\ = 8\pi(hc)^{-3}\varepsilon_a\sqrt{\varepsilon_a^2 - m_\alpha^2 c^4}\,\Delta\varepsilon_a. \tag{A.4.4}$$

Emission coefficient of particle I in process (A.3.3) from integration of (A.3.12) is

$$\eta_a^I(t) = \frac{\hbar^2 c^4}{8(4\pi)^2} \sum_{c,d,j,s,k} C_a(\varepsilon_1)\Delta\mu_j \Delta\mu_s \Delta\phi_k \times |M_{fi}|^2 \times \\ \times \frac{p_2}{\varepsilon_1[1-(\beta_1/\beta_2)\vec{n}_1\cdot\vec{n}_2]} \times \frac{Y_c^{III}(t)}{\varepsilon_c}\frac{Y_d^{IV}(t)}{\varepsilon_d} \times \left[1 \pm \frac{Y_a^I(t)}{\bar{Y}_a^I}\right]\left[1 \pm \frac{Y_b^{II}(t)}{\bar{Y}_b^{II}}\right], \tag{A.4.5}$$

where index j denotes polar angle zone of incoming particle IV, index s denotes polar angle zone of outgoing particle II, index k denotes azimuthal

angle zone of outgoing particle II, and

$$C_a(\varepsilon_1) = \begin{cases} \dfrac{\varepsilon_a - \varepsilon_1}{\varepsilon_a - \varepsilon_{a-1}}, & \varepsilon_{a-1} < \varepsilon_1 < \varepsilon_a, \\ \dfrac{\varepsilon_{a+1} - \varepsilon_1}{\varepsilon_{a+1} - \varepsilon_a}, & \varepsilon_a < \varepsilon_1 < \varepsilon_{a+1}, \\ 0, & \text{otherwise.} \end{cases} \tag{A.4.6}$$

In integration of (A.3.12) over the zone one can integrate out the δ-function $\int \delta(\varepsilon_1 - \varepsilon) d\varepsilon_1 \longrightarrow 1$. However, when energies of incoming particles are fixed on the grid, the energies of outgoing particles are not on the grid. Hence an interpolation (A.4.6) is adopted, which enforces the exact number of particles and energy conservation in each two-particle process due to redistribution of outgoing particle α with energy ε over two energy zones $\Omega_n^\alpha, \Omega_{n+1}^\alpha$ with $\varepsilon_n < \varepsilon < \varepsilon_{n+1}$.

The redistribution of final particles should also satisfy requirements of quantum statistics. Therefore if a process occurs, when final particle should be distributed over the quantum states which are fully occupied, such process is forbidden. Thus we introduce the Bose enhancement/Pauli blocking coefficients in (A.4.3) and (A.4.5) as

$$\left[1 \pm \frac{Y_a^\alpha(t)}{\bar{Y}_a^\alpha}\right] = \min\left(1 \pm \frac{Y_n^\alpha(t)}{\bar{Y}_n^\alpha}, 1 \pm \frac{Y_{n+1}^\alpha(t)}{\bar{Y}_{n+1}^\alpha}\right). \tag{A.4.7}$$

The sum over angles μ_j, μ_s, ϕ_k can be found once and for all at the beginning of the calculations. We then store in the program for each set of the incoming and outgoing particles the corresponding terms and redistribution coefficients given by Eq. (A.4.6).

Extension of this scheme to three-particle interactions is straightforward. However, unlike two-particle case where pairs of indices I, II and III, IV can be interchanged, in three-particle case there is no such symmetry. Then we give absorption and emission coefficients for incoming and outgoing particles in processes (A.3.13) and (A.3.14) separately. Considering the direct process (A.3.13), finite difference representation of absorption coefficient for

incoming particle I in (A.3.26) is

$$\chi_a^I(t)Y_a^I(t) = \frac{\alpha r_e^2 c^3}{2(4\pi)^2} \sum_{b,j,s,k,f,p,r} \Delta\mu_j \Delta\mu_s \Delta\phi_k \Delta\varepsilon_f \Delta\mu_p \Delta\phi_r \times \\ \times X \times \frac{p_4 p_5}{\varepsilon_3[1-(\beta_3/\beta_4)\vec{n}_3\cdot\vec{n}_4]} \times \frac{Y_a^I(t)}{\varepsilon_a}\frac{Y_b^{II}(t)}{\varepsilon_b} \times \\ \times \left[1 \pm \frac{Y_c^{III}(t)}{\bar{Y}_c^{III}}\right]\left[1 \pm \frac{Y_d^{IV}(t)}{\bar{Y}_d^{IV}}\right]\left[1 \pm \frac{Y_f^{V}(t)}{\bar{Y}_f^{V}}\right], \quad \text{(A.4.8)}$$

and emission coefficient for outgoing particle III is

$$\eta_c^{III}(t) = \frac{\alpha r_e^2 c^3}{2(4\pi)^2} \sum_{a,b,j,s,k,f,p,r} \Delta\mu_j \Delta\mu_s \Delta\phi_k \Delta\varepsilon_f \Delta\mu_p \Delta\phi_r \times \\ \times C_a(\varepsilon_3) \times X \times \frac{p_4 p_5}{\varepsilon_3[1-(\beta_3/\beta_4)\vec{n}_3\cdot\vec{n}_4]} \times \frac{Y_a^I(t)}{\varepsilon_a}\frac{Y_b^{II}(t)}{\varepsilon_b} \times \\ \times \left[1 \pm \frac{Y_c^{III}(t)}{\bar{Y}_c^{III}}\right]\left[1 \pm \frac{Y_d^{IV}(t)}{\bar{Y}_d^{IV}}\right]\left[1 \pm \frac{Y_f^{V}(t)}{\bar{Y}_f^{V}}\right], \quad \text{(A.4.9)}$$

where indices f, p, r denote energy, polar angle and azimuthal angle zone of outgoing particle V, respectively. Considering the inverse process (A.3.14), emission coefficient for the outgoing particle I is

$$\eta_a^I(t) = \frac{\alpha r_e^2 c^5 h^3}{4(4\pi)^3} \sum_{c,s,k,d,j,f,p,r} \Delta\mu_s \Delta\phi_k \Delta\mu_j \Delta\mu_p \Delta\phi_r \times \\ \times C_a(\epsilon_1) \times X \times \frac{p_2}{\varepsilon_1[1-(\beta_1/\beta_2)\vec{n}_1\cdot\vec{n}_2]} \frac{Y_c^{III}(t)}{\varepsilon_c}\frac{Y_d^{IV}(t)}{\varepsilon_d}\frac{Y_f^{V}(t)}{\varepsilon_f} \times \\ \times \left[1 \pm \frac{Y_a^{I}(t)}{\bar{Y}_a^{I}}\right]\left[1 \pm \frac{Y_b^{II}(t)}{\bar{Y}_b^{II}}\right], \quad \text{(A.4.10)}$$

while absorption coefficient for the incoming particle III is

$$\chi_c^{III}(t)Y_c^{III}(t) = \frac{\alpha r_e^2 c^5 h^3}{4(4\pi)^3} \sum_{s,k,d,j,f,p,r} \Delta\mu_s \Delta\phi_k \Delta\mu_j \Delta\mu_p \Delta\phi_r \times$$
$$\times X \times \frac{p_2}{\varepsilon_1[1-(\beta_1/\beta_2)\vec{n}_1\cdot\vec{n}_2]} \frac{Y_c^{III}(t)}{\varepsilon_c} \frac{Y_d^{IV}(t)}{\varepsilon_d} \frac{Y_f^{V}(t)}{\varepsilon_f} \times$$
$$\times \left[1 \pm \frac{Y_a^I(t)}{\bar{Y}_a^I}\right] \left[1 \pm \frac{Y_b^{II}(t)}{\bar{Y}_b^{II}}\right], \quad \text{(A.4.11)}$$

where indices s and k denote polar and azimuthal angle zones of outgoing particle II, respectively; index j denotes polar angle zone of incoming particle IV, and indices f, p, r denote energy, polar angle and azimuthal angle zone of particle V, respectively.

In these sums (A.4.8–A.4.11) summation over angles μ_j, μ_s, ϕ_k, μ_p, ϕ_r again can be performed once and for all at the beginning of the calculations. Representation of discretized collisional integral for particle I and energy zone a in processes (A.3.2, A.3.3, A.3.13, A.3.14) is

$$\frac{dY_a^I}{dt} = -\sum A \times Y_a^I(t)Y_b^{II}(t) \times \left[1 \pm \frac{Y_c^{III}(t)}{\bar{Y}_c^{III}}\right] \left[1 \pm \frac{Y_d^{IV}(t)}{\bar{Y}_d^{IV}}\right] +$$
$$+ \sum B \times Y_c^{III}(t)Y_d^{IV}(t) \times \left[1 \pm \frac{Y_a^I(t)}{\bar{Y}_a^I}\right] \left[1 \pm \frac{Y_b^{II}(t)}{\bar{Y}_b^{II}}\right] -$$
$$- \sum C \times Y_a^I(t)Y_b^{II}(t) \times \left[1 \pm \frac{Y_c^{III}(t)}{\bar{Y}_c^{III}}\right] \left[1 \pm \frac{Y_d^{IV}(t)}{\bar{Y}_d^{IV}}\right] \left[1 \pm \frac{Y_f^{V}(t)}{\bar{Y}_f^{V}}\right] +$$
$$+ \sum D \times Y_c^{III}(t)Y_d^{IV}(t)Y_f^{V}(t) \times \left[1 \pm \frac{Y_a^I(t)}{\bar{Y}_a^I}\right] \left[1 \pm \frac{Y_b^{II}(t)}{\bar{Y}_b^{II}}\right], \quad \text{(A.4.12)}$$

where constant coefficients A, B, C, D are obtained from the summation over angles in the sums (A.4.3, A.4.5, A.4.8, A.4.10). The full Boltzmann equation (A.4.2) contains similar sums for all processes from Tab. A.2. Each individual term in these sums appears in the system of discretized Boltzmann equations four or five times in emission and absorption coefficients for each particle entering a given process. Then each term can be computed only once and

added to all corresponding sums, that is the essence of our *"reaction-oriented" approach*.

In our method exact energy and number of particles conservation laws are satisfied. The number of energy intervals is typically 20, while internal grid of angles has 32 points in μ and 64 in ϕ. The system under consideration has several characteristic times for different processes, and therefore the resulting system of ordinary differential equations (A.4.2) is stiff. We use Gear's method (Hall and Watt, 1976) to integrate the system numerically.

A.5. Rates of three-particle interactions

In previous works Aksenov et al. (2007, 2009); **?** three-particle interactions were taken into account only approximately. Since in nondegenerate plasma triple interactions have rates smaller than the binary ones by a factor α, it was shown that kinetic equilibrium is established well before three-particle interaction become essential. Once the kinetic equilibrium is reached, each collision integral contains multipliers proportional to

$$F_i = \exp \frac{\nu_i}{\theta_i}, \tag{A.5.1}$$

called fugacity. The calculation of emission and absorption coefficients can then be performed using the well established thermal equilibrium rates Svensson (1984), multiplied by the corresponding fugacities.

When quantum corrections are taken into account the simplification discussed above does not apply. The three-particle interactions have to be computed from first principles, as described above. Here we present the rates of three-particle processes in thermal equilibrium in relativistic plasma. In non-degenerate case these rates are given in Svensson (1982a, 1984).

Once relaxation is finished, the right hand side of Boltzmann equations for photons and pairs vanishes. However, coefficients for individual processes listed in Table A.2 do not. In Fig. A.2 we show normalized emission and absoprtion coefficients (η/n and χ) for electrons (left panel) and photons (right panel) in direct and inverse process of double Compton scattering $e + \gamma \longleftrightarrow e' + \gamma' + \gamma''$ in thermal equilibrium at temperature $\theta = 1$ as functions of electron energy, measured in units of mc^2. This equilibrium is reached on the grid with 20 intervals in energy and 16 and 32 intervals in

angles ϑ and ϕ, respectively. Given strong anisotropy of matrix elements for three-particle processes, this grid is still relatively coarse. However, given the computational performance of current computers and intrinsic difficulties in applying well established parallel computational schemes to the code this is best one can reach. Nevertheless, one can see regular behaviour of emission and absorption coefficients everywhere except the very last interval which should be excluded from the analysis. One can also see the increase of all emission and absorption coefficients for photons (except for absorption in direct process) as photon energy decreases below the value mc^2. In Fig. A.3 we show the same normalized emission and absorption coefficients for electron-electron bremsstrahlung process $e_1 + e_2 \longleftrightarrow e_1' + e_2' + \gamma$. While the direct emission and absorption coefficients for electrons in this process are almost independent on electron energy, the inverse ones grow as a power law. Interestingly, different behaviour is seen for emission and absorption coefficients of photons. While both decrease with photon energy, the former saturates at energies at relativistic energies, and the latter continues to decrease as a power law. In Fig. A.4 we present the same normalized emission and absorption coefficients for the radiative pair production process $e + \gamma \longleftrightarrow e' + e^+ + e^-$. One can see the exponential cut-off due to energy threshold for all coefficients of electrons, except for absorption in the direct process. Finally, total emission and absorption coefficients for all three-particle processes is shown in Fig. A.5. As expected, the coefficients for direct and inverse processes almost coincide, indicating that the system has relaxed to an equilibrium on the grid. By comparison of these results one can see that at this temperature the energy dependence of emission and absorption coefficients of electrons is determined by the electron bremsstrahlung process, especially at energies above mc^2. Interestingly, the emission and absorption coefficients of photons behave in nontrivial way. At nonrelativistic energies, the total emission coefficient in direct reactions is equal to the total absorption coefficient in inverse ones. Also, the total absorption coefficient in direct reactions is equal to the total emission coefficient in inverse ones. However, at energies above mc^2 they interchange.

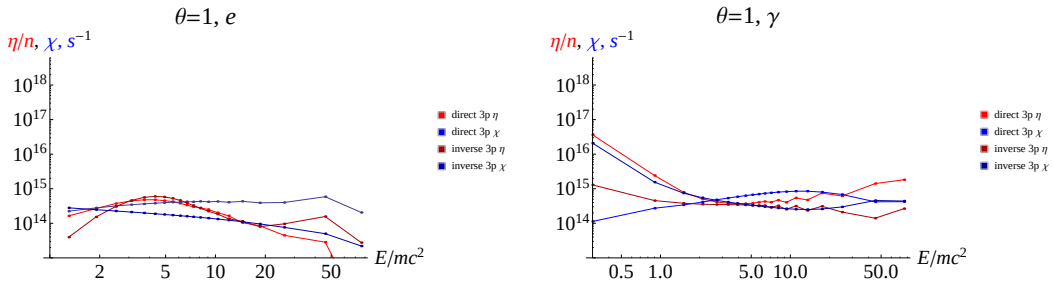

Figure A.2.: Normalized emission (red) and absoprtion (blue) coefficients for electrons (left panel) and photons (right panel) in direct (light) and inverse (dark) process of double Compton scattering in thermal equilibrium at temperature $\theta = 1$ as functions of electron energy, measured in units of mc^2.

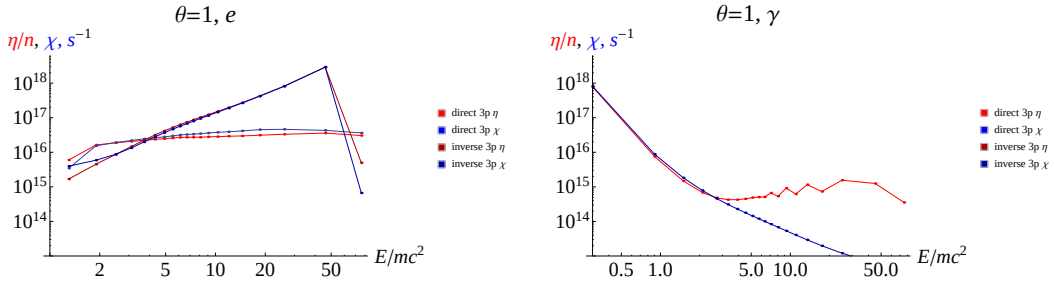

Figure A.3.: The same as in Fig. A.2, but for direct and inverse electron-electron bremsstrahlung for electrons.

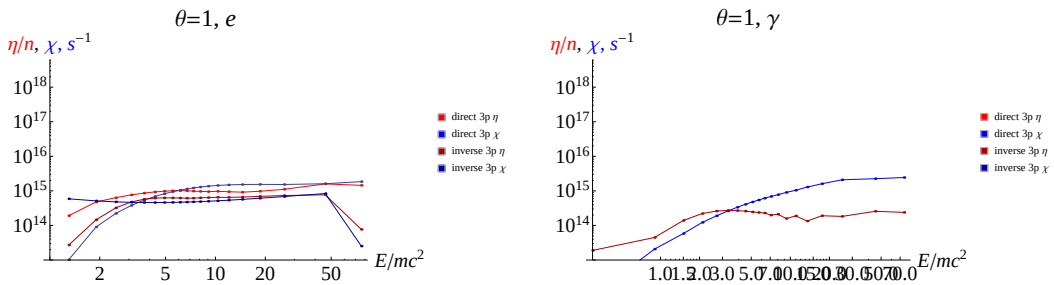

Figure A.4.: The same as in Fig. A.2, but for direct and inverse radiative pair production for electrons.

A.6. Characteristic time scales of plasma relaxation

We solved numerically Boltzmann equation (A.3.1) in two cases. Initially only photons are present with constant spectral energy density and total energy density $\rho = 10^{23}$ erg/cm^3 and $\rho = 10^{29}$ erg/cm^3. Such energy densities corresponds to the temperature θ in thermal equilibrium of 0.3 and 8, respectively.

In Figs. A.6 and A.7 we present number density, energy density, temperature and chemical potential of photons and pairs in both cases. We also show the difference between quantum and Boltzmann statistics by including and omitting the Pauli blocking and Bose enhancement factors in evolution equations (A.4.12). Time is expressed in units of Compton time

$$\tau_C = \frac{1}{\sigma_T n_\pm c}, \tag{A.6.1}$$

where $n_\pm$ is number density of pairs in thermal equilibrium, σ_T is Thomson cross section.

Timescales of relaxation to thermal equilibrium for quantum (classical) statistics nearly coincide: $15\tau_C$ ($18\tau_C$) for $\rho = 10^{23}$ erg/cm^3, and $27\tau_C$ ($23\tau_C$) for $\rho = 10^{29}$ erg/cm^3. Inspection of Figs. A.6 and A.7 indicates that both temperatures and chemical potentials of leptonic and photon components become nearly equal when the total number density of particles shown by blue

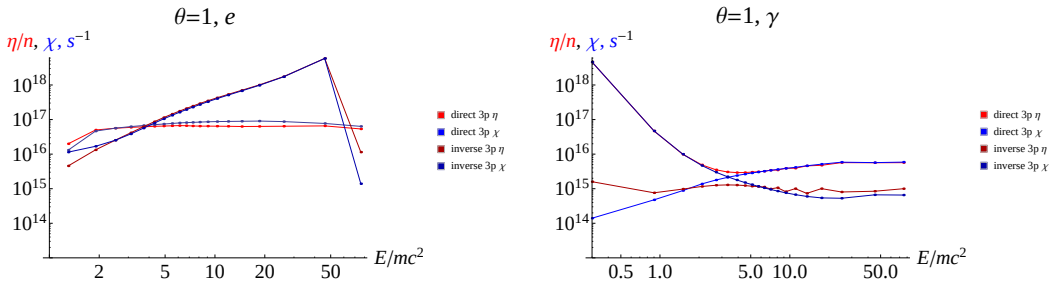

Figure A.5.: Total normalized emission (red) and absoprtion (blue) coefficients for electrons (left panel) and photons (right panel) in all direct (light) and inverse (dark) three-particle processes in thermal equilibrium at temperature $\theta = 1$ as functions of electron energy, measured in units of mc^2.

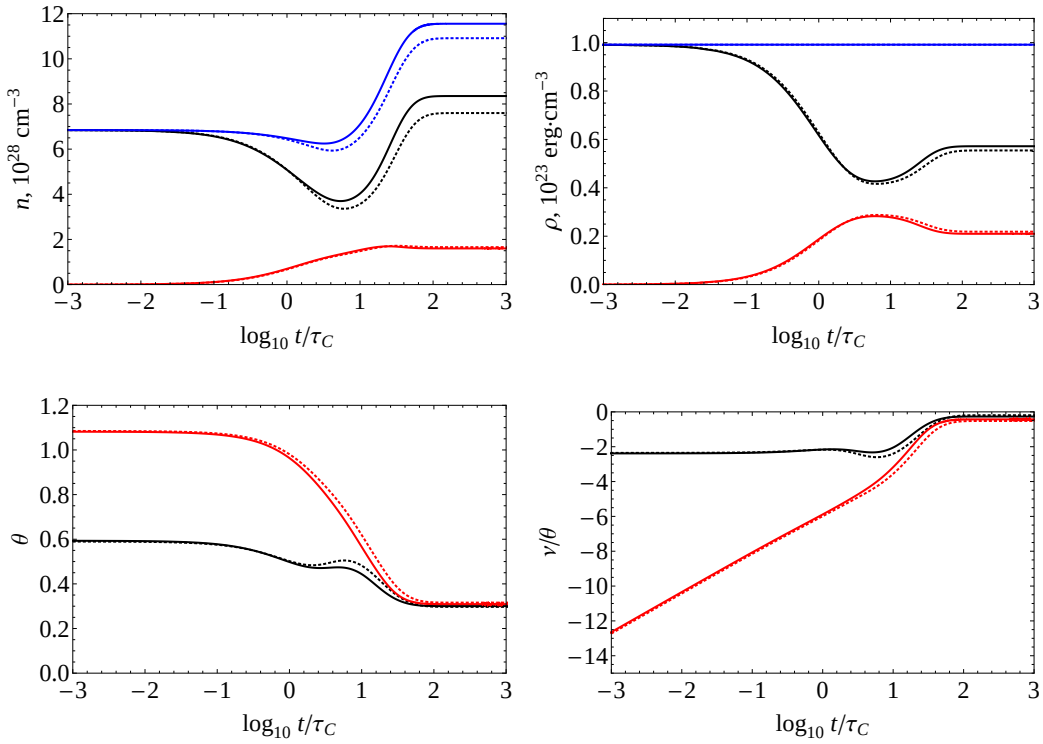

Figure A.6.: Comparison of evolution of number n and energy ρ densities, dimensionless temperature θ, chemical potential ξ, for quantum (solid curves) and classical (dotted curves) statistics with total energy density $\rho = 10^{23}$ erg/cm^3. Black and red curves correspond to photons and pairs, respectively, blue curve gives the sum of densities.

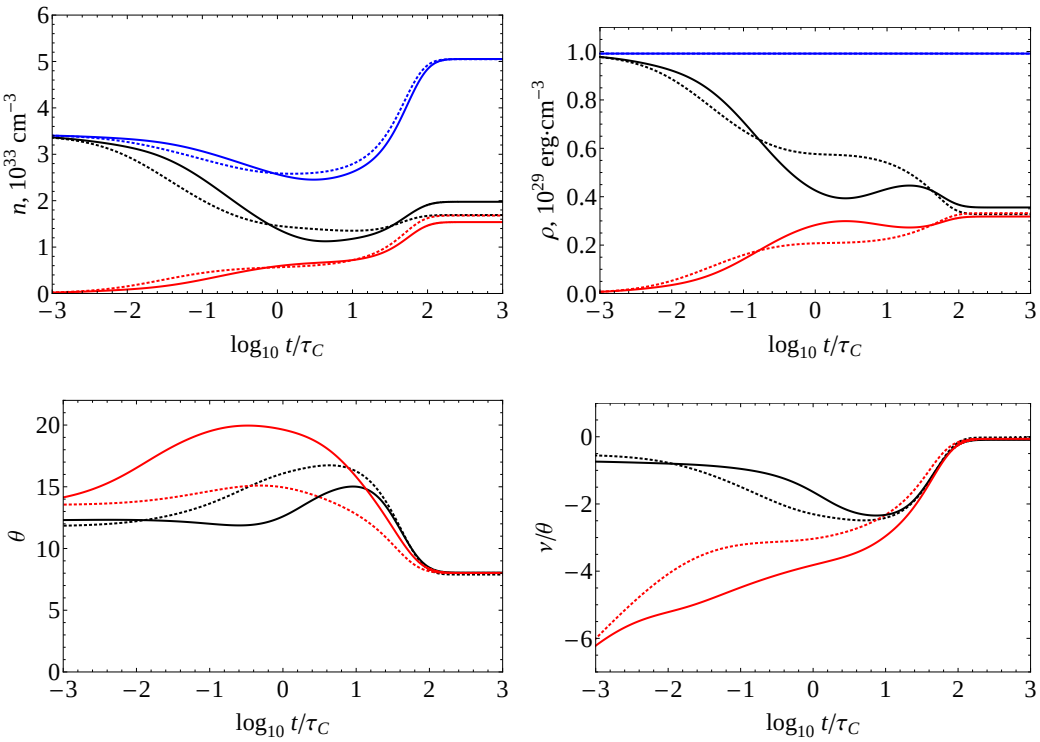

Figure A.7.: The same as in Fig. A.6, but for total energy density $\rho = 10^{29}$ erg/cm^3.

curves is almost constant. This fact indicates that three-particle interactions become relevant when almost detailed balance (kinetic equilibrium) is established by two-particle interactions (Aksenov et al., 2007). Notice, however, that due to energy dependence of reaction rates the characteristic timescale on which kinetic equilibrium is established is larger than Compton time (A.6.1). For the same reason the characteristic timescale on which thermal equilibrium is established is smaller than the simple estimate $\alpha^{-1}\tau_C$. Thus the ratio of the timescales of kinetic and thermal equilibrium is no longer α but higher. This fact shows why the exact treatment of three-particle interactions, especially for high energy densities, becomes important.

In Figs. A.8 and A.9 we show spectral evolution for both our initial conditions. The final spectra shown for $t = 10^3\tau_C$ are in good agreement with Planck/Fermi-Dirac distribution functions, correspondingly, obtained for the given energy density, typically within 5 % accuracy. Notice that at the Compton time both electron/positron and photon spectra are far from equilibrium shape, with the only exception of leptonic spectrum for $\rho = 10^{23}$ erg/cm^3. This quick relaxation of leptonic component is due to large Coulomb logarithm for non-relativistic temperatures.

A.7. Conclusions

In this Chapter we consider relaxation of nonequilibrium optically thick pair plasma to complete thermal equilibrium by integrating numerically relativistic Boltzmann equations with exact QED two-particle and three-particle collision integrals. Quantum nature of particle statistics is accounted for in collision integrals by the corresponding Bose enhancement and Pauli blocking factors.

We point out that unlike classical Boltzmann equation for binary interactions such as scattering, more general interactions are typically described by four collision integrals for each particle that appears both among incoming and outgoing particles.

The partial summations over angles in three-particle processes appears to be the most time-consuming part of the numerical solution of Boltzmann equation. Typical number of points in calculations is 10^{12}.

Our numerical results indicate that the rates of three-particle interactions become comparable to those of two-particle ones for temperatures exceeding the electron rest-mass energy. Thus three particle interactions such as

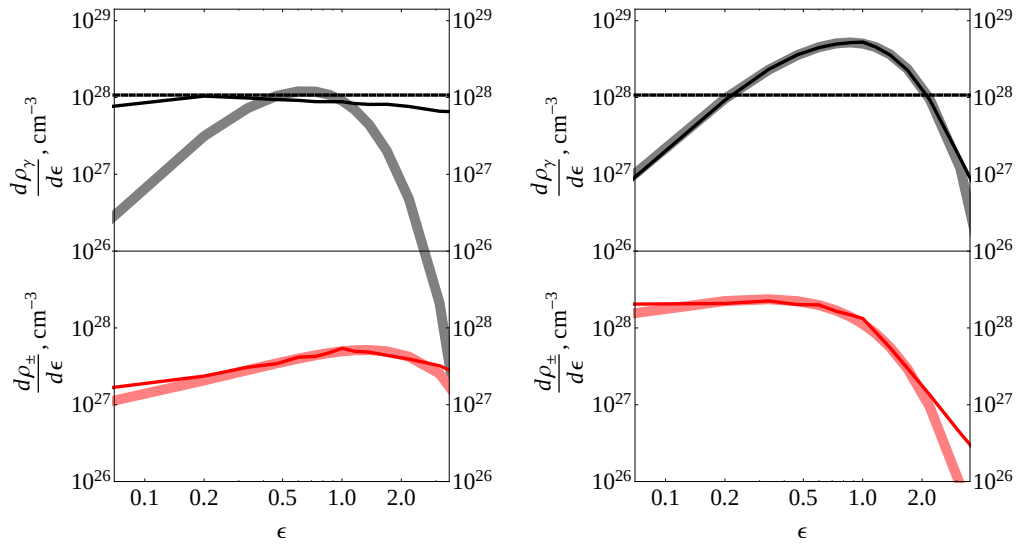

Figure A.8.: Numerical spectral energy densities of photons (black line) and pairs (red line) at $t = \tau_C$ (left) and at $t = 10^3\tau_C$ (right) for $\rho = 10^{23}$ erg/cm^3. Thick curves show the corresponding Bose-Einstein and Fermi-Dirac distributions with the same number and energy densities, respectively. Dashed thin line shows initial photon spectrum.

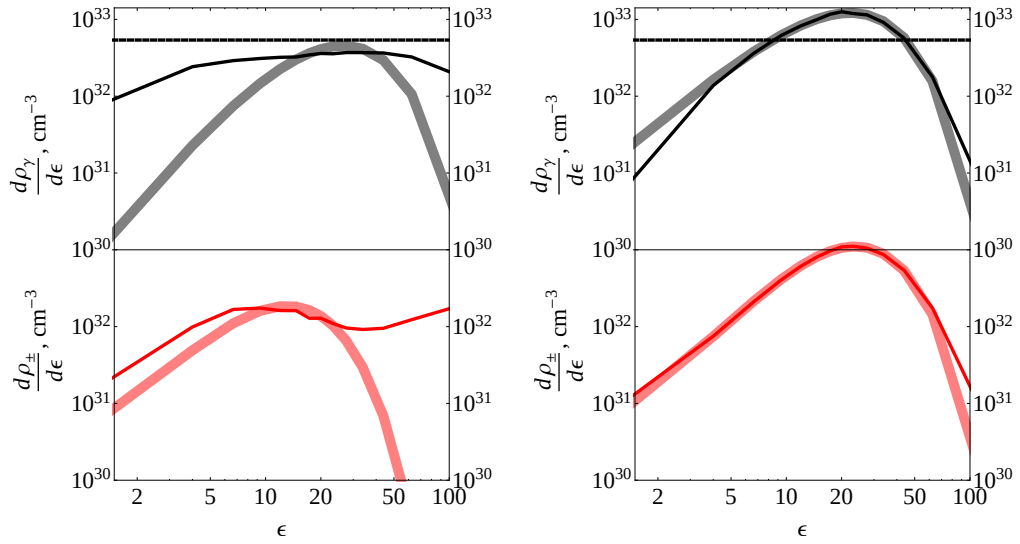

Figure A.9.: The same as in Fig. A.8 for $\rho = 10^{29}$ erg/cm^3.

relativistic bremsstrahlung, double Compton scattering, and radiative pair creation become essential not only for establishment of thermal equilibrium, but also for correct estimation of interaction rates, energy losses etc.

B. Transparency of an instantaneously created electron-positron-photon plasma

B.1. Introduction

The problem of the release of a large amount of energy in a small volume has been considered for the first time by Fermi (1950), who proposed a statistical theory for computing high energy collisions of protons with multiple production of particles. Landau (1953) noticed that the initial expansion of the system can be treated within relativistic hydrodynamics. Due to highly relativistic velocities of the colliding particles, the region of collision appears to be highly contracted in one direction. Consequently the problem can be reduced to one dimensional relativistic hydrodynamics in plane geometry. Landau found an approximate solution of this problem. Later on, an exact solution has been given by Khalatnikov (1954).

A similar problem has been considered in application to Gamma Ray Bursts (GRBs) within spherical geometry. Goodman (1986) considered the fate of a large quantity of energy in photons and electron-positron pairs, initially confined to a sphere in equilibrium at temperature above MeV, and then allowed to expand freely. He solved numerically the relativistic hydrodynamics equations. He found that the plasma expands and cools down to non relativistic temperatures. Then due to the exponential dependence of pairs density on temperature and consequently on radius, the system becomes transparent suddenly. He computed the energy distribution of the photon flux received by a distant observer by integrating over the volume of the system at the moment of transparency. The spectrum was found to be nearly thermal.

An approximate analytic solution for the problem of relativistic spherical expansion into vacuum of an instantly created ultra-relativistic plasma has been given by Bisnovatyi-Kogan and Murzina (1995). In this paper we used this solution in order to find the observed spectra from transparency of electron-proton-photon plasma. The problem is intrinsically dynamic with the photosphere evolving rapidly with time. The only method available to compute the photospheric emission in such dynamical case is the one by Ruffini et al. (2013b). This method solves the radiative transfer equation assuming the source function to be isotropic and thermal.

The applications of the results presented in our paper are twofold. Firstly in the case of very low baryon contamination, it is a natural extension of Ruffini et al. (2013b) who considered finite wind profiles. It also finds direct application in the interpretation of the spectra of some GRBs in the context of the Fireshell model, see e.g. Ruffini et al. (2007) and references therein. Indeed, Muccino et al. (2013) analysed the short GRB090227B and interpreted the thermal first episode as an almost pure electron-positron-photon plasma reaching transparency. One has to keep in mind that the photospheric component of long duration (on the order of seconds) seen in some bursts cannot be explained within this model. It is usually interpreted within the relativistic wind model of Paczynski (1990).

B.2. Approximate solution of the relativistic hydrodynamics equations

Starting from the laws of energy and momentum conservation, and by imposing the equation of state $\epsilon_c = 3P$, one finds:

$$\frac{\partial}{\partial t}\left(4v\gamma^2\epsilon\right) + \frac{\partial}{\partial r}\left[(4v^2\gamma^2+1)\epsilon\right] + \frac{8v^2\gamma^2\epsilon}{r} = 0 \tag{B.2.1}$$

$$\frac{\partial}{\partial t}\left[(4\gamma^2-1)\epsilon\right] + \frac{\partial}{\partial r}\left(4v\gamma^2\epsilon\right) + \frac{8v\gamma^2\epsilon}{r} = 0, \tag{B.2.2}$$

where v is such that $\gamma = (1-v^2)^{1/2}$.

Bisnovatyi-Kogan and Murzina (1995) makes the following change of variables $\xi = t - r$, $g = \gamma^2/r^2$, $\epsilon_1 = \epsilon r^4$, $\epsilon_1 = \epsilon_{10}\exp(-4\tau)$, $g = g_0\exp(2\phi)$, $y_1 = y/(2g) = r/(2\gamma^2)$, $x_1 = \tau - (\phi/\sqrt{3})$ and $x_2 = \tau + (\phi/\sqrt{3})$. Then the

solution is extracted from the value of two functions f and $\tilde{f}$ such that:

$$f = e^{-(1+\sqrt{3}/2)x_1} e^{-(1-\sqrt{3}/2)x_2} \xi \tag{B.2.3}$$

$$= f_1(0) I_0(\sqrt{x_1 x_2}) + \int_0^{x_2} \frac{df_1(x_2')}{dx_2'} I_0(\sqrt{x_1(x_2 - x_2')}) dx_2' \tag{B.2.4}$$

$$+ \int_0^{x_1} \frac{df_2(x_1')}{dx_1'} I_0(\sqrt{(x_1 - x_1')x_2}) dx_1', \tag{B.2.5}$$

$$\tilde{f} = e^{-(1+\sqrt{3}/2)x_1} e^{-(1-\sqrt{3}/2)x_2} y_1 \tag{B.2.6}$$

$$= \tilde{f}_1(0) I_0(\sqrt{x_1 x_2}) + \int_0^{x_2} \frac{d\tilde{f}_1(x_2')}{dx_2'} I_0(\sqrt{x_1(x_2 - x_2')}) dx_2' \tag{B.2.7}$$

$$+ \int_0^{x_1} \frac{d\tilde{f}_2(x_1')}{dx_1'} I_0(\sqrt{(x_1 - x_1')x_2}) dx_1', \tag{B.2.8}$$

where I_0s is the Bessel function and f_1, f_2, $\tilde{f}_1$ and $\tilde{f}_2$ are the following boundary functions

$$f_1(x_2) = (\xi_{a1} + \xi_a e^{-kx_2}) e^{-(1-\sqrt{3}/2)x_2}, \tag{B.2.9}$$

$$\tilde{f}_1(x_2) = (\xi_a y_a e^{-(1+k-\sqrt{3}/2)x_2}, \tag{B.2.10}$$

$$f_2(x_1) = \xi_b e^{-x_1} + \xi_{b1} e^{-(1+\sqrt{3}/2)x_1}, \tag{B.2.11}$$

$$\tilde{f}_2(x_1) = (2 - \sqrt{3}) \xi_b e^{-x_1}, \tag{B.2.12}$$

where ξ_a, ξ_{a1}, ξ_b, and ξ_{b1} are:

$$\xi_a = (2 - \sqrt{3}) \frac{\xi_b}{\xi_a}, \tag{B.2.13}$$

$$\xi_{a1} - \xi_b = \xi_b - \xi_a = \xi_0 \tag{B.2.14}$$

$$= \sqrt{\frac{\delta_{fit}}{2g_0}} \sqrt{\frac{1}{2 - \sqrt{3}}} \left(1 + \frac{2 - \sqrt{3}}{2 + \sqrt{3}} \frac{k - \sqrt{3}}{k}\right), \tag{B.2.15}$$

where finally we imposed $\xi_{a1} = 0$ and $\xi_0 = |\xi_{b1}|$.

The hydrodynamic profile is obtained in the following way: firstly, the equation $\xi - (1/y) - t = 0$ links x_1 and x_2 at a given time by using Eq.(B.2.3) to Eq.(B.2.3), secondly the functions f and $\tilde{f}$ are mapped for a given interval of x_1 (and correspondingly x_2), and finally the hydrodynamical profile is determined by using

$$\epsilon = \frac{2\epsilon_{10} g_0 f \tilde{f}}{\xi r^3} \tag{B.2.16}$$

$$\Gamma = \sqrt{\frac{rf}{2\xi\tilde{f}}}, \tag{B.2.17}$$

where r and ξ are computed using Eq.(B.2.3).

B.3. Equation of state

To obtain a realistic profile of the shell, we used the solution of Bisnovatyi-Kogan and Murzina (1995) described below, that is valid for the ultra-relativistic equation of state $\epsilon = 3P$, where ϵ is the co-moving energy density and P is the pressure, and ultra-relativistic expansion velocity $v \approx c$. For an optically thick system of electron-positron pairs and photons, all particles give a contribution to the equation of state.

Assuming thermal equilibrium, one can find the equation of state in this system. It is presented in Fig.B.1 for different values of the dimensional co-moving temperature T.

At high temperatures $k_B T \gg m_e c^2$, where k_B is the Boltzmann constant, m_e the electron mass and c the speed of light, the equation of state is ultra-relativistic. At non-relativistic temperatures ($k_B T \ll m_e c^2$), the equation of state is also ultra-relativistic since the contribution of non-relativistic electron-positron pairs is small (see also Goodman (1986)). As can be seen from Fig.B.1 the maximum deviation from the value $1/3$ is achieved at the temperature $k_B T = 0.33 m_e c^2$ and it amounts for 12%. This fact justifies the ultra-relativistic equation of state in the optically thick electron-positron-photon plasma. It is also known that such plasma, being optically thick, expands with acceleration and reaches ultra-relativistic velocity of expansion before becoming transparent (c.f. Goodman (1986)). Consequently the solution of Bisnovatyi-Kogan and Murzina (1995) can be applied to this system.

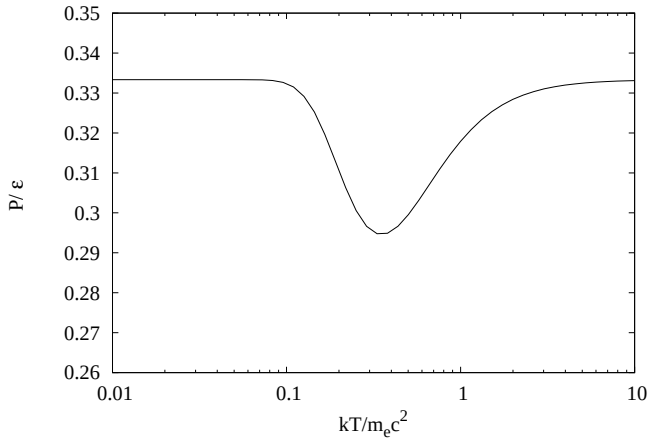

Figure B.1.: Equation of state of the optically thick electron-positron-photon plasma as a function of the co-moving temperature T.

The analytical solution of the relativistic hydrodynamic equations given by Bisnovatyi-Kogan and Murzina (1995) allows to compute the Lorentz factor Γ and co-moving energy density ϵ at arbitrary laboratory time t and laboratory radius r:

$$\epsilon(t,r) = \frac{2\epsilon_{10} g_0 f(t,r)\tilde{f}(t,r)}{\xi r^3}, \tag{B.3.1}$$

$$\Gamma(t,r) = \sqrt{\frac{rf(t,r)}{2\xi\tilde{f}(t,r)}}, \tag{B.3.2}$$

where f and $\tilde{f}$ are given in section B.2, $\xi = ct - r$ measures the depth within the shell with g_0 and ϵ_{10} being parameters of the solution[1]. For large t, the solution describes a thin shell with constant laboratory width (see Piran et al. (1993); Ruffini et al. (1999, 2000)) propagating radially with $\Gamma \gg 1$, see Fig.B.2.

From the co-moving energy density, the co-moving temperature can be found as $T(t,r) = (c\epsilon(t,r)/(4\sigma_{SB}))^{1/4}$, where σ_{SB} is the Stefan-Boltzmann constant. Electron-positron-photon plasma with macroscopic size, gets transparent when the temperature decreases to the value $k_B T \sim 0.04 m_e c^2$

[1]The formula (3.21) for the Lorentz factor in the Bisnovatyi-Kogan and Murzina (1995) paper contains a misprint.

Ruffini et al. (2013b). At such non-relativistic temperature, the co-moving number density of pairs is given by (e.g. Sampson (1962)):

$$n_c^{\pm}(t,r) = 4\left(\frac{m_e}{h}\right)^3 \left(\frac{2\pi k_B T(t,r)}{m_e}\right)^{\frac{3}{2}} \exp\left(-\frac{m_e c^2}{k_B T(t,r)}\right), \tag{B.3.3}$$

where h is the Planck constant.

B.4. Computation of observed flux and spectrum

The transparency of the shell occurs when its optical depth for Compton scattering reaches unity. For a shell, it writes Ruffini et al. (2013b):

$$\tau(t,r,\phi_0) = \int_r^{R_{out}} \sigma_T n_c^{\pm} \Gamma(1-\beta\cos\phi)\frac{dR}{\cos(\phi)}, \tag{B.4.1}$$

where ϕ is the laboratory angle between the radial direction and the four momentum of the photon, ϕ_0 is that angle at the initial radius from which the integration is performed, β is the speed in units of the speed of light, r is the radius of emission of the photon and R_{out} is the radius at which the photon leaves the shell. The integration has to be performed along the world line of a photon.

Ref. Ruffini et al. (2013b) proposed two different approximations to compute the light-curves and the spectra: the fuzzy and the sharp photosphere ones. In the sharp photosphere approximation, the energy contained in a small volume is assumed to be released instantly at the time, radius and angle given by the condition $\tau(t,r,\phi) = 1$. Then the laboratory energy dE emitted in a laboratory solid angle $d\Omega$ is equal to $dE = 3\epsilon dV d\Omega/(8\Lambda^4)$, where $\Lambda = \Gamma(1-\beta\cos\phi)$ is the Doppler factor, dV is the laboratory volume associated with the emission. In order to compute the light-curves, dE is integrated over the photosphere for a given arrival time $t_a = t_e - \cos(\phi)(r_e/c)$, where r_e and t_e are the radial position and the laboratory time of the emitting region, $t_a = 0$ for a photon emitted at the origin. The spectra are computed assuming that the energy is released with the Planck spectrum in the co-moving frame, with the co-moving temperature given by the co-moving energy density at the point of emission. Then the intensity of radiation in the frequency range

$d\nu_l$, solid angle $d\Omega_l$ is given by:

$$I_\nu d\nu_l d\Omega_l = \int \frac{2h}{c^2} \frac{\nu_l^3 d\nu_l d\Omega_l dA}{\exp\left(\frac{h\nu_l}{kT_l}\right) - 1},$$

where the quantities with index l are measured in the laboratory frame, $d\Omega_l$ measures the angular size of the detector. The integration over the surface dA is performed to take into account the emitting area at the photosphere. Due to the exponential dependence of the optical depth on the radial coordinate (see Eq.(B.3.3) and Eq.(B.4.1)) the transition from the optically thick to the optically thin condition is indeed sharp. This fact justifies the sharp photosphere approximation in this problem.

The basis of the fuzzy photosphere approximation is the transfer equation for the specific intensity I_ν along the ray. Its formal solution is (see e.g Eq.(1.29) of Rybicki and Lightman (1979)):

$$I_\nu = I_\nu(0)\exp(-\tau_\nu) + \int_0^{\tau_\nu} \exp(\tau_\nu - \tau_\nu^{'}) S_\nu d\tau_\nu^{'} \tag{B.4.2}$$

where S_ν is the source function. At large optical depth, it is well known that the source function for scattering corresponds to a thermal isotropic distribution of photon, with temperature $T(r,t)$. In addition, for energy dominated outflows, Beloborodov (2011) showed that coherent scattering preserves the isotropy of the radiation field, together with the blackbody shape of the spectrum, like if radiation is propagating in vacuum. In fact, a freely propagating photon in an accelerating shell with $\Gamma \propto r$ does not change its angle in the co-moving frame. This later condition is actually used to obtain the approximate analytic solution by Bisnovatyi-Kogan and Murzina (1995). Since the radiation diffusion is negligible for accelerating shells Ruffini et al. (2013b), we can use the source function as a thermal Planck function $S_\nu = B_\nu(T(t,r))$ and Eq.(B.4.2) can be integrated numerically. Then the flux at a given arrival time is obtained by integration over the frequencies weighted by the surface of emission, while the total flux is obtained by additional integration over the arrival time.

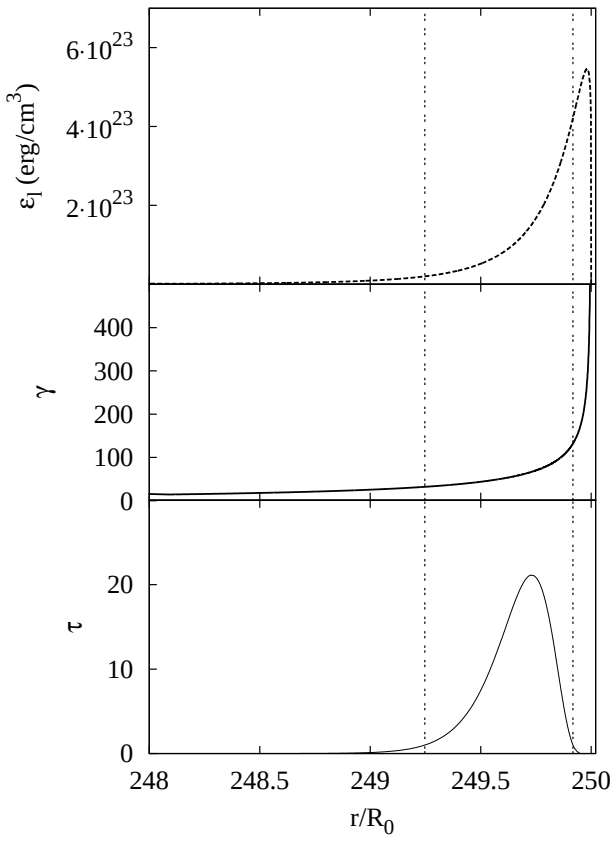

Figure B.2.: Laboratory energy density (top), Lorentz factor (middle) and optical depth (bottom) radial profiles at $t = 250R_0/c$. The two vertical lines represent the radii at which $\tau(t, r, \phi = 0) = 1$. The main part of the energy has already been emitted, as can be seen from the top panel.

B.5. Numerical results

We now apply the approximate analytic solution of relativistic hydrodynamic equations obtained by Bisnovatyi-Kogan and Murzina (1995) to optically thick electron-positron plasma. The parameters entering Eq.(B.3.1) and Eq.(B.3.2) can be related to the total energy E_0 confined to a sphere of radius R_0 as follows:

$$R_0 = h_{shell} = 3\sqrt{\frac{\delta_{fit}}{g_0}}, \tag{B.5.1}$$

$$E_0 = 4\pi g_0 \epsilon_{10} \times 1.3 h_{shell}, \tag{B.5.2}$$

$$\delta_{fit} = 2.2 \times 10^{-2}. \tag{B.5.3}$$

We perform the computation for $E_0 = 10^{54}$erg and $R_0 = 10^8$cm, corresponding to the initial temperature $k_B T_0 = 6.5$MeV. Such parameters are typical within the Fireshell model of GRBs (see e.g. Ruffini et al. 2007). We fixed the parameter k to the value $1 + \sqrt{3}/2$, as prescribed by Bisnovatyi-Kogan and Murzina (1995).

The radial profiles of the laboratory energy density ϵ_l, Lorentz factor and optical depth are displayed in Fig.B.2 at $t = 250 R_0/c$. Since the solution of Bisnovatyi-Kogan and Murzina (1995) does not reproduce the separation between the front of the shell and the light surface, the relative position of a photon inside the shell does not change substantially with time if it propagates radially. The shell is photon thick Ruffini et al. (2013b): photons decouple because locally the pairs density decreases too fast to sustain collisions.

The dependence of the optical depth on ξ at a given laboratory time t follows closely the variation of the co-moving energy density: from the outer boundary toward the centre it firstly increases and then decreases. This behaviour has to be contrasted with the one found by Ruffini et al. (2013b) for a simple shell profile of relativistic wind with finite duration: the optical depth as a function of ξ increases up to a saturation value from which it stays constant up to the inner boundary of the outflow. This implies that the emission time t_e on the line of sight is increasing with the depth ξ inside the shell. In our more complex profile the outer and inner part of the shell become transparent before the central part: there are two photospheres for a given laboratory time t_e. However, at a given arrival time t_a there is only one photosphere: the emission from the inner part of the shell arrives to the observer

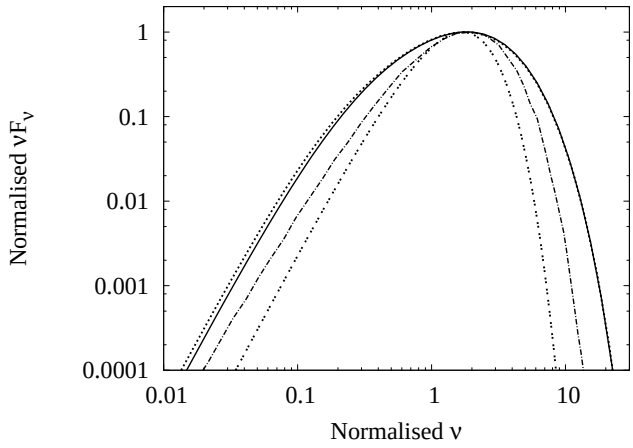

Figure B.3.: Time integrated spectra: solid line-fuzzy approximation, dotted line-sharp approximation, dotted-dashed line-spectrum from Goodman (1986) and double-dashed line-Planck spectrum. For the sake of comparison these two last ones have been shifted to lower energy by a factor 2.3.

later.

Fig.B.3 displays the time-integrated spectra from sharp and fuzzy approximations, as well as the one obtained by Goodman (1986) which has been shifted to lower energy by a factor 2.3. He obtained the observed spectrum by integration both over angles of emission and over the radial coordinate at a fixed laboratory time corresponding to the moment of transparency on the line of sight, see the lower panel of Fig.B.2. This region of integration is shown in grey in Fig.B.4. In our computation the dynamics of the photosphere is taken into account explicitly: for each arrival time the spectrum from the surface defined by $\tau(r, t, \phi_0) = 1$ is computed. Eq.(B.4.1) shows that the optical depth increases with ϕ_0, so the points satisfying $\tau = 1$ for a given ξ are shifted to larger time and radius than the one on the line of sight. This surface is displayed schematically by Fig.B.4. Finally an integration is performed over arrival times.

This explains the two differences between our result and the one of Goodman. Firstly the time integrated spectrum is broader at low energy because the observed temperature of a fluid element out of the line of sight is decreased in our computation. Secondly the peak energy is shifted to lower energy because of the joint effect of increased volume of emission and de-

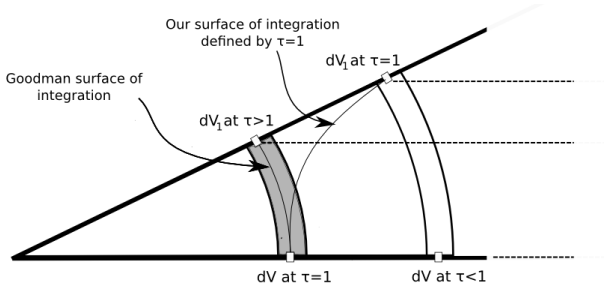

Figure B.4.: Illustration of the difference in computation methods by Goodman and ours. The grey region corresponds to the shell at the laboratory time for which the optical depth of a photon propagating radially equals unity. It is the region in which the spectrum is computed by Goodman (1986). The shell is also represented at a larger laboratory time with the curve linking dV to dV_1 being a schematic representation of the $\tau = 1$ surface at a given depth ξ.

creased observed temperature out of the line of sight.

The low energy slopes are close in all cases and are dominated by the high latitude emission. On the contrary the high energy part of the spectrum is dominated by the photons emitted along the line of sight, for which the profile of temperatures plays an important role.

The light-curves for sharp and fuzzy approximations are presented on Fig.B.5. Both approximations give close results, even if the raising part is not resolved for the sharp photosphere approximation. Because of the narrow profile of the laboratory energy density, the emission reaches its maximum and shortly later decreases: there is no plateau emission lasting the light-crossing time as reported by Ruffini et al. (2013b) for a finite wind. That is because they considered a different radial profile for the shell. Nevertheless the time needed to emit 90% of the energy is of the order of R_0/c.

B.6. Discussion

In our computation we used the simplifying assumption that the pairs recombine efficiently, so their number density is given everywhere by Eq.(B.3.3). Nevertheless Grimsrud and Wasserman (1998) studied their recombination by considering the Boltzmann equation in the case of a static and infinite

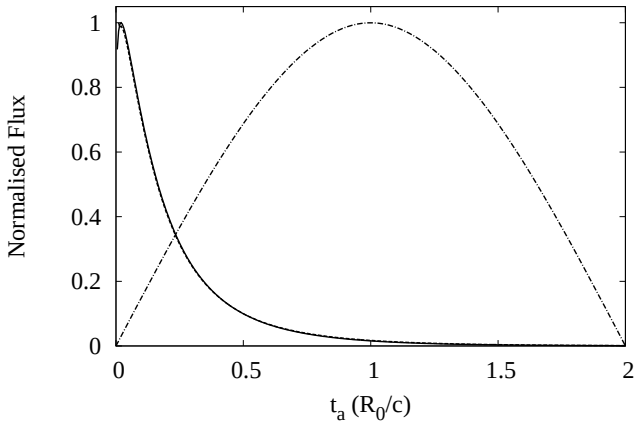

Figure B.5.: Light-curves for fuzzy (continuous curve) and sharp (dashed curve) photosphere. They are nearly undistinguishable. For comparison the light-curve that would be obtained from an optically thin ball of radius R_0 uniformly filled by isotropic radiation is displayed by the dash-dotted line.

wind. They showed that the pairs recombination process freezes out at the radius $R_{\pm}$, smaller than R_{ph}. Above $R_{\pm}$, the co-moving pair density decreases proportionally to r^{-3}. The same effect is taken into account in the Fireshell model, see Ruffini et al. (1999, 2000). The ratio between the optical depth for Compton scattering and pairs recombination process is:

$$\frac{\tau_{\pm}}{\tau} = \frac{\sigma_{\pm}}{\sigma_T} \approx 0.8,$$

where $\sigma_{\pm}$ is the cross section for the pairs recombination process. The co-moving temperature at $R_{\pm}$ can be found by solving Eq.(54) of Grimsrud and Wasserman (1998). We found $k_B T_{\pm} \sim 0.042 m_e c^2$, being close from the photosphere where the temperature is $k_B T \sim 0.040 m_e c^2$ (see e.g. Ruffini et al. (2013b).

It implies that the optical depth increases when considering the freeze out of pairs recombination process, which leads to a small increase in the value of R_{ph}. Secondly the optical depth for the pairs at R_{ph} is given by:

$$\tau_{\pm\gamma}(R_{ph}) = \tau(R_{ph}) \times \frac{n_{\gamma}}{n_{\pm}} \gg 1,$$

where the inequality holds because $\tau(R_{ph}) = 1$ by definition, and $n_\gamma \gg n_\pm$. It follows that even when the radiation streams freely, the pairs are still strongly coupled to it and keep being accelerated by the radiative pressure: their Lorentz factor $\Gamma_\pm$ increases proportionally to r. For such outflow, Beloborodov (2011) showed that the isotropy of the radiation field is preserved in the accelerating co-moving frame of pairs and that its temperature drops as r^{-1}. This means that the observed temperature is constant, and no effect on the spectrum is expected.

The last point left to be discussed is the influence of the profile of temperatures within the shell. Aksenov et al. (2013) considered the decoupling of photons from ultra-relativistic coasting winds with different profiles for the electron temperature. They showed that the spectral index at low energy depends strongly on the chosen profile. Such kind of temperature dependence naturally arises when considering a realistic profile for the expanding plasma. Nevertheless the position of a photon in the shell does not change substantially during the expansion below R_{ph} for accelerated outflows, so no influence of the temperature profile on the photon Comptonization close to the photosphere is expected in the spectrum. At larger radii when the radiation streams freely and crosses the shell, the Compton parameter y is much smaller than unity as the temperature is not relativistic and $\tau < 1$, hence distortion of the spectrum is small.

B.7. Conclusion

We have considered the analytical solution from Bisnovatyi-Kogan and Murzina (1995) for the spherical expansion of a large amount of energy in a small volume and applied it to electron-positron plasma initially confined to a macroscopic volume. Considering the dynamical evolution of the shell, we computed the flux and the energy distribution of the photospheric emission as seen by a distant observer at rest in the laboratory frame.

We found that the spectrum is broader than the Planck one and than the one of Goodman (1986) and shifted to lower energy, because of the integration over impact parameters (or angles between the line of sight and the radial direction) in the dynamical photosphere. The numerical results obtained by the sharp and fuzzy photosphere approximations coincide.

We additionally presented the light-curve from such event, showing that

the maximum of the emission is reached in a short time scale compared to the light-crossing time of the shell R_0/c. Then the flux decays sharply.

C. Spreading of ultrarelativistically expanding shell: an application to GRBs

C.1. Introduction

Optically thick pair plasma with baryon loading is assumed to power GRBs in many models considered in the literature, see, e.g., Piran (1999), Meszaros (2006), Ruffini et al. (2009). Such plasma is self accelerated to large bulk Lorentz factors due to initial energy dominance. Due to relativistic kinematics in laboratory reference frame it forms a shell with width approximately equal to its initial size. When the plasma becomes transparent to Compton scattering a flash of radiation is emitted. In the literature such emission is often associated with so-called precursors (Lazzati, 2005). In the fireshell model (Ruffini et al., 2009) this emission is called the Proper GRB (P-GRB).

For typical baryonic loading parameters of observed GRBs $10^{-3} < B < 10^{-2}$, where $B = Mc^2/E_0$, Mc^2 is total baryonic rest mass energy, E_0 is total energy released in the source of GRB, the fraction of energy emitted at transparency can reach several percents of the total energy. Considering that typical duration of long GRBs is of the order of hundreds of seconds, and P-GRB typically lasts for less than few seconds (Ruffini et al., 2009) luminosities of both events are comparable in magnitude.

Early treatments assuming the absence of baryons and thin shell approximation (Bianco et al., 2001), and non instantaneous energy release (Ruffini et al., 2005b) produced estimations of P-GRBs duration $\sim 10^{-2} - 10^{-1}$ sec for the progenitor mass range $10 - 10^3 M_\odot$, much larger than the naive estimation of the gravitational collapse time $\sim GM/c^3 \simeq 5 \cdot 10^{-6} M/M_\odot$ sec, where G is Newton's constant, M is black hole mass, c is the speed of light. Observed durations of P-GRBs (Ruffini et al., 2009) of most energetic GRBs is of the order of several seconds. Main purpose of this paper

is to outline a possibility of resolution of this tension considering different mechanisms of spreading of ultrarelativistically expanding shell.

The paper is organized as follows. In Sec. 2 the hydrodynamic phase of GRB is discussed, hydrodynamical spreading mechanism is recalled, and results of its application to GRBs are shown. In Sec. 3 the concept of thermal spreading is introduced, evaluation of spreading for relativistic Maxwellian distribution function is performed, and the results of thermal spreading computation are applied to GRBs. Discussion of the spreading effects on the duration of P-GRB and conclusions follow in the last section.

C.2. Hydrodynamic phase and optical depth of GRBs

Energy, entropy and baryonic number conservation laws for each differential subshell of ultrarelativistically expanding shell imply (Ruffini and Vereshchagin, 2013)

$$\begin{aligned} (p+\rho)\Gamma^2 r^2 dr &= \text{const}, \\ \sigma\Gamma r^2 dr &= \text{const}, \\ n\Gamma r^2 dr &= \text{const}, \end{aligned} \tag{C.2.1}$$

where ρ and p are respectively comoving energy density and pressure, σ and n are respectively comoving entropy and comoving baryon number density, Γ is Lorentz factor, and r is laboratory radial coordinate. Assuming polytropic equation of state

$$p = (\gamma - 1)\,\rho, \quad \sigma = \rho^{\gamma}, \tag{C.2.2}$$

where γ is the thermal index, from (C.2) each differential subshell has

$$\Gamma \propto r, \quad \rho \propto r^{-4}, \quad n \propto r^{-3}, \tag{C.2.3}$$

during the energy dominated phase with $\gamma = 4/3$. The transition from energy to matter domination with $\gamma = 1$ occurs at $R_{eq} \simeq R_0/B$, where R_0 is initial size of the energy dominated region. During the matter dominated phase for $r \gg R_{eq}$

$$\Gamma \simeq B^{-1} = \text{const}, \quad \rho \propto r^{-2}, \quad n \propto r^{-2}. \tag{C.2.4}$$

In Ruffini et al. (2013b) we computed the optical depth and dynamics of P-GRB for the case when Γ is constant across the shell. General expression for the optical depth of the shell is

$$\tau = \int_R^{R^*} \sigma_T n \Gamma (1-\beta) dr \tag{C.2.5}$$

where σ_T is Thomson's cross section and R^* is the radius at which light ray emitted from the inner boundary of the shell at radius R crosses its outer boundary. For large baryonic loading with

$$B \gg 1 \times 10^{-3} E_{54}^{-1/5} R_8^{2/5}, \tag{C.2.6}$$

where $R_0 = R_8 10^8$ cm, $E_0 = E_{54} 10^{54}$ erg, optical depth of the shell is

$$\tau = \tau_0 \left(\frac{R_0}{R} \right)^2, \tag{C.2.7}$$

where $\tau_0 = \sigma_T n_0 R_0$, n_0 is given by equation (C.2.11) with $r_0 = R_0$. Equation (C.2.7) correspond to the photon thin asymptotics (Ruffini et al., 2013b) of equation (C.2.5) defined by the condition $R^* - R = 2\Gamma^2 R_0 \ll R$.

The observed duration of P-GRB is determined in this asymptotics by the process of radiative diffusion (Ruffini et al., 2013b)

$$\Delta t_a = \frac{t_D}{2\Gamma^2} \simeq 0.12 E_{54}^{1/3} B_{-2}^{5/3} R_8^{1/3} \text{ s}, \tag{C.2.8}$$

where $B = B_{-}2 10^{-2}$ and time of diffusion t_D was found by solution of radiative transfer equation.

All these results are derived assuming constant Lorentz factor across the shell. Hence the width of the shell remains constant during its expansion. This fact has been used within the fireshell model and termed as the "constant thickness approximation", provided that the baryon loading is not too heavy $B \leq 10^{-2}$ (Ruffini et al., 2000). Hydrodynamic analytical (Shemi and Piran (1990), Bisnovatyi-Kogan and Murzina (1995)) and numerical (Piran et al. (1993), Mészáros et al. (1993)) calculations show that Lorentz factor gradient is developing during shell expansion that leads to spreading of the shell at sufficiently large radii at the matter dominated phase.

At this phase of expansion each differential subshell is expanding with al-

most constant speed $v = \beta c \simeq c(1 - 1/2\Gamma^2)$, so the spreading of the shell is determined by the radial dependence of the Lorentz factor $\Gamma(r)$. In a variable shell there can be regions with $\Gamma(r)$ decreasing with radius and $\Gamma(r)$ increasing with radius. At sufficiently large radii only the regions with increasing Γ contribute to the spreading of the shell. From equations of motion of external and internal boundaries of this region we obtain (Piran et al., 1993) the thickness of the region as function of radial position of the region

$$l(R) = R_0 + \frac{R}{2}\left(\frac{1}{\Gamma_i^2} - \frac{1}{\Gamma_e^2}\right), \tag{C.2.9}$$

where Γ_e and Γ_i are Lorentz factors at external and internal boundaries, R_0 is the width of the region at small R, R being the radial position of inner boundary. Let us consider such a region in two limiting cases:

a) when relative Lorentz factor difference is strong, $\Delta\Gamma = \Gamma_e - \Gamma_i \gtrsim \Gamma_i$;

b) when relative Lorentz factor difference is weak, $\Delta\Gamma = \Gamma_e - \Gamma_i \ll \Gamma_i$.

In the case a) the second term in parenthesis in equation (C.2.9) can be neglected, and we obtain that the spreading becomes efficient at $R > R_b = 2\Gamma_i^2 R_0$, see Mészáros et al. (1993) and Piran et al. (1993). In the case b) we find the corresponding critical radius of hydrodynamical spreading $R_b = (\Gamma_i/\Delta\Gamma)\Gamma_i^2 l \gg \Gamma_i^2 R_0$. From equation (C.2.9) one can see that in both cases for $R \gg R_b$ width of the shell is increasing linearly with radius $l(R) \simeq (\Delta\Gamma/\Gamma_i)R/\Gamma_i^2$.

The discussion above corresponds to the case b) since for weak Lorentz factor difference $R_b \gg R_{tr}$. In what follows we focus on the case a) and derive corresponding relations assuming strong relative Lorentz factor difference across the shell. Let us take an element of fluid with constant number of particles dN in the part of the shell with gradient of Γ. Internal boundary of the element is moving with velocity v, and external one is moving with velocity $v + dv = v + \frac{dv}{dr}dr$, where dr is the differential thickness at some fixed laboratory time $t = 0$ and derivative dv/dr is taken at the same laboratory time. Then at time t the width of the element is $dl = dr + tdv$, its radial position is $R(t) = r_0 + vt$, where r_0 ia initial radial position of the element,

and corresponding laboratory density is

$$n_l = \frac{dN}{dV} = \frac{dN}{4\pi R^2 \left(1 + t\frac{dv}{dr}\right) dr} = n_0 \frac{r_0^2}{R^2 \left(1 + t\frac{dv}{dr}\right)}, \tag{C.2.10}$$

where

$$n_0 = \frac{dN}{dV_0} = \frac{dN}{4\pi r_0^2 dr}. \tag{C.2.11}$$

At large enough t using $R \simeq ct$ we have in contrast with (C.2.4)

$$\Gamma \simeq \text{const}, \quad \rho \propto r^{-4}, \quad n \propto r^{-3}, \tag{C.2.12}$$
$$R \gg R_b = \frac{1}{\Gamma^3} \left(\frac{d\Gamma}{dr}\right)^{-1}.$$

In order to compute the integral (C.2.5) we need to find the expression for baryonic number density along the light ray. Taking into account hydrodynamical spreading (C.2.9) we obtain

$$n = \frac{n_0}{\Gamma} \left(\frac{R_0}{r}\right)^2 \frac{1}{1 + \frac{2r}{\Gamma}\frac{d\Gamma}{dr}}, \tag{C.2.13}$$

that is exact in ultrarelativistic limit. Notice the difference between equations (C.2.13) and (C.2.10): in the former case $d\Gamma/dr$ is computed along the light ray, while in the latter case dv/dr is computed along the radial coordinate at fixed laboratory time. The expression (C.2.13) reduces to equation (C.2.4) when $d\Gamma/dr = 0$. Instead when the second term in the denominator of the expression (C.2.13) dominates, namely when $r \gg \Gamma(d\Gamma/dr)^{-1}$, density radial dependence coincides with the one given by relations (C.2.12).

An estimate for $d\Gamma/dr$ can be given for strong relative Lorentz factor difference $\Delta\Gamma \sim \Gamma$ in the shell

$$\frac{d\Gamma}{dr} \sim \frac{\Delta\Gamma}{\Delta r} \sim \frac{\Gamma}{2\Gamma^2 R_0} = \frac{1}{2\Gamma R_0}, \tag{C.2.14}$$

where $\Delta r \sim 2\Gamma^2 R_0$ is the distance inside the shell along the light ray. Numerical results from Piran et al. (1993), Mészáros et al. (1993) and analytical ones from Bisnovatyi-Kogan and Murzina (1995) support this estimate.

Integrating expression (C.2.14) we obtain Lorentz factor dependence on radial coordinate along the light ray

$$\Gamma(r) \sim \sqrt{\frac{r-R}{R_0}}. \tag{C.2.15}$$

Since we are interested in the asymptotics when the hydrodynamical spreading is essential, we can assume in the integral (C.2.5) $r \gg R$ and $R^* \gg R$. Under these conditions the optical depth is

$$\tau = \frac{\tau_0}{8}\left(\frac{R_0}{R}\right)^2. \tag{C.2.16}$$

This result coincide with equation (C.2.7) up to a numerical factor. However its physical meaning is different. It represents photon thick asymptotics of equation (C.2.5), since $R^* \gg R$.

Transparency radius is defined by equating (C.2.16) to unity and is given by

$$R_{tr} \simeq \left(\frac{\sigma_T B E_0}{32\pi\, m_p c^2}\right)^{1/2} = 2\times 10^{14} B_{-2}^{1/2} E_{54}^{1/2}\ \text{cm}, \tag{C.2.17}$$

where m_p is proton mass. At the radius of transparency the width of the shell (C.2.9) spreads up to

$$\Delta l_{hydr} \simeq 10^{10}\, B_{-2}^{1/2}\, E_{54}^{1/2}\, \Gamma_2^{-2}\ \text{cm}, \tag{C.2.18}$$

where $\Gamma_i = 100\Gamma_2$.

In this case radiative diffusion is irrelevant and duration of P-GRB is then given by the time of arrival of photons emitted from the shell all the way up to R_{tr}

$$\Delta t_a \simeq \frac{R_{tr}}{2\Gamma_i^2 c} = 0.3\, B_{-2}^{1/2}\, E_{54}^{1/2}\, \Gamma_2^{-2}\ \text{s}. \tag{C.2.19}$$

In contrast to equation (C.2.8) in the case of strong Lorentz factor difference, namely with $\Gamma_i < (2B)^{-1}$, this duration can be of the order of several seconds with agreement with observations.

C.3. Thermal spreading

We now determine the velocity spread of particles as a function of comoving temperature T and bulk Lorentz factor Γ for relativistic Maxwellian distribution. Based on this result we compute the value of thermal spreading of expanding shell.

The distribution of particles in the momentum space in the laboratory frame is a Lorentz-boosted Maxwellian

$$f(p_x, p_y, p_z) = A \exp\Bigg(-\frac{1}{mc\theta}\Big[m^2c^2 + {p_y}^2 + {p_z}^2 + \Big(\Gamma p_x - \sqrt{(\Gamma^2 - 1)(m^2c^2 + \mathbf{p}^2)} \Big)^2 \Big]^{1/2} \Bigg), \quad \text{(C.3.1)}$$

where we assumed that the relative motion of the frames is along their x-axes and $\theta = kT/mc^2$ is dimensionless comoving temperature.

Velocity dispersion in the x-direction is

$$D(v_x) = M(v_x^2) - M^2(v_x), \quad \text{(C.3.2)}$$

where $M(\chi)$ denotes the average value of χ, which is defined by the convolution with the distribution function (C.3.1)

$$M(\chi) = \frac{\int d^3\mathbf{p}\, \chi(\mathbf{p}) f(\mathbf{p})}{\int d^3\mathbf{p}\, f(\mathbf{p})}. \quad \text{(C.3.3)}$$

The above written integrals cannot be computed analytically, but their numerical approximations can be found.

Numerical issues in the velocity dispersion calculations by (C.3.2) arise from the fact that for high Γ we need to subtract two numbers $M(v^2)$ and $M^2(v)$ which are very close to each other and to c^2. This leads to substantial reduction of accuracy. A different formula for dispersion

$$D(v_x) = M([v_x - M(v_x)]^2) \quad \text{(C.3.4)}$$

proves to be more convenient. The spread of particle velocities is then

$(\Delta v)_{therm} = \sqrt{D(v)}$.

For nonrelativistic comoving temperatures the correct asymptotics is

$$\left(\frac{\Delta v}{c}\right)_{\theta \ll 1} = \Gamma^{-2}\theta^{1/2}. \tag{C.3.5}$$

The case of ultrarelativistic comoving temperature ($\theta \gg 1$) is more interesting. Starting close to the maximal value $1/\sqrt{2}$, the velocity spread for $10 \lesssim \Gamma \lesssim \theta$ reaches approximately

$$\left(\frac{\Delta v}{c}\right)_{10 \lesssim \Gamma \lesssim \theta} \simeq \Gamma^{-3/2}, \tag{C.3.6}$$

which means that the dispersion is independent on the temperature. For $\Gamma \gg \theta$ the asymptotics (C.3.5) is restored just up to a multiplier close to unity

$$\left(\frac{\Delta v}{c}\right)_{1 \ll \theta \ll \Gamma} \simeq 1.16\,\Gamma^{-2}\theta^{1/2}. \tag{C.3.7}$$

Our results suggest that (C.3.6) gives absolute upper limit for the velocity spread, and temperature dependence of (C.3.5) and (C.3.7) reduce the spread even further.

Initial temperature of the plasma formed in the source of GRB can be estimated from its initial size $R_0 \sim 10^8$ cm and total energy released

$$10^{48}\ \text{erg} < E_0 < 10^{55}\ \text{erg}.$$

Assuming that the temperature is determined by e^+e^- pairs only

$$\frac{E_0}{V_0} = \frac{3E_0}{4\pi R_0^3} = aT_0^4 \tag{C.3.8}$$

we get for initial temperature

$$0.40 < \frac{kT_0}{m_e c^2} < 22. \tag{C.3.9}$$

At radiation dominated phase the comoving temperature of the plasma decreases as $T \simeq T_0 R_0/r$, at matter dominated phase as $T \simeq T_0 B^{1/3}(R_0/r)^{2/3}$.

Now we compute the thermal spreading at both phases.

For the first phase the reasonable approximation of Lorentz factor is

$$\Gamma(t) \simeq \sqrt{1 + \left(\frac{ct}{R_0}\right)^2}.$$

Due to the nature of Lorentz transformations in constantly accelerated frame the final spreading of the shell $\Delta l_1 = \int_0^t \Delta v \, dt$ appears to be finite even if we extend this phase infinitely in time, and the main part of the spreading is connected with initial part of motion with relatively small Γ.

While the temperature of protons in the source of GRB is nonrelativistic $\theta \ll 1$, velocity spread is given by (C.3.5) which in energy dominated phase leads to the spreading

$$\frac{\Delta l_1}{R_0} \lesssim 2.2\sqrt{\frac{kT_0}{m_p c^2}} = 0.18\, E_{54}^{1/8}\, R_8^{-3/8}. \tag{C.3.10}$$

In the matter dominated phase the additional spreading of the shell is

$$\frac{\Delta l_2}{R_0} \simeq 3B^{7/3}\sqrt{\frac{kT_0}{m_p c^2}}\left(\frac{R_{tr}}{R_0}\right)^{1/3} = \\ = 6.7 \cdot 10^{-4}\, E_{54}^{7/24}\, R_8^{-17/24}\, B_{-2}^{5/2}, \tag{C.3.11}$$

when $R_{tr} \gg R_0$. Comparing to the hydrodynamical spreading for reasonable GRB parameters the spreading coming from both (C.3.10) and (C.3.11) is negligible.

Note that velocity dispersion in any case does not exceed the value given by equation (C.3.6) with $\theta \gg 1$

$$\frac{\Delta l_1}{R_0} = \frac{1}{R_0}\int_0^{t_1} \Delta v(t) dt \lesssim \frac{1}{R_0}\int_0^{\infty} c\Gamma(t)^{-3/2} dt \simeq 2.6, \tag{C.3.12}$$

which gives an absolute maximum of the thermal spreading on the energy dominated phase.

C.4. Conclusions

In this paper we considered two mechanisms of spreading of relativistically expanding plasma shell. We also discuss their implications for the duration of electromagnetic signal from transparency of the plasma.

Firstly, following the proposal of Piran et al. (1993) hydrodynamical spreading of relativistically expanding shell is estimated. Secondly, thermal spreading is considered. Assuming relativistic Maxwellian distribution function we determined the velocity dispersion depending on temperature and the Lorentz factor of the bulk motion.

We then applied these results to GRBs within the framework of the fireshell model. It is shown that thermal spreading provides negligible spreading for typical parameters of GRBs. Instead, hydrodynamical spreading results in the increase of the duration of P-GRB. For nonspreading shells characterized by almost constant Lorentz factor distribution within the shell the duration of P-GRB is determined by the time of diffusion, see equation (C.2.8). If strong Lorentz factor difference is present within the shell, hydrodynamical spreading prevents occurrence of photon thin asymptotics and leads to duration of P-GRB given by equation (C.2.19).

Our results imply that for high enough baryon loading and energy of the burst the duration of the P-GRB is not determined by the initial size of the plasma R_0, but by the value of the hydrodynamical spreading, reaching up to several seconds.

D. Relativistic spotlight effect

Winds of high velocity particles moving outwards from their source are common in astrophysics: the best known example is stellar wind, see e.g. Lamers and Cassinelli (1999). Winds may exhibit relativistic velocities as in cases of active galactic nuclei Faucher-Giguère and Quataert (2012), gamma ray bursts Meszaros (2006) or pulsars Kirk et al. (2009).

It is well known that the mean free path of photons in relativistically moving medium is anisotropic, see e.g. (Rybicki and Lightman, 1979, §4.9). For relativistic wind this implies a peculiar shape of the photosphere seen by a distant observer Abramowicz et al. (1991). In particular, a steady spherical wind with constant radial velocity has the photosphere $r = r_{ph}(\theta)$ given by Pe'er (2008); Beloborodov (2011)

$$r_{ph}(\theta) = \tau_0 R_0 \left(\frac{\theta}{\sin\theta} - \beta \right), \tag{D.0.1}$$

where r is radius and θ is the polar angle around the line of sight of the observer, $\tau_0 = \sigma n_0 R_0$, σ is scattering cross section, $n(r) = n_0 (r/R_0)^{-2}$ is the laboratory density of the wind with constant radial velocity $v = \beta c$, c is the speed of light, n_0 is the density at the base of the wind with radius R_0. The value of radius $R_{ph} = r_{ph}(\theta = 0)$ on the line of sight is referred to as photospheric radius of the wind $R_{ph} = \tau_0 R_0 (1 - \beta) \simeq \tau_0 R_0 / (2\Gamma^2)$, where the last equality holds for large bulk Lorentz factor Γ of the wind, $\Gamma = \left(1 - \beta^2\right)^{-1/2} \gg 1$. In what follows we assume this is always the case.

However, only a small part of the entire photosphere within the relativistic beaming angle $\theta_b = 1/\Gamma$ around the line of sight has the radius $r_{ph}(\theta) \sim R_{ph}$. For $\theta \gg \theta_b$ the radial coordinate of the photosphere is much larger, $r_{ph}(\theta) \sim \tau_0 R_0 \simeq \Gamma^2 R_{ph}$. Hence the photosphere of the relativistic wind described by Eq. (D.0.1) is concave due to a narrow dip along the line of sight. This specific shape of the photosphere plays a crucial role in determination of observational properties of emission originating at the photosphere, see

e.g. Bégué et al. (2013). In fact, almost all radiation originating from the optically thick region of the wind comes to the observer from the part of the photosphere within the relativistic beaming angle around the line of sight.

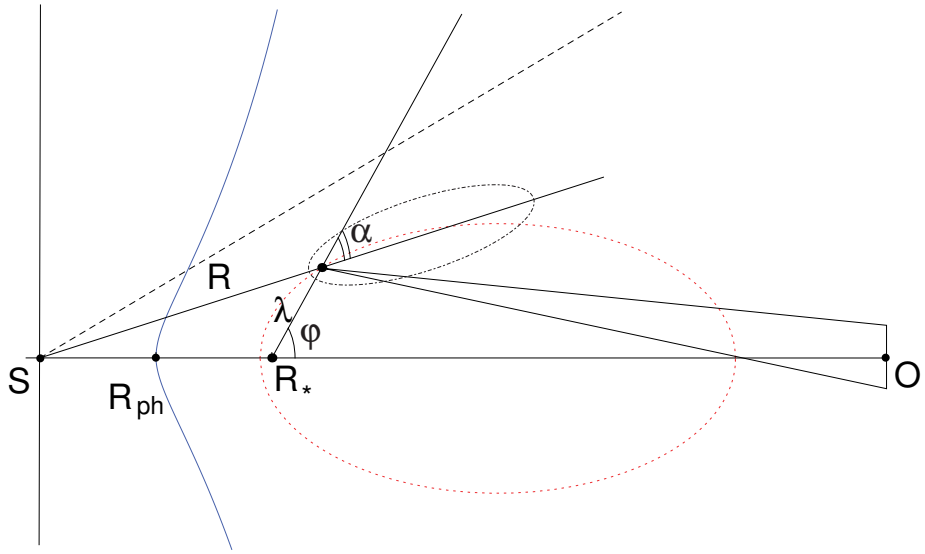

Figure D.1.: Geometry of photon scattering. Photons are emitted isotropically from the source at $R_\star > R_{ph}$. Most photons emitted at the angle φ with the line of sight are scattered at the distance λ from the source in the point with radial coordinate R. In this point the angle between the direction of photon propagation and the velocity of the wind is α. The photosphere of the wind is shown as thin blue curve. The ellipse of local mean free path, given by Eq. (D.0.3) is shown as dotted red curve. The scattering indicatrix is shown by dashed-dotted curve. Observer's detector is located to the right in point O.

In this Letter we discuss another effect of this anisotropy in relativistic wind. Consider an isotropic stationary point source of photons located on the line of sight at the radial position $r = R_\star$, see Fig. D.1. When such a source is located beyond the photospheric radius of relativistic wind with $R_{ph} \lesssim R_\star \lesssim R_{ph}\Gamma^2$ its intensity for a distant observer gets enhanced by a large factor up to Γ^4. For ultrarelativistic winds occurring e.g. in GRBs the Lorentz factor may be as large as $\sim 10^3$. Consequently, the source of photons may be located far above the photospheric radius, up to $10^6 R_{ph}$, and its intensity may be enhanced up to 10^{12} times! Due to large anisotropy in the mean free path of photons only small fraction of them reaches the observer

without any scattering. For all photons emitted beyond some critical angle $\varphi_{\max}$ around the line of sight the wind is opaque. It means that at some point along their trajectories where the optical depth becomes sufficiently large, they start to scatter. This point with coordinates $r = R$, $\theta = \varphi - \alpha$ is shown on Fig. D.1. The scattering indicatrix has a preferential direction, which is the radial direction of the wind. Thus an essential part of photons is scattered also towards the observer. The most important aspect here is that for large Γ the drastic compression of the ellipse of the mean free path, shown in Fig. D.1 by dashed curve, occurs. This effect is accompanied with the compression of the scattering indicatrix. For very large Γ practically all light emitted from the source is channeled towards the observer along its line of sight. Hence the wind plays a role of a reflector which concentrates the scattered emission within a narrow angle with the line of sight.

The large enhancement in intensity as seen by a distant observer is due to two effects: the preferential scattering of photons in radial direction and the increase of photon energy after the scattering by a factor $\sim \Gamma^2$. We will refer to this phenomenon as *relativistic spotlight effect*. In what follows we give a quantitative description of this effect.

Consider photons emitted at angle $\varphi > \varphi_{\max}$ from the point source described above, see Fig. D.1. The optical depth of the wind between two points with coordinates $(R_\star, 0)$ and $(R, \varphi - \alpha(R))$ is given by Beloborodov (2011)

$$\tau(R_\star, \varphi, R) = \tau_0 \frac{R_0}{R_\star} \left[\frac{\varphi - \alpha(R)}{\sin\varphi} - \beta \left(1 - \frac{R_\star}{R} \right) \right], \qquad \text{(D.0.2)}$$

where $\alpha(R)$ is the angle between the direction of wind velocity and the direction of photon propagation. The expression (D.0.1) is recovered from this formula for $\tau(r_{ph}, \theta, \infty) = 1$. Since $R_\star > R_{ph}$ the wind is transparent for small angles $\varphi < \varphi_{\max}$, where $\varphi_{\max}$ is determined by the condition $\tau(R_\star, \varphi_{\max}, \infty) = 1$. Due to strong dependence on φ the wind is opaque for $\varphi > \varphi_{\max}$. Moreover, the ratio $\tau(R_\star, \varphi \gg \varphi_{\max}, \infty)/\tau(R_\star, \varphi = 0, \infty)$ is on the order of Γ^2. Photons with angles $\varphi > \varphi_{\max}$ will be scattered for the first time near the point with coordinates defined by equating expression (D.0.2) to unity. The distance of this point to the source is approximately given by the local mean free path Abramowicz et al. (1991)

$$\lambda(R_\star, \varphi) = \frac{1}{\sigma n(R_\star)(1 - \beta\cos\varphi)} = \frac{R_\star^2}{\tau_0 R_0 (1 - \beta\cos\varphi)}. \qquad \text{(D.0.3)}$$

This equation describes an ellipse with eccentricity β and focus located at the point $R_\star$, see Fig. D.1.

Due to relativistic bulk motion of electrons the photons are scattered into the radial direction of the wind motion with $\alpha \lesssim \theta_b$. The scattering indicatrix is shown in Fig. D.1 by a dashed-dotted curve. Since the optical depth in this new direction is small most photons will escape after single scattering event [1]. Moreover, the inverse Compton scattering typically increases the energy of the photon by a factor Γ^2, providing an effective way to extract the wind energy and momentum. Actually, the interaction between the electron and the photon can be considered as Thomson scattering in the reference frame comoving with the wind, as soon as electrons in the wind have nonrelativistic temperature and initial energy of photons is $\epsilon \lesssim m_e c^2/\Gamma$, where m_e is electron mass.

For simplicity we assume that photons emitted with angle φ with respect to the line of sight are scattered exactly at the distance λ from the source. The distant observer sees only part of the scattered photons that arrive at the detector, see Fig. D.1. The intensity measured by this observer depends on the angular size of the ellipse defined by Eq. (D.0.3) as seen from the origin. For $R_\star < \Gamma R_{ph}$ the angular size of this ellipse is less than θ_b. In this case photons are scattered in the narrow beam with angular spread θ_b around the line of sight, independently on the position of the source $R_\star$. The larger is the Lorentz factor, the larger is the intensity seen by the distant observer. This is due to the fact, that both ellipses shown in Fig. D.1 become highly compressed with increasing Γ. For $R_\star > \Gamma R_{ph}$ the angular size of the scattering ellipse exceeds θ_b and the amount of scattered photons reaching the observer is reduced. This is due to the fact that photons are scattered into a wider cone. The intensity seen by the distant observer in this case decreases as $R_\star^{-2}$.

These results are confirmed by integration of photon and energy fluxes towards the observer over the ellipse given by Eq. (D.0.3) with the scattering indicatrix which is isotropic in the reference frame comoving with the wind, see Figs. D.2 and D.3. The analytic expressions are cumbersome, but can be approximated by simple formulae. For $R_\star < 2\Gamma^2 R_{ph}$ the enhancement of the

[1] Indeed, Monte-Carlo simulations show that the average number of photon scatterings is changing from 2 to 0.5 for $R_{ph} \lesssim R_\star \lesssim R_{ph}\Gamma^2$ (D. Bégué, private communication).

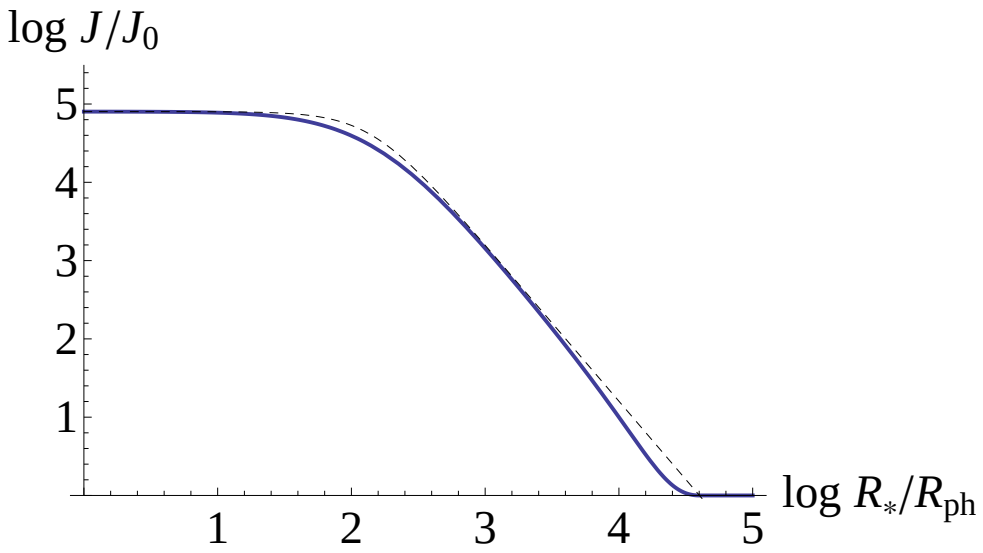

Figure D.2.: Enhancement of the photon number intensity J/J_0 along the line of sight as function of the radial position of the photon source in relativistic steady winds with $\Gamma = 100$. Dashed line shows approximate results obtained by Eq. (D.0.4).

photon number intensity is

$$J/J_0 \simeq \frac{8\Gamma^2}{1 + R_\star^2/(2\Gamma^2 R_{ph}^2)}, \tag{D.0.4}$$

while the enhancement of intensity is

$$I/I_0 \simeq \frac{16\Gamma^4}{1 + R_\star^2/(2\Gamma^2 R_{ph}^2)}. \tag{D.0.5}$$

For $R_\star > 2\Gamma^2 R_{ph}$ the spotlight effect is negligible, as at this radius the medium is transparent in almost all directions. The observed intensity enhancement is shown in Figs. D.2 and D.3 as function of the position $R_\star$ of the isotropic source of photons for the bulk Lorentz factor of the wind $\Gamma = 100$. The agreement between analytic results and their approximations (D.0.4) and (D.0.5) improves for higher Γ.

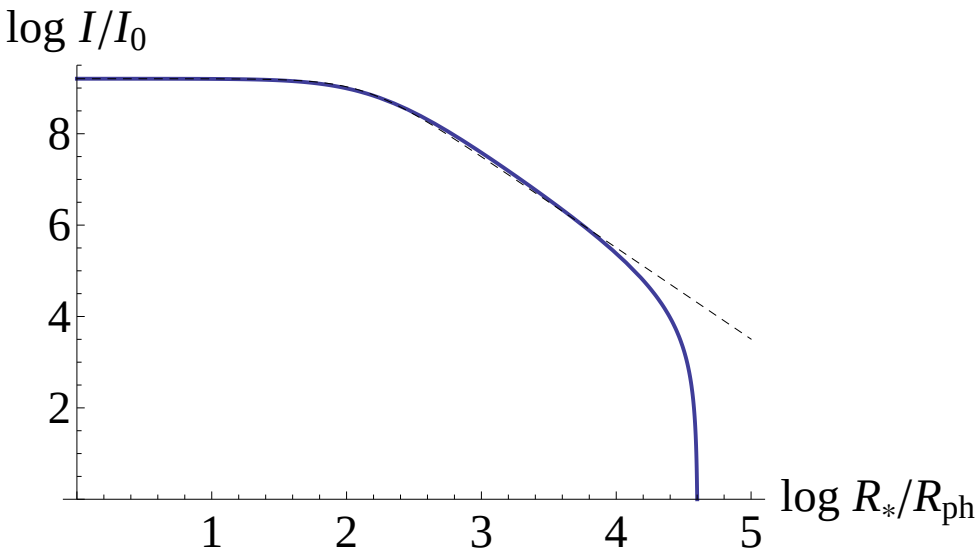

Figure D.3.: The same as in Fig. D.2 for the intensity I/I_0. Dashed line shows approximate results obtained by Eq. (D.0.5).

One may consider an extended stationary isotropic source of photons in the rest frame of the observer with the center located on the line of sight in the same range of radii $R_{ph} \lesssim R_\star \lesssim R_{ph}\Gamma^2$. When the transverse size

of the source is larger than $R_\star/\Gamma$ the photon flux for a distant observer is equivalent to that of a spherical shell with the radius $R_\star$ emitting with the same surface brightness in the absence of the wind. Since most photons are upscattered and their laboratory energy increases by a factor Γ^2 the energy flux is increased by the same factor Γ^2, compared to the case without the wind.

The enhancement of the intensity is due to the kinetic energy of relativistic wind. It is interesting to note that this kinetic energy can be efficiently extracted by the photons[2]. One can estimate the luminosity of the stationary spherical source $L_\star$ required for deceleration of the wind. The wind is traditionally characterized Paczynski (1990) by its luminosity $L = \Gamma \dot{M} c^2$, where $\dot{M}$ is the rest mass ejection rate. The deceleration of the wind by the spotlight effect changes the form of the photosphere given by Eq. (D.0.1), making it less concave. Then for $L_\star \gtrsim \dot{M}c^2/\Gamma$ the kinetic energy of the wind is extracted almost entirely and the relativistic spotlight effect disappears.

The enhancement of intensity of a photon source by a factor $\sim \Gamma^4$ is also known in several different contexts: the reflection off relativistically moving mirror (Einstein, 1905, p. 915); the emission of a source, relativistically moving towards the observer (Rybicki and Lightman, 1979, Eq. (4.97)). Nevertheless, the spotlight effect cannot be reduced to either of the two: the enhancement of the static source is due to the presence of relativistic medium providing strong anisotropy of the optical depth. In particular, in both above mentioned cases the enhancement of the intensity does not depend on position of the source, unlike the effect considered here, c.f. Eq. (D.0.5).

This phenomenon may find an application in GRB physics, provided the photon source is located within the relativistic beaming cone around the line of sight. This requirement is rather natural in relativistic context. The problem of conversion of kinetic energy into radiation is well known. The mechanism described above provides an efficient solution to this problem. In fact, when only a fraction $1/\Gamma^2$ of the kinetic energy of relativistic outflow is converted into soft photons emitted *isotropically* in the rest frame of the observer, such photons will extract large part of the kinetic energy of the outflow. For instance, in the relativistic outflow with $\Gamma \sim 300$ thermal photons with temperature 1 eV will be upscattered to energies $\sim$ 300 keV, typical for GRB

[2]In the model of Lazzati et al. (2000) the propagation of relativistic wind through photon bath was considered. However the estimation of ratio of photons dragged by the wind in transparent region (considered here) is incorrect, since the authors did not take into account the anisotropy of the optical depth properly.

spectra.

E. On the structure of the circumburst medium in the fireshell model of Gamma-Ray Bursts

E.1. Introduction

In the fireshell model, see Ruffini et al. (2009) and references therein, the light-curve of long Gamma-Ray Burst (GRB) prompt emission is composed of a thermal signal (P-GRB) at early time, followed by the peak of the emission originating from the interaction of the relativistic shell with the circumburst medium (CBM). This model has been successfully applied to numerous burst, see e.g. Ruffini et al. (2001, 2002); Izzo et al. (2012); Penacchioni et al. (2012, 2013); Muccino et al. (2013).

In order to fit the spectra, the model uses the additional assumption of thermal energy emission in the co-moving frame of the shell. To obtain the observed temperature, the volume of emission has to be reduced by introducing the filling factor $\mathcal{R}$, which is interpreted as the ratio of the emitting surface to the total visible area, leading to the interpretation that the CBM is composed of clouds, which in turn are made of filaments, see Ruffini et al. (2005a). Each filament is responsible for small local deceleration of the shell.

In this work, we are interested in the case for which each filament produces strong deceleration of a part of the shell interacting with it. We introduce an additional parameter to constrain the filaments and use the relativistic energy and momentum conservation laws to constrain the interaction between a filament and the shell.

The paper is organized as follows. In section 2, the treatment is described. Section 3 deals with the new parameter used to constrain the filament. It is followed by the description of the interaction between a filament and the

shell. And we conclude by estimating the parameters of a cloud such that the properties of GRB light-curve and spectrum are recovered together with two additional conditions: the filaments are optically thick and strong deceleration within filaments occurs.

E.2. Long GRB prompt emission in the fireshell model

In the fireshell model Ruffini et al. (2009), the main part of long GRB prompt emission is assumed to originate from a relativistic shell that interacts with the CBM with some average density n. There are three levels of description of this medium.

The first level considers the CBM to be homogeneous, with density typically $n \sim 1$ cm^{-3} (see Ruffini et al. (2001) and references therein). The interaction results in gradual deceleration of the shell and a smooth light-curve that raises up to the maximum and then decays. The emission lasts from few seconds to few hundreds seconds. The characteristic radius of interaction can be defined by considering that the initial Lorentz factor Γ of the shell has been divided by a factor of two at that radius. In other words, half of the kinetic energy of the shell is extracted. The radius of deceleration reads:

$$r_d = \left(\frac{9E}{8\pi m_p c^2 \Gamma^2 n}\right)^{\frac{1}{3}} \sim 2.9 \times 10^{17} E_{54}^{\frac{1}{3}} \Gamma_2^{-2/3} n_0^{-1/3} \text{cm} \tag{E.2.1}$$

where m_p is the proton mass, c the speed of light, E the total isotropic energy of the burst, see also e.g. Rees and Meszaros (1992) for a similar treatment in the fireball model. In Eq.(1) and below we define any quantity X_n such that $X = 10^n X_n$.

The second level of description introduces over-dense (called clouds) regions at rest in the laboratory frame. Assuming spherical symmetry, they are described by concentric shells, defined by the following parameters with their typical values: the density $n_c \sim 10^2$ cm^{-3}, thickness $l_c \sim 10^{15}$cm and radial position $R_c \sim 10^{16}$cm. Such clouds have a typical mass $10^{-7} M_\odot$ Ruffini et al. (2002). The interactions between each cloud and the shell result in variability over the smooth light-curve discussed above. Each spike of

a typical duration of few seconds is associated to one cloud. The interactions between each clood and the shell is described by the relativistic energy and momentum conservation equations for inelastic collision. All the internal energy generated in the interaction is assumed to be radiated away instantly ("fully radiative condition", see *e.g.* Ruffini et al. (2009)).

The third level of description considers inhomogeneities inside a cloud called filaments. The only constraint on the filaments is given by the filling factor $\mathcal{R} = A_{eff}/A$, where A_{eff} is the area that emits at each given time and A is the total visible area Ruffini et al. (2005a). This last parameter takes into account the relativistic beaming. This level of description is used to model observed spectra of GRBs Ruffini et al. (2005a). For not very energetic bursts ($E < 10^{53}$ergs) the emission is assumed to be thermal in the co-moving frame of the shell, while for more energetic bursts ($E > 10^{54}$ergs) the co-moving spectrum is phenomenologically modified Patricelli et al. (2012). $\mathcal{R}$ is determined by associating the peak energy to the observed temperature T_{ob} obtained by considering the co-moving internal energy $d\epsilon$ created in the interaction during the co-moving time $d\tau$:

$$T_{ob} = 2\Gamma \left(\frac{d\epsilon}{\sigma_{SB} A \mathcal{R} d\tau} \right)^{\frac{1}{4}}, \tag{E.2.2}$$

where $A = 4\pi R_c^2$ is the area of interaction. The numerical value of the filling factor $\mathcal{R}$ changes from cloud to cloud, but it is always infered from observations to be small, $\mathcal{R} \ll 1$, with typical values 10^{-8}, see *e.g.* Bernardini et al. (2007); Dainotti et al. (2007); Caito et al. (2009); Muccino et al. (2013). Only a small fraction of the total area of the shell is interacting with filaments at a given laboratory time t. It is implicitly assumed that the resulting variation in the Lorentz factor at a given cross-section of the cloud is small. Such small perturbations are neglected and the shell, characterised by an average Lorentz factor Γ, is assumed to be decelerated gradually by many consecutive interactions with filaments.

The modelling of the light curves and spectra requires 4 local parameters for each spike: l_c, n_c, R_c and $\mathcal{R}$, and the global parameter n.

Below we discuss the following problems which were not completely covered in the previous treatement:

- what are the implications of the filling factor $\mathcal{R}$ on the physical properties of the filaments?

- how the dynamics of the shell is affected by the filamentary structure? In particular, is it possible to decelerate to non-relativistic velocities only a small part of the shell by a single filament?

In order to answer these questions we propose to extend the model by the introduction of one additional parameter and by making several additional assumptions about the filaments.

E.3. New description of filaments and its implication

For simplicity we assume all filaments to be identical. For definiteness, we also assume they have cylindrical shape[1] with the axis aligned with the radial direction and characterized by the parameters: l_f (length), r_f (radius) and n_f (density). Besides we assume that the distribution of filaments is homogeneous inside the cloud.

In addition, we introduce a new parameter Ω such that $\sum s = \Omega A$ where $s = \pi r_f^2$ is the surface of a filament and the sum is running over all filaments in the cloud. A physical interpretation of Ω is given if one considers a small area of the shell Δs such that $\Delta s \ll s$. Then since the filaments are uniformly distributed in a cloud, Ω can be interpreted as the average number of filaments interacting with Δs while the shell propagates through the cloud. In particular $\Omega > 1$ implies that Δs will propagate through more than one filament, so there is an overlap between them. For this reason, Ω is referred to as overlap factor. A schematic representation of $\mathcal{R}$ and of Ω is given by Figure E.1.

Now the model for one cloud involves 8 parameters: n_c, l_c, R_c, r_f, l_f, n_f, $\mathcal{R}$ and Ω. But these parameters are not independent. To get the relation between them, let us first consider a section of the cloud of length δl such that $\delta l \ll l_f$. The number of particles in this section of the cloud is $N_c = A n_c \delta l$ while the number of particles in filaments of that section is $N_f = \sum' s n_f \delta l$, where the sum is running over all filaments *that are intersected by the cross-section of the cloud under consideration* (here $\sum' s = A_{eff}$). By considering that the number of particles is the same in both pictures (since the mass is the same), we write

[1] The geometrical shape of a filament only changes the following results by a factor of order 1.

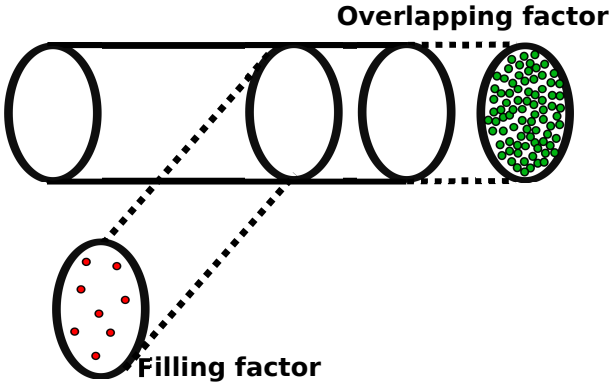

Figure E.1.: Schematic representation of a cloud. The filling factor $\mathcal{R}$ corresponds to the ratio between the area of the red dots (filaments) and the total area of the cloud, while Ω is the ratio between the area of the green dots (projection of *all* the filaments in the cloud) and the total area.

$N_c = N_f$ and obtain:

$$n_c A = n_f A_{eff}.$$

That gives Ruffini et al. (2005a); Muccino et al. (2013):

$$n_f = \frac{n_c}{\mathcal{R}} \tag{E.3.1}$$

Finally, using particle number conservation in the whole cloud, which gives immediately $n_c l_c = \Omega l_f n_f$, and Eq.(E.3.1), one obtains the following relation:

$$l_f = \frac{\mathcal{R}}{\Omega} l_c \tag{E.3.2}$$

One can then compute the optical depth for Compton scattering of such filament by combining Eq.(E.3.1) and Eq.(E.3.2) (n_f is assumed to be constant through a filament):

$$\tau_f = \sigma_T n_f l_f = \frac{\sigma_T n_c l_c}{\Omega} \tag{E.3.3}$$

where $\sigma_T = 6.65 * 10^{-25} \mathrm{cm}^{-2}$ is the Thomson cross section. In the case $\Omega > 1$, the optical depth of the cloud τ_c is given by the sum of the contributions of

all the filaments on the line of sight.

For the typical values $n_c = 10^2 \mathrm{cm}^{-3}$, $l_c = 10^{15}\mathrm{cm}$ and $\mathcal{R} = 10^{-8}$ given by Ruffini et al. (2005a), we find: $n_f = 10^{10}\mathrm{cm}^{-3}$, $l_f = 10^7\mathrm{cm}$ and $\tau_c = \sigma_T n_c l_c \sim 10^{-8}$.

In the fireshell model, the evolution of the shell is computed by considering its interaction with the clouds. The filaments are introduced only to compute the spectra: their influence on the dynamics is neglected. It has two consequences: first, the interaction between the filament and the shell results in small deceleration, and second, it is required that $\Omega \gg 1$ to have efficient energy extraction from the interaction between the shell and the cloud.

Alternatively, one can assume $\Omega \lesssim 1$. The lower limit on Ω is the value of $\mathcal{R}$ since the length of a filament can not exceed the length of the cloud. Considering the definition of Ω as the ratio between the interacting area of the shell $\sum s$ and A, we see that for $\Omega < 1$, the shell will not interact with the cloud on its total area A, but only with a fraction Ω of it. As a consequence, the amount of energy extracted from the shell by the cloud is less than ΩE_k, where E_k is the total kinetic energy of the shell before the interaction starts.

Thus, efficient extraction of energy by one cloud requires that Ω is not too small, say $0.1 < \Omega \lesssim 1$. From Eq.(E.3.3), we find that the density in one cloud should then be of the order of $n_c \sim 10^{10}\mathrm{cm}^{-3}$ for $l_c = 10^{15}\mathrm{cm}$ (as given by Ruffini et al. (2005a)) to have optically thick filaments. Let us also note that the constraints on $\mathcal{R}$ and Ω are independent.

E.4. Dynamics of the shell

The relativistic energy and momentum conservation equations for an inelastic collision between the shell and a cloud can be found e.g. in Ruffini et al. (2009). Here we consider the same equations to describe the interaction between the shell and a filament. They take the following form:

$$m_{shell}\Gamma + m_f = \left(m_{shell} + m_f + \frac{\epsilon}{c^2}\right)\Gamma_m \tag{E.4.1}$$

$$m_{shell}\sqrt{\Gamma^2 - 1} = \left(m_{shell} + m_f + \frac{\epsilon}{c^2}\right)\sqrt{\Gamma_m^2 - 1} \tag{E.4.2}$$

where Γ_m is the Lorentz factor of the merged system after the collision, m_{shell} and m_f are the baryonic masses of the interacting part of the shell and that of the filament, and ϵ is the internal energy in the co-moving frame of the

merged mass created in the interaction. We also have used the fact that the filament is assumed to be initially at rest in the laboratory frame.

Using Eq.(E.4.1) and Eq.(E.4.2) we can express the ratio of the masses m_{shell} and m_f as a function of Γ and Γ_m:

$$\frac{m_f}{m_{shell}} = \Gamma \left[\left(\frac{1-\Gamma^{-2}}{1-\Gamma_m^{-2}} \right)^{\frac{1}{2}} - 1 \right] \equiv \Gamma f(\Gamma, \Gamma_m) \tag{E.4.3}$$

Figure E.2 displays the ratio Γ_m/Γ as a function of m_f/m_{shell} according to Eq.(E.4.3). For $m_f \sim m_{shell}/\Gamma$, small deceleration occurs and the final Lorentz factor is comparable to the initial Lorentz factor $\Gamma_m \sim \Gamma$. This is the case adopted in the fireshell model. For larger mass of the filaments strong deceleration occurs. For $m_f \sim \Gamma m_{shell}$, we have $\Gamma_m \sim 1$, which means that the merged system moves with non-relativistic speed after the interaction.

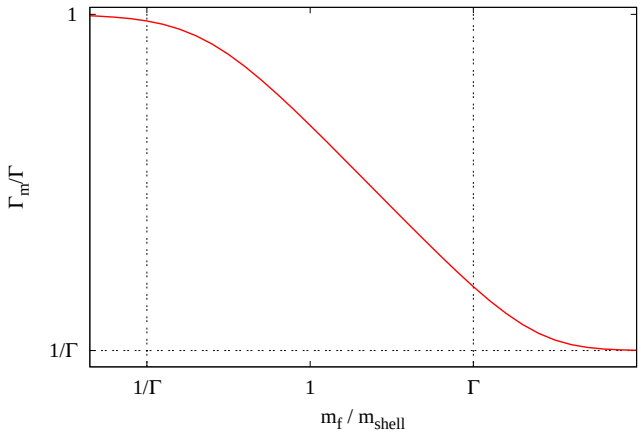

Figure E.2.: Ratio between the final (Γ_m) and the initial (Γ) Lorentz factors as a function of the ratio m_f/m_{shell} according to Eq.(E.4.3). Here $\Gamma = 100$, but qualitatively the dependence remains the same for all $\Gamma \gg 1$.

The model of inelastic collision adopted in our treatment following Ruffini et al. (2009) contains the assumption that after the interaction the system is merged and has a unique Lorentz factor Γ_m. This is only possible in case of tight coupling between particles in the merged system. This tight coupling requires that the mean free path of all particles (protons, electrons,

photons) is much less than the size of the merged system. Then the natural requirement is that the optical depth of the filaments defined in Eq.E.3.3 is larger than one. It is also required by the assumption of thermal emission in the co-moving frame of the merged system, see Ruffini et al. (2005a).

For the mass of the cloud, considered here as a spherical shell concentric to the origin of the burst (Ruffini et al., 2001), we have $M_c = n_c V_c m_p = 4\pi R_c^2 l_c n_c m_p$ and then we find:

$$M_c > 1.6 * 10^{-4}\, \Omega \tau_f \left(\frac{R_c}{10^{14}\mathrm{cm}} \right)^2 M_\odot. \tag{E.4.4}$$

In order to obtain the radial position of the cloud R_{dec} at which the interaction should happen, we can express the mass of the shell interacting with a filament and the mass of the filament in the form:

$$m_f = \pi l_f r_f^2 m_p n_f \tag{E.4.5}$$

$$m_{shell} = \frac{E r_f^2}{4\Gamma^2 R_c^2}. \tag{E.4.6}$$

Finally by using Eq.(E.4.3), we obtained the radius at which the filament has to be placed to decelerate up to an arbitrary Γ_m the part of shell that interacts with it:

$$R_{dec} = \sqrt{\frac{E f(\Gamma, \Gamma_m)}{4\pi m_p c^2 l_f n_f}} = \sqrt{\frac{E f(\Gamma, \Gamma_m)\sigma_T}{4\pi m_p c^2 \tau_f}}. \tag{E.4.7}$$

In the following, we discuss both extreme cases with slight and complete deceleration, as well as the intermediate one.

E.5. Deceleration regimes

E.5.1. Slight deceleration ($\Gamma_m \sim \Gamma$ with $m_f \sim m_{shell}/\Gamma$)

First we consider the case in which the shell is still highly relativistic after the interaction. For the numerical evaluation we chose $\Gamma_m/\Gamma = 1/2$, the standard condition determining the deceleration radius Rees and Meszaros (1992), which means that the interaction extracts 50% of the kinetic energy of

the interacting section of the shell. Using Eq.(E.4.7) we obtain:

$$R_{dec} = 7.3 * 10^{13} \left(\frac{E}{10^{54}\text{erg}}\right)^{1/2} \left(\frac{\Gamma}{10^2}\right)^{-1} \tau_f^{-1/2}\text{cm}.$$

The typical duration of the emission from the interaction between a cloud and the shell is:

$$\delta t_a = l_c/(2\Gamma_m^2 c) < R_{dec}/(2\Gamma_m^2 c) \tag{E.5.1}$$

$$< 0.48 \left(\frac{E}{10^{54}\text{erg}}\right)^{1/2} \left(\frac{\Gamma}{10^2}\right)^{-3} \tau_f^{-1/2}\text{s}, \tag{E.5.2}$$

which is smaller than the typical variability time-scale expected from the interaction of the relativistic shell and a cloud. For $\Omega \gg 1$, this estimate also gives the duration of the emission. While for $\Omega < 1$ this estimate gives the time-scale of the variability associated with the cloud.

E.5.2. Complete deceleration ($\Gamma_m \sim 1$ with $m_f \sim \Gamma m_{shell}$)

In this section we consider the case when the interaction between a filament and the shell leads to a deceleration up to almost non-relativistic speed of the interacting part of the shell, choosing $\Gamma_m = 2$.

For $\Omega > 1$, the kinetic energy of the shell would be completely extracted by this single interaction. On the contrary for $\Omega \lesssim 1$, only Ω part of the energy is extracted and the part of the shell that does not interact with the filaments of that cloud moves with the original Lorentz factor Γ, being able to interact with other clouds at larger distances.

The deceleration radius are found to be of the order of:

$$R_{dec} = 2.3 * 10^{15} \left(\frac{E}{10^{54}\text{erg}}\right)^{\frac{1}{2}} \left(\frac{\Gamma}{10^2}\right)^{\frac{1}{2}} \tau_f^{-\frac{1}{2}}\text{cm}. \tag{E.5.3}$$

Since the emission is isotropic and not relativistically collimated, the time

scale of emission is found by:

$$\delta t_a = \frac{2R_{dec}}{c} = 1.5 * 10^5 \left(\frac{E}{10^{54}\text{erg}}\right)^{\frac{1}{2}} \left(\frac{\Gamma}{10^2}\right)^{\frac{1}{2}} \tau_f^{-\frac{1}{2}} \text{s}. \quad \text{(E.5.4)}$$

This time scale does not correspond to the typical ones observed in GRBs.

E.5.3. Intermediate regime

We have seen that if one imposes the optical depth of the filament to be larger than one, none of the regimes studied above reproduces the typical time scales observed in GRBs. It is necessary to consider low relativistic speed ($\Gamma_m \sim 20$ after interaction) to establish a regime consistent with the observations. We can find both the radial position of the cloud R_{dec} and Γ_m as:

$$\Gamma_m = 19 \left(\frac{E}{10^{54}\text{erg}}\right)^{\frac{1}{6}} \tau_f^{-\frac{1}{6}} \left(\frac{\delta t}{10\text{s}}\right)^{-\frac{1}{3}} \quad \text{(E.5.5)}$$

$$R_{dec} = 2.2 * 10^{14} \left(\frac{E}{10^{54}\text{erg}}\right)^{\frac{1}{3}} \tau_f^{-\frac{1}{3}} \left(\frac{\delta t}{10\text{s}}\right)^{\frac{1}{3}} \text{cm}, \quad \text{(E.5.6)}$$

where δt is the typical duration of one spike. Since $\Gamma_m \ll \Gamma$, almost all the kinetic energy is extracted from the interaction with the filaments. To explain further variability in the light curve (subsequent spikes), we must require that $\Omega \lesssim 1$ to have energy left in the shell, and a subsequent delay between the emission from the interaction with two clouds.

Let us call Δt_a the delay between two spikes in the light-curve of a GRB. With $\Omega \lesssim 1$, a part of the shell is strongly decelerated by the first cloud, while the other part coasts with the initial Lorentz factor up to the second cloud. The delay between the two emissions is given by

$$\Delta t_a = \frac{R_{c,2} - R_{c,1}}{2\Gamma^2 c^2} = 0.17 \left(\frac{\Delta R}{10^{14}\text{cm}}\right) \left(\frac{\Gamma}{10^2}\right) \text{s}. \quad \text{(E.5.7)}$$

In order to have Δt_a of the order of few seconds, it is required either large radii of interaction of the order of few 10^{15}cm, or deceleration of the shell

between the two clouds.

Increasing the radii of interaction is impossible. Indeed the energy is fixed, as well as the duration of one spike to some seconds, leaving only the optical depth as a free parameter, and Eq.(E.5.6) shows that optically thick filaments constrains the radius of interaction to be smaller than $2.2 * 10^{14}$cm.

Actually, substantial deceleration of the shell can take place between the two clouds by interaction with the constant CBM. By decreasing the Lorentz factor of the part of the shell that did not interact with the first cloud from Γ to $\bar{\Gamma}$, an estimate of Δt_a is given by $\Delta t_a = \Delta R/(2\bar{\Gamma}^2 c)$. For instance, if between the two clouds, the Lorentz factor is decreased by a factor of 3, then Δt_a is 10 times larger than if no deceleration had taken place. The mass required between the two clouds is of the order of $m_{shell}/\Gamma \ll M_c$, given by Eq.(E.4.4).

E.6. Estimation of $\mathcal{R}$ and n_f with $\Omega < 1$

It is not possible to follow the approach of Ruffini et al. (2005a) to constrain the filling factor $\mathcal{R}$ from the observed temperature. Indeed they apply the energy and momentum conservation equations to the interaction *between the shell and a cloud*, considering that the filaments are only responsible for slight deceleration of the shell and that $\Omega \gg 1$, which implies that the shell decelerates on average by its interaction with many filaments. Here we apply the energy and momentum conservation equations to the interaction *between the shell and a filament*, with no further assumption on Ω and on the deceleration of the shell by a filament.

So we can constrain $\mathcal{R}$ from the energy emitted from all the filaments. The observed temperature of the emission from one filament writes:

$$T_{ob,fil} = 2\Gamma_m \left(\frac{\epsilon_f}{a V_f'} \right)^{\frac{1}{4}},$$

where ϵ_f is the co-moving internal energy created in the interaction of *one* filament with the shell and V_f' is the co-moving volume of a filament. Since this last quantity is not known, one can consider the sum over all the filaments in

the cloud:

$$T_{ob,fil} = 2\Gamma_m \left(\frac{\epsilon_{tot}}{4\pi a R_c^2 l_f^{'}} \right)^{\frac{1}{4}},$$

where $\epsilon_{tot}\Omega$ is the total energy released in all the filaments and the co-moving volume is $V_f^{'} = 4\pi R^2 \Omega l_f^{'}$ with $l_f^{'}$ being the co-moving length of a filament. Finally, when using Eq.(E.3.2) and $l_f^{'} = \Gamma_m l_f$, one obtains:

$$T_{ob,fil} = 2\Gamma_m \left(\frac{\epsilon_{tot}\Omega}{4\pi a R_c^2 \mathcal{R} \Gamma_m l_c} \right)^{\frac{1}{4}},$$

to be compared with Eq.(E.2.2). The filling factor writes:

$$\mathcal{R} = \left(\frac{2\Gamma_m}{T_{ob}} \right)^4 \frac{\Omega \epsilon_{tot}}{4\pi a R_c^2 \Gamma_m l_c}.$$

Γ_m and ϵ_{tot} are given by the conservation of energy and momentum. From Eq.(E.4.1) and (E.4.2) it comes:

$$\frac{\epsilon_{tot}}{m_{shell} c^2} = \left(\frac{\Gamma}{\Gamma_m} - 1 \right) + \Gamma f(\Gamma, \Gamma_m) \left(\frac{1}{\Gamma_m} - 1 \right), \tag{E.6.1}$$

where m_{shell} is given by $E/(\Gamma c^2)$.

The final expression for $\mathcal{R}$ is

$$\mathcal{R} = \frac{2^4 \Gamma_m^3}{T_{ob}^4} \frac{\Omega m_s c^2 \left[\left(\frac{\Gamma}{\Gamma_m} - 1 \right) + \Gamma f(\Gamma, \Gamma_m) \left(\frac{1}{\Gamma_m} - 1 \right) \right]}{4\pi a R^2 l_c}. \tag{E.6.2}$$

The dependence of $\mathcal{R}$ as a function of Γ_m/Γ is given by Fig.(E.3) for $E = 2 \times 10^{53}$erg, $R = 10^{14}$cm, $\Omega = 0.5$ and $k_B T_{ob} = 500$keV.

E.7. Discussion

Our analysis shows that when the interaction between the shell and the clouds is considered in the fireshell model, $\Omega \gg 1$ is implicitly assumed. In other words, there is significant ovelap between numerous filaments. The

typical values for the cloud parameters are given by Ruffini et al. (2005a): $n_c = 10^2 \mathrm{cm}^{-3}$, $l_c = 10^{15}\mathrm{cm}$ and $\mathcal{R} = 10^{-8}$.

Here we consider the interaction between the shell and a filament. In order to justify the assumption that the energy is thermal in the co-moving frame after interaction, we require $\tau_f > 1$ and express the radius at which the filament has to be placed as a function of the resulting Lorentz factor. With $\tau_f > 1$, it follows that each filament contains a large mass, which in turn results in a small deceleration radius, see Eq.(E.5.6), as compared to those adopted in the previous treatment within the fireshell model.

When assuming that $\Omega < 1$, it is needed that the interaction results in rather strong deceleration of the interacting parts of the shell with Γ_m of the order of few tens in order to recover the variability time-scale of the order of 1s. In this situation, the parameters of a cloud are $l_c < R_c \lesssim 10^{14}\mathrm{cm}$, $\mathcal{R} \sim 10^{-10}$ (imposed by the observed temperature), $n_c \sim 10^{12}\mathrm{cm}^{-3}$ (imposed by $\tau_f > 1$). The parameters of each individual filaments are also constrained $n_f \sim 10^{22}\mathrm{cm}^{-3}$ (a factor of 10 denser than air) and $l_f \sim 10^3\mathrm{cm}$.

In addition, in order to recover the delay between two spikes in the light-curve due to interactions with two clouds, together with the constrain of optically thick filaments, it is required that the Lorentz factor of the shell decreases substantially between the two clouds by interacting with the CBM. Its density can be estimated to be of the order of $n = 1.6 \times 10^{10}\mathrm{cm}^{-3} E_{54} \Gamma_2^{-2} R_{14}^{-3}$.

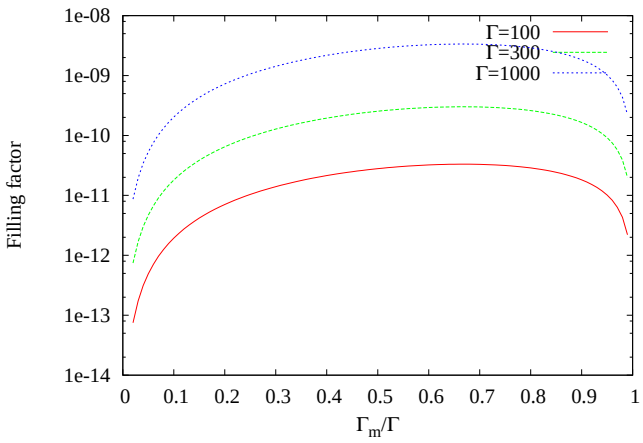

Figure E.3.: $\mathcal{R}$ as a function of Γ_m/Γ is given by Fig.(E.3) for $E = 2 \times 10^{53}\mathrm{erg}$, $R_c = 10^{14}\mathrm{cm}$, $\Omega = 0.5$ and $k_B T_{ob} = 500\mathrm{keV}$.

One can also attempt a third approach in which an homogeneous deceleration of the shell is taking place at the same time as the interaction with filaments.

Finally, note that there is a similar theoretical treatment of the interaction between the GRB ejecta and a shell of matter by Badjin et al. (2013) to explain the thermal component in the UV-range in the late afterglow. Starting from the requirement that the ISM shell is optically thick, they determined its mass and density, finding $n \sim 10^{11}\mathrm{cm}^{-3}$, similar to our estimate. Since they also require the prompt emission to be seen, they additionally assume that the surface of interaction of the relativistic outflow is only a fraction of the total visible area, which in our work translates to $\Omega < 1$.

E.8. Conclusion

In the context of the fireshell model, in addition to the filling factor $\mathcal{R}$ we have introduced a new parameter Ω which is interpreted as the average number of filaments that interact with a small area of the shell while it propagates through the cloud. We found that $\Omega \gg 1$ is implicitly assumed in the fireshell model.

In addition, with the parameters of the clouds adopted in the fireshell model, we have shown that the requirement that the optical depth of either a filament or a cloud be larger than one is not consistent with the condition $\Omega \gg 1$, see Eq.(E.3.3) . However the application of relativistic energy and momentum conservation equations to inelastic collision between the relativistic shell and the filaments requires tight coupling between particles in the merged system. In other words, it requires the condition $\tau_f > 1$.

Adopting the energy and momentum conservation approach and requiring the filaments to be opaque, we studied the interaction between the relativistic shell and the filaments and identified the typical parameters relevant for the description of the light-curves of Gamma Ray Bursts. In particular we found that all the requirements (optical depth larger than unity, variability timescale and duration) can be accounted for if a cloud of large mass (comparable with a fraction of a solar mass, see Eq.(E.4.4)) is placed at a radius of the order of 10^{14}cm or less, see Eq.(E.5.6), leading to large deceleration of parts of the shell.

F. Thermal emission from the interaction of GRBs and supernova ejecta

F.1. Introduction

A thermal X-ray component, regularly coupled with a flare, is observed in the early afterglow of many gamma-ray bursts (GRBs), for instance, GRB 060729, 081007, 090618, 130427A, see more examples inPage et al. (2011); Sparre and Starling (2012); Starling et al. (2012); Ruffini et al. (2014a,b). Some possible mechanisms were proposed, in the literature there is no consensus. The traditional shockwave breakout model has difficulties in generating the observed high luminosity in a distant radius Ghisellini et al. (2007); Starling et al. (2012). In ref. Friis and Watson (2013), the authors link the afterglow thermal radiation to the prompt phase via photospheric emission from the jet, but from the observation, the cooling of thermal components in the prompt phase and in the afterglow follows different trends, see an example in Fig.F.3. In ref.Pe'er et al. (2006), the thermal emission is interpreted as coming from a hot plasma "cocoon" heated by the GRB jet, but this model requires much higher Lorentz factors (on the order of 10) than the ones inferred from the observations.

In this paper, we attempt to explain the thermal component in the early afterglow by considering the interaction of GRB outflow with a baryonic shell encircling a GRB source. In the particular paradigm of induced gravitational collapse (IGC), see e.g. Ruffini et al. (2014a) and references therein, such shell is interpreted as a supernova (SN) ejecta. IGC delineates a missive star exploding as a SN in a close binary system, the companion neutron star accretes a partial SN ejecta and gravitationally collapses to a blackhole, GRB occurs simultaneously. The mechanisms of GRB energy engine and explosive dynamics in the prompt phase are described by fireshell model, see e.g. Ruffini et al.

(2010); Ruffini et al. (2009) and references therein. Such a GRB then interacts with the rest of the supernova ejecta, accelerates and heats the supernova ejecta, as a consequence, the supernova ejecta expands mild-relativistically and emits the thermal radiation.

The content is organized as follows. In Section F.2 we solve the equations of relativistic energy-momentum conservation in order to recover the amount of thermal energy and velocity of the shell after the collision with the GRB ejecta, also the photon diffusion is considered. In Section F.3 we compute the resulting temperature and estimate the optical depth of the shell. We apply the model in Section F.4 and consider the cases of 6 GRBs, including the prototype GRB 090618. Conclusions follow.

F.2. Velocity and internal energy

Assuming the SN ejecta is a shell comprised of baryonic clumps with different sizes and thicknesses at radius R from the SN source, the clumps near the GRB are thinner than the more distant ones as a result of the accretion by the initial neutron star. The circumstances we deal with in this paper have $R > 10^{12}$ cm, two orders of magnitude larger than the distance ($< 10^{10}$ cm) between binary stars in the IGC paradigm, therefore R is also considered approximatively as the distance between the shell and the GRB Fryer et al. (2014). This shell interacts with the GRB ultra-relativistic outflow. Here we approximate the total energy of GRB outflow as the observed isotropic energy E_{iso}. In practice, the shell may not fully cover the sphere, also the GRB outflow may be jetted, so in the following computation, we only consider the interacting part, involving a portion of the shell with area $4\pi\epsilon R^2$ and the associated mass $M = \epsilon M_s$, the energy of GRB outflow interacting with this portion of shell $E = \epsilon E_{iso}$, where ϵ is a fractional factor and M_s is a mass of the spherical shell. For simplicity, in the following text, when we mention the shell, it means the interacting part of the shell.

F.2.1. Interaction

Interaction transfers energy and momentum from the GRB outflow to the clumps of the shell. Energy-momentum conservation reads

$$E + Mc^2 = \left(Mc^2 + W\right)\Gamma, \tag{F.2.1}$$

$$\frac{E}{c} = \left(M + \frac{W}{c^2}\right)\Gamma v, \tag{F.2.2}$$

where $\Gamma = \left[1 - (v/c)^2\right]^{-1/2}$ is the Lorentz factor of radial motion of the shell, c is the speed of light, W is internal energy. These equations can be used to find the internal energy and the velocity of the shell after the interaction. If the shell remains opaque, the internal energy of the shell is transformed into its kinetic energy resulting in acceleration. At the phase of acceleration the radial momentum is not conserved, and equation (F.2.2) in the above set cannot be used. The final velocity after the acceleration phase can be found from the energy conservation alone, namely from equation (F.2.1). For having concise expressions, we neglect the initial energy and momentum of the shell, which only affects less than 5% and 12% of the temperature and mass respectively for our cases.

In order to solve equations (F.2.1) and (F.2.2) we introduce the new variables

$$\eta = \frac{E}{Mc^2}, \qquad \omega = \frac{W}{Mc^2}, \qquad u = \Gamma\frac{v}{c} \tag{F.2.3}$$

we rewrite the energy-momentum conservation

$$\eta = (\omega + 1)\sqrt{u^2 + 1} - 1, \tag{F.2.4}$$

$$\eta = (\omega + 1)\, u. \tag{F.2.5}$$

The solution to this system reads

$$u = \frac{\eta}{\sqrt{1 + 2\eta}}, \qquad \frac{W}{E} = \frac{\omega}{\eta} = \frac{1}{u} - \frac{1}{\eta}. \tag{F.2.6}$$

In nonrelativistic and ultrarelativistic asymptotics, respectively, the solution

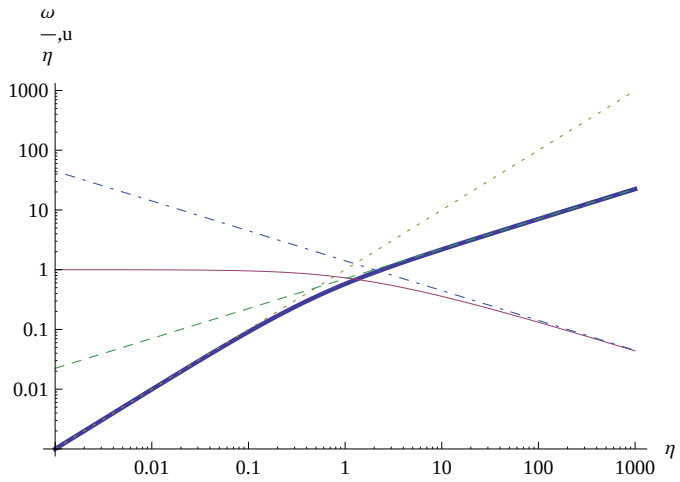

Figure F.1.: Two functions are shown: the dimensionless velocity parameter $u = \Gamma v/c$ of the shell after the interaction with photons (thick), as function of the parameter $\eta = E/(Mc^2)$, as well as the ratio between the internal energy and the initial energy in photons (thin), $\omega/\eta = W/E$, as function of the same parameter η. Dotted (dashed) line shows the nonrelativistic (ultrarelativistic) asymptotics for u, while the dash-dotted line shows the ultrarelativistic asymptotics for W/E.

becomes

$$u \simeq \frac{v}{c} \simeq \eta \ll 1, \qquad \omega \simeq \eta, \tag{F.2.7}$$

$$u \simeq \Gamma \simeq \sqrt{\frac{\eta}{2}} \gg 1, \qquad \frac{\omega}{\eta} \simeq \sqrt{\frac{2}{\eta}}. \tag{F.2.8}$$

This solution is illustrated in Figure F.1. These results imply the following. On the one hand, when the energy in photons is much less than the rest mass of the shell, $E \ll Mc^2$, most of the energy is transferred into internal energy $W \simeq E$, and the resulting velocity of the shell is nonrelativistic, $v/c \simeq E/(Mc^2)$. On the other hand, for $E \gg Mc^2$ the transfer of momentum is inefficient. We have $\Gamma \simeq \sqrt{E/(2Mc^2)}$ and $W/(Mc^2) \simeq \sqrt{2Mc^2/E}$. The shell is accelerated to ultrarelativistic velocity, but some energy goes into internal energy as well. This internal energy will then be transferred into kinetic one during the acceleration phase.

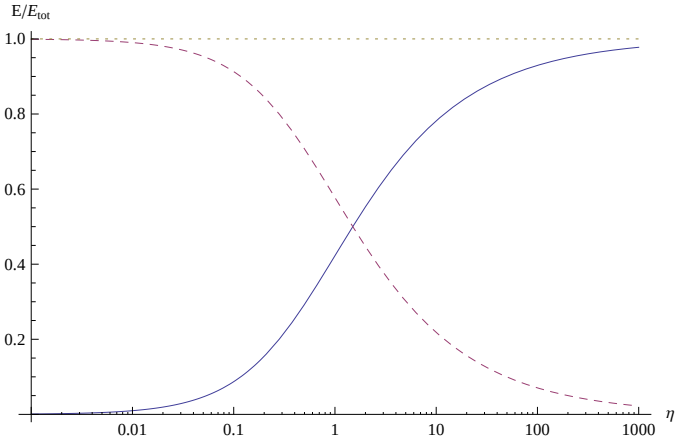

Figure F.2.: The ratio between internal (dashed) and kinetic (solid) energy to initial energy (dotted) after the interaction. In nonrelativistic case with $\eta \ll 1$ all the energy of the GRB ejecta is transformed into internal energy (heat) of the baryonic shell. In ultrarelativistic case with $\eta \gg 1$ the energy of the GRB ejecta is transformed mostly in kinetic energy of the shell.

In Figure F.2 we present the ratio between internal and kinetic energy of the shell to initial energy of the system, composed of the GRB ejecta and the baryonic shell, computed after the interaction. One can see that in the nonrelativistic case with $E \ll Mc^2$ all the energy of the GRB ejecta is transformed into internal energy of the baryonic shell. In contrast, in ultrarelativistic case with $E \gg Mc^2$ the energy of the GRB ejecta is transformed mostly in kinetic energy of the shell. Notice the striking similarity with the corresponding diagram for the energies emitted in the P-GRB and in the extended afterglow, in units of the total energy of the plasma within the fireshell model, see e.g. Figure 5 in Ruffini et al. (2009).

F.2.2. Acceleration

If the shell is spherically symmetric, assuming all energy is ultimately transferred into kinetic energy of the shell ($W \ll Mc^2$) from the energy conservation, equation (F.2.1), one has

$$\Gamma - 1 = \frac{E}{Mc^2} = \frac{E_{iso}}{M_s c^2} = \eta, \tag{F.2.9}$$

Again, in nonrelativistic and ultrarelativistic asymptotics, respectively, one finds

$$\frac{v}{c} \simeq \sqrt{2\eta}, \qquad \eta \ll 1, \tag{F.2.10}$$

$$\Gamma \simeq \eta, \qquad \eta \gg 1. \tag{F.2.11}$$

As a matter of fact, the values of velocity (Lorentz factor) after the interaction are always smaller than the final values, reached after the acceleration phase.

Note that in the derivation in this Section we never used the condition $W \ll Mc^2$. This condition is valid in GRBs context as baryons after collision never reach relativistic temperatures, $kT \ll m_p c^2$.

F.3. Temperature and optical depth

The comoving temperature of the shell T_c is found from the condition $W = 4\pi\epsilon a R^2 l T_c^4$. The observed temperature for the source with angle ϑ with respect to the line of sight is

$$T = \frac{T_c}{\Gamma\left(1 - \beta\cos\vartheta\right)} = \frac{\sqrt{1+2\eta}}{1+\eta-\eta\cos\vartheta}\left(\frac{\omega}{\eta}\frac{F}{al}\right)^{1/4}, \tag{F.3.1}$$

where $F = \epsilon E_{iso} / \left(4\pi\epsilon R^2\right) = E_{iso} / \left(4\pi R^2\right)$ is isotropic energy flux. This expression gives, respectively, in nonrelativistic and ultrarelativistic asymptotics

$$T \simeq \left(\frac{F}{al}\right)^{1/4}, \qquad E \ll Mc^2, \tag{F.3.2}$$

$$T \simeq 2\Gamma\left[\frac{F}{al}\left(\frac{2}{\eta}\right)^{1/2}\right]^{1/4}, \qquad E \gg Mc^2, \tag{F.3.3}$$

where in eq. (F.3.3) we assume that the source is on the line of sight.

The shell will emit photons from its photosphere. The case of ultrarelativistic photosphere with $\Gamma \gg 1$ is treated in Ruffini et al. (2013b), see also recent review Vereshchagin (2014). From now on assume that the photosphere is not ultrarelativistic. We still retain fully relativistic expression (F.3.1). The validity of the treatment in the previous section requires that the shell is opaque,

namely its optical depth τ is large. The latter is given by

$$\tau = \sigma n l = \frac{\sigma M}{4\pi\epsilon R^2 Z m_p} \gg 1, \tag{F.3.4}$$

where σ is Thomson cross section m_p is proton mass, Z is atomic number. Further acceleration of the shell, considered above, is possible only of the shell is still opaque during the acceleration phase.

The emission from the photosphere occurs due to radiative diffusion from the interior of the shell. The emission lasts until all energy diffuses out from the shell. The characteristic diffusion time form a clump with a given thickness is

$$t_D = \frac{l^2}{D} = 3\tau\frac{l}{c}, \tag{F.3.5}$$

where $D = c/(3\sigma n)$ is the diffusion coefficient for photons. Since $\tau \gg 1$ we have $l \ll ct_D$. The density decrease in diffusion coefficient due to expansion of the shell can be neglected if the diffusion time is less than the dynamical time of expansion R/v, namely if

$$3\tau\frac{v}{c} \ll \frac{R}{l}. \tag{F.3.6}$$

In the opposite case one has to consider the effects of expansion and the thermal spreading of the baryonic shell after interaction with photons on the diffusion time. In any case, this effect reduces the diffusion time.

Note that equations (F.2.8) and especially (F.3.3) are relevant in the context of the fireshell model Ruffini et al. (2009) as they describe the values of the Lorentz factor of the PEMB pulse and its temperature at the moment after the collision of the PEM pulse with the baryonic remnant. The asymptotic expression (F.2.11) describes the Lorentz factor of the PEMB pulse under the condition $\eta < 10^4$.

F.4. Application

From the observation one can derive the isotropic energy via the observed flux and redshift, and by fitting the light curve and spectra, one can obtain the evolution of temperature from thermal emission, as well as the velocity of expansion. In practice, the satellites do not cover all the energy band, what

we can have are only given temperatures with given duration. The *Swift*-XRT is the most widely used instrument on detecting the GRB afterglow, it covers $0.3 \sim 10$ KeV. In other words, by analyzing the data from *Swift*-XRT, we can only obtain the thermal temperature in soft X-ray band, and the corresponding duration. For example, in Fig.7 of Ruffini et al. (2014b), clearly the temperature of blackbody radiation from 196 s to 461 s is within the scope *Swift*-XRT, temperature cools along the time. Therefore here we adopt three parameters E_{iso}, t_D and u given by the observations, then we deduce the temperature using the above equations for the comparison with the observational one. It is convenient to rewrite equation (F.3.1) using equations (F.2.6) and (F.3.5) as

$$\begin{aligned} T &= X(u)F^{1/2}\left(a\frac{m_pc^2}{3\sigma}Zct_D\right)^{-1/4} \\ &\simeq 2.13X(u)E_{iso,52}^{1/2}R_{13}^{-1}t_{100}^{-1/4}Z_{10}^{-1/4}\text{keV}, \end{aligned} \tag{F.4.1}$$

where $E_{52} = E/10^{52}$erg, $R_{13} = R/10^{13}$cm, $t_{100} = t_D/100$s, $Z_{10} = Z/10$,

$$\begin{aligned} X &= \frac{1}{\sqrt{u}}\frac{1}{\sqrt{1+u^2}-u\cos\vartheta}\left(\frac{u+\sqrt{1+u^2}-1}{2u^2+2u\sqrt{1+u^2}+1}\right)^{1/4} \\ &= \begin{cases} u^{-1/4}, & u \ll 1, \\ 2^{3/4}u^{1/4}, & u \gg 1 \end{cases} \end{aligned} \tag{F.4.2}$$

is a slowly varying function of u which decreases as $u^{-1/4}$ for $u < 1$ and increases as $u^{1/4}$ for $u > 1$, with $X(u = 1, \vartheta = 0) \approx 1.7$.

In fact, in most cases thermal component in soft X-ray contains small fraction of the GRB energy, see table F.1. The baryonic shell may not necessary be spherically symmetric as we assumed, clumps have different thickness. The thinner clumps have earlier emission with higher temperature, and vice versa. The small ratio between thermal energy in X-ray and GRB energy can be explained assuming small ratio of the total surface of relatively thin baryonic clumps to the total spherical area at that radius. Naturally in the IGC paradigm, these thin clumps are accumulated around the accreting source, the progenitor of GRB. Some similar ideas in treatment of thermal emission in GRBs are discussed in Badjin et al. (2013); Pe'er et al. (2006).

F.4.1. The case of GRB 090618

A thermal component has been inferred from observations of the early X-ray afterglow in GRB 090618. Following Izzo et al. (2012) and Ruffini et al. (2014a) we summarize the parameters:

- isotropic energy of GRB $E_{iso} = 2.9 \times 10^{53}$ erg,
- observed duration of the thermal component in Episode 3, $t = 150$ s,
- observed temperature T is decreasing from 1 keV to 0.3 keV.

Two alternative models were presented to explain this component: a relativistic wind model (e.g. Friis and Watson (2013)) and a mild-relativistic shell model Ruffini et al. (2014a). Here we focus on the second one. In the model described above we neglected the initial kinetic energy of the shell and assumed that the interaction between the GRB ejecta and the shell results in two effects: heating of the shell and its acceleration. The parameters of the shell were inferred from observations Ruffini et al. (2014a):

- radius $R = 10^{13}$ cm,
- velocity $0.75 < v/c < 0.89$.

These parameters are quite close to those discussed above. The observed trend of decreasing temperature can be explained by the expansion of the shell, neglected in our simplified treatment in Section F.3. Given relativistic velocities of the shell, neither nonrelativistic nor ultrarelativistic approximations can be used to infer the parameters of the clump. Instead, the full analytic solution (F.2.6) must be used. So from equation (F.2.6) we determine

$$3.0 < \eta < 8.1,$$

then knowing the energy in the thermal component the mass is

$$0.02 M_\odot < M_s < 0.05 M_\odot,$$

then the optical depth of the clump is found from equation (F.3.4), and it is

$$1.3 \times 10^4 < Z\tau < 3.4 \times 10^4,$$

then the length of the clump is obtained from equation (F.3.5) and it gives

$$4.4 \times 10^7 \mathrm{cm} < \frac{l}{Z} < 1.2 \times 10^8 \mathrm{cm}.$$

Again, with these parameters the constraint equation (F.3.6) is satisfied.

It is clear from Figure F.2, that with these parameters the energy of GRB ejecta is divided nearly equally between kinetic energy of the shell and its internal energy.

Assuming the shell is composed of hydrogen with $Z = 1$ the temperature of the shell is 8.62 keV, which is a factor 9 higher than the observed one. Instead, if the shell is composed of radioactive elements produced at the supernova explosion, the atomic number should be around $Z = 26$, which gives for the temperature a much closer value to the one observed, namely 3.8 keV. Clearly, in our simplified treatment this coincidence is remarkable. In fact, we assumed that the temperature and density distribution in the shell are uniform. However, realistic temperature and density profiles will give smaller temperature at the photosphere, compared to the temperature in the interior of the shell.

Our model predicts that in non-relativistic case ($\eta \lesssim 1$) practically all kinetic energy of the GRB outflow is transferred into internal energy of the baryonic shell, namely $W \simeq E$. In the case of GRB 090618 we have $W \simeq E/2$. However, the total energy in the thermal component is estimated to be only $E_{BB} = 2.1 \times 10^{49}$ erg. This can be explained if only a small fraction ($\epsilon \simeq 0.005$) of the GRB ejecta actually interacts with thin baryonic clumps. Recall that our model is also valid without imposing the spherical symmetry. It implies that the mass of thin baryonic material around the GRB source is $M \sim 10^{-4} M_\odot$. This is the lower limit to the total mass of baryonic material around the source. The rest of the material can be much more massive and thicker.

If the GRB ejecta is spherical, interaction of this ejecta with the main part of the SN remnant will increase the internal energy of the ejecta, thus contributing to the bolometric luminosity of the optical SN light curve. This effect can explain why the nickel mass inferred in GRB-SN systems is systematically higher than in other Ibc type SN .

In the IGC paradigm, accretion contributes to the emission of first seconds, while in the fireball model, photospheric emission could exist in the beginning. In both cases, as a result, thermal emission could be detected if its fluence is sufficient. For GRB 090618, a decreasing thermal temperature within

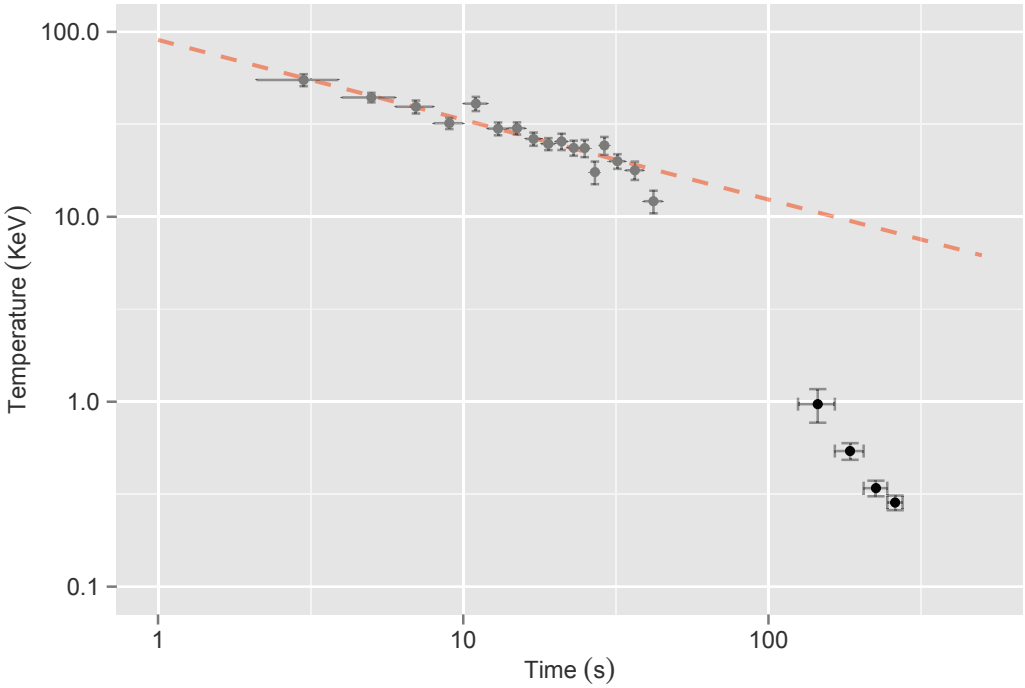

Figure F.3.: Temperature of the thermal component in the prompt emission (grey points) and in the afterglow (black points). The single power-law fitting of the temperature in the prompt emission clearly shows its extrapolation lays much higher than the temperature in the afterglow. The value of temperature comes from Ruffini et al. (2014a); Izzo et al. (2012).

the first 50 s is observed, and we extrapolate this temperature by a single power-law till hundreds of seconds and find that the extrapolated value is much higher than the observed one, as shown in Figure F.3. This consideration Begue (2014) supports that the thermal component in the afterglow has a different origin, as in this article we adopt the proposal from IGC paradigm, generated by the collision of GRB afterglow and a baryonic shell.

GRB	z	E_{iso} ($\times 10^{52}$ erg)	R_c ($\times 10^{13}$ cm)	$t_{d,c}$ ($\times$100s)	ν ($\times 10^{10}$ cm/s)	$T_{obs,c}$ (KeV)	T (KeV)	E_{bb} ($\times 10^{50}$
060218	0.033	0.0053	0.039	25.40	0.040	0.18	5.18	0.063
100316D	0.070	0.0060	0.093	5.53	0.39	0.19	1.83	0.095
081007	0.53	0.15	0.13	0.45	2.15	0.47	5.45	0.42
060729	0.54	1.60	0.58	1.45	2.34	0.32	2.62	4.92
090618	0.54	41	1.00	0.98	2.45	0.97	4.85	24.00
130427A	0.34	140	1.20	2.65	2.40	0.50	9.77	28.68

Table F.1.: Observational parameters and deduced temperature of 5 supernova associated GRBs, subscript 'c' presents the comoving frame. Observational data is taken from Ruffini et al. (2014a,b); Izzo et al. (2012); Starling et al. (2012).

F.4.2. More Examples

In order to have a more general comparison, we adopt 5 more GRBs with isotropic energy from 10^{49} erg to 10^{54} erg, all these GRBs show supernova signal either from the spectral aspect or a bump in the optical lightcurve is detected. To find a thermal component, two conditions are required due to the capacity of satellites, that the flux of thermal component is sufficient and the ratio of thermal flux versus total flux is prominent, the thermal flux within the observed duration t_D adopted in this article fulfills these two conditions. With this consideration, t_D should be shorter than the real thermal emission time, however, a great fraction of the total thermal energy is released during t_D, it's reasonable to employ the observed t_D as an approximation.

Table (F.1) shows the observational parameters and the temperature deduced from equation (F.4.1), and the ratio (defined as ϵ) of observed total thermal energy E_{bb} in Episode 3 versus isotropic energy, in Figure F.4, we demonstrate and fit the E_{iso} and E_{bb} relation, which shows approximately

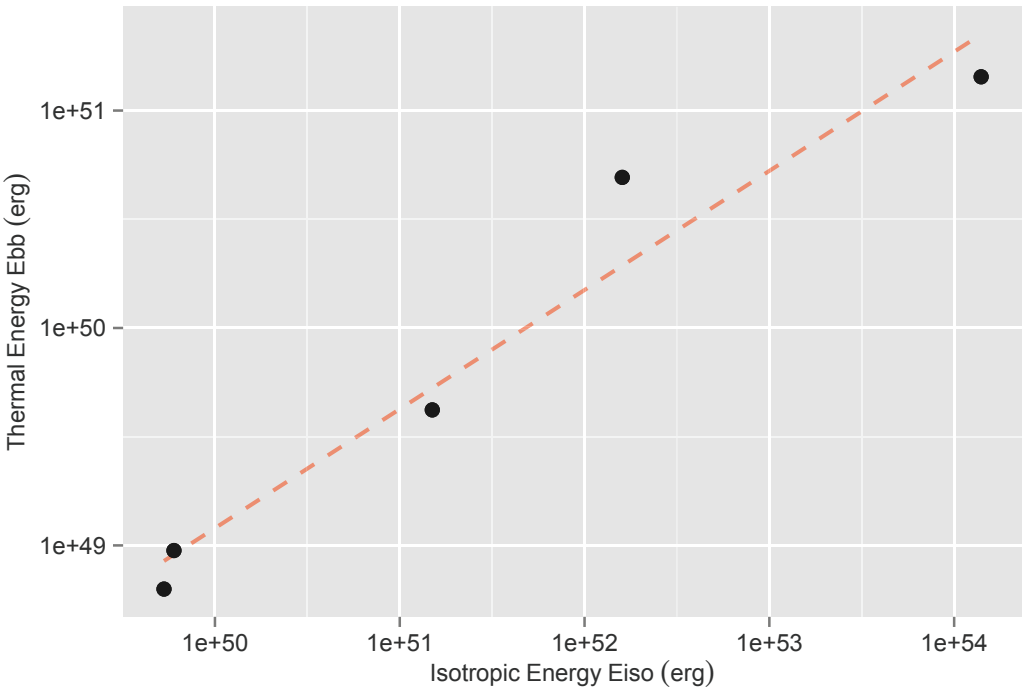

Figure F.4.: Isotropic energy versus thermal energy, dashed line displays a simple power-law fitting of the GRBs in Table F.1, the power-law index is 0.6, as $E_{\rm bb} \propto E_{\rm iso}^{0.6}$.

$E_{bb} \propto E_{iso}^{0.6}$. We notice that in reality, radius R and temperature T are not constants, common pattern are found as radius increases while temperature decreases within the duration t_D. But some GRBs in our sample do not provide adequate data for having precise time resolved analysis, instead, averaged values are given for all the 5 GRBs.

The temperature deduced are universally higher than the observed ones, and a trend that the deduced temperature increases along with the observed temperature can be found. These results are within our expectation, because equation (F.4.1) depicts the average temperature, measured in the interior of the shell. In reality, a temperature distribution profile should be taken into consideration, and a steep gradient of temperature always exists at the outer edge which emits thermal photons. Detailed simulation will be given elsewhere.

F.5. Conclusions

The observed parameters of the thermal component in the Episode 3 of emission in GRB 090618 are reproduced by considering the interaction of the GRB outflow with the thin baryonic shell having mass of $10^{-4} M_{\odot}$ and thickness of 10^8 cm. In addition, thermal temperature of 5 more GRBs, namely 060218, 100316D, 081007, 060729, 130427A, with observed thermal emission in the early afteglow were analysed, and the parameters of associated baryonic shells are obtained.

Our results suggest an alternative explanation of the observed thermal signal in the early afterglow of some GRBs. While in Friis and Watson (2013) this signal is associated with the photospheric emission from relativistic wind, in our approach this emission is due to nonrelativistic photosphere of a thin baryonic shell, energized and accelerated by the associated GRB.

G. Relativistic kinetic theory and its applications

G.1. Introduction

Kinetic theory (KT) was born in the XIX century, the golden age of classical physics. Based on the atomic picture of a medium Boltzmann (2011) properties such as heat and electrical conductivity, as well as viscosity and diffusion found natural explanations. The term originates from the Greek where $\kappa\iota\nu\eta\sigma\iota\zeta$ means motion. In fact all these properties of the medium may be understood to be emerging from its microscopical structure and motion.

KT now has to be considered in a wider framework of statistical mechanics appearing at the end of XIX century essentially in the works of Maxwell, Boltzmann and Gibbs. It should be emphasized that the main ideas and principles of KT influenced the development of many other sciences, including the mathematics (probability theory, ergodic theory), biology (evolutionary biology, population genetics) and economics (financial markets, econophysics).

Within physics, KT is closely related to statistical physics, thermodynamics, hydro- and gasdynamics. Today one can say that the main task of kinetic theory is explanation of various macroscopic properties of a medium based on known microscopic properties and interactions. In a general context, KT is a microscopic theory of nonequilibrium systems. Indeed, all the above mentioned fields of physics such as e.g. thermodynamics assume that the medium is in its most probable microphysical state, called equilibrium. Clearly, any macroscopic manifestation of deviations from this microscopic equilibrium should be considered within KT.

The first classical applications of KT concerned gases. A successful description of ideal and nonideal gases has been reached within the framework of Newtonian mechanics. With the discovery of Special Relativity KT had to be reformulated in a Lorentz invariant fashion, to make it compatible with

existence of a limiting velocity, the speed of light. Indeed, the generalization of Maxwell-Boltzmann equilibrium distributions to relativistic case was obtained already in 1911 Jüttner (1911). It soon became clear that there is another natural arena for application of KT which is plasma physics Landau (1936, 1937). The major difference between plasma and gas is the existence of long range forces, which has been accommodated by introduction of the mean field description Vlasov (1938). Formulation of relativistic KT has been completed in the 1960s and is presented in several monographs, see e.g. Synge (1957); Groot et al. (1980); Cercignani and Kremer (2002).

Since basic phenomena in the microworld are described on a quantum language, KT uses extensively quantum theory. In fact, basic principles and equations of KT may be derived from Quantum Field Theory, see Groot et al. (1980).

The purpose of these lecture notes is, however, not to review the foundations of KT that would require an entire dedicated monograph. In this paper I will only remind basic concepts of KT and introduce the necessary mathematical apparatus. The main goal is essentially to show a wide area of applications of KT, spanning from astrophysical compact objects to the whole Universe in its evolution.

G.2. Basic concepts

G.2.1. Distribution function

In classical (also relativistic) mechanics a complete description of a system composed of N interacting particles is given by their N equations of motion. In non-relativistic kinetic theory one deals with a space of positions and velocities of these particles, the configuration space. In relativistic kinetic theory it is replaced by the *phase space* $\mathcal{M}$ of positions and momenta. In principle, equivalent description of the system is given by a function $F(\Gamma)$ of $6N$ independent variables, defined on $\mathcal{M}$. An equation can be formulated for this function, called the Liouville equation, that can be written apparently in a very simple form

$$\frac{dF(\Gamma)}{ds} = 0, \tag{G.2.1}$$

where the derivative is over the proper time. However, its complexity is equivalent to the complexity of original N-body problem, and in majority

of cases it cannot be addressed directly.

A tremendous simplification occurs for some systems, where N is very large. Under certain conditions, which will be discussed below in Sec. G.6, they can be described by a function defined on the 6-dimensional phase space $\mathcal{M}^6$. Such function depends only on 7 variables: 3 space coordinates, 3 momentum components, and time. In such a case the DF is called the *one particle distribution function* (DF) $f(x^\mu, p^\mu)$. This is the basic object used in statistical (probabilistic) description of a system composed of large number of particles. For brevity in what follows denote[1] the coordinates in momentum space as $x = x^\mu = (ct, \mathbf{x})$, $p = p^\mu = (p^0, \mathbf{p})$, where c is the speed of light. Notice that p^0 is not an independent variable and it satisfies the relativistic energy equation $p^0 = \sqrt{\mathbf{p}^2 + m^2c^2}$. The DF is defined such that the integral

$$N \equiv \int_{\mathcal{M}^6} f(\mathbf{p}, \mathbf{x}, t) d^3p d^3x, \tag{G.2.2}$$

gives the total number of particles. Notice that the integral is clearly Lorentz invariant. The invariance of the distribution function itself is not obvious from such a definition and will be demonstrated explicitly below in Sec. G.2.3. Then one observes that $f(x, p)d^3pd^3x$ is an average number of particles having momenta in the range $(\mathbf{p}, \mathbf{p}+d^3p)$ and coordinates in the range $(\mathbf{x}, \mathbf{x}+d^3x)$ at the moment t, and the integral (G.2.2) is taken in the whole phase space $\mathcal{M}^6$.

Notice that despite symmetrical form of $f(x, p)$ there is a conceptual difference between x and p. In particular, the integral

$$n(\mathbf{x}, t) \equiv \int_{-\infty}^{+\infty} f d^3p \tag{G.2.3}$$

is assumed to be finite, leading to certain restrictions on $f(p)$. In particular, when the DF is isotropic in momentum space, $p^2 f(|p|)$ should decrease with increasing momentum for $|p| \gg 1$ fast enough, at least faster than $1/|p|$; it also should not increase with decreasing momentum for $|p| \ll 1$ faster than $1/|p|$.

[1] In what follows Greek indices run from 0 to 3, while Latin ones run from 1 to 3. Einstein summation rule is adopted.

G.2.2. Averaging and macroscopic quantities

It is important to keep in mind that the DF defined by eq. (G.2.2) is not accessible directly to measurements. In any experiment or observation one has to deal with averaged quantities. While a microscopic state is defined on the phase space by the DF, it is useful to introduce a macroscopic quantity $A(x)$ as

$$A(x) \equiv \int_{-\infty}^{+\infty} A(x,p) d^3p. \tag{G.2.4}$$

Particle density (G.2.3) is the simplest example. By definition the macroscopic quantity does not depend on momentum, but only on coordinates and time. Such quantity may be further averaged in space or time as follows

$$\langle A \rangle_{\text{time}} (\mathbf{x}) \equiv \lim_{T\to\infty} \frac{1}{T} \int_0^T A(x) dt, \qquad \langle A \rangle_{\text{space}} (t) \equiv \lim_{V\to\infty} \frac{1}{V} \int_{\mathcal{V}} A(x) d^3x. \tag{G.2.5}$$

The averaging may also be made on finite time T and in finite volume V then the limits in front of integrals in eq. (G.2.5) are omitted.

In contrast to space and time averaging, statistical (or ensemble) averaging for a quantity $A(x,p)$ is defined as

$$\langle A \rangle_{\text{ens}} \equiv \frac{1}{N} \int_{\mathcal{M}^6} A(x,p) f(x,p) d^3p d^3x. \tag{G.2.6}$$

While experiments deal with space and time averaged quantities, theory usually works with ensemble averaged ones. The connection between macroscopic and microscopic quantities from the one hand, but also space-time averaged quantities and ensemble averaged ones from the other hand, is required. An important concept called *statistical equilibrium* requires that any macroscopically large part of the system has macroscopic physical quantities being equal to their statistical average values. For one particle DF this statement can be represented as follows

$$\frac{1}{V} \int_{\mathcal{V}} \int_{-\infty}^{+\infty} A(x,p) d^3p d^3x = \frac{\int_{\mathcal{V}} \int_{-\infty}^{+\infty} A(x,p) f(x,p) d^3p d^3x}{\int_{\mathcal{V}} \int_{-\infty}^{+\infty} f(x,p) d^3p d^3x}, \tag{G.2.7}$$

where $\mathcal{V}$ is an arbitrary macroscopic volume.

One of the most important theorems in statistical mechanics states that for *ergodic systems* the time averaged quantity should be equal to its ensemble average. In a specific case when the system is described by one particle DF it is reduced to

$$\lim_{T\to\infty}\frac{1}{T}\int_0^T A(x,p)dt = \frac{1}{N}\int_{\mathcal{M}^6} A(x,p)f(x,p)d^3pd^3x. \tag{G.2.8}$$

Note that it is difficult to prove ergodicity of a given physical system. Nevertheless, ergodicity is often assumed in practice.

G.2.3. Invariance of one particle DF

The one particle DF defined by (G.2.2) is not written in a Lorentz invariant way. However, it is an invariant, as demonstrated below following Ochelkov et al. (1979); Groot et al. (1980), see also Debbasch et al. (2001). Consider the system of particles of equal mass m with coordinates $\mathbf{x}_i(t)$ and momenta $\mathbf{p}_i(t)$. By definition, from the statistical point of view, the one particle DF is the averaged particle density in momentum space, see e.g. Debbasch and van Leeuwen (2009a), that is

$$f(\mathbf{p},\mathbf{x},t) = \left\langle \sum_i \delta^3\left[\mathbf{p}-\mathbf{p}_i(t)\right]\delta^3\left[\mathbf{x}-\mathbf{x}_i(t)\right]\right\rangle_{\text{ens}}. \tag{G.2.9}$$

In a relativistic context, it is natural to introduce an eight-dimensional one-particle phase space $\mathcal{M}^8$. In such phase space the variable p^0 is not necessarily related to $\mathbf{p}$, likewise t is not related to $\mathbf{x}$. At the end of any calculations involving $\mathcal{M}^8$ the physical results can be recovered by restricting every equation to the sub-manifold of the mass-shell where $p^0 > 0$. Introducing in this way a new quantity

$$\mathcal{F}(x,p) = 2\Theta(p^0)\delta(p^\mu p_\mu - m^2c^2)f(\mathbf{p},\mathbf{x},t), \tag{G.2.10}$$

where the term $\Theta(p^0)\delta(p^\mu p_\mu - m^2c^2)$ is Lorentz scalar, one has to show that this function is a Lorentz scalar. Recalling the identity

$$\delta\left(Z(x)\right) = \sum_i \left|\frac{dZ}{dx}\right|^{-1}\delta\left(x-x_i\right), \tag{G.2.11}$$

where x_i are the roots of the equation $Z(x) = 0$, rewrite eq. (G.2.10) using (G.2.9) as

$$\mathcal{F}(x,p) = \left\langle \sum_i \frac{1}{p_i^0(t)} \delta^3 \left[\mathbf{p} - \mathbf{p}_i(t)\right] \delta \left[p - p_i^0(t)\right] \delta^3 \left[\mathbf{x} - \mathbf{x}_i(t)\right] \right\rangle_{\text{ens}}. \quad \text{(G.2.12)}$$

Introducing additional integration over a delta function as

$$\mathcal{F}(x,p) = \int dt \left\langle \sum_i \frac{1}{p_i^0(t_i)} \delta \left[t - t_i\right] \delta^3 \left[\mathbf{p} - \mathbf{p}_i(t_i)\right] \delta \left[p - p_i^0(t_i)\right] \delta^3 \left[\mathbf{x} - \mathbf{x}_i(t_i)\right] \right\rangle_{\text{ens}} \quad \text{(G.2.13)}$$

and using the relation $ds_i = \frac{mc}{p_i^0(t_i)} dt_i$ one can show that $\mathcal{F}(x,p)$ is a scalar since

$$\mathcal{F}(x,p) = \frac{1}{mc} \int ds \left\langle \sum_i \delta^4 \left[x - x_i(s)\right] \delta^4 \left[p - p_i(s)\right] \right\rangle_{\text{ens}}, \quad \text{(G.2.14)}$$

where $x_i(s)$ and momenta $p_i(s)$ are trajectories in $\mathcal{M}^8$. The last expression can be understood as the ensemble averaged and time integrated Klimontovich one particle DF, see e.g. Zakharov (2000) and Sec. G.3.1 below.

G.2.4. Important macroscopic quantities

One can define an invariant quantity instead of eq. (G.2.3) as

$$j^\mu(\mathbf{x},t) \equiv c \int p^\mu f \frac{d^3p}{p^0} = c \int \mathcal{F}(x,p) p^\mu d^4p, \quad \text{(G.2.15)}$$

where both f and d^3p/p^0 are scalars. This *first moment* of the DF is the particle four-flux. Its spatial part represents usual three-vector flux $\mathbf{j}(\mathbf{x},t) \equiv c \int \mathbf{v} f d^3p$, where $\mathbf{v} = c\mathbf{p}/p^0$ is the velocity of a relativistic particle with momentum $\mathbf{p}$, $u^\mu = dx^\mu/ds$.

Analogously, the *second moment* can be constructed

$$T^{\mu\nu}(\mathbf{x},t) \equiv c \int p^\mu p^\nu f \frac{d^3p}{p^0}, \quad \text{(G.2.16)}$$

and so on. The quantity $T^{\mu\nu}$ is a symmetric tensor by construction. It represents an energy-momentum tensor of the system of particles. It should be noted that in eq. (L.0.1) only rest mass energy and kinetic energy of particles are taken into account, excluding their potential energy.

One more important quantity is entropy flux defined as

$$S^{\mu}(\mathbf{x},t) \equiv -k_B c \int p^{\mu} f \frac{d^3p}{p^0} \left[\log\left(h^3 f\right) - 1\right], \tag{G.2.17}$$

where two new constants appear: k_B is Boltzmann's constant and h is a dimensional parameter needed to make the argument of the logarithm dimensionless.

Unlike non-relativistic kinetic theory, in its relativistic counterpart macroscopic velocity can be defined in different ways. Two widespread definitions are due to Eckart Eckart (1940) and Landau and Lifshitz Landau and Lifshitz (1959):

$$U^{\mu}_{\mathrm{E}} \equiv \frac{cj^{\mu}}{\sqrt{j^{\mu}j_{\mu}}} \qquad \text{or} \qquad U^{\mu}_{\mathrm{LL}} \equiv \frac{cT^{\mu\nu}U_{\nu}}{\sqrt{U_{\rho}T^{\rho\sigma}T_{\sigma\tau}U^{\tau}}}. \tag{G.2.18}$$

While U^{μ}_{E} can be interpreted as the average velocity of particles, U^{μ}_{LL} can be understood as the average velocity of energy-momentum transfer.

G.3. Kinetic equation

This section follows the derivation presented in Groot et al. (1980). One can introduce a scalar quantity

$$\Delta J = \frac{1}{c}\int_{\Delta^3\sigma} d^3\sigma_{\mu} j^{\mu} = \int_{\Delta^3\sigma} d^3\sigma_{\mu} \int \frac{d^3p}{p^0} p^{\mu} f, \tag{G.3.1}$$

where the time-like four-vector $d^3\sigma_{\mu}$ is an oriented three-surface element of a plane space-like surface σ, the quantity $\Delta^3\sigma$ is a small element and the last equality follows from eq. (G.2.15). In the Lorentz frame where $d^3\sigma_{\mu}$ is purely timelike it has components $(d^3x, 0, 0, 0)$. In this frame

$$\Delta J = \int_{\Delta^3\sigma} \int f\left(x,p\right) d^3p d^3x, \tag{G.3.2}$$

which is just an average number of world lines crossing the segment $\Delta^3\sigma$. Considering those world lines which have momenta in the range $\Delta^3 p$ around $\mathbf{p}$, one can get

$$\Delta J = \int_{\Delta^3\sigma}\int_{\Delta^3 p} f\left(x,p\right) d^3p d^3x. \tag{G.3.3}$$

Accepting this interpretation, consider world lines given by eq. (G.3.1) which later cross another segment $\Delta^3\hat{\sigma}$. Since there are no collisions it is possible to write

$$\int_{\Delta^3\hat{\sigma}} d^3\sigma_\mu \int_{\Delta^3 p} \frac{d^3p}{p^0} p^\mu f - \int_{\Delta^3\sigma} d^3\sigma_\mu \int_{\Delta^3 p} \frac{d^3p}{p^0} p^\mu f = 0, \tag{G.3.4}$$

or in other way

$$\int_{\Delta^3 x} d^3\sigma_\mu \int_{\Delta^3 p} \frac{d^3p}{p^0} p^\mu f = 0, \tag{G.3.5}$$

where $\Delta^3 x$ is the surface of Minkowski space element $\Delta^4 x$. Applying Gauss' theorem one gets

$$\int_{\Delta^4 x} d^4x \int_{\Delta^3 p} \frac{d^3p}{p^0} p^\mu \partial_\mu f = 0, \tag{G.3.6}$$

where $\partial_\mu = \left(c^{-1}\partial/\partial t, \nabla\right)$, $\Delta^3 x$ and $\Delta^3 p$ are some arbitrary hypersurfaces in the phase space.

The basic equation represents *time evolution* of the DF due to microscopic interactions in the system. In absence of any interactions between particles it represents continuity of the four-vector $p^\mu f$ and it follows from eq. (G.3.6) as

$$p^\mu \partial_\mu f = 0. \tag{G.3.7}$$

Written in the vector notation

$$\frac{\partial f}{\partial t} + \mathbf{v}\cdot\nabla f = 0. \tag{G.3.8}$$

In general case both collisions and external forces alter eq. (G.3.7) and the kinetic equation becomes

$$p^\mu \partial_\mu f + mF^\mu \frac{\partial f}{\partial p^\mu} = \mathrm{St}\, f, \tag{G.3.9}$$

where F^μ represents an external four-force, St f is the collision integral. This is the *relativistic transport equation*.

One of the main goals of KT is to establish the form of the collision integral. Consider an elastic collision

$$1+2 \longrightarrow 1'+2', \tag{G.3.10}$$

where particles 1 and 2 have masses m_1 and m_2, momenta p^μ and k^μ which changed after the collision to p'^μ and k'^μ respectively. Energy-momentum conservation gives

$$p^\mu + k^\mu = p'^\mu + k'^\mu. \tag{G.3.11}$$

The average number of such collisions is proportional to 1) the number of particles per unit volume with momenta p^μ in the range d^3p, 2) the number of particles per unit volume with momenta k^μ in the range d^3k and 3) the intervals $d^3p'^\mu$, $d^3k'^\mu$ and d^4x. The proportionality coefficients, depending only on four-momenta before and after the collision are represented as $W\left(p,k \mid p',k'\right) / \left(p^0k^0p'^0k'^0\right)$. The quantity $W\left(p,k \mid p',k'\right)$ is called the transition rate and it is a scalar. By this process particles leave the phase volume d^3p around p^μ. Collisions also bring particles back into this volume by the inverse process with the corresponding rate $W\left(p',k' \mid p,k\right)$.

Then Boltzmann equation can be written as

$$\int_{\mathcal{V}}\int_{\mathcal{P}} p^\mu \partial_\mu f \frac{d^3p}{p^0} d^4x = \frac{1}{2}\int_{\mathcal{V}}\int_{\mathcal{P}}\int \frac{d^3p}{p^0}\frac{d^3p'}{p'^0}\frac{d^3k}{k^0}\frac{d^3k'}{k'^0}\times \tag{G.3.12}$$
$$\times\left[f\left(x,p'\right)f\left(x,k'\right)W\left(p',k' \mid p,k\right) - f\left(x,p\right)f\left(x,k\right)W\left(p,k \mid p',k'\right)\right]d^4x,$$

or in differential form

$$p^\mu\partial_\mu f = \frac{1}{2}\int \frac{d^3p'}{p'^0}\frac{d^3k}{k^0}\frac{d^3k'}{k'^0}\times \tag{G.3.13}$$
$$\times\left[f\left(x,p'\right)f\left(x,k'\right)W\left(p',k' \mid p,k\right) - f\left(x,p\right)f\left(x,k\right)W\left(p,k \mid p',k'\right)\right].$$

The same equation in vector notation becomes

$$\frac{\partial f}{\partial t} + \mathbf{v}\cdot\nabla f = \frac{1}{2}\int d^3p'd^3k^3k'\left[f\left(x,p'\right)f\left(x,k'\right)w_{p'k';pk} - f\left(x,p\right)f\left(x,k\right)w_{pk;p'k'}\right], \tag{G.3.14}$$

where $w_{pk;p'k'} = cW\left(p,k \mid p',k'\right) / \left(p^0k^0p'^0k'^0\right)$. If in this expression particle

momenta are substituted by their velocities, this equation will coincide with the one derived first by Boltzmann Boltzmann (2011). Notice that the factor $1/2$ in front of collision integral is due to indistinguishability of particles.

G.3.1. Boltzmann equation in General Relativity

The derivation of Boltzmann equation in General Relativity is presented here following Zakharov (2000), for more details see Chernikov (1962, 1963b); Debbasch and van Leeuwen (2009a,b).

Let us start by introducing the 8-dimensional phase space $\mathcal{M}^8$. The distribution function $\mathcal{F}^K(x,p)$ in this phase space is defined Beliaev and Budker (1956) such that

$$j^\mu = \int u^\mu \mathcal{F}^K(x,p)\, d^4p \tag{G.3.15}$$

is the usual particle-current four-vector (G.2.15). Define the Klimontovich DF Klimontovich (1960a)

$$\mathcal{F}^K(x,p) = \frac{1}{mc}\sum_i \int ds \delta^4\left[x - x_i(s)\right]\delta^4\left[p - p_i(s)\right], \tag{G.3.16}$$

where $ds = \left(g_{\mu\nu}dx^\mu dx^\nu\right)^{1/2}$ is the proper time. Notice that eq. (G.2.14) defined above is nothing but the ensemble averaged function (G.3.16). The equations of motion for each particle in the gravitational field are

$$mc\frac{dx^\mu}{ds} = p^\mu, \qquad mc\frac{dp^\mu}{ds} = -\Gamma^\mu_{\nu\lambda}p^\nu p^\lambda, \tag{G.3.17}$$

where the $\Gamma^\mu_{\nu\lambda}$ are the Christoffel symbols. Using the property

$$\frac{d}{ds}\delta\left[x - g(s)\right] = -\frac{d}{dx}\delta\left[x - g(s)\right]\frac{dg}{ds} \tag{G.3.18}$$

from the identity

$$\int ds \frac{d}{ds}\left\{\delta^4\left[x - x_i(s)\right]\delta^4\left[p - p_i(s)\right]\right\} = 0 \tag{G.3.19}$$

one can obtain

$$\frac{\partial\left(p^{\mu}\mathcal{F}^{K}\right)}{\partial x^{\mu}}-\frac{\partial}{\partial p^{\mu}}\left(\Gamma_{\nu\lambda}^{\mu}p^{\nu}p^{\lambda}\mathcal{F}^{K}\right)=0. \tag{G.3.20}$$

Using another identity

$$\frac{\partial p^{\mu}}{\partial x^{\mu}}-\frac{\partial}{\partial p^{\mu}}\left(\Gamma_{\nu\lambda}^{\mu}p^{\nu}p^{\lambda}\right)=0, \tag{G.3.21}$$

see Zakharov (2000), and applying to eq. (G.3.20) the averaging procedure with $\mathcal{F}=\left\langle \mathcal{F}^{K}(x,p)\right\rangle_{\text{ens}}$ one finally gets

$$p^{\mu}\frac{\partial\mathcal{F}}{\partial x^{\mu}}-\Gamma_{\nu\lambda}^{\mu}p^{\nu}p^{\lambda}\frac{\partial\mathcal{F}}{\partial p^{\mu}}=0. \tag{G.3.22}$$

This is the collisionless kinetic equation for the distribution function defined in $\mathcal{M}^{8}$. As for the DF $f(\mathbf{p},\mathbf{x},t)$ defined in $\mathcal{M}^{6}$ the corresponding equation can be obtained using eq. (G.2.10) and integrating eq. (G.3.22) over p^{0}. As the result one has

$$p^{\mu}\frac{\partial f}{\partial x^{\mu}}-\Gamma_{\nu\lambda}^{i}p^{\nu}p^{\lambda}\frac{\partial f}{\partial p^{i}}=0. \tag{G.3.23}$$

Finally, assuming that it is possible to introduce a local Lorentz frame and define the expressions for $\mathrm{St}\, f$ in that frame, one can write by analogy with eq. (G.3.9) the general expression for the Boltzmann equation as

$$p^{\mu}\frac{\partial f}{\partial x^{\mu}}-\Gamma_{\nu\lambda}^{i}p^{\nu}p^{\lambda}\frac{\partial f}{\partial p^{i}}=\mathrm{St}\, f. \tag{G.3.24}$$

This equation has to be compared with eq. (G.3.9): in General Relativity the curved nature of space-time results in a term similar to the external force in eq. (G.3.9). Another form of Boltzmann equation can be written in a different form, similar to eq. (G.3.13) by introducing the Cartan covariant derivative

$$\nabla_{\mu}\Phi(x,p)\equiv\frac{\partial\Phi}{\partial x^{\mu}}+\Gamma_{\mu\nu}^{\lambda}p_{\lambda}\frac{\partial\Phi}{\partial p_{\nu}}. \tag{G.3.25}$$

Then for the ensemble averaged DF one has

$$p^{\mu}\nabla_{\mu}f(x,p)=\mathrm{St}\, f. \tag{G.3.26}$$

Comparing this last expression with eq. (G.3.13) one can see that, as often occurs in General Relativity, usual derivative in eq. (G.3.13) is substituted with the covariant derivative in eq. (G.3.26).

G.3.2. Uehling-Uhlenbeck collision integral

In this section the collision integral of eq. (G.3.13) is obtained for the case of elastic collision between two classical particles. When particles follow quantum statistics it is still possible to use the collision integral Uehling and Uhlenbeck (1933); Uehling (1934) which is phenomenologically modified as follows

$$\begin{gathered}\mathrm{St}\, f = \frac{1}{2}\int \frac{d^3p'}{p'^0}\frac{d^3k}{k^0}\frac{d^3k'}{k'^0}\times \\ \times\left\{f\left(x,p'\right) f\left(x,k'\right)\left[1+\theta\varphi\left(x,p\right)\right]\left[1+\theta\varphi\left(x,k\right)\right] W\left(p',k' \mid p,k\right) - \right. \\ \left. -f\left(x,p\right) f\left(x,k\right)\left[1+\theta\varphi\left(x,p'\right)\right]\left[1+\theta\varphi\left(x,k'\right)\right] W\left(p,k \mid p',k'\right)\right\},\end{gathered} \tag{G.3.27}$$

where $f\left(x,p\right) = g\varphi\left(x,p\right)/\left(2\pi\hbar\right)^3$, g is the degeneracy factor, $\theta = \pm 1, 0$ for respectively Bose-Einstein, Fermi-Dirac and Boltzmann statistics. Comparing this expression to eq. (G.3.13) one finds additional multipliers $1 \pm \left(2\pi\hbar\right)^3 f\left(x,p\right)/g$, which guarantee that equilibrium distribution functions are indeed Bose-Einstein and Fermi-Dirac ones, respectively, see e.g. Chernikov (1964a); Ehlers (1973).

G.3.3. Cross-section

An important concept describing the strength of particle interactions is the cross-section. It plays an important role in the case of two particle collisions, which is the most simple and hence the most studied case. This concept will be illustrated for the process of scattering (G.3.10).

It is possible to introduce Mandelstam (1958) the following invariant variables

$$s = \left(p^\mu + k^\mu\right)^2, \qquad t = \left(p^\mu - p'^\mu\right)^2. \tag{G.3.28}$$

They prove technically useful, but they also possess a physical interpretation: sc^2 is the square of the energy in the center of mass reference system, t is related to the scattering angle in this system: $\cos\vartheta - 1 = 2t/\left(s - 4m_1m_2c^2\right)$.

Then one may rewrite

$$W\left(p,k \mid p',k'\right) = s\sigma\left(s,\vartheta\right)\delta^4\left(p^\mu + k^\mu - p'^\mu - k'^\mu\right), \tag{G.3.29}$$

where $\sigma\left(s,\vartheta\right)$ is the differential cross-section for a given process. Remind Berestetskii et al. (1982) that the cross-section is defined through

$$dw = jd\sigma, \tag{G.3.30}$$

where dw is the probability of the process per unit time and unit volume and

$$j = \left[\left(p^\mu k_\mu\right)^2 - \left(m_1 m_2 c^2\right)^2\right]^{1/2} \tag{G.3.31}$$

is invariant flux of particles in initial state. It is possible to show Groot et al. (1980) that

$$\int \frac{d^3p'}{p'^0}\frac{d^3k'}{k'^0}\frac{1}{j}W\left(p,k \mid p',k'\right) = \int \sigma d\Omega = \int d\sigma. \tag{G.3.32}$$

Then, using the detailed balance condition

$$W\left(p,k \mid p',k'\right) = W\left(p',k' \mid p,k\right) \tag{G.3.33}$$

one may write Boltzmann equation as

$$p^\mu \partial_\mu f = \frac{1}{2}\int \frac{d^3k}{k^0}\sigma\left[f\left(x,p'\right)f\left(x,k'\right) - f\left(x,p\right)f\left(x,k\right)\right]d\Omega, \tag{G.3.34}$$

or in vector notation as

$$\frac{\partial f}{\partial t} + \mathbf{v}\cdot\nabla f = \frac{1}{2}\int d^3k\sigma v\left[f\left(x,p'\right)f\left(x,k'\right) - f\left(x,p\right)f\left(x,k\right)\right]d\Omega, \tag{G.3.35}$$

where $v = cj/\left(p^0k^0\right)$ is the particles relative velocity.

G.4. Conservation laws and relativistic hydrodynamics

In this Section following Groot et al. (1980) the conservation laws fulfilled by the macroscopic quantities are derived, namely the *particle number* conservation, the *entropy* conservation and the *energy-momentum* conservation, see also Chernikov (1963a, 1964b).

Consider a mixture of D components whose particles may interact by elastic and inelastic collisions, conserving their total number. Boltzmann equations for each DF $f_k\left(x, p_k\right)$ then read

$$p_k^\mu \partial_\mu f_k = \sum_{l=1}^{D} C_{kl}\left(x, p_k\right), \tag{G.4.1}$$

where Latin indices now denote the species kind (not to be confused with tensor indices) and

$$C_{kl}\left(x, p_k\right) = \frac{1}{2} \sum_{i,j=1}^{D} \int \frac{d^3 p_l}{p_l^0} \frac{d^3 p_i}{p_i^0} \frac{d^3 p_j}{p_j^0} \left(f_i f_j W_{ij|kl} - f_k f_l W_{kl|ij}\right). \tag{G.4.2}$$

An important property of collision integrals follows from the microscopic conservation laws fulfilled at each interaction, namely

$$F = \sum_{k,l=1}^{D} \int \frac{d^3 p_k}{p_k^0} \psi_k(x) C_{kl}(x, p_k) = 0, \tag{G.4.3}$$

where $\psi_k(x)$ are so called summational invariants

$$\psi_k(x) = a_k(x) + p_k^\mu b_\mu(x), \tag{G.4.4}$$

they are arbitrary functions, except for the constraint that $a_k(x)$ is additively conserved in all reactions, i.e.

$$a_i(x) + a_j(x) = a_k(x) + a_l(x), \tag{G.4.5}$$

and $b_\mu(x)$ is an arbitrary vector. The proof of eq. (G.4.3) is based on eq. (G.4.5) and on energy-momentum conservation in a binary reaction $p_i^\mu + p_j^\mu = p_k^\mu +$

p_l^μ. In particular, for elastic scattering

$$\int \frac{d^3p_k}{p_k^0} C_{kl}(x, p_k) = 0. \tag{G.4.6}$$

Now it is possible to show how the basic equations of relativistic hydrodynamics, namely the particle number conservation (continuity) equation and the energy-momentum conservation equations arise from Boltzmann equation.

Consider the case when in eq. (G.4.4) $b_\mu(x) = 0$ and $a_k(x) = q_k a(x)$, where $a(x)$ is an arbitrary function. Then from eqs. (G.4.1) and (G.4.2) one has

$$\sum_{k=1}^{D} q_k \int \frac{d^3p_k}{p_k^0} p_k^\mu \partial_\mu f_k = 0. \tag{G.4.7}$$

Recalling the definition (G.2.15) for each component

$$j_k^\mu = c \int \frac{d^3p_k}{p_k^0} p_k^\mu f_k, \tag{G.4.8}$$

one gets

$$\partial_\mu J^\mu = 0, \quad J^\mu = \sum_{k=1}^{D} q_k j_k^\mu, \tag{G.4.9}$$

where q_k is a charge (e.g. electric, leptonic, baryonic). In particular, with $q = 1$ this is just particle number conservation. Similarly the conservation law for the total particle number can be obtained. In particular, for elastic scattering using eq. (G.4.6) one finds

$$\partial_\mu j_k^\mu = 0. \tag{G.4.10}$$

Consider now the case $a_k(x) = 0$. Then from eq. (G.4.3) one finds

$$\sum_{k,l=1}^{D} \int \frac{d^3p_k}{p_k^0} p_k^\mu C_{kl} = 0. \tag{G.4.11}$$

Substituting this into eqs. (G.4.1) and (G.4.2) and recalling the definition (L.0.1) one gets

$$\partial_\nu T^{\mu\nu} = 0, \tag{G.4.12}$$

where

$$T^{\mu\nu} = c \sum_{k=1}^{D} \int \frac{d^3 p_k}{p_k^0} p_k^\mu p_k^\nu f_k, \tag{G.4.13}$$

is the energy-momentum tensor of the mixture. Equations (G.4.9) and (G.4.11) represent basic equations of relativistic hydrodynamics, see e.g. Mihalas and Mihalas (1984).

G.5. Entropy and equilibrium

In this Section the concept of thermodynamic equilibrium will be discussed from the point of view of kinetic theory.

G.5.1. $\mathcal{H}$-theorem

First let us show, following Groot et al. (1980), that the quantity defined as divergence of four-vector (G.2.17) as

$$\sigma(x) \equiv \partial_\mu S^\mu, \tag{G.5.1}$$

can never decrease. For alternative derivation see Chernikov (1963b). From eqs. (G.2.17) and (G.5.1) it follows

$$\sigma = -k_B c \int \frac{d^3 p}{p^0} \left[\log\left(h^3 f\right)\right] p^\mu \partial_\mu f. \tag{G.5.2}$$

Substituting Boltzmann equation (G.3.9) into this expression one get

$$\sigma = -k_B c \int \frac{d^3 p}{p^0} \left[\log\left(h^3 f\right)\right] Stf + k_B c \int \frac{d^3 p}{p^0} \left[\log\left(h^3 f\right)\right] F^\mu \frac{\partial f}{\partial p^\mu}. \tag{G.5.3}$$

Assume that the force satisfies the following properties: $p^\mu F_\mu = 0$ and $\frac{\partial F^\mu}{\partial p^\mu} = 0$. The former condition means that the force is mechanical and does not alter particle rest mass. Then the second contribution in eq. (G.5.3) can be written as

$$2k_B c \int d^4 p \frac{\partial}{\partial p^\mu} \left\{\Theta(p^0)\delta(p^\mu p_\mu - m^2 c^2) f \left[\log\left(h^3 f\right) - 1\right] F^\mu\right\}, \tag{G.5.4}$$

and it vanishes, provided that the integrand is decreasing fast enough for large momenta in the sense defined above.

The first contribution can be rewritten as

$$\sigma = -\frac{1}{4}k_B c \sum_{i,j,k,l} \int \frac{d^3p_i}{p_i^0}\frac{d^3p_j}{p_j^0}\frac{d^3p_k}{p_k^0}\frac{d^3p_l}{p_l^0}\left[\log\left(\frac{f_k f_l}{f_i f_j}\right)\right] f_i f_j W_{ij|kl}. \tag{G.5.5}$$

Now using the property

$$\sum_{i,j,k,l} \int \frac{d^3p_i}{p_i^0}\frac{d^3p_j}{p_j^0}\frac{d^3p_k}{p_k^0}\frac{d^3p_l}{p_l^0}\left(f_k f_l - f_i f_j\right) W_{ij|kl} = 0, \tag{G.5.6}$$

which follows from the bilateral normalization condition Groot et al. (1980) one finally gets

$$\sigma = \frac{1}{4}k_B c \sum_{i,j,k,l} \int \frac{d^3p_i}{p_i^0}\frac{d^3p_j}{p_j^0}\frac{d^3p_k}{p_k^0}\frac{d^3p_l}{p_l^0} A\left(y\right) f_i f_j W_{ij|kl}, \tag{G.5.7}$$

where

$$A\left(y\right) = y - \log y - 1 \geq 0, \qquad y = \frac{f_k f_l}{f_i f_j}. \tag{G.5.8}$$

Since $A\left(y\right)$ is a non-negative function, eq. (G.5.7) implies that $\sigma \geq 0$. This completes the proof of the Boltzmann $\mathcal{H}$-theorem.

Notice that $\sigma = 0$ holds if and only if

$$f_i\left(x, p_i\right) f_j\left(x, p_j\right) = f_k\left(x, p_k\right) f_l\left(x, p_l\right). \tag{G.5.9}$$

This condition is satisfied, as can be seen from eq. (G.3.34) when collision integral in the RHS of Boltzmann equation vanishes. This case is identified as *local equilibrium*. In fact, the equilibrium DF is characterized by the following macroscopic quantities as parameters: density, temperature, 4-velocity. It is possible to show this by turning to a simple system with binary collisions and rewrite the condition (G.5.9) as

$$\log\left(h^3 f_1\right) + \log\left(h^3 f_2\right) = \log\left(h^3 f_1'\right) + \log\left(h^3 f_2'\right). \tag{G.5.10}$$

It is clear that the quantity $\log\left(h^3 f\right)$ is a summational invariant. The most

general summational invariant, as discussed above, is a linear combination of a constant and p^μ. Then one particle distribution function in equilibrium is

$$f^{eq} = \frac{1}{h^3} \exp\left[a(x) + b_\mu(x) p^\mu\right] \tag{G.5.11}$$

with arbitrary space- and time-dependent parameters $a(x)$ and $b_\mu(x)$.

However, DF f^{eq} will be a solution of the Boltzmann equation only if it turns to zero also its LHS. Then the parameters of eq. (G.5.11) should satisfy

$$p^\mu \partial_\mu a(x) + p^\mu p^\nu \partial_\mu b_\nu(x) + m b_\mu(x) F^\mu(x,p) = 0, \tag{G.5.12}$$

which should be an identity for arbitrary p^μ. When the DF satisfies eq. (G.5.12) it is called *global equilibrium* DF f^{EQ}.

In the absence of external field f^{EQ} reduces to the Jüttner Jüttner (1911) momentum distribution

$$f^{EQ}(p) = \frac{1}{h^3} \exp\left[\frac{\phi - p^\mu U_\mu}{k_B T}\right], \tag{G.5.13}$$

where ϕ, T and U_μ are parameters, $U^\mu U_\mu = c^2$, h and k_B are Planck's and Boltzmann's constants.

It is possible now to compute such important macroscopic quantities as the number density, the energy density and the pressure of a system in local equilibrium. Using the definition (G.2.15) and $j^\mu = n U^\mu$ one has

$$n = \frac{j^\mu U_\mu}{c^2} = \frac{1}{ch^3} \exp\left(\frac{\phi}{k_B T}\right) \int \frac{d^3p}{p^0} p^\mu U_\mu \exp\left(\frac{-p^\nu U_\nu}{k_B T}\right). \tag{G.5.14}$$

The integral, being a scalar, can be evaluated in the rest frame, where $U^\mu = (c,0,0,0)$ by introducing polar coordinates and dimensionless variables $\theta = k_B T / \left(mc^2\right)$, $\nu = \phi / \left(mc^2\right)$ and $y = c\sqrt{\mathbf{p}^2 + m^2c^2} / \left(k_B T\right)$. The result is

$$n = \frac{4\pi}{\lambda_C^3} \exp\left(\frac{\nu}{\theta}\right) K_2\left(\theta^{-1}\right), \tag{G.5.15}$$

where $\lambda_C = \frac{\hbar}{mc}$ and

$$K_n\left(\theta^{-1}\right) = \frac{2^{n-1}(n-1)!}{(2n-2)!} z^{-n} \int_z^\infty dy \left(y^2 - \theta^{-2}\right)^{n-\frac{3}{2}} y \exp(-y) \tag{G.5.16}$$

is the modified Bessel function of the second kind.

In full analogy, using the definition of the energy-momentum tensor and $T^{\mu\nu} = c^{-2}\rho U^\mu U^\nu - p\Delta^{\mu\nu}$, where $\Delta^{\mu\nu} = g^{\mu\nu} - c^{-2}U^\mu U^\nu$, one can compute the energy density ρ and pressure p as follows

$$\rho = \frac{T^{\mu\nu}U_\mu U_\nu}{c^2} = \frac{1}{c}\int \frac{d^3p}{p^0}\left(p^\mu U_\mu\right)^2 f^{EQ}, \tag{G.5.17}$$

$$p = -\frac{1}{3}T^{\mu\nu}\Delta_{\mu\nu} = -\frac{c}{3}\int \frac{d^3p}{p^0}p^\mu p^\nu \Delta_{\mu\nu} f^{EQ}. \tag{G.5.18}$$

Performing the integrals one finally gets

$$\rho = 4\pi\frac{mc^2}{\lambda_C^3}\exp\left(\frac{\nu}{\theta}\right)\left[3\theta^2 K_2\left(\theta^{-1}\right) + \theta K_1\left(\theta^{-1}\right)\right], \tag{G.5.19}$$

$$p = 4\pi\frac{mc^2}{\lambda_C^3}\exp\left(\frac{\nu}{\theta}\right)\theta^2 K_2\left(\theta^{-1}\right). \tag{G.5.20}$$

Introducing the enthalpy as $h_e = (\rho + p)/n$ one obtains

$$h_e = mc^2\frac{K_3\left(\theta^{-1}\right)}{K_2\left(\theta^{-1}\right)}. \tag{G.5.21}$$

Finally, the entropy density is given by

$$s = \frac{S^\mu U_\mu}{c^2} = -\frac{k_B}{c}\exp\left(\frac{\phi}{k_B T}\right)\int \frac{d^3p}{p^0}p^\mu U_\mu\left(\frac{\varphi - p^\nu U_\nu}{k_B T} - 1\right)\exp\left(\frac{-p^\nu U_\nu}{k_B T}\right). \tag{G.5.22}$$

Taking into account eqs. (G.5.15) and (G.5.19) this integral gives

$$s = \frac{1}{T}(\rho - \phi n) + k_B n. \tag{G.5.23}$$

Finally, for the thermal index $\Gamma = c_p/c_v$, which is the ratio of specific heat capacities

$$c_p = \left(\frac{\partial h_e}{\partial T}\right)_p, \quad c_v = \left(\frac{\partial\left(\rho/n\right)}{\partial T}\right)_v, \tag{G.5.24}$$

one has

$$\frac{\Gamma}{\Gamma-1}=\theta^{-2}+5\left(\frac{h_e}{\theta}\right)-\left(\frac{h_e}{\theta}\right)^2, \tag{G.5.25}$$

and the limiting cases are

$$\Gamma\to\begin{cases}\frac{5}{3}, & \theta\to 0,\\ \\ \frac{4}{3}, & \theta\to\infty.\end{cases} \tag{G.5.26}$$

In Fig. G.1 the dependence $\Gamma(\theta)$ computed using eqs. (G.5.25) and (G.5.21) is shown. Non-relativistic and ultra-relativistic asymptotics are clearly visible. Interestingly, at temperatures $k_BT\sim mc^2$ usually considered mildly relativistic this function is already close to its ultra-relativistic value.

Combining expressions (G.5.15), (G.5.19), (G.5.20), (G.5.23) and (G.5.21) above one find the perfect gas laws

$$\begin{aligned}&p=nk_BT,\\ &p=(\Gamma-1)\,\rho,\\ &\phi=h_e-Ts.\end{aligned} \tag{G.5.27}$$

Note that the traditional scheme of thermodynamics is recovered if we identify T as temperature, ϕ as the chemical (Gibbs) potential.

G.5.2. Relativistic Maxwellian distribution

It is instructive to consider relativistic Maxwell distribution of particles with somewhat more attention. Considering eq. (G.5.13) in the local rest frame

$$f^{LEQ}=\frac{1}{h^3}\exp\left(\frac{\nu}{\theta}\right)\exp\left(-\frac{\gamma}{\theta}\right), \tag{G.5.28}$$

where $\gamma=p^0/(mc)$, using eq. (G.2.3) and comparing it with eq. (G.5.15) one gets

$$f=\frac{dn}{d\gamma}=\frac{4\pi}{\lambda_C^3\theta K_2\left(\theta^{-1}\right)}\exp\left(\frac{\nu}{\theta}\right)\gamma\sqrt{\gamma^2-1}\exp\left(-\frac{\gamma}{\theta}\right). \tag{G.5.29}$$

The function $f(\beta)$ with $\beta = |\mathbf{v}|/c$ is shown in Fig. G.2 for selected values of the dimensionless temperature, each curve is normalized to unity. While the distribution function with the lowest temperature $\theta = 0.02$ reminds a classical Maxwellian, the one with the highest temperature $\theta = 1.78$ it is already far from it: the effect of limiting velocity is clearly visible.

G.5.3. Generalized continuity equation

Up to now only such interactions where particle conservation is satisfied were discussed. An obvious example is scattering. However, there are processes where particle conservation does not hold. The simplest example annihilation of particles-antiparticle pair in two photons and the inverse process of pair creation from two photons. Even if total number of particles (both pairs and photons) is conserved, individual number of particles in each component can change. Consider this process in more details

$$e^+ + e^- \longleftrightarrow \gamma_1 + \gamma_2, \tag{G.5.30}$$

with the corresponding energy-momentum conservation $p_- + p_+ = k_1 + k_2$. For positron (electron) from eq. (G.3.13) one has[2]

$$p^\mu \partial_\mu f_\pm = \int \frac{d^3p_\mp}{p^0_\mp}\frac{d^3k_1}{k^0_1}\frac{d^3k_2}{k^0_2}\left[f_1 f_2 W\left(k_1, k_2 \mid p_\pm, p_\mp\right) - f_\pm f_\mp W\left(p_\pm, p_\mp \mid k_1, k_2\right)\right], \tag{G.5.31}$$

where $f_\pm = f(x, p_\pm)$, etc. From eqs. (G.3.30) and (G.3.31) one gets

$$\frac{d^3k_1}{k^0_1}\frac{d^3k_2}{k^0_2} W\left(p_\pm, p_\mp \mid k_1, k_2\right) = j d\sigma, \tag{G.5.32}$$

$$v_{\text{rel}} = \sqrt{\left(\mathbf{v}_- - \mathbf{v}_+\right)^2 - \left(\mathbf{v}_- \times \mathbf{v}_+\right)^2} = j\frac{c}{p^0_\pm p_{0\mp}},$$

[2]Electrons and positrons are distinguishable particles and hence there is no factor $1/2$ in front of the collision integral.

where $v_{\rm rel}$ is the relative velocity between electron and positron. Then integrating eq. (G.5.31) over $\frac{d^3p_\pm}{p^0_\pm}$ and using eq. (G.5.32) one obtains

$$\partial_\mu \int \frac{d^3p_\pm}{p^0_\pm} p^\mu f_\pm = \int \frac{d^3p_\pm}{p^0_\pm}\frac{d^3p_\mp}{p^0_\mp}\frac{d^3k_1}{k^0_1}\frac{d^3k_2}{k^0_2} f_1 f_2 W\left(k_1,k_2 \mid p_\pm,p_\mp\right) - \\ - \int \frac{d^3p_\pm}{p^0_\pm}\frac{d^3p_\mp}{p^0_\mp} f_\pm f_\mp j d\sigma. \tag{G.5.33}$$

In view of eq. (G.2.3) and second equation in (G.5.32) the annihilation rate is defined as

$$n_\pm n_\mp \left\langle \sigma v \right\rangle_{ann} \equiv c \int \frac{d^3p_\pm}{p^0_\pm}\frac{d^3p_\mp}{p^0_\mp} f_\pm f_\mp j d\sigma. \tag{G.5.34}$$

This is an invariant quantity, as can be seen from analysis of the RHS. Notice, that the LHS in eq. (G.5.33) is nothing but derivative of the particle four-flux (G.2.15). In equilibrium this quantity is conserved, see eq. (G.4.10). So that in equilibrium

$$c \int \frac{d^3p_\pm}{p^0_\pm}\frac{d^3p_\mp}{p^0_\mp}\frac{d^3k_1}{k^0_1}\frac{d^3k_2}{k^0_2} f_1 f_2 W\left(k_1,k_2 \mid p_\pm,p_\mp\right) = n^{eq}_\pm n^{eq}_\mp \left\langle \sigma v \right\rangle_{ann}. \tag{G.5.35}$$

Thus one can write

$$\partial_\mu j^\mu_\pm = \left\langle \sigma v \right\rangle_{ann} \left(n^{eq}_+ n^{eq}_- - n_+ n_-\right), \tag{G.5.36}$$

and it reduces to eq. (G.4.10) in thermal equilibrium, since in equilibrium particle non conserving interactions balance each other. This equation finds numerous applications, especially in cosmology, since it is much easier to solve compared to integro-differential eq. (G.3.13).

G.6. Relativistic BBGKY hierarchy

In this section following de Jagher and Sluijter (1988), the derivation of relativistic Bogoliubov–Born–Green–Kirkwood–Yvon hierarchy is briefly illustrated, see also Klimontovich (1960a),Kuz'menkov (1978),Naumov (1981),Polyakov (1988) and Hakim (2011). The basic idea in this approach is that any many-body system can be characterized by the set of equations of

motion under given interaction. Applying averaging to Klimontovich distribution functions one can derive the infinite chain of equations (hierarchy) for many particle distribution functions.

For definiteness let us discuss a system of charged particles of equal mass with the corresponding electromagnetic interaction. In that case it is convenient to use for the four-momentum $p^\mu \longrightarrow p^\mu - \frac{q}{c}A^\mu$, where A^μ is the vector potential of the electromagnetic field. The equations of motion are

$$\frac{dp^\mu}{ds} = -\frac{q}{c}F^{\mu\nu}u_\nu, \quad p^\mu = mu^\mu, \quad u^\mu = \frac{dx^\mu}{ds}, \tag{G.6.1}$$

where $F^{\mu\nu}$ is the electromagnetic field tensor, u^μ is the particle four-velocity. For the point particle the four-current is

$$j^\mu = q\int u^\mu \delta^4\left[x^\nu - x^\nu\left(s\right)\right]ds. \tag{G.6.2}$$

Recalling the definition (G.3.16) of the Klimontovich DF one may proceed in analogy with Sec. G.3.1. Using eq. (G.6.1) one arrives to the Klimontovich equation

$$p^\mu \partial_\mu \mathcal{F}^K - \frac{q}{c}p_\mu F^{\mu\nu}\frac{\partial \mathcal{F}^K}{\partial p^\nu} = 0. \tag{G.6.3}$$

This equation has to be supplemented by the Maxwell field equations

$$\partial_\mu F^{\mu\nu} = 4\pi J^\nu, \quad \varepsilon_{\mu\nu\sigma\rho}\partial^\nu F^{\sigma\rho} = 0. \tag{G.6.4}$$

These equations are the basis for derivation of the hierarchy. Notice that these equations are used in numerical simulations (particle-in-cell algorithms). Solutions of eqs. (G.6.3), (G.6.4) are approximate solutions to the Vlasov-Maxwell system with the accuracy $\mathcal{O}(\mu)$, where $\mu = \left(n\lambda_D^3\right)^{-1}$, see e.g. Sigov (2001) is the plasma parameter, λ_D is the Debye length, see eq. (G.7.8) below, n is density.

The usual approach in statistical physics of a many-body system is to start with the Liouville theorem for ensemble density. In order to generalize the treatment to include fields with infinite degrees of freedom one has to consider linear spaces. Assume that relativistic Hamilton equations are valid (in symbolic form)

$$\frac{dX}{ds} = G\left[X\left(s\right), s\right], \tag{G.6.5}$$

and they are supplied with initial conditions $X(s = s_0) = X_0$. Introducing the N-particle phase space with coordinates X being the element of the linear space and probability density $F(X, s)$ in this phase space, after rather lengthy derivation one can show that Liouville's theorem holds

$$\frac{\partial}{\partial s}F(X,s) + F(X,s)\frac{\partial}{\partial X}\cdot G(X,s) + G(X,s)\cdot\frac{\partial}{\partial X}F(X,s) = 0. \qquad \text{(G.6.6)}$$

Then one has to apply statistical averaging to eqs. (G.6.3) and (G.6.4), which have to be rewritten in the Hamiltonian form. This can be done by introducing a hypersurface S on which initial conditions are given and which determines a scalar that can be used as a time parameter. Then a linear space is constructed in which a point can be interpreted as a state vector for the system at the surface S. Assume that fields $F^{\mu\nu}$ restricted on S can be regarded as an element of a Hilbert space with a set of orthonormal coordinates denoted by $|\Psi_i\rangle$.

It is possible to show that statistical averaging and differentiation with respect to s commute, i.e.

$$\left\langle \frac{d}{ds}A(X,s)\right\rangle_{\text{ens}} = \frac{d}{ds}\left\langle A(X,s)\right\rangle_{\text{ens}}. \qquad \text{(G.6.7)}$$

Introducing the one-particle DF (G.2.14) as $\mathcal{F}(x,p) = \left\langle \mathcal{F}^K(x,p)\right\rangle_{\text{ens}}$, averaged fields $\left\langle \sum_i F^{\mu\nu}(s)\,|\Psi_i\rangle\right\rangle_{\text{ens}}$ and currents $\left\langle q\int p^\mu \mathcal{F}^K(x,p)\,d^4p\right\rangle_{\text{ens}}$ it is possible to write down the hierarchy

$$\begin{aligned} u^\mu\partial_\mu\mathcal{F}(x,p) &= \frac{1}{p_\sigma u^\sigma}\left\{\Delta_{\mu\nu}p^\mu\partial^\nu f + \frac{q}{c}p_\mu F^{\mu\nu}\frac{\partial f}{\partial p^\nu} + \frac{q}{c}p_\mu\frac{\partial I^{\mu\nu}}{\partial p^\nu}\right\},\\ u^\sigma\partial_\sigma F^{\mu\nu}(x) &= 4\pi\Delta^{\mu\nu}_\lambda\left(J^\lambda - \Delta_{\eta\sigma}\partial^\eta F^{\sigma\lambda}\right) + \Delta^{\mu\nu}_{\sigma\lambda\rho}\partial^\sigma F^{\lambda\rho}, \qquad \text{(G.6.8)}\\ u^\mu\partial_\mu I^{\mu\nu}(x,p) &= ... \end{aligned}$$

where

$$I^{\mu\nu}(x,p) = \left\langle \left[F^{\mu\nu}(x) - \left\langle F^{\mu\nu}\right\rangle_{\text{ens}}\right]\left[\mathcal{F}^K(x,p) - \mathcal{F}(x,p)\right]\right\rangle_{\text{ens}} \qquad \text{(G.6.9)}$$

is the particle-field correlation, $\Delta^{\mu\nu} = g^{\mu\nu} + U^\mu U^\nu$ is a projection operator and

$$\Delta^{\mu\nu}_\lambda = u^\mu\Delta^\nu_\lambda - u^\nu\Delta^\mu_\lambda, \quad \Delta^{\mu\nu}_{\sigma\lambda\rho} = \left(\Delta^\mu_\sigma\Delta^\nu_\rho - \Delta^\nu_\sigma\Delta^\mu_\rho\right)u_\lambda. \qquad \text{(G.6.10)}$$

Dynamical equation for $I^{\mu\nu}(x,p)$ contains particle variance, field variance

$$g_{12}(x,p_1,p_2) = \left\langle \left[\mathcal{F}^K(x,p_1) - f(x,p_1)\right]\left[\mathcal{F}^K(x,p_2) - f(x,p_2)\right]\right\rangle_{\text{ens}}, \tag{G.6.11}$$
$$G^{\mu\nu\rho\sigma}(x) = \left\langle \left[F^{\mu\nu}(x) - \left\langle F^{\mu\nu}\right\rangle_{\text{ens}}\right]\left[F^{\rho\sigma}(x) - \left\langle F^{\rho\sigma}\right\rangle_{\text{ens}}\right]\right\rangle_{\text{ens}},$$

as well as triple correlations and so on, for details see de Jagher and Sluijter (1988). The system (G.6.8) is the relativistic Bogoliubov–Born–Green–Kirkwood–Yvon hierarchy. Like in non-relativistic theory this hierarchy is infinite.

Notice that Klimontovich in his original derivation Klimontovich (1960b) of relativistic kinetic equation neglecting radiation used solution of Maxwell equations for the four-potential A_μ. Hence in his chain of equations only particle-particle correlation functions such as $g_{12}(x,p_1,p_2)$ appear, see also Kuz'menkov (1978).

In order to close the system (G.6.8) additional assumptions are needed. In plasma physics with Coulomb interactions between particles the rapid attenuation of correlations principle Bogoliubov (1946, 1962) is usually adopted. Notice that such a principle may be considered as a consequence of ergodicity of the system Smolyansky (1968). In this way the assumption of no correlation between particles

$$\begin{aligned} \mathcal{G}(x,p_1,p_2) &= \mathcal{F}(x,p_1)\,\mathcal{F}(x,p_2), \\ \mathcal{G}(x,p_1,p_2,p_3) &= \mathcal{F}(x,p_1)\,\mathcal{F}(x,p_2)\,\mathcal{F}(x,p_3), \\ &\ldots \end{aligned} \tag{G.6.12}$$

leads to the system of Vlasov-Maxwell equations

$$p^\mu \partial_\mu \mathcal{F} - \frac{q}{c} p_\mu F^{\mu\nu} \frac{\partial \mathcal{F}}{\partial p^\nu} = 0, \tag{G.6.13}$$

$$\partial_\mu F^{\mu\nu} = 4\pi q \int \frac{d^3p}{p^0} p^\mu \partial_\mu \mathcal{F}, \quad \varepsilon_{\mu\nu\sigma\rho}\partial^\nu F^{\sigma\rho} = 0. \tag{G.6.14}$$

Taking into account nonvanishing two point correlation function, but neglecting three point correlations results in the Belyaev-Budker equation Beliaev and Budker (1956). For its derivation from the BBGKY hierarchy see Klimontovich (1960b), Naumov (1981) and Polyakov (1988). The result in-

stead of eq. (G.6.13) is

$$u^\mu \partial_\mu \mathcal{F} = -\frac{\partial K_\mu}{\partial p^\mu},$$

$$K_\mu = \frac{2\pi \left(qq'\right)^2 \Lambda}{c^2} \int d^4p' \frac{\left(u_\lambda u'_\lambda\right)^2}{c\left[\left(u_\lambda u'_\lambda\right)^2 - 1\right]^{\frac{3}{2}}} B_{\mu\nu} \left(\mathcal{F}\frac{\partial \mathcal{F}'}{\partial p'_\nu} - \mathcal{F}'\frac{\partial \mathcal{F}}{\partial p_\nu}\right), \quad \text{(G.6.15)}$$

$$B_{\mu\nu} = \left\{\left[\left(u_\lambda u'_\lambda\right)^2 - 1\right]\delta_{\mu\nu} - u_\mu u_\nu - u'_\mu u'_\nu - u_\lambda u'_\lambda \left(u_\mu u'_\nu + u'_\mu u_\nu\right)\right\},$$

where Λ is Coulomb logarithm, see eq. (G.7.22) below, primed and unprimed values correspond to two incoming particles, and the mean field is neglected. In non-relativistic case Landau (1936, 1937) this equation reduces to

$$\frac{\partial f}{\partial t} + \mathbf{v}\frac{\partial f}{\partial \mathbf{r}} + q\left(\mathbf{E} + \frac{1}{c}\mathbf{v}\times\mathbf{B}\right)\frac{\partial f}{\partial \mathbf{p}} = -\frac{\partial s_a}{\partial p_a}, \quad \text{(G.6.16)}$$

$$s_a = 2\pi q^2 \Lambda \int \left(f\frac{\partial f'}{\partial p'_b} - f'\frac{\partial f}{\partial p_b}\right)\frac{\left(\mathbf{v}-\mathbf{v}'\right)^2 \delta_{ab} - \left(v_a - v'_a\right)\left(v_b - v'_b\right)}{\left(|\mathbf{v}-\mathbf{v}'|\right)^3} d^3p'.$$

Recall that in dilute plasma collisions with small momentum transfer dominate. For this reason the Coulomb collision integral in non-relativistic plasma is usually approximated by the Fokker-Planck diffusive term. Such approximation actually becomes invalid for relativistic plasma with $k_B T \gtrsim m_e c^2$, where m_e is electron mass, since at these temperatures pairs of electrons and positrons form, see Sec. G.8 below. Description of such relativistic plasma requires the full Boltzmann collision integral.

It has to be noted that both system (G.6.13), (G.6.14) and equation (G.6.15) are microscopic equations in the sense that they define one particle distribution functions for discrete sources and corresponding electromagnetic fields.

The system of particles interacting via gravitational mean field is described Zakharov (2000) by the Einstein-Vlasov system of equations

$$R^{\mu\nu} - \frac{1}{2}g^{\mu\nu}R + g^{\mu\nu}\Lambda = \frac{8\pi G}{c^4} c \int \frac{d^3p}{p^0} p^\mu p^\nu \mathcal{F}^K \quad \text{(G.6.17)}$$

$$p^\mu \frac{\partial \mathcal{F}^K}{\partial x^\mu} - \Gamma^i_{\nu\lambda} p^\nu p^\lambda \frac{\partial \mathcal{F}^K}{\partial p^i} = 0,$$

where $\mathcal{F}^K$ is the Klimontovich DF defined by eq. (G.3.16). These equations form the basis for microscopic gravity. For mathematical aspects see recent review Andréasson (2011).

Macroscopic gravitation theory should be derived from these equations by applying the averaging procedure. Following the discussion in Sec. G.6 it is expected that correlations should appear in both equations after the averaging and represent matter-field, matter-matter and field-field correlations. An attempt to construct such equations up to the second order terms in interaction is made in Zakharov (2000).

G.7. Gases and plasmas

Having derived basic kinetic equation in Sec. G.3 and G.6 let us turn to their application. Dilute gas and plasma are traditionally considered as primary applications for KT. The generalization to relativistic case of KT for gas required mainly terminological changes Synge (1957). However, KT of plasma had to be build on relativistic basis from the beginning since Maxwell equations, being intrinsically relativistic, are necessarily a natural part of it. Besides, in relativistic domain (at relativistic temperatures) many qualitatively new phenomena occur in plasma. In order to understand these phenomena, as well as to provide the physical foundations for the derivation of the Boltzmann and Vlasov equations discussed in the previous section, it is very useful to discuss characteristic quantities in both gases and plasmas.

G.7.1. Plasma frequency

Let us start from the Maxwell equations (G.6.4) and assume that particles move collectively with velocity v given by the equation of motion

$$m\frac{\partial U^\mu}{\partial x^\nu} = -\frac{q}{c}F^\mu_\nu, \tag{G.7.1}$$

Taking 0-1 components in eq. (G.6.4) one has

$$m\frac{d\left(\gamma\beta\right)}{dt} = qE, \quad \frac{dE}{dt} = -4\pi qn\beta, \tag{G.7.2}$$

where $\beta = v/c$ and $\gamma = \left(1-\beta^2\right)^{-1/2}$. Differentiating the first equation with respect to time one gets, see e.g. Benedetti et al. (2011)

$$\frac{d^2u}{dt} + \frac{4\pi q^2 n}{m}\frac{u}{\sqrt{1+u^2}} = 0, \quad u = \gamma\beta. \tag{G.7.3}$$

This equation describes nonlinear Langmuir oscillations (reducing to harmonic ones for $v \ll c$) with the frequency given by

$$\omega_p^2 = \frac{4\pi q^2 n}{m\gamma}. \tag{G.7.4}$$

This parameter is one of the most fundamental ones and it is called *plasma frequency*.

G.7.2. Correlations in plasma

In order to determine other characteristic quantities of plasma one needs to consider the notion of correlation in plasma. It is well known that the correlation function in a medium composed of particles interacting via Coulomb potential is divergent. However, since a neutral plasma contains both positive and negative charges in equal amount, the field of a charged particle in plasma is different from the Coulomb field. In order to illustrate this point consider a charged particle at rest in the origin, see e.g. Chen (1984) and Silin (1998). The system of equations (G.6.13) and (G.6.14) simplifies for this case and there remain only two of them:

$$\mathbf{v}_i\frac{\partial f_i}{\partial \mathbf{r}} - q_i\frac{\partial \varphi}{\partial \mathbf{r}}\frac{\partial f_i}{\partial \mathbf{p}_i} = 0, \quad \Delta\varphi = -4\pi\sum_i q_i n_i - 4\pi q\delta\left(r\right), \tag{G.7.5}$$

where φ is electrostatic potential, and for clarity the DF defined in eq. (G.2.2) is used instead of $\mathcal{F}$. In order to solve these equations one has to set up the boundary conditions. Assume that the electric field vanishes at infinity, i.e. $\varphi\left(\infty\right) = 0$. Assume also that the DF far from the origin is the Maxwell-Boltzmann one (G.5.28), that is

$$f_i\left(\gamma_i\right) \propto n_i \exp\left(-\frac{\gamma_i m_i c^2 + q_i\varphi(r)}{k_B T}\right). \tag{G.7.6}$$

Then taking into account charge conservation $\sum_i q_i n_i = 0$ one can get for the potential

$$\Delta\varphi = -4\pi q\delta(r) + 4\pi \sum_i q_i n_i \left[1 - \exp\left(-\frac{q_i\varphi}{k_B T}\right)\right]. \tag{G.7.7}$$

At large radii $|q_i\varphi| \ll k_B T$ and instead of eq. (G.7.7) a linear equation is obtained

$$\Delta\varphi - \frac{1}{\lambda_D^2}\varphi = -4\pi q\delta(r), \quad \lambda_D^2 = \frac{k_B T}{\sum_i 4\pi q_i^2 n_i}. \tag{G.7.8}$$

and it gives the solution for the electric potential in equilibrium plasma

$$\varphi = \frac{q}{r}\exp\left(-\frac{r}{\lambda_D}\right). \tag{G.7.9}$$

This result implies that at large distances the Coulomb field of the point charge is screened.

Define now a two-particle *spatial* correlation function in equilibrium as

$$f_2(1,2) = f_1(\gamma_1) f_1(\gamma_2) g(r), \tag{G.7.10}$$

where the functions $f_i(\gamma_i)$ are given by eq. (G.5.29), $r = |\mathbf{x}_2 - \mathbf{x}_1|$ and $g(r)$ is called radial distribution function . Using the normalization $\int f_i(\gamma_i)\, d\gamma_i = 1$ one can introduce the *total correlation function*

$$\xi(r) = g(r) - 1 \ll 1, \tag{G.7.11}$$

where $\xi(r)$ is zero for uncorrelated particles. For dilute plasma in a state close to equilibrium Klimontovich (1997) this function is

$$\xi(r) = -\frac{1}{k_B T}\frac{q^2}{r}\exp\left(-\frac{r}{\lambda_D}\right), \tag{G.7.12}$$

which means that the correlation radius for this plasma is $r_{cor} \sim \lambda_D$.

G.7.3. Gravitational correlations in expanding Universe

Unlike for the electromagnetic interactions, there is no Debye screening in the gravitational interactions since there is no negative mass. In an expanding

Universe it is possible, however, to introduce the gravitational correlation radius. Following Zakharov (2000) consider the Poisson-Vlasov equations in the comoving coordinates

$$\frac{\partial f}{\partial t}+\frac{\mathbf{u}}{a^2}\frac{\partial f}{\partial \mathbf{q}}-\frac{\partial \Phi}{\partial \mathbf{q}}\frac{\partial f}{\partial \mathbf{u}}=0, \quad \Delta\Phi=\frac{4\pi G}{a}\int f d^3u-a^3\rho_0, \tag{G.7.13}$$

where ρ_0 is the average density, Φ is gravitational potential. Here comoving coordinates $\mathbf{q}$ and velocities $\mathbf{u}$ are related to the physical ones as usual

$$\mathbf{q}=\frac{\mathbf{x}}{a\left(t\right)}, \quad \mathbf{u}=a\left(t\right)\left[\mathbf{v}-H\left(t\right)\mathbf{x}\right], \tag{G.7.14}$$

where $a\left(t\right)$ is cosmological scale factor. By comparison of eqs. (G.7.13) and (G.7.5) one finds that the average density in eq. (G.7.13) plays the role of opposite charge particles. By analogy with eq. (G.7.7) considering a gravitating particle in a uniform media, insert in eq. (G.7.13) instead of $a^3\rho_0$ a new density

$$a^3\rho=a^3\rho_0\exp\left(-\frac{m\Phi}{k_BT}\right). \tag{G.7.15}$$

In the physical coordinates one obtains

$$\Delta\Phi=4\pi G\rho\left[\exp\left(-\frac{m\Phi}{k_BT}\right)-1\right], \tag{G.7.16}$$

which is similar to eq. (G.7.7). For large distances it reduces to

$$\frac{1}{r^2}\frac{d}{dr}\left(r^2\frac{d\Phi}{dr}\right)+\frac{4\pi G\rho_0 m}{k_BT}\Phi=0, \tag{G.7.17}$$

which gives

$$\Phi\propto\frac{1}{r}\cos\left(\frac{r}{r_g}\right), \quad r_g^2=\frac{k_BT}{4\pi G\rho_0 m}. \tag{G.7.18}$$

It is important that this dependence, being introduced in the correlation function

$$g_{ab}=f_{ab}-f_af_b\propto\exp\left(\frac{\Phi\left(\mathbf{r}_1,\mathbf{r}_2\right)}{k_BT}-1\right). \tag{G.7.19}$$

leads to finite integrals at infinity.

G.7.4. Coulomb collisions

Consider Coulomb collision with large impact parameter and, consequently, small deflection angle ϑ, measured in the center-of-mass system. The transport cross-section in non-relativistic case Lifshitz and Pitaevskii (1981) is

$$\sigma_t = \int (1 - \cos\vartheta)\, d\sigma \simeq \frac{1}{2}\int \vartheta^2 d\sigma. \tag{G.7.20}$$

Here the differential cross section with small angles is given by the Rutherford formula

$$d\sigma = \frac{8\pi \left(qq'\right)^2}{\mu^2 \left(v - v'\right)^4} \frac{d\vartheta}{\vartheta^3}, \tag{G.7.21}$$

where prime denotes the second particle. Then the total cross-section is

$$\sigma_t = \frac{4\pi \left(qq'\right)^2}{\mu^2 \left(v - v'\right)^4}\Lambda, \qquad \Lambda = \log\left(L\right) = \int \frac{d\vartheta}{\vartheta}. \tag{G.7.22}$$

This result shows that in non-relativistic plasma, due to the long-range nature of the electromagnetic interactions the "collision" process occurs at large distances between particles.

Consider now *Coulomb logarithm* in relativistic plasma. Electron-electron or electron-positron collisions are then described by Møller and Bhabha cross-sections, instead of (G.7.21). In this case the Born approximation has to be used since the relative velocity v_r between particles is larger than αc and then

$$L = \frac{m\left\langle v\gamma\right\rangle}{h}\lambda_D \simeq \vartheta_{\min}^{-1}. \tag{G.7.23}$$

In thermal equilibrium, using eqs. (G.7.8) and (G.5.15) one finds

$$\left\langle \frac{v}{c}\gamma \right\rangle = 3\theta + \frac{K_1\left(\theta^{-1}\right)}{K_2\left(\theta^{-1}\right)} \underset{\theta\to\infty}{\longrightarrow} 3\theta, \tag{G.7.24}$$

so in relativistic case one has

$$\log\left(\Lambda\right) = \frac{3}{4\pi^{3/2}}\theta^{\frac{3}{2}}\left(\alpha\lambda_C^3 n\right)^{-\frac{1}{2}} \underset{\theta\to\infty}{\longrightarrow} \mathcal{O}(1), \tag{G.7.25}$$

where α is the fine structure constant. This result implies that the mean free path due to Compton scattering $l_C = \frac{1}{n\sigma_T}$and the one due to Coulomb scattering $l_C = \frac{1}{\log(\Lambda)\sigma_T}$ become equal in the ultra-relativistic case. This formula shows also that for relativistic plasmas, when $\log(\Lambda) \simeq \mathcal{O}(1)$ the momentum transfer in Coulomb collisions is no longer small, and so the Fokker-Planck approximation (G.6.15) does not hold.

G.7.5. Characteristic distances

Following Klimontovich (1983) let us compare the characteristic distances in gas and plasma: the correlation radius r_{cor}, the average distance between particles r_{av} and the mean free path l.

For dilute gas interactions between particles occur when they approach each other, so the correlation length is $r_{cor} \sim r_0$, where r_0 is the particle (atom or molecule) size. Average distance between particles is determined from particle density n as $r_{av} \sim n^{-1/3}$. The mean free path, i.e. the average distance that particles travel without interactions is $l \sim (n\sigma)^{-1} \sim \left(nr_0^2\right)^{-1}$, where in the last relation the fact that the cross-section in gas is typically $\sigma \sim r_0^2$ is used.

For dilute plasma, as discussed above, $r_{cor} \sim \lambda_D$. The mean free path is instead $l \sim \left(n\lambda_D^2\right)^{-1}$.

From these quantities it is possible to construct dimensionless parameters characterizing a given medium: for dilute plasma and gas, respectively

$$\mathfrak{g}_p = \frac{1}{n\lambda_D^3} \ll 1, \quad \mathfrak{g}_g = nr_0^3 \ll 1. \tag{G.7.26}$$

Relativistic plasma in thermal equilibrium is always dilute, see Fig. G.3. In general the following inequalities hold for gas and plasma

$$\begin{aligned} r_{cor} \ll r_{av} \ll l, \quad &\text{(gas)} \\ r_{av} \ll r_{cor} \ll l. \quad &\text{(plasma)} \end{aligned} \tag{G.7.27}$$

It is clear that in dilute gas interaction occurs only when two particles encounter or "collide" with each other. Correlations between particles may be neglected before and after the collision. In dilute plasma the situation is opposite. A given particle is interacting simultaneously with many particles located in the Debye sphere around this particle with radius λ_D. It means

that particles move in the mean electromagnetic field, created by many other particles. This field has to be averaged over some volume, smaller than the Debye volume λ_D^3, but larger than the interparticle volumes r_{av}^3. The Vlasov approximation (G.6.13),(G.6.14) is valid when the rate of particle collisions is smaller than the rate of change of these averaged electromagnetic field. In other words, the relaxation lengths are much larger than the size of the system L.

Now it is possible to justify the derivation of the Boltzmann equation in Sec. G.3, where only binary interactions have been considered and interactions between three particles, four particles, and so on were neglected. Indeed, triple collisions in gas are much less probable than binary collisions, since the correlation function $C(1,2)$ is small, see e.g. Liboff (2003)

$$C(1,2) = f_2(1,2) - f_1(1) f_1(2) \sim \mathfrak{g}_g f_2(1,2), \tag{G.7.28}$$

where $f_2(1,2)$ is two particle DF, $f_1(1)$ and $f_1(2)$ stand for one particle DF of particle one and two, respectively. Analogously, $C(1,2,3) \sim \mathfrak{g}_g f_3(1,2,3)$ and so on.

From the kinetic point of view physically infinitesimally small scales should satisfy the inequalities

$$r_{ph} \ll L, \quad n r_{ph}^3 \gg 1, \tag{G.7.29}$$

where L is the characteristic size in the problem (the size over which DF changes significantly). Then one has for such kinetic infinitesimally small scales

$$\begin{aligned} &r_K \ll l, \quad (\text{gas}) \\ &r_K \ll \lambda_D. \quad (\text{plasma}) \end{aligned} \tag{G.7.30}$$

From the hydrodynamic point of view the relaxation scale is a function of the characteristic size L and of one of the three dissipation coefficients: diffusion D, viscosity ν and heat conductivity χ. The corresponding physically infinitesimally small scale satisfies the following inequality

$$r_{HD} \ll \frac{vL^2}{D^*}, \quad D^* = \max(D, \nu, \chi). \tag{G.7.31}$$

The transition from kinetic level of description to the hydrodynamic one is

realized by the introduction of the physical *Knudsen number*

$$Kn = \frac{r_{ph}}{L} \ll 1. \tag{G.7.32}$$

The approximate methods of solutions of the Boltzmann equation (such as Hilbert, Chapman-Enskog, Grad methods, see e.g. Cercignani and Kremer (2002) and Liboff (2003)) use Kn as a small parameter for expansion of kinetic equations. The ratio of the two infinitesimally small scales (kinetic and hydrodynamic ones) is

$$\frac{r_K}{r_{HD}} \sim \mathfrak{g}_g^{3/10} Kn^{6/5} \leq 1, \tag{G.7.33}$$

where equality corresponds to the maximal Knudsen number (minimal scale L) when a common hydrodynamic and kinetic description of the system is still possible.

G.7.6. Relativistic degeneracy

If the temperature of plasma decreases for a given density of particles it may become degenerate Landau and Lifshitz (1980). The same phenomenon occurs when particle density increases, but the temperature is fixed. It is useful to construct the temperature-density diagram, see Fig. G.4.

The characteristic temperature which separates non-degenerate from degenerate systems is defined by

$$\theta_F \equiv \frac{E_F}{m_e c^2}, \tag{G.7.34}$$

where E_F is Fermi energy, corresponding to Fermi momentum

$$p_F = \left(3\pi^2 n\right)^{\frac{1}{3}} \hbar. \tag{G.7.35}$$

For a relativistic gas the total energy and momentum are related $E^2 = p^2c^2 + m_e^2c^4$. Equating the kinetic energy $E - m_e c^2$ to the Fermi energy the

degeneracy temperature is obtained

$$\theta_F = \left[\left(3\pi^2\right)^{\frac{4}{3}} \left(\lambda_C n^{\frac{1}{3}}\right)^2 + 1\right]^{1/2} - 1. \tag{G.7.36}$$

Define the degeneracy parameter

$$\mathcal{D} = \frac{\theta}{\theta_F}. \tag{G.7.37}$$

Note that it is related to the degeneracy parameter introduced in Groot et al. (1980) as $\mathcal{D}' = \frac{\theta^3}{n\lambda_C^3} \simeq \mathcal{D}^3$. Definition (G.7.37) takes into account both non-relativistic and ultra-relativistic asymptotics in eq. (G.7.36). As can be seen from Fig. G.4 even in thermal equilibrium relativistic plasma becomes degenerate, though this degeneracy is weak.

G.7.7. Landau damping

Following Lifshitz and Pitaevskii (1981) consider non-relativistic linear Landau damping with a simplified treatment. More details, including non-linear damping are given in the mathematical treatise Mouhot and Villani (2011), see also Klimontovich (1997). Consider a homogeneous isotropic plasma with DF $f_0(p)$. Assume that a weak electromagnetic field is present, which induces a small perturbation on DF such that $f = f_0(p) + \delta f$. In isotropic plasma magnetic field in eqs. (G.6.13),(G.6.14) is not important, then linearized eq. (G.6.13) becomes

$$\frac{\partial \delta f}{\partial t} + \mathbf{v} \cdot \nabla \delta f = q\mathbf{E}\frac{\partial f_0}{\partial \mathbf{p}}, \tag{G.7.38}$$

where δf and $\mathbf{E}$ are, respectively, DF and electric field perturbations. Assuming that $\delta f \sim \exp\left[i\left(\mathbf{kr} - \omega t\right)\right]$, $\mathbf{E} \sim \exp\left[i\left(\mathbf{kr} - \omega t\right)\right]$, the solution is

$$\delta f = \frac{q\mathbf{E}}{i\left(\mathbf{k}\cdot\mathbf{v} - \omega\right)} \cdot \frac{\partial f_0}{\partial \mathbf{p}}. \tag{G.7.39}$$

The dielectric constant, given by $4\pi\mathbf{P} = \left(\varepsilon - 1\right)\mathbf{E}$ can be found, observing that

$$i\mathbf{k}\cdot\mathbf{P} = -\rho = q\int \delta f d^3p. \tag{G.7.40}$$

Since the function δf has a pole at $\omega = \mathbf{k}\cdot\mathbf{v}$ the integral above should be evaluated using the Landau rule $\omega \to \omega + i0$. The result is

$$\varepsilon = 1 - \frac{4\pi q^2}{k^2}\int \mathbf{k}\cdot\frac{\partial f_0}{\partial \mathbf{p}}\frac{d^3p}{(\mathbf{k}\cdot\mathbf{v} - \omega - i0)}. \tag{G.7.41}$$

It means that the dielectric constant has an imaginary part. Introducing the DF along x-axis and choosing the direction of $\mathbf{k}$ along the same axis one gets

$$\mathrm{Im}\,(\varepsilon) = -\frac{4\pi q^2 m}{k^2}\frac{df\,(p_x)}{dp_x}. \tag{G.7.42}$$

Non-vanishing $\mathrm{Im}\,(\varepsilon)$ means that the electric field looses energy with the rate

$$Q = -\left|\mathbf{E}\right|^2\frac{\pi m q^2}{2k^2}\frac{df\,(p_x)}{dp_x}. \tag{G.7.43}$$

This is collisionless damping of electromagnetic waves as established by Landau Landau (1946). The validity condition for this result is $\lambda_D \ll \frac{2\pi}{k} \ll L$.

Actually, the damping of electromagnetic field oscillations in non-relativistic case is exponentially weak. In contrast, in ultra relativistic case there are two possibilities: when phase velocity of the wave is smaller than the speed of light the damping is strong; in the opposite case the damping is absent Buti (1962). This result is generally confirmed for electron-positron plasma Laing and Diver (2006).

G.8. Pair plasma

In this section a special case of plasma will be considered, when both negative and positive charge carriers have equal masses: electron-positron plasma. Electron-positron plasma is of interest in many fields of physics and astrophysics. In cosmology during the lepton era ultra-relativistic electron-positron pairs contribute to the matter content of the Universe Weinberg (2008). The cosmic microwave background radiation is created at the black body photosphere Khatri and Sunyaev (2012), around the cosmic redshift $z = 10^6$.

In astrophysics comparable energy densities are expected to be reached in gamma-ray bursts sources, hence electron-positron pairs play an essen-

tial role there Piran (2005). Indications exist that the pair plasma is present also in active galactic nuclei Wardle et al. (1998), in the center of our Galaxy Churazov et al. (2005), around hypothetical quark stars Usov (1998). In the laboratory pair plasma is expected to appear in the fields of ultra intense lasers Blaschke et al. (2006), see also Benedetti et al. (2013) and Ruffini et al. (2010) for review.

In many stationary astrophysical sources the pair plasma is thought to be in thermodynamic equilibrium. A detailed study of the relevant processes Bisnovatyi-Kogan et al. (1971), Weaver (1976), Lightman (1982), Gould (1982), Stepney and Guilbert (1983), Coppi and Blandford (1990), radiation mechanisms Lightman and Band (1981), possible equilibrium configurations Lightman (1982), Svensson (1982a), Guilbert and Stepney (1985) and spectra Zdziarski (1984) in an optically thin pair plasma has been carried out. Particular attention has been given to collisional relaxation process Gould (1981), Stepney (1983), pair production and annihilation Svensson (1982b), relativistic bremsstrahlung Gould (1980), Haug (1985), double Compton scattering Lightman (1981), Gould (1984).

An equilibrium occurs if the sum of all reaction rates vanishes, see eq. (G.5.9) and discussion that follows. For instance, electron-positron pairs are in equilibrium when the net pair production (annihilation) rate is zero. This can be achieved by variety of ways and the corresponding condition can be represented as a system of algebraic equations Svensson (1984). However, the main assumption made in all the above mentioned works is that the plasma is assumed to obey relativistic quantum statistics. The latter is shown to be possible, in principle, in the range of temperatures up to 10 MeV Bisnovatyi-Kogan et al. (1971),Stepney (1983). It will be shown that independently of a wide set of initial conditions, thermal equilibrium forms for the phase space distribution functions are recovered during the process of thermalization by two body and three body direct and inverse particle-particle collisions. The pair plasma is assumed to be optically thick. Although moderately thick plasmas have been treated in the literature Guilbert and Stepney (1985), only qualitative description Bisnovatyi-Kogan et al. (1971),Svensson (1982a) was available for large optical depths until recently Aksenov et al. (2007),Aksenov et al. (2009).

G.8.1. Basic parameters

Consider a mildly relativistic plasma with average energy per particle $0.1 \lesssim \frac{\epsilon}{\mathrm{MeV}} \lesssim 10$. Before formulating the relativistic kinetic equations for the electron-positron plasma recall the basic plasma parameters and their typical values. The plasma parameter (G.7.26) for electron-positron plasma is typically $\mathfrak{g}_p = (n_- \lambda_D^3)^{-1} \sim 10^{-3}$, here $\lambda_D = \frac{c}{\omega}\sqrt{\theta_-}$ is the Debye length (G.7.8), $\theta_- = k_B T_- / (mc^2)$ is the dimensionless temperature, $\omega = \sqrt{4\pi q^2 n_- / m}$ is the plasma frequency, n_- is the electron number density, m is its mass. It implies that the relativistic Boltzmann equations for one particle distribution functions can be used to describe an electron-positron plasma. The classicality parameter $\varkappa = e^2/(\hbar v_r) = \alpha/\beta_r < 1$, where $v_r = \beta_r c$ is the mean relative velocity of particles. It means that in electron-positron plasma a quantum description of scattering is required. The Coulomb logarithm is $\Lambda = \mathcal{M}\lambda_D v_r \gamma_r / \hbar$, where $\mathcal{M}$ is the reduced mass. Since this expression contains the Debye length, which is defined only for a thermal plasma, the expression (G.7.25) for relativistic Coulomb logarithm will be used. As already mentioned in Sec. G.7.6 a relativistic plasma may be degenerate, but in what follows such relativistic degeneracy will be neglected.

Intensity of interaction of photons with other particles is characterized by the optical depth

$$\tau = \int_{\mathcal{L}} \sigma \, (n_- + n_+) \, dl, \tag{G.8.1}$$

where σ is the cross-section and the integral (G.8.1) is taken over the lightlike worldline $\mathcal{L}$. In what follows consider the case in which plasma linear dimensions R exceed the photon mean free path $\lambda_\gamma = (n_- \sigma)^{-1}$, thus $\tau \gg 1$.

When admixture of protons and electrons is allowed it may be characterized by an additional parameter, the baryonic loading

$$B = \frac{n_p M c^2}{\rho_r}, \tag{G.8.2}$$

where M is the proton mass, ρ_r is the energy density in relativistic component (electrons, positrons and photons).

In thermal equilibrium, while e^+e^- are relativistic, with average energies $\epsilon_\pm \sim mc^2 \sim k_B T$, protons are not with kinetic energies $M v_p^2 \sim k_B T$, and thus $\frac{v_p}{c} \sim \sqrt{\frac{m}{M}}$. Also in equilibrium with $\epsilon_\pm \geq mc^2$ one has $\rho_\pm \approx n_\pm mc^2$ and

thus the density ratio between protons and pairs is $\frac{n_p}{n_\pm} \sim \frac{m}{M}B$. Since electron is subject to interaction with both electrons (positrons) and photons, one has for the ratio of mean free paths, see e.g. Groot et al. (1980)

$$\frac{\lambda_\gamma}{\lambda_\pm} = \log(\Lambda) + \frac{n_\pm + n_p}{n_\gamma}. \tag{G.8.3}$$

Note that there are two natural parameters for perturbative expansion in various expressions: the fine structure constant $\alpha \simeq 1/137$ and the ration between electron and proton masses $m/M \simeq 1/1836$.

G.8.2. Kinetic equation and collision integrals

Relativistic Boltzmann equations (G.3.9) for homogeneous isotropic plasma are

$$\frac{1}{c}\frac{\partial f_i}{\partial t} - \nabla U \frac{\partial f_i}{\partial \mathbf{p}} = \mathrm{St}\, f, \tag{G.8.4}$$

where U is a potential due to external force, $f_i(\epsilon, t)$ are distribution functions and the index i stands for electrons, positrons and photons. The second term on the LHS of eq. (G.8.4) describes the mean field produced by all particles, plus an external field. Particle collisions, including Coulomb ones, are taken into account by collision terms on the RHS. Particle motion between collisions is assumed to be subject to the mean field, which is neglected. This is an assumption, but in dense collision dominated plasma this assumption is justified, see e.g. Groot et al. (1980). Then eq. (G.8.4) reduces to a coupled system of partial-integro-differential equations

$$\frac{1}{c}\frac{\partial f_i}{\partial t} = \sum_q \left(\eta_i^q - \chi_i^q f_i\right), \tag{G.8.5}$$

where η_i^q and χ_i^q are the emission and the absorption coefficients for a given process q Mihalas and Mihalas (1984).

The elementary interactions between particles are described by the quantum field theory. In the case under consideration this is quantum electrodynamics. These coefficients have to be computed from the probability of a given process, expressed as function of the corresponding matrix element. In general, for a process involving a outgoing and b incoming particles the

Binary interactions	Radiative and pair producing variants
Møller and Bhabha scattering $e_1^{\pm} e_2^{\pm} \longrightarrow e_1^{\pm\prime} e_2^{\pm\prime}$ $e^{\pm} e^{\mp} \longrightarrow e^{\pm\prime} e^{\mp\prime}$	Bremsstrahlung $e_1^{\pm} e_2^{\pm} \longleftrightarrow e_1^{\pm\prime} e_2^{\pm\prime} \gamma$ $e^{\pm} e^{\mp} \longleftrightarrow e^{\pm\prime} e^{\mp\prime} \gamma$
Single Compton scattering $e^{\pm}\gamma \longrightarrow e^{\pm}\gamma'$	Double Compton scattering $e^{\pm}\gamma \longleftrightarrow e^{\pm\prime}\gamma'\gamma''$
Pair production and annihilation $\gamma\gamma' \longleftrightarrow e^{\pm} e^{\mp}$	Radiative pair production and three photon annihilation $\gamma\gamma' \longleftrightarrow e^{\pm} e^{\mp} \gamma''$ $e^{\pm} e^{\mp} \longleftrightarrow \gamma\gamma'\gamma''$
	$e^{\pm}\gamma \longleftrightarrow e^{\pm\prime} e^{\mp} e^{\pm\prime\prime}$

Table G.1.: Microphysical processes in the pair plasma.

differential probability per unit time is ($\hbar = c = 1$)

$$dw = c(2\pi\hbar)^4 \delta^{(4)}\left(\mathfrak{p}_f - \mathfrak{p}_i\right) \left|M_{fi}\right|^2 V \left[\prod_b \frac{\hbar c}{2\epsilon_b V}\right] \left[\prod_a \frac{d\mathbf{p}'_a}{(2\pi\hbar)^3} \frac{\hbar c}{2\epsilon'_a}\right], \quad \text{(G.8.6)}$$

where $\mathbf{p}'_a$ and ϵ'_a (ϵ_b) are respectively momenta and energies of outgoing (incoming) particles, M_{fi} are the corresponding matrix elements, $\delta^{(4)}$ stands for energy-momentum conservation, V is the normalization volume. The list of processes that are relevant for optically thick electron-positron plasma is given in Tab. G.1.

The list of the leptonic processes involving protons is given in Tab. G.2.

Each of the above mentioned reactions is characterized by the corresponding time-scale and optical depth. For Compton scattering of an electron, for instance, one has

$$t_{\rm cs} = \frac{1}{\sigma_T n_{\pm} c}, \qquad \tau_{\rm cs} = \sigma_T n_{\pm} R, \quad \text{(G.8.7)}$$

where $\sigma_T = \frac{8\pi}{3}\alpha^2(\frac{\hbar}{mc})^2$ is the Thomson cross-section, R is the linear size of plasma. There are several time-scales in this problem that characterize the condition of detailed balance between direct and inverse reactions, namely

- Pair production, Compton and electron-electron scattering: $t_{\gamma e} \sim t_{\gamma e} \sim (\sigma_T n c)^{-1}$;

Binary interactions	Radiative and pair producing variants
Coulomb scattering $p_1 p_2 \longrightarrow p_1' p_2'$ $pe^{\pm} \longrightarrow p' e^{\pm\prime}$	Bremsstrahlung $p_1 p_2 \longleftrightarrow p_1' p_2' \gamma$ $pe^{\pm} \longleftrightarrow p' e^{\pm\prime} \gamma$
	$pe_1^{\pm} \longleftrightarrow p' e_1^{\pm\prime} e^{\pm} e^{\mp}$
Single Compton scattering $p\gamma \longrightarrow p'\gamma'$	Double Compton scattering and radiative pair production $p\gamma \longleftrightarrow p'\gamma'\gamma''$
	$p\gamma \longleftrightarrow p' e^{\pm} e^{\mp}$

Table G.2.: Microphysical processes involving protons in the pair plasma.

- Cooling: $t_{br} = \alpha^{-1} t_c$;
- Proton-proton: $\left(n_p t_{pp}\right)^{-1} \approx \sqrt{\frac{m}{M}} \left(n_- t_{ee}\right)^{-1}, \qquad v_p \approx \sqrt{\frac{m}{M}} v_e, \qquad v_e \approx c$;
- Electron-proton: $t_{ep}^{-1} \approx \frac{\epsilon_{\pm}}{Mc^2} t_{ee}^{-1}, \qquad \epsilon_{\pm} \ll \epsilon_p$;
- Proton Compton scattering: $\left(n_p t_{\gamma p}\right)^{-1} \approx \left(\frac{\epsilon}{Mc^2}\right)^2 \left(n_- t_{\gamma e}\right)^{-1}, \qquad \epsilon \geq mc^2$;
- Dynamical time-scale: $t_{hyd} \sim R/c$.

As example of collision integral consider the absorption coefficient for Compton scattering which is given by

$$\chi^{\text{cs}} f_\gamma = \int d\mathbf{k}' d\mathbf{p} d\mathbf{p}' W_{\mathbf{k}',\mathbf{p}';\mathbf{k},\mathbf{p}} f_\gamma(\mathbf{k}, t) f_\pm(\mathbf{p}, t), \tag{G.8.8}$$

where $\mathfrak{p}$ and $\mathfrak{k}$ are the four-momenta of electron (positron) and photon respectively, $\mathbf{p}$ and $\mathbf{k}$ are their three-momenta, $d\mathbf{p} = d\epsilon_\pm do \epsilon_\pm^2 \beta_\pm / c^3$, $d\mathbf{k}' = d\epsilon_\gamma' \epsilon_\gamma'^2 do_\gamma' / c^3$ and the transition rate $W_{\mathbf{k}',\mathbf{p}';\mathbf{k},\mathbf{p}}$ is related to the differential transition probability $dw_{\mathbf{k}',\mathbf{p}';\mathbf{k},\mathbf{p}}$ per unit time as

$$W_{\mathbf{k}',\mathbf{p}';\mathbf{k},\mathbf{p}} d\mathbf{k}' d\mathbf{p}' \equiv V dw_{\mathbf{k}',\mathbf{p}';\mathbf{k},\mathbf{p}}, \quad dw_{\mathbf{k}',\mathbf{p}';\mathbf{k},\mathbf{p}} = w_{\mathbf{k}',\mathbf{p}';\mathbf{k},\mathbf{p}} d\mathbf{k}' d\mathbf{p}'. \tag{G.8.9}$$

One integration over $d\mathbf{p}'$ as $\int d\mathbf{p}' \delta(d\mathbf{k} + d\mathbf{p} - d\mathbf{k}' - d\mathbf{p}') \to 1$ can be readily performed. Then it is necessary to take into account the momentum conser-

vation in the next integration over $d\mathbf{k}'$, namely

$$\int d\epsilon'_\gamma \delta(\epsilon_\gamma + \epsilon_\pm - \epsilon'_\gamma - \epsilon'_\pm) \to \frac{1}{|\partial(\epsilon'_\gamma + \epsilon'_\pm)/\partial\epsilon'_\gamma|} \equiv J_{\rm cs}, \tag{G.8.10}$$

where the Jacobian of the transformation is $J_{\rm cs} = \frac{1}{1-\beta'_\pm \mathbf{b}'_\gamma \cdot \mathbf{b}'_\pm}$, where $\mathbf{b}_i = \mathbf{p}_i/p$, $\mathbf{b}'_i = \mathbf{p}'_i/p'$ and $\mathbf{b}'_\pm = (\beta_\pm \epsilon_\pm \mathbf{b}_\pm + \epsilon_\gamma \mathbf{b}_\gamma - \epsilon'_\gamma \mathbf{b}'_\gamma)/(\beta'_\pm \epsilon'_\pm)$. Finally, for the absorption coefficient one has

$$\chi^{\rm cs} f_\gamma = -\int \frac{do'_\gamma d\mathbf{p}}{(2\pi)^2} \frac{\epsilon'_\gamma |M_{fi}|^2 \hbar^2 c^2}{16\epsilon_\pm \epsilon_\gamma \epsilon'_\pm} J_{\rm cs} f_\gamma(\mathbf{k}, t) f_\pm(\mathbf{p}, t), \tag{G.8.11}$$

where the matrix element squared, see e.g. Berestetskii et al. (1982), is

$$|M_{fi}|^2 = 2^6 \pi^2 \alpha^2 \left[\frac{m^2c^2}{s - m^2c^2} + \frac{m^2c^2}{u - m^2c^2} + \left(\frac{m^2c^2}{s - m^2c^2} + \frac{m^2c^2}{u - m^2c^2} \right)^2 \right.$$
$$\left. - \frac{1}{4} \left(\frac{s - m^2c^2}{u - m^2c^2} + \frac{u - m^2c^2}{s - m^2c^2} \right) \right], \tag{G.8.12}$$

$s = (\mathfrak{p} + \mathfrak{k})^2$ and $u = (\mathfrak{p} - \mathfrak{k}')^2$ are invariants, $\mathfrak{k} = (\epsilon_\gamma/c)(1, \mathbf{e}_\gamma)$ and $\mathfrak{p} = (\epsilon_\pm/c)(1, \beta_\pm \mathbf{e}_\pm)$ are energy-momentum four-vectors of photons and electrons, respectively, $d\mathbf{p} = d\epsilon_\pm do \epsilon_\pm^2 \beta_\pm / c^3$, $d\mathbf{k}' = d\epsilon'_\gamma \epsilon'^2_\gamma do'_\gamma / c^3$ and $do = d\mu d\phi$.

As example of triple interactions consider the relativistic bremsstrahlung

$$e_1 + e_2 \leftrightarrow e'_1 + e'_2 + \gamma'. \tag{G.8.13}$$

For the time derivative, for instance, of the distribution function f_2 in the direct and in the inverse reactions (G.8.13) one has

$$\dot{f}_2 = \int d\mathbf{p}_1 d\mathbf{p}'_1 d\mathbf{p}'_2 d\mathbf{k}' \left[W_{\mathbf{p}'_1, \mathbf{p}'_2, \mathbf{k}'; \mathbf{p}_1, \mathbf{p}_2} f'_1 f'_2 f'_k - W_{\mathbf{p}_1, \mathbf{p}_2; \mathbf{p}'_1, \mathbf{p}'_2, \mathbf{k}'} f_1 f_2 \right] =$$
$$= \int d\mathbf{p}_1 d\mathbf{p}'_1 d\mathbf{p}'_2 d\mathbf{k}' \frac{c^6 \hbar^3}{(2\pi)^2} \frac{\delta^{(4)}(P_f - P_i) |M_{fi}|^2}{2^5 \epsilon_1 \epsilon_2 \epsilon'_1 \epsilon'_2 \epsilon'_\gamma} \left[f'_1 f'_2 f'_k - \frac{1}{(2\pi\hbar)^3} f_1 f_2 \right], \tag{G.8.14}$$
$$d\mathbf{p}_1 d\mathbf{p}_2 W_{\mathbf{p}'_1, \mathbf{p}'_2, \mathbf{k}'; \mathbf{p}_1, \mathbf{p}_2} \equiv V^2 dw_1, \quad d\mathbf{p}'_1 d\mathbf{p}'_2 d\mathbf{k}' W_{\mathbf{p}_1, \mathbf{p}_2; \mathbf{p}'_1, \mathbf{p}'_2, \mathbf{k}'} \equiv V dw_2,$$

A finite difference method with a computational grid in the phase space can

	Interaction	Parameters of DFs
I	e^+e^- scattering	$\theta_+ = \theta_-$, $\forall\nu_+$,ν_-
II	$e^\pm p$ scattering	$\theta_p = \theta_\pm$, $\forall\nu_\pm$,ν_p
III	$e^\pm\gamma$ scattering	$\theta_\gamma = \theta_\pm$, $\forall\nu_\gamma$,$\nu_\pm$
IV	pair production	$\nu_+ + \nu_- = 2\nu_\gamma$, if $\theta_\gamma = \theta_\pm$
V	Tripe interactions	ν_γ, $\nu_\pm = 0$, if $\theta_\gamma = \theta_\pm$

Table G.3.: Thermodynamic quantities under detailed balance conditions for a given process.

be used for numerical solution of eq. (G.8.5), see Aksenov et al. (2009). In what follows a concrete example of numerical solution of the system of relativistic Boltzmann equations (G.8.5) will be discussed. In order to interpret this solution it is necessary to introduce the notion of kinetic equilibrium Aksenov et al. (2007).

G.8.3. Kinetic and thermal equilibria

The number of conservation laws in the problem under consideration imply the existence of some relations between thermodynamic quantities in equlibrium. The following conservation laws exist: energy conservation $\frac{d}{dt}\sum_i \rho_i = 0$, particle number conservation for binary reactions $\frac{d}{dt}\sum_i n_i = 0$, baryonic number conservation $\frac{dn_p}{dt} = 0$ and charge conservation $n_- = n_+ + n_p$. The condition for the chemical potentials coming from detailed balance conditions is $\varphi_+ + \varphi_- = 2\varphi_\gamma$.

The kinetic equilibrium is defined as the state when the detailed balance condition is satisfied for any binary process. In this state distribution functions have the following form

$$f_i(\varepsilon) = \frac{2}{(2\pi\hbar)^3}\exp\left(-\frac{\varepsilon - \nu_i}{\theta_i}\right), \tag{G.8.15}$$

with chemical potential $\nu_i \equiv \frac{\phi_i}{mc^2}$ and temperature $\theta_i \equiv \frac{k_B T_i}{m_e c^2}$, where $\varepsilon \equiv \frac{\epsilon}{m_e c^2}$ is the energy of the particle. In particular, detailed balance conditions with respect to a given direct and inverse process listed in Tab. G.1 leads to the following constraints on temperatures and chemical potentials in eq. (G.8.15):

Provided conditions I-IV in Tab. G.3 are satisfied, one can obtain the relation between two couples of quantities: total the number density and the total energy density on the one hand, and temperature and the chemical potential on the other hand. In particular, for photons

$$n_\gamma = \frac{1}{V_0}\exp\left(\frac{\nu_\gamma}{\theta}\right)2\theta^3, \qquad \frac{\rho_\gamma}{n_\gamma mc^2} = 3\theta, \qquad V_0 = \frac{1}{8\pi}\left(\frac{2\pi\hbar}{mc}\right)^3. \quad \text{(G.8.16)}$$

From eqs. (G.5.15) and (G.5.19) for non-degenerate pairs

$$n_\pm = \frac{1}{V_0}\exp\left(\frac{\nu_\pm}{\theta}\right)j_1(\theta), \qquad \frac{\rho_\pm}{n_\pm mc^2} = j_2(\theta), \quad \text{(G.8.17)}$$

and for non-relativistic protons

$$n_p = \frac{1}{V_0}\sqrt{\frac{\pi}{2}}\left(\frac{M}{m}\right)^{3/2}\exp\left(\frac{\nu_p - M/m}{\theta}\right)\theta^{3/2}, \qquad \frac{\rho_p}{Mn_pc^2} = 1 + \frac{3}{2}\frac{m}{M}\theta, \quad \text{(G.8.18)}$$

where

$$j_1(\theta) = \theta K_2(\theta^{-1}) \to \begin{cases} \sqrt{\frac{\pi}{2}}e^{-\frac{1}{\theta}}\theta^{3/2}, & \theta \to 0 \\ 2\theta^3, & \theta \to \infty \end{cases}, \quad \text{(G.8.19)}$$

$$j_2(\theta) = \frac{3K_3(\theta^{-1}) + K_1(\theta^{-1})}{4K_2(\theta^{-1})} \to \begin{cases} 1 + \frac{3}{2}\theta, & \theta \to 0 \\ 3\theta, & \theta \to \infty \end{cases}.$$

With nonzero baryon loading (G.8.2) in kinetic equilibrium $\theta_+ = \theta_- = \theta_\gamma = \theta_\mathrm{k}$, but it may be that $\theta_p \neq \theta_\mathrm{k}$. Summing up energy densities

$$\sum_{e^+,e^-,\gamma}\rho_i = \frac{mc^2}{V_0}\left\{\left[1 - \frac{n_pV_0}{j_1(\theta_\mathrm{k})}\exp\left(-\frac{\nu_+}{\theta_\mathrm{k}}\right)\right]^{\frac{1}{2}} \times \right. \quad \text{(G.8.20)}$$

$$\left. \times 6\theta_\mathrm{k}^4\exp\left(\frac{\nu_+}{\theta_\mathrm{k}}\right) + \left[2j_1(\theta_k)\exp\left(\frac{\nu_+}{\theta_\mathrm{k}}\right) - n_pV_0\right]j_2(\theta_\mathrm{k})\right\},$$

and analogously for number densities

$$\sum_{e^+,e^-,\gamma} n_i = \frac{1}{V_0}\left\{\left[1-\frac{n_p V_0}{j_1(\theta_\mathrm{k})}\exp\left(-\frac{\nu_+}{\theta_\mathrm{k}}\right)\right]^{\frac{1}{2}}\times \right. \tag{G.8.21}$$
$$\left.\times 6\theta_\mathrm{k}^4\exp\left(\frac{\nu_+}{\theta_\mathrm{k}}\right)+2j_1(\theta_\mathrm{k})\exp\left(\frac{\nu_+}{\theta_\mathrm{k}}\right)\right\}.$$

Equations (G.8.20) and (G.8.21) represent the relations between (ρ, n) and $(\nu_+, \theta_\mathrm{k})$. Conservation laws allow to determine the rest of chemical potentials, obtained from the following relations

$$\exp\left(\frac{\nu_-}{\theta_\mathrm{k}}\right)=\exp\left(\frac{\nu_+}{\theta_\mathrm{k}}\right)+\frac{n_p V_0}{j_1(\theta_\mathrm{k})}, \tag{G.8.22}$$

$$\exp\left(\frac{\nu_\gamma}{\theta_\mathrm{k}}\right)=\exp\left(\frac{\nu_+}{\theta_\mathrm{k}}\right)\left[1+\frac{n_p V_0}{j_1(\theta_\mathrm{k})}\exp\left(-\frac{\nu_+}{\theta_\mathrm{k}}\right)\right]^{\frac{1}{2}}, \tag{G.8.23}$$

The temperature and chemical potential of protons can be found separately.

In thermal equilibrium ν_γ vanishes and one has

$$\nu_- = \theta_\mathrm{k}\mathrm{arcsinh}\left[\frac{n_p V_0}{2j_1(\theta_\mathrm{k})}\right], \qquad \nu_+ = -\nu_-, \tag{G.8.24}$$

which both reduce to $\nu_- = \nu_+ = 0$ for $n_p = 0$. At the same time, for $n_p > 0$ one always has $\nu_- > 0$ and $\nu_+ < 0$ in thermal equilibrium. In order to determine the Coulomb logarithm as function of particle energies, one can use the relation (G.7.23). The minimal scattering angle in thermal relativistic plasma in the center of mass system Haug (1985) is

$$\theta_\mathrm{min} = \frac{2\hbar}{\mathcal{M}cD}\frac{\gamma_r}{(\gamma_r+1)\sqrt{2(\gamma_r-1)}}, \tag{G.8.25}$$

where the maximum impact parameter (neglecting the effect of protons) is $D = \frac{c^2}{\omega}\frac{p_0}{\epsilon_{10}}$, where p_0 and ϵ_{10} are CM quantities, and the invariant Lorentz factor of relative motion is

$$\gamma_r = \frac{1}{\sqrt{1-\left(\frac{v_r}{c}\right)^2}} = \frac{\epsilon_1\epsilon_2 - \mathbf{p}_1\mathbf{p}_2c^2}{m_1m_2c^4}. \tag{G.8.26}$$

The Coulomb logarithm is

$$\log(\Lambda) = \frac{1}{2} - \log\left(\sqrt{2}\sin\theta_{\min}\right). \tag{G.8.27}$$

G.8.4. Numerical example

G.8.5. Numerical example

Consider now an example of thermalization of initially non-equilibrium electron-positron plasma, following Aksenov et al. (2009). The following initial conditions are adopted: flat initial spectral energy densities $E_i(\epsilon_i) = \frac{4\pi\epsilon_i^3\beta_i f_i}{c^3} = \text{const}$, with total energy density $\rho = 10^{24}\text{erg/cm}^3$. Plasma is dominated by photons with small amount of electron-positron pairs, the ratio between energy densities in photons and in electron-positron pairs $\rho_\pm/\rho_\gamma = 10^{-5}$. Baryonic loading parameter $B = 10^{-3}$, corresponding to $\rho_p = 2.7 \times 10^{18}\text{erg/cm}^3$. The energy density in each component of plasma changes, as can be seen from Fig. G.5, keeping constant the total energy density shown by dotted line in Fig. G.5, as the energy conservation requires. As early as at 10^{-23} sec the energy starts to redistribute between electrons and positrons from the one hand and photons from the other hand essentially by the pair-creation process. This leads to equipartition of energies between these particles at 3×10^{-15} sec. Concentrations of pairs and photons equalize at 10^{-14} sec, as can be seen from Fig. G.6. From this moment temperatures and chemical potentials of electrons, positrons and photons tend to be equal, see Fig. G.7 and Fig. G.8 respectively, and it corresponds to the approach to kinetic equilibrium.

This is quasi-equilibrium state since total number of particles is still approximately conserved, as can be seen from Fig. G.6, and triple interactions are not yet efficient. At the moment $t_1 = 4 \times 10^{-14}$ sec, shown by the vertical line on the left in Fig. G.7 and Fig. G.8, the temperature of photons and pairs is $\theta_\text{k} \simeq 1.5$, while the chemical potentials of these particles are $\nu_\text{k} \simeq -7$. Concentration of protons is so small that their energy density is not affected by the presence of other components; also proton-proton collisions are inefficient. In other words, protons do not interact yet and their spectra are not yet of equilibrium form, see Fig. G.9. The temperature of protons start to change only at 10^{-13} sec, when proton-electron Coulomb scattering becomes efficient.

As can be seen from Fig. G.8, the chemical potentials of electrons, positrons and photons evolved by that time due to triple interactions. Since chemical potentials of electrons, positrons and photons were negative, the particles were in deficit with respect to the thermal state. This caused the total number of these particles to increase and consequently the temperature to decrease. The chemical potential of photons reaches zero at $t_2 = 10^{-12}$ sec, shown by the vertical line on the right in Fig. G.7 and Fig. G.8, which means that electrons, positrons and photons are now in thermal equilibrium. However, protons are not yet in equilibrium with other particle since their spectra are not thermal, as shown in the lower part of Fig. G.9.

Finally, the proton component thermalize with other particles at 4×10^{-12} sec, and from that moment plasma is characterized by unique temperature, $\theta_{\rm th} \simeq 0.48$ as Fig. G.7 clearly shows. Protons have final chemical potential $\nu_p \simeq -12.8$.

This state is characterized by thermal distribution of all particles as can be seen from Fig. G.10. There initial flat as well as final spectral densities are shown together with fits of particles spectra with the values of the common temperature and the corresponding chemical potentials in thermal equilibrium.

In this particular example relaxation time-scales towards kinetic and thermal equilibria have been determined. One can similarly determine relaxation time-scales as the function of total energy density ρ and baryon loading parameter B in wide range range of these parameters. This was done in Aksenov et al. (2010).

G.9. Collisionless and self-gravitating systems

The kinetic approach is remarkably useful in studying collisionless systems. In such systems particle do not collide, but interact via long range forces such as gravitational and electromagnetic fields. The basic equations governing evolution of the system are, respectively, Vlasov-Einstein and Vlasov-Maxwell equations. In this Section systems interacting via electromagnetic and gravitatinal fields will be discussed.

G.9.1. Plasma instabilities

In Sec. G.7.7 damping of waves in collisionless plasma were discussed. This process suppresses the amplitude of initial perturbations thus bringing the system to an equilibrium. The opposite can happen, namely initially small perturbation can grow with time: this process is generally referred to as instability. There are many plasma instabilities occurring when different plasma flows, particles with different masses and electromagnetic fields interact Mikhailovskii (1975). The focus will be on two particular kinds, which are thought to occur in astrophysical conditions: *Weibel* and *two stream* instabilities.

The Weibel instability is a plasma instability present in homogeneous or nearly-homogeneous electromagnetic plasmas which possess an anisotropy in momentum (velocity) space. In the linear limit the instability causes exponential growth of electromagnetic fields in the plasma which helps to restore momentum space isotropy.

The two stream instability can be thought of as the inverse of Landau damping, where the existence of a greater number of particles that move slower than the wave phase velocity as compared with those that move faster, leads to an energy transfer from the wave to the particles. Again, focus will be on non-relativistic case for simplicity, see Achterberg and Wiersma (2007) for Weibel instability in relativistic plasma and Dieckmann (2005) for relativistic two-stream instability, see also Bret et al. (2008).

Following Weibel (1959) consider an electron-ion plasma, where electrons have an anisotropic DF $f_0(\mathbf{v})$. The equations for first order perturbations are obtained from the Vlasov-Maxwell equations (G.6.13),(G.6.14) as

$$\frac{\partial \delta f}{\partial t} + \mathbf{v}\cdot\frac{\partial \delta f}{\partial \mathbf{r}} + \frac{q}{m}\left[\mathbf{v}\times\mathbf{B}_0\right]\cdot\frac{\partial \delta f}{\partial \mathbf{v}} = -\frac{q}{m}\left[\mathbf{E}+\mathbf{v}\times\mathbf{B}\right]\cdot\frac{\partial f_0}{\partial \mathbf{v}}, \tag{G.9.1}$$

where magnetic field $\mathbf{B}_0$ is included for generality. In analogy with Sec. G.7.7 assume that perturbations of DF and electromagnetic fields fields are of the form $\exp\left[-i\left(\mathbf{k}\cdot\mathbf{r}-\omega t\right)\right]$. Then it follows

$$i\left(\omega+\mathbf{k}\cdot\mathbf{v}\right)\delta f - \frac{q}{m}\mathbf{B}_0\cdot\left[\mathbf{v}\times\frac{\partial \delta f}{\partial \mathbf{v}}\right] = -\frac{q}{m\omega}\left\{\omega\mathbf{E}\cdot\frac{\partial f_0}{\partial \mathbf{v}} + \left[\mathbf{k}\times\mathbf{E}\right]\cdot\left[\mathbf{v}\times\frac{\partial f_0}{\partial \mathbf{v}}\right]\right\}, \tag{G.9.2}$$

where the effect of anisotropy is seen on the RHS. Actually the external magnetic field $\mathbf{B}_0$ is not necessary for the development of instability, it is included

for generality. Assume $\mathbf{k} \parallel \hat{\mathbf{z}}$, $\mathbf{E} \perp \mathbf{k}$ and consider a special case of distribution function

$$f_0 = \frac{n}{(2\pi)^{3/2} u_0^2 u_3} \exp\left(-\frac{v_x^2 + v_y^2}{2u_0^2} - \frac{v_z^2}{2u_3^2}\right). \tag{G.9.3}$$

Now taking $\mathbf{B}_0 = 0$, $\omega \gg u_3 k$ it is possible to integrate the dispersion relation and get

$$\omega^4 - \left(\omega_p^2 + k^2\right)\omega^2 - u_0^2 \omega_p^2 k^2 = 0, \tag{G.9.4}$$

where $\omega_p^2 = \frac{4\pi q^2 n}{m}$ is the usual plasma frequency. This equation has four roots

$$\omega = \pm\left\{\frac{1}{2}\left[\omega_p^2 + k^2 \pm \sqrt{\left(\omega_p^2 + k^2\right)^2 + 4u_0^2\omega_p^2 k^2}\right]\right\}^{1/2}, \tag{G.9.5}$$

and the one corresponding to both "$-$" signs is negative imaginary. It is the source of instability. This solution is valid only when $u_0 \gg u_3$ (velocity dispersion in $\hat{\mathbf{z}}$ direction is much smaller than in other directions).

The two stream instability occurs for instance when there is a stream of particles uniformly distributed in space through a plasma at rest (counter streaming beams etc.). Consider electron-ion plasma with electron density n_e, and electrons with much smaller density n'_e stream through it with constant velocity $\mathbf{v}$ (total charge is zero).

Following the same steps as before the dispersion relation can be obtained, see e.g. Lifshitz and Pitaevskii (1981). In this case one has

$$\left(\frac{\omega_e}{\omega}\right)^2 + \left(\frac{\omega'_e}{\omega - \mathbf{k}\cdot\mathbf{v}}\right)^2 = 1, \quad \omega_e^2 = \frac{4\pi q^2 n_e}{m}, \quad \omega_e'^2 = \frac{4\pi q^2 n'_e}{m}, \tag{G.9.6}$$

and one should search for its solution of the form $\omega = \mathbf{k}\cdot\mathbf{v} + \delta$, where $\delta \ll \mathbf{k}\cdot\mathbf{v}$. The solution is

$$\delta = \pm\frac{\omega'_e}{\sqrt{1 - \left(\omega_e/\mathbf{k}\cdot\mathbf{v}\right)^2}}. \tag{G.9.7}$$

For $\mathbf{k}\cdot\mathbf{v} \ll \omega_e$ purely imaginary δ is found, which again means the presence of instability. The linear analysis presented above shows that initially small perturbations grow exponentially with time. Actually, as soon as validity condition $\delta f \ll f_0$ breaks down, the non-linear character of instabilities has

to be considered.

G.9.2. Collisionless shock waves

Such instabilities are present in relativistic regime as well. They may play a crucial role in the Gamma-Ray Burst phenomena, where interaction between two streams moving relativistically with respect to each other is expected Spitkovsky (2008b). Similar plasma instabilities are expected also in experiments with ultra-intense lasers Fiuza et al. (2012).

The growth rates for linear Weibel and two-stream instabilities are, respectively

$$\Gamma_W \propto \left(\frac{n_e'}{n_e}\right)^{1/2}, \quad \Gamma_{TS} \propto \left(\frac{n_e'}{n_e}\right)^{1/3}, \tag{G.9.8}$$

see e.g. Silva (2006). The typical wavelengths are similar

$$\lambda_W \simeq \frac{c}{\omega_e}, \quad \lambda_{TS} \simeq \frac{v}{\omega_e}, \tag{G.9.9}$$

where v is velocity of plasma stream. It is remarkable that currently numerical experiments in three dimensions, see e.g. Frederiksen et al. (2004),Spitkovsky (2008a), allow studying not only development of instabilities at their linear stage, but also following them on much longer time-scales, where saturation occurs and complex electromagnetic field patterns emerge.

G.9.3. Free streaming

Gas of self-gravitating particles in a flat space time is also known to be unstable Jeans (1902). Following Bisnovatyi-Kogan and Zel'Dovich (1971) consider Vlasov-Poisson equations (G.7.13) for collisionless particles in expanding Universe

$$\frac{\partial f}{\partial t} + \mathbf{v}\cdot\frac{\partial f}{\partial \mathbf{r}} - \frac{\partial \Phi}{\partial \mathbf{r}}\cdot\frac{\partial f}{\partial \mathbf{v}} = 0, \quad \Delta\Phi = 4\pi G\rho, \tag{G.9.10}$$

where $\rho = m\int f d^3\mathbf{v}$ is mass density of particles. The background solution for a Newtonian universe with zero spatial curvature is

$$\rho = \frac{1}{6\pi G t^2}, \quad \Phi = \frac{2}{3}\pi G\rho\,(t)\,r^2, \quad \frac{\partial\Phi}{\partial\mathbf{r}} = \frac{2}{9}\frac{\mathbf{r}}{t^2}. \tag{G.9.11}$$

Solving the corresponding linearized equations for a perturbed Maxwellian distribution with temperature θ by integration over characteristics the gravitational potential is found

$$\varphi(t) = \frac{2}{t^{2/3}} \int_0^t \varphi(t') \, \tau \exp\left(-\frac{9}{4} k^2 \theta \tau^2\right) dt', \quad \tau = t^{-1/3} - t'^{-1/3}, \quad \text{(G.9.12)}$$

where $\Phi = \exp(ik\xi)\,\varphi(t)$.

For long waves the exponential is substituted by unity and the result is

$$\varphi(t) \propto t^{-5/3}, \quad \delta\rho/\rho \propto t^{2/3}, \quad \text{(G.9.13)}$$

which is the usual result of gravitational instability in matter dominated phase of the Universe, see e.g. Weinberg (2008). For short waves with $\frac{9}{4}k^2\theta \gg t^{1/3}$ using the method of steepest descents one finds

$$\varphi(t) \propto \exp\left[\frac{1}{9}\sqrt{\frac{2e\lambda^3}{\pi}}\frac{1}{t}\right], \quad \lambda = \frac{9}{4}k^2\theta, \quad \text{(G.9.14)}$$

which means perturbations are damped with time. This phenomenon is similar to Landau damping in plasma and is called *gravitational Landau damping* (or *free streaming*). Distribution function with two counter streams has been studied as well in Bisnovatyi-Kogan and Zel'Dovich (1971), but it was found that this does not lead to additional instability. For the formulation of the problem within General Relativity see Bond and Szalay (1983).

Note that the treatment of perturbations in hydrodynamic limit shows oscillations of perturbations at small scales, see e.g. Lattanzi et al. (2003), instead of damping. These oscillations occur due to interplay between gravity and pressure. Hence the hydrodynamic treatment does not capture an essential phenomenon in self-gravitating systems.

This result of kinetic theory is so remarkable that it has been one of the main reasons why purely hot dark matter cosmological scenarios were rejected, see e.g. White et al. (1983). In fact, light particles which decouple from primordial plasma when relativistic have the free streaming scale Padmanabhan (1993)

$$l_{FS} \simeq 0.5 \left(\frac{m_{DM}}{1\,\mathrm{keV}}\right)^{-4/3} (\Omega_{DM} h^2)^{1/3}\,\mathrm{Mpc}, \quad \text{(G.9.15)}$$

where m_{DM} is particle mass, Ω_{DM} is the fraction of the dark matter in the

critical density of the Universe, $H = 100h$ km/s/Mpc is the Hubble parameter. On the scale smaller than l_{FS} structures cannot form as any perturbations are exponentially suppressed. A corresponding mass scale has an order of supercluster of galaxies or even larger if the particle mass is $m_{DM} < 30\,\mathrm{eV}$, implying that dark matter cannot consist mainly of particles with such mass.

G.9.4. Phase mixing and violent relaxation

The phenomenon of phase mixing is thought to be important in formation of galaxies and large scale structure of the Universe, see e.g. Binney and Tremaine (2008). For illustration of this phenomenon let us consider an example. Assume particles are placed in a rectangular potential well and each one moves with constant velocity, see Fig. G.11. When particles hit the wall they change the direction of the velocity. While in the beginning only lower half of the phase space is filled, in course of time the distribution function tends to fill all the phase space. While the *fine grained DF* f stays constant by the Liouville theorem, the *coarse grained DF* decreases. Another example of phase mixing is given in Binney and Tremaine (2008).

Relaxation mechanism related to phase mixing is found by Linden-Bell Lynden-Bell (1967). It should operate in a newly formed gravitationally bound collisionless systems such as galactic halo or cluster of galaxies. When a star moves in a fixed potential Φ its specific energy is constant $\epsilon = \frac{1}{2}v^2 + \Phi$. When the potential is time varying $\Phi(\mathbf{x}, t)$, the energy is not constant

$$\frac{d\epsilon}{dt} = \frac{1}{2}\frac{dv^2}{dt} + \frac{d\Phi}{dt} = \mathbf{v}\cdot\left(\frac{d\mathbf{v}}{dt} + \nabla\Phi\right) + \frac{\partial\Phi}{\partial t} = \left.\frac{\partial\Phi}{\partial t}\right|_{\mathbf{x}(t)}. \tag{G.9.16}$$

This is a mechanism of redistributing particles in the phase space, i.e. relaxation. It differs from particle collisions, because the energy change does not depend on mass. Linden-Bell derived also the relaxation time-scale, which is

$$t_{LB} \simeq \frac{3}{4\sqrt{2\pi G\langle\rho\rangle}} = \frac{3}{8\pi}P, \tag{G.9.17}$$

where P is the typical radial period of the orbit of a star in the galaxy.

G.9.5. Dark matter structure formation

The processes discussed above provide a mechanism to form the structure in the Universe. Almost homogeneous matter initially has small density fluctuations being subject to gravitational instability. Structures become gravitationally bound, detach from the Hubble flow, relax by phase mixing and violent relaxation, and end up as virialized equilibrium systems. The process repeats on larger and larger scales. This bottom-up picture of structure formation is called *hierarchical clustering*, and it is supported by numerical simulations. There are additional physical effects such as merging of smaller structures that influence and possibly even dominate structure formation.

The largest success of the numerical N-body simulations resulted in so called Navarro-Frenk-While profile of dark mater halos Navarro et al. (1996). The dark matter halo density profile is inferred from numerical simulations, and has a universal shape with mass density profile

$$\frac{\rho}{\rho_c} = \frac{\delta_c}{(r/r_s)\,(1 + r/r_s)^2}, \tag{G.9.18}$$

where ρ_c is the critical density, δ_c is the characteristic density, r_s is the scale radius. It should be noted that other halo profiles are suggested in the literature which may give better agreement with measurements of rotation curves of galaxies.

G.10. Conclusions

These brief lecture notes summarize the material presented during five lectures during XV Brazilian School of Cosmology and Gravitation. The idea has been to illustrate not only the theoretical progress in kinetic theory in relativistic domain, but also to acknowledge the rapid development of its applications, especially in the field of astrophysics and cosmology. Many processes in these fields can be understood on the basis of hydrodynamics. However, the study of phenomena which generally involve *non-equilibrium* processes require a different approach, based on kinetic theory.

I could only touch upon several phenomena, providing references in which interested reader could find more details. Much more phenomena remain even not mentioned: the choice is due to personal interests of the author.

Phenomena that I did not cover include, among others, reheating after inflation, cosmic recombination, cosmological nucleosynthesis, primordial magnetic fields generation, particle acceleration in shocks, Sunyaev–Zeldovich effect. I conclude with a general remark: that astrophysics and cosmology are natural fields of application of kinetic theory, since basic requirements of the theory such as large number of particles are easily satisfied.

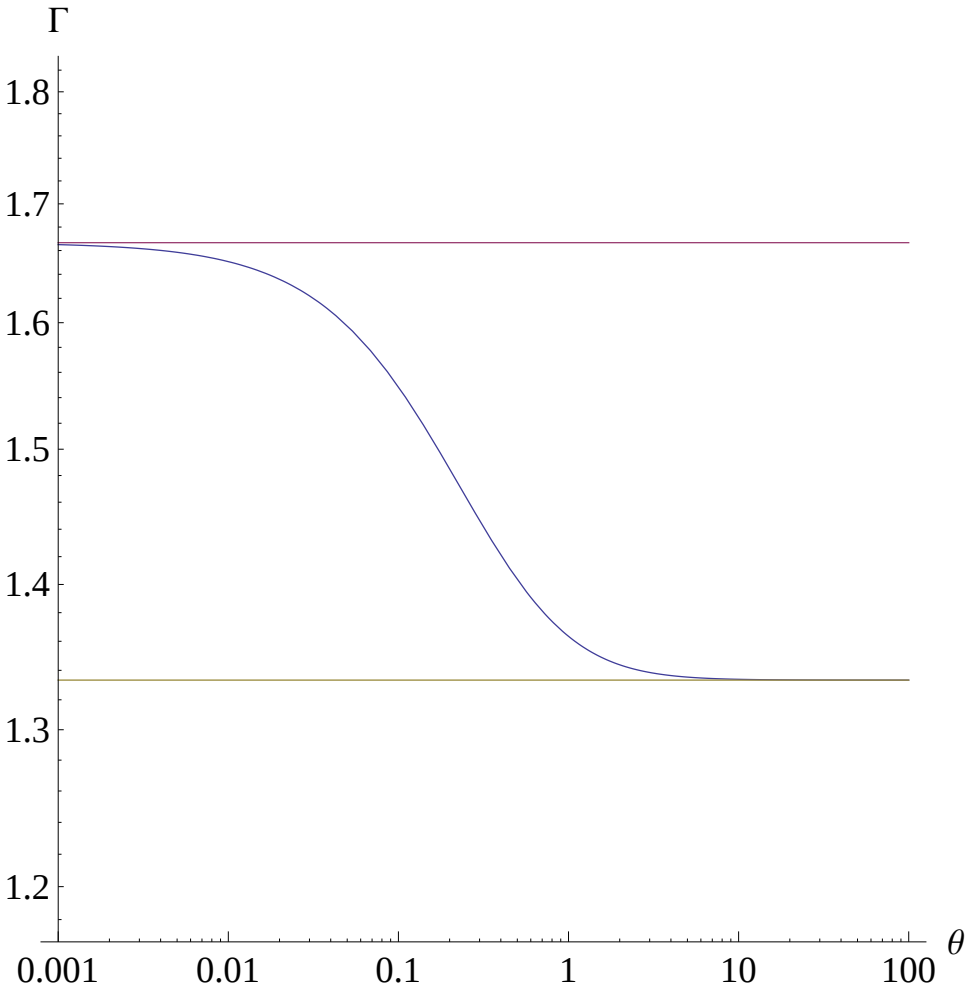

Figure G.1.: The thermal index of relativistic gas as function of dimensionless temperature.

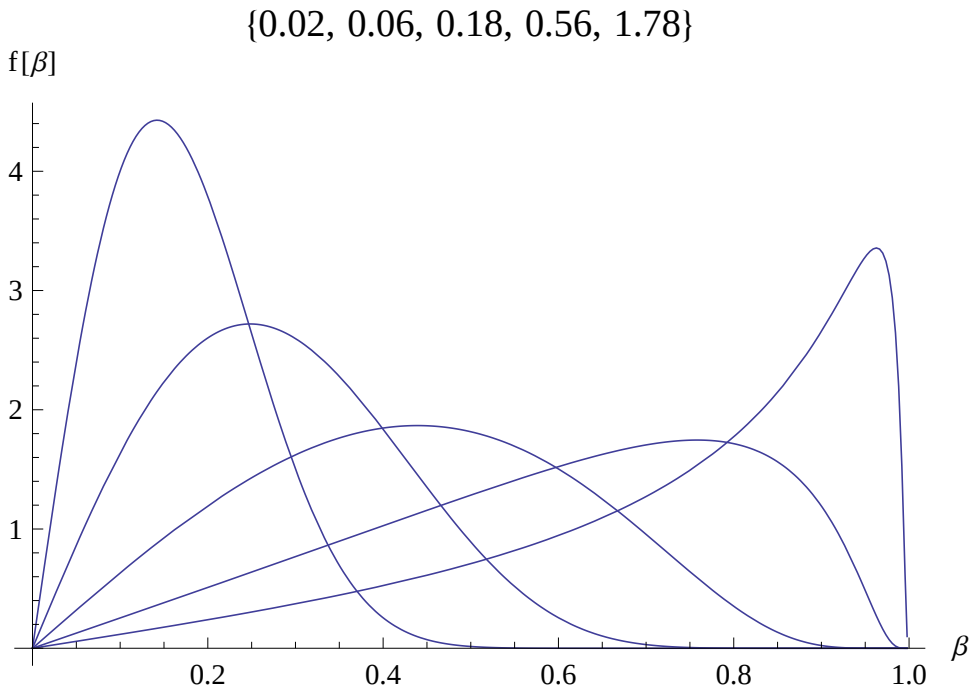

Figure G.2.: Relativistic Maxwellian distribution function for selected values of dimensionless temperature.

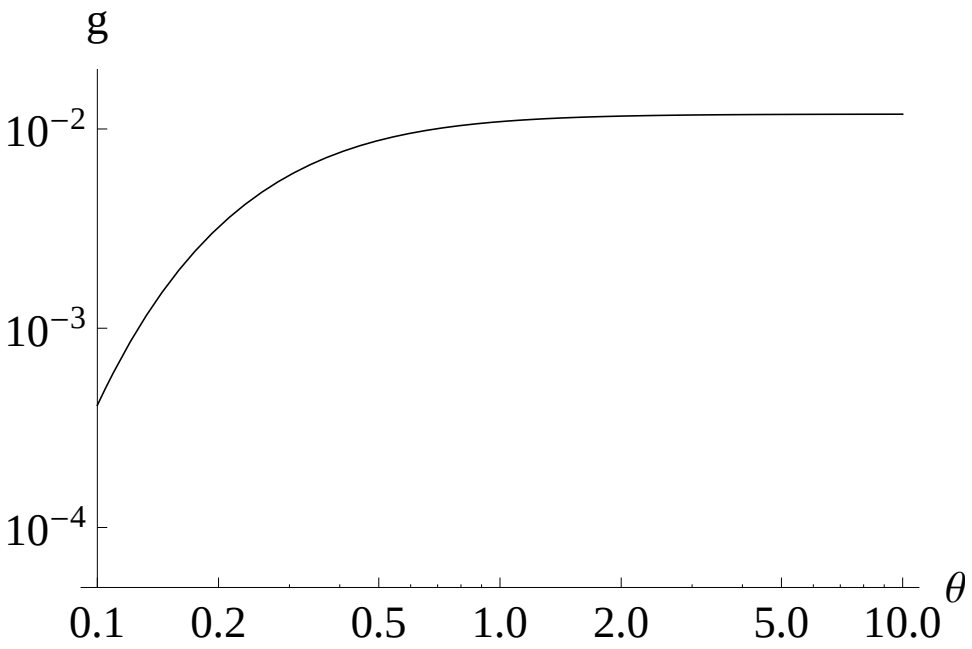

Figure G.3.: The plasma parameter of relativistic plasma in thermal equilibrium as function of dimensionless temperature.

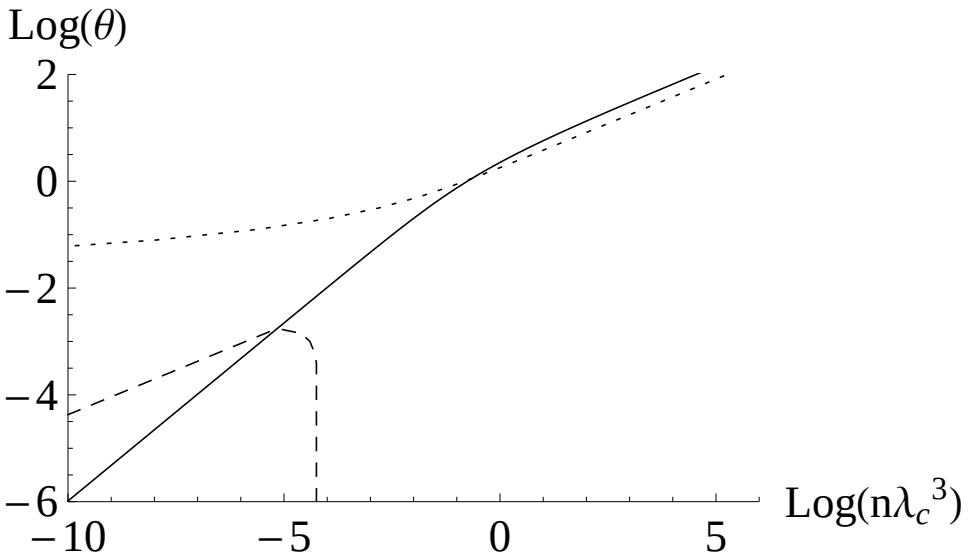

Figure G.4.: The temperature-density diagram for relativistic plasma. Solid line corresponds to the condition $\mathcal{D} = 1$. To the right of this curve $\mathcal{D} < 1$ and plasma is degenerate. Dashed curve corresponds to the condition $\mathfrak{g}_p = 1$. Above this curve $\mathfrak{g}_p < 1$ and plasma is ideal. Dotted curve corresponds to thermal electron-positron plasma.

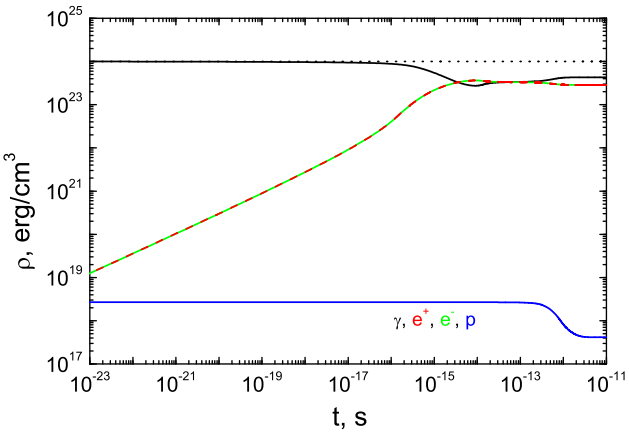

Figure G.5.: Depencence on time of energy densities of electrons (green), positrons (red), photons (black) and protons (blue) for initial conditions I. Total energy density is shown by dotted black line. Interaction between pairs and photons operates on very short time-scales up to 10^{-23} sec. Quasi-equilibrium state is established at $t_{\rm k} \simeq 10^{-14}$ sec which corresponds to kinetic equilibrium for pairs and photons. Protons start to interact with then as late as at $t_{\rm th} \simeq 10^{-13}$ sec.

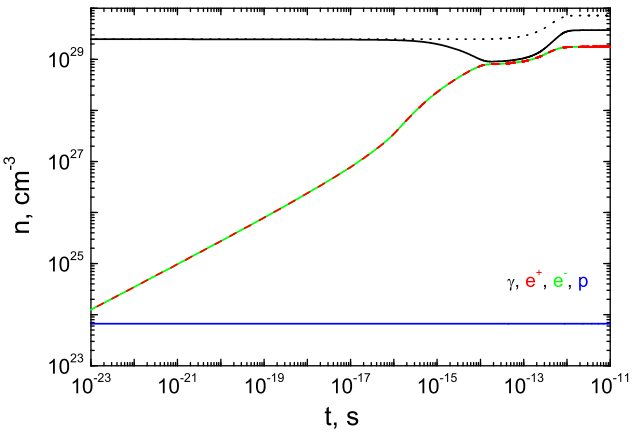

Figure G.6.: Depencence on time of concentrations of electrons (green), positrons (red), photons (black) and protons (blue) for initial conditions I. Total number density is shown by dotted black line. In this case kinetic equilibrium between electrons, positrons and photons is reached at $t_{\rm k} \simeq 10^{-14}$ sec. Protons join thermal equilibrium with other particles at $t_{\rm th} \simeq 4 \times 10^{-12}$ sec.

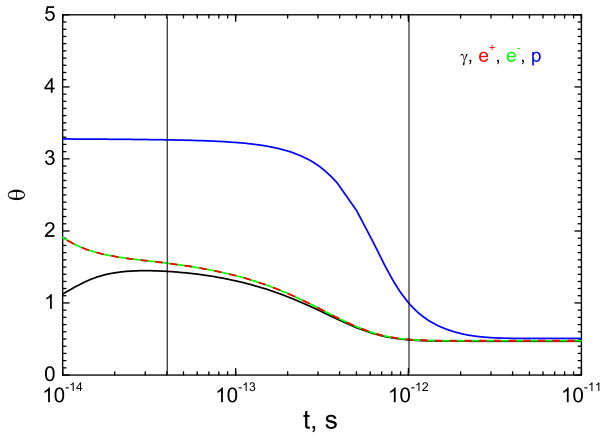

Figure G.7.: Depencence on time of dimensionless temperature of electrons (green), positrons (red), photons (black) and protons (blue) for initial conditions I. The temperature for pairs and photons acquires physical meaning only in kinetic equilibrium at $t_{\rm k} \simeq 10^{-14}$ sec. Protons are cooled by the pair-photon plasma and acquire common temperature with it as late as at $t_{\rm th} \simeq 4 \times 10^{-12}$ sec.

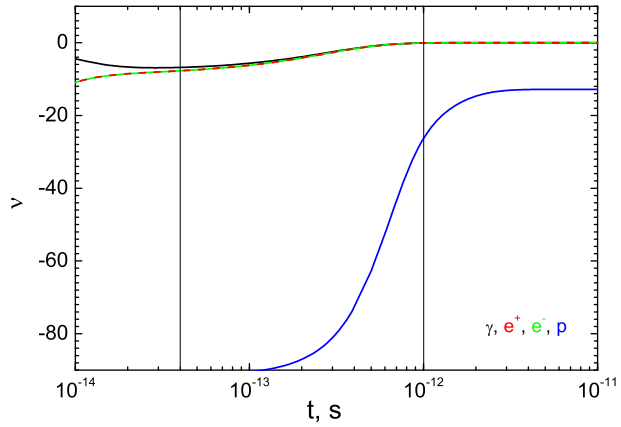

Figure G.8.: Depencence on time of dimensionless chemical potential of electrons (green), positrons (red), photons (black) and protons (blue) for initial conditions I. The chemical potential for pairs and photons acquires physical meaning only in kinetic equilibrium at $t_{\rm k} \simeq 10^{-14}$ sec, while for protons this happens at $t_{\rm th} \simeq 4 \times 10^{-12}$ sec. At this time chemical potential of photons has evolved to zero and thermal equilibrium has been already reached.

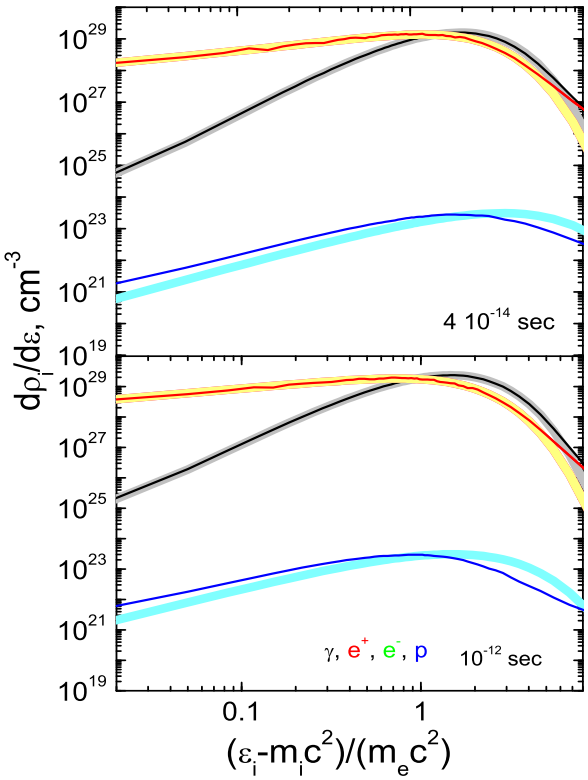

Figure G.9.: Spectral density as function of particle energy for electrons (green), positrons (red), photons (black) and protons (blue) for initial conditions I at intermediate time moments $t_1 = 4 \times 10^{-14}$ sec (upper figure) and $t_2 = 10^{-12}$ sec (lower figure). Fits of the spectra with chemical potentials and temperatures corresponding to thermal equilibrium state are also shown by yellow (electrons and positrons), grey (photons) and light blue (protons) thick lines. The upper figure shows the spectra when kinetic equilibrium is established for the first time between electrons, positrons and photons while the lower figure shows the spectra at thermal equilibrium between these particles. On both figures protons are not yet in equilibrium neither with themselves nor with other particles.

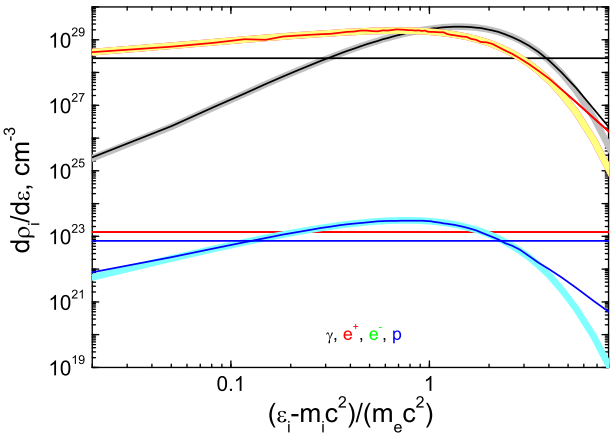

Figure G.10.: Spectral density as function of particle energy are shown as before at initial and final moments of the computations. The final photon spectrum is black body one.

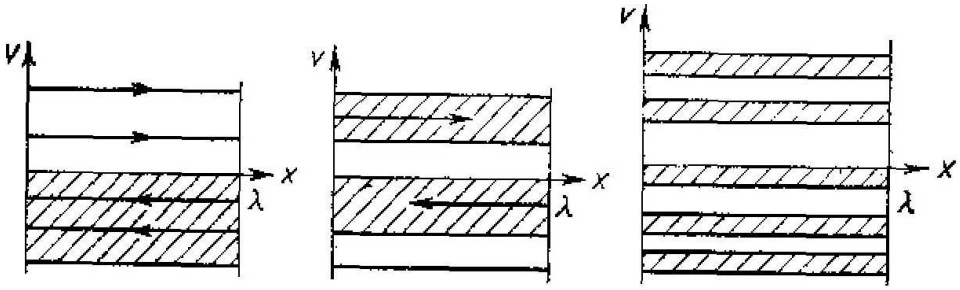

Figure G.11.: Phase space of particles moving in rectangular potential well, see Artsimovich and Sagdeev (1979), p. 80.

H. The distribution of dark matter in galaxies based quantum treatments

H.1. INTRODUCTION

One of the most quoted papers in the study of the dark-matter distribution in galactic halos is certainly the work of Tremaine & Gunn Tremaine and Gunn (1979), in which the authors established a lower limit on the mass of neutrinos composing galactic halos by considering an isothermal classical distribution of self-gravitating particles and imposing quantum constraints on the phase space density in the core of the galaxies. That treatment presenting a peculiar mixture of quantum and classical considerations has always attracted the attention and the suspicion of many astrophysicists and theoretical physicists. In particular, the opinion of one of us (R. Ruffini) was that a self-consistent treatment of quantum constraints in a self-consistent quantum description of the microphysical system was needed. A long effort so started.

H.2. HISTORICAL REVIEW: TWO PIONEERING WORKS

One of the preliminary works in order to prove the analogy and the differences between a classical and a quantum self-gravitating system was advanced within a Newtonian approach in Ref. Ruffini and Stella (1983). There, the problem of a semi-degenerate system of fermions under a gravitational interaction was approached, and that model was compared and contrasted with the classical King model. The authors of Ref. 2 proposed a distribution

function built for non-relativistic particles:

$$f(v) = \frac{1 - \exp\left[-j^2(v_e^2 - v^2)\right]}{\exp\left[j^2(v^2 - \bar{\mu})\right] + 1}, \; v \leq v_e$$
$$= 0, \qquad\qquad v > v_e,$$

where v_e is the escape velocity. In the limit $v_e \to \infty$, the usual Fermi distribution is obtained. The other two constant parameters are $j^2 = m/(2kT)$ and $\bar{\mu} = 2\mu/m$. The relevance of this $f(v)$ is that it is an extension of the King model to the case of a Fermi gas. Moreover, if the degeneracy parameter $\theta = j^2\bar{\mu}$ is defined, when $\theta \to -\infty$, the non-degenerate limit is reached, and the distribution function used by King is recovered. Instead, when $j^2 \to \infty$ and $\bar{\mu} \to v_e^2$, the degenerate limit is obtained, and the escape velocity is associated with the Fermi energy. The energy integral,

$$E = v^2/2 + V(r)\,, \tag{H.2.1}$$

together with the Jeans theorem for spherical systems, allowed them to simply relate the escape velocity to the gravitational potential by $v_e^2 = -2V$ (V being 0 at the surface of the configuration). They finally solved the Poisson equation for $W = -2j^2V$, with the mass density being given by $\rho \propto \int f(v)v^2dv$, which is related to W via the j parameter.

For simplicity, in an attempt to understand the physical interpretation of the parameters, only the value for the central degeneracy parameter was assumed for the sake of example,

$$\theta(0) \equiv \theta_0 = 0\,, \tag{H.2.2}$$

and no other values for θ_0 were explored at the time. Different normalized mass density solutions were given for different values of $W(0) \equiv W_0$, as shown in Fig. H.1. Under these special conditions, the analogy between a self-gravitating system of fermions and the King model was proven, and a first attempt was made to justify the Tremaine & Gunn limit.

It soon became clear that these solutions, although interesting in reproducing the classical results of the King profiles for a self-gravitating fermion gas, were really extremely restrictive and were not representative of the general solutions for a relativistic self-gravitating system of massive fermions. These restrictions correspond to three different constraints: 1) $\theta_0 = 0$; 2) the ap-

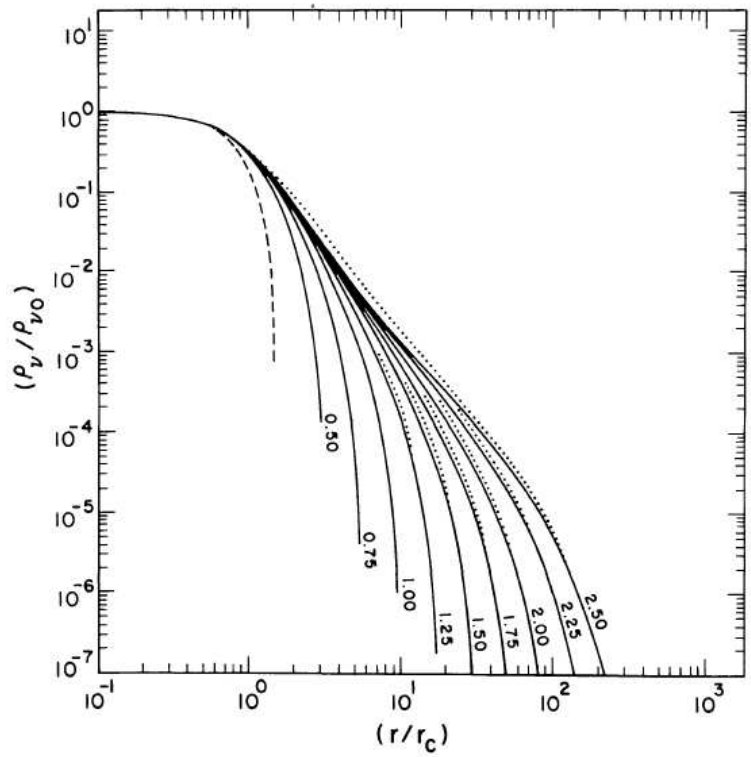

Figure H.1.: Normalized density profiles for different values of W_0 and fixed $\theta_0 = 0$. The dotted curve corresponds to the analogous King profiles while the dashed curve represents the degenerate limit (taken from Ref. 2 with permission).

plication of a cut-off in the phase space, which implies the elimination of an important family of solutions; and 3) the use of a non-relativistic Newtonian approach.

A fundamental step was taken by Gao et al. (1990) to include special relativity, as well as general relativity effects in the phase space of the distribution function. Thus, they considered the relativistic Fermi-Dirac distribution function for the 'inos' without any cut-off in their momentum space; i.e., $f(\epsilon) = (\exp[(\epsilon - \mu)/(kT)] + 1)^{-1}$, where $\epsilon(p) = \sqrt{c^2p^2 + m^2c^4} - mc^2$ is the particle's kinetic energy and μ the chemical potential with the particle rest-energy subtracted off. They wrote the system of Einstein equations in the spherically-symmetric metric $g_{\mu\nu} = diag(e^{\nu}, -e^{\lambda}, -r^2, -r^2\sin^2\theta)$, where ν and λ depend only on the radial coordinate r, together with the thermodynamic equilibrium conditions of Tolman (1930), and Klein (1949),

$$e^{\nu/2}T = const., \quad e^{\nu/2}(\mu + mc^2) = const.,$$

in the following dimensionless way:

$$\frac{d\hat{M}}{d\hat{r}} = 4\pi\hat{r}^2\hat{\rho}\,, \tag{H.2.3}$$

$$\frac{d\theta}{d\hat{r}} = \frac{\beta_0(\theta - \theta_0) - 1}{\beta_0}\frac{\hat{M} + 4\pi\hat{P}\hat{r}^3}{\hat{r}^2(1 - 2\hat{M}/\hat{r})}\,, \tag{H.2.4}$$

$$\frac{d\nu}{d\hat{r}} = \frac{\hat{M} + 4\pi\hat{P}\hat{r}^3}{\hat{r}^2(1 - 2\hat{M}/\hat{r})}\,, \tag{H.2.5}$$

$$\beta_0 = \beta(r)e^{\frac{\nu(r)-\nu_0}{2}}\,. \tag{H.2.6}$$

The following dimensionless quantities were introduced: $\hat{r} = r/\chi$, $\hat{M} = GM/(c^2\chi)$, $\hat{\rho} = G\chi^2\rho/c^2$ and $\hat{P} = G\chi^2P/c^4$, where $\chi = 2\pi^{3/2}(\hbar/mc)(m_p/m)$ is a dimensional factor that has a unit of length and scales as m^{-2}, with $m_p = \sqrt{\hbar c/G}$ being the Planck mass. The temperature and degeneracy parameters are, $\beta = kT/(mc^2)$ and $\theta = \mu/(kT)$, respectively. For a relativistic and semi-degenerate Fermi gas the mass density ρ and pressure P are expressed in terms of the standard infinite integrals in momentum space weighted with the $f(\epsilon)$ already given (see Ref. Gao et al. (1990)).

In Ref. Gao et al. (1990) the initial condition problem for the variables of the system, $\theta(r)$, $\beta(r)$, $\nu(r)$, and $M(r)$, was solved by using $M_0 = 0$ at $r = 0$ (indi-

cated by a subscript '0') while using arbitrary values for the temperature and the degeneracy parameters β_0 and θ_0, respectively. In Figs. H.2–H.3, different normalized mass density solutions for different $\theta_0 < 0$ and $\theta_0 \geq 0$, respectively, are shown for a fixed non-relativistic central temperature parameter β_0.

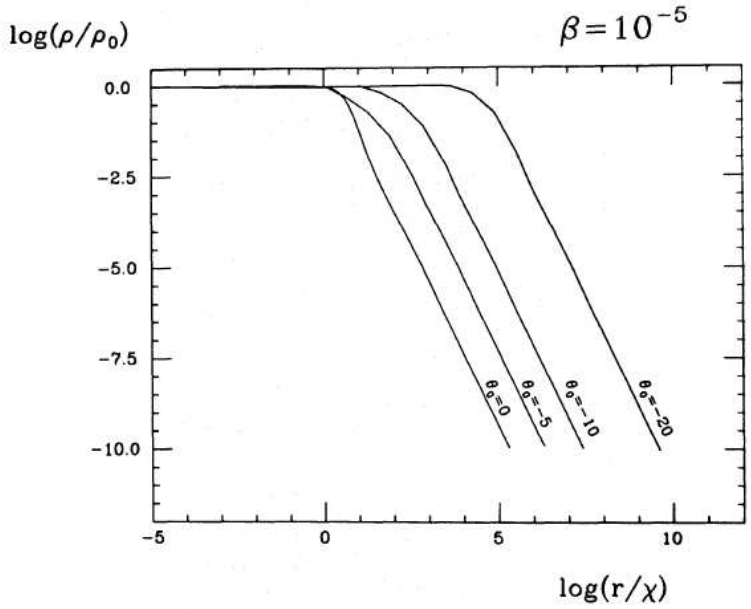

Figure H.2.: Different density profiles for different $\theta_0 < 0$ and fixed β_0 in dimensionless variables. Note the simple cored plus r^{-2} morphology (taken from Ref. Gao et al. (1990) with permission).

It is important to note that the system in Eqs. (K.2.1)–(K.2.4) has no particle mass (m) dependence when solved in the dimensionless variables while instead the physical magnitudes, such as those of r and ρ, have an explicit dependence on m through the dimensional factor $\chi(m)$. Because the authors of Ref. Gao et al. (1990) were mainly interested in the general properties of the solutions without going through the physical magnitudes, no particle mass constraints were used.

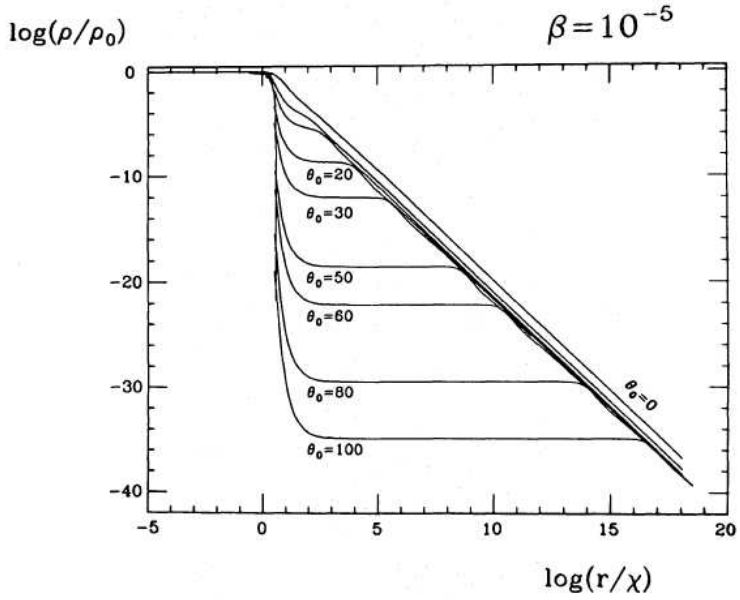

Figure H.3.: Different density profiles for different $\theta_0 \geq 0$ and fixed β_0 in dimensionless variables. Note the more complex core plus 'plateau' plus r^{-2} morphology (taken from Ref. Gao et al. (1990) with permission).

H.3. NOVEL PROCEDURE AND DISCUSSION

We recently returned to the Gao et al. work and propose a completely different way for solving the boundary condition problem for the system in Eqs. (K.2.1)–(K.2.4) in order to be consistent with the observationally-inferred values of typical dark matter halos in spiral galaxies as given in Ref. de Blok et al. (2008). Namely, using initial conditions $M_0 = v_0 = 0$ and arbitrary θ_0 (depending on the chosen central degeneracy) and defining the halo radius r_h at the onset of the flat rotation curve, we solve an eigenvalue problem for the central temperature parameter β_0 until the observed halo circular velocity v_h is obtained. Then, we solve a second eigenvalue problem for the particle mass m until the *observed* halo mass M_h is reached at the radius r_h.

The quest has been to use all this information in order to put constraints on the mass of the 'ino' in galactic halos by introducing the observational properties that may be utilized in this research. Interestingly enough, as detailed in Ref. Ruffini et al. (2014), only for an specific range of $\theta_0 > 0$ can these two eigenvalue problems be solved together, implying, as a consequence, a novel morphology for the density profiles, as well as a novel particle-mass bound associated with it, is reached. The density profiles present a quantum degenerate core, followed by a low degeneracy plateau, until they reach the r^{-2} Boltzmannian region corresponding to the flat part in the rotation curve. In Fig. H.4, we show a family of density profiles for different values of θ_0 that fulfills the mentioned halo constraints. We also plott for comparison the purely Boltzmannian curve, which agrees with the same *observed* halo magnitudes. As can be seen from Fig. H.4, we obtain from this novel analysis a more stringent lower mass bound for the 'ino' mass m, which is ~ 10 times higher than the ones inferred in Refs. 2 and 1. That is, $m \geq 0.42$ keV$/c^2$ for typical spiral galaxies.

Interestingly the quantum and relativistic treatment of the configurations considered here are characterized by the presence of central-cored structures unlike the typical cuspy configurations obtained from a classic non-relativistic approximation, such as the ones of numerical N-body simulations in Ref. Navarro et al. (1997). This naturally leads to a possible solution to the well-known core-cusp discrepancy de Blok et al. (2001a).

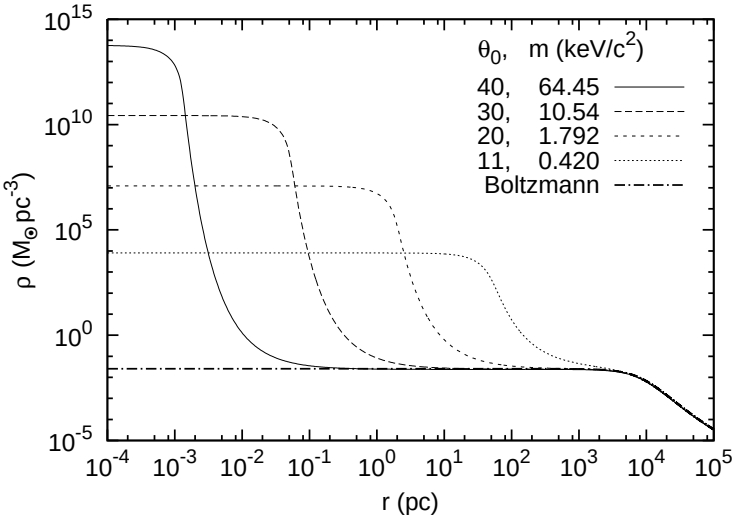

Figure H.4.: Physical density profiles for a specific ino masses m and central degeneracies θ_0 fulfilling the observational constraints $M_h = 1.6 \times 10^{11} M_\odot$ and $v_h = 168$ km/s at $r_h = 25$ Kpc (as taken from Ref. 7 and detailed in Ref. 8). The dot-dashed line represents the purely Boltzmannian profile for comparison.

I. A novel core-halo distribution of dark matter in galaxies

The problem of identifying the masses and the fundamental interactions of the dark matter particles is currently one of the most fundamental issues in physics and astrophysics. As we will show some inferences can already be derived from general considerations based on quantum statistics and gravitational interactions. Specific constraints on the values of the mass of the particles can be established using the rotation curves of galaxies. Indeed, already Tremaine and Gunn Tremaine and Gunn (1979), in addition of recalling previous cosmological considerations on massive neutrinos Cowsik and McClelland (1972); Weinberg (1972); Gott et al. (1974); Lee and Weinberg (1977), addressed the issue of the dark matter component in galactic halos. They made the following assumptions: 1) that the central region of these bound systems of self-gravitating massive neutrinos resemble classical Newtonian isothermal gas spheres with a core radius given by the King radius ; 2) that their velocity distribution is Maxwellian and the maximum phase-space density is $\rho_0 m^{-4}(2\pi\sigma^2)^{-3/2}$, m being the neutrino mass, ρ_0 the central density, σ the one-dimensional velocity dispersion, and $r_K^2 = 9\sigma^2/(4\pi G\rho_0)$ the King radius; 3) they further assume that the above maximum phase-space density at the center of the configurations cannot exceed, by Liouville's theorem, the phase-space neutrinos density at decoupling, $2g/h^3$ (g = particle helicity) . Consequently they obtained a limit on the particle mass

$$m > 101 \left(\frac{1}{g}\frac{100\mathrm{km/s}}{\sigma}\frac{1\ \mathrm{kpc}}{r_K}\right)^{1/4} \mathrm{eV}/c^2\,, \tag{I.0.1}$$

In this Letter we formulate an alternative proposal to the general problem of the dark matter distribution in galaxies with the following order: 1) we assume that the dark matter phase-space density is described Fermi-Dirac quantum statistics; 2) that the equilibrium equations for the configurations be

solved, for completeness, within a general relativistic treatment; 3) only after having identified the physical properties of the equilibrium configurations, constraints on the mass of the inos are inferred from observable quantities. As a direct outcome of this new approach it is exemplified how the determination of the ino mass, far from being derived imposing constraints on the phase-space distribution of a King-like core, e.g. Tremaine and Gunn (1979), it is obtained from a more composite equilibrium structure.

Following Gao et al. (1990); Ruffini et al. (2013a), we here consider a system of general relativistic self-gravitating bare massive fermions in thermodynamic equilibrium. No additional interactions are initially assumed for the fermions besides their fulfillment of quantum statistics and the relativistic gravitational equations. In particular, we do not assume weakly interacting particles as in Tremaine and Gunn (1979). We refer to this *bare* particles more generally as *inos*, leaving the possibility of additional fundamental interactions to be determined by further requirements to be fulfilled by the model. Already this treatment of bare fermions leads to a new class of equilibrium configurations and, correspondingly, to new limits to the ino mass. This is a necessary first step in view of a final treatment involving additional interactions to be treated self-consistently, as we will soon indicate.

The density and pressure of the fermion system are given by $\rho = m(2/h^3)\int f_p\left[1+\epsilon/(mc^2)\right]d^3p$ and $P = [2/(3h^3)]\int f_p\left[1+\epsilon/(2mc^2)\right]\epsilon/\left[1+\epsilon/(mc^2)\right]d^3p$, where the integration is over all the momentum space, $f_p = (\exp[(\epsilon-\mu)/(kT)]+1)^{-1}$ is the distribution function, $\epsilon = \sqrt{c^2p^2+m^2c^4}-mc^2$ is the particle kinetic energy, μ is the chemical potential with the particle rest-energy subtracted off, T is the temperature, k is the Boltzmann constant, h is the Planck constant, c is the speed of light, and m is the ino's particle mass. We do not include the presence of anti-fermions, i.e. we consider temperatures $T \ll mc^2/k$.

The Einstein equations for the spherically symmetric metric $g_{\mu\nu} = diag(e^{\nu}, -e^{\lambda}, -r^2, -r^2\sin^2\theta)$, where ν and λ depend only on the radial coordinate r, together with the thermodynamic equilibrium conditions of Tolman (1930), $e^{\nu/2}T$ =constant, and Klein (1949), $e^{\nu/2}(\mu+mc^2)$ =constant, can be written as Gao et al. (1990)

$$\frac{d\hat{M}}{d\hat{r}} = 4\pi\hat{r}^2\hat{\rho}, \quad \frac{d\nu}{d\hat{r}} = \frac{\hat{M} + 4\pi\hat{P}\hat{r}^3}{\hat{r}^2(1 - 2\hat{M}/\hat{r})}, \tag{I.0.2}$$

$$\frac{d\theta}{d\hat{r}} = -\frac{1 - \beta_0(\theta - \theta_0)}{\beta_0}\frac{d\nu}{d\hat{r}}, \quad \beta_0 = \beta(r)e^{\frac{\nu(r)-\nu_0}{2}}. \tag{I.0.3}$$

The following dimensionless quantities were introduced: $\hat{r} = r/\chi$, $\hat{M} = GM/(c^2\chi)$, $\hat{\rho} = G\chi^2\rho/c^2$, $\hat{P} = G\chi^2P/c^4$, where $\chi = 2\pi^{3/2}(\hbar/mc)(m_p/m)$, with $m_p = \sqrt{\hbar c/G}$ the Planck mass, and the temperature and degeneracy parameters, $\beta = kT/(mc^2)$ and $\theta = \mu/(kT)$, respectively.

The system variables are $[M(r), \theta(r), \beta(r), \nu(r)]$. We integrate Eqs. (I.0.2–I.0.3) for given initial conditions at the center, $r = 0$, in order to be consistent with the observed dark matter halo mass $M(r = r_h) = M_h$ and radius r_h, defined in our model at the onset of the flat rotation curves. The circular velocity is $v(r) = \sqrt{GM(r)/[r - 2GM(r)/c^2]}$ which at $r = r_h$, is $v(r = r_h) = v_h$.

It is interesting that a very similar set of equations have been re-derived in 2002 in Bilic et al. (2002) apparently disregarding the theoretical approach already implemented in 1990 in Gao et al. (1990). They integrated the Einstein equations fixing a fiducial mass of the ino of $m = 15\ \mathrm{keV}/c^2$, and they derived a family of density profiles for different values of the central degeneracy parameter at a fixed temperature consistent with an asymptotic circular velocity $v_\infty = 220\ \mathrm{km/s}$. They conclude that a self-gravitating system of such inos could offer an alternative to the interpretation of the massive black hole in the core of SgrA* Ghez et al. (2008). Although this result was possible at that time, it has been superseded by new constraints imposed by further observational limits on the trajectory of S-stars such as S1 and S2 Ghez et al. (2008); Gillessen et al. (2009).

In this Letter we give special attention to the flat rotation curves and their asymptotic value at infinity. We integrate our system of equations using different boundary conditions to the ones imposed in Bilic et al. (2002) and reaching different conclusions. We first apply this model to typical spiral galaxies, similar to our own galaxy, adopting dark matter halo parameters de Blok et al. (2008); Sofue et al. (2009):

$$r_h = 25\ \mathrm{k}pc,\ v_h = 168\ \mathrm{k}m/s,\ M_h = 1.6 \times 10^{11} M_\odot\,. \tag{I.0.4}$$

The initial conditions are $M(0) = 0$, $\nu(0) = 0$, $\theta(0) = \theta_0$ and $\beta(0) = \beta_0$. We integrate Eqs. (I.0.2–I.0.3) for selected values of θ_0 and m, corresponding to different degenerate states of the gas at the center of the configuration. The value of β_0 is actually an eigenvalue which is found by a trial and error procedure until the observed values of v_h and M_h at r_h are obtained. We show in Fig. I.1 the density profiles and the rotation curves as a function of the distance for a wide range of parameters (θ_0, m), for which the boundary conditions in (I.0.4) are exactly fulfilled.

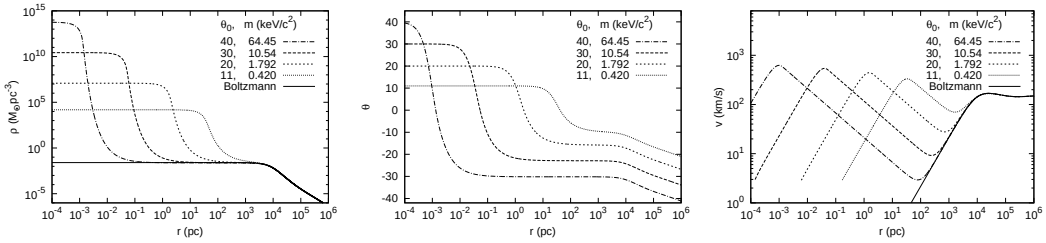

Figure I.1.: Mass density (left panel), degeneracy parameter (central panel), and rotation velocity curves (right panel) for specific ino masses m and central degeneracies θ_0 fulfilling the observational constraints (I.0.4). The density solutions are contrasted with a Boltzmannian isothermal sphere with the same halo properties. It is clear how the Boltzmann distribution, is as it should be, independent of m. All the configurations for $r \sim r_h$ asymptotically approaches the Boltzmann distribution. All the configurations, for any value of θ_0 and corresponding m, converge for $r \gtrsim r_h$ to the classical Boltzmannian isothermal distribution.

The phase-space distribution encompasses both the classical and quantum regimes. Correspondingly, the integration of the equilibrium equations leads to three marked different regimes (see Fig. I.1): a) the first consisting in a core of quantum degenerate fermions. These cores are characterized by having $\theta(r) > 0$. The core radius r_c is defined by the first maximum of the velocity curve. A necessary condition for the validity of this quantum treatment of the core is that the interparticle mean-distance, l_c, be smaller or of the same order, of the thermal de Broglie wavelength of the inos, $\lambda_B = h/\sqrt{2\pi mkT}$. As we show below (see Fig. I.2), this indeed is fulfilled in all the cases here studied . b) A second regime where $\theta(r)$ goes from positive to negative values for $r > r_c$, all the way up to the so called classical domain where the quantum corrections become negligible. This transition region consists in a sharply

decreasing density followed by an extended plateau. c) The classical regime described by Boltzmann statistics and corresponding with $\theta(r) \ll -1$ (for $r \gtrsim r_h$), in which the solution tends to the Newtonian isothermal sphere with $\rho \sim r^{-2}$, where the flat rotation curve sets in.

We define the core mass, the circular velocity at r_c, and the core degeneracy as $M_c = M(r_c)$, $v_c = v(r_c)$ and $\theta_c = \theta(r_c)$, respectively. In Table K.1 we show the core properties of the equilibrium configurations in spiral galaxies, for a wide range of (θ_0, m). For any selected value of θ_0 we obtain the correspondent ino mass m to fulfill the halo properties (I.0.4), after the above eigenvalue problem of β_0 is solved.

θ_0	m (keV/c^2)	r_c (pc)	$M_c(M_\odot)$	v_c (km/s)	θ_c
11	0.420	3.3×10^{1}	8.5×10^{8}	3.3×10^{2}	2.1
25	4.323	2.5×10^{-1}	1.4×10^{7}	4.9×10^{2}	5.5
30	10.540	4.0×10^{-2}	2.7×10^{6}	5.4×10^{2}	6.7
40	64.450	1.0×10^{-3}	8.9×10^{4}	6.2×10^{2}	8.9
58.4	2.0×10^{3}	9.3×10^{-7}	1.2×10^{2}	7.5×10^{2}	14.4
98.5	3.2×10^{6}	3.2×10^{-13}	7.2×10^{-5}	9.8×10^{2}	21.4

Table I.1.: Core properties for different equilibrium configurations fulfilling the halo parameters (I.0.4) of spiral galaxies.

It is clear from Table K.1 and Fig. I.1 that the mass of the core M_c is strongly dependent on the ino mass, and that the maximum space-density in the core is considerably larger than the maximum value considered in Tremaine and Gunn (1979) for a Maxwellian distribution. Interestingly, as can be seen from Fig. I.1, the less degenerate quantum cores in agreement with the halo observables (I.0.4), are the ones with the largest sizes, of the order of halo-distance-scales. In this limit, the fermion mass acquires a sub-keV minimum value which is larger, but comparable, than the corresponding sub-keV Gunn & Tremaine bound (I.0.1), for the same halo observables. Indeed, Eq. (I.0.1) gives a lower limit $m \approx 0.05$ keV$/c^2$ using the proper value for the King radius, $r_K \simeq 8.5$ kpc, for $\sigma = \sqrt{2/5} v_h$ and $\rho_0 = 2.5 \times 10^{-2} M_\odot/\mathrm{pc}^3$, associated to the Boltzmannian density profile in Fig. I.1.

In the case of a typical spiral galaxy, for an ino mass of $m \sim 10$ keV$/c^2$, and a temperature parameter $\beta_0 \sim 10^{-7}$, obtained from the observed halo rotation velocity v_h, the de Broglie wavelength λ_B is higher than the interparticle mean-distance in the core l_c, see Fig. I.2, safely justifying the quantum-

statistical treatment applied here.

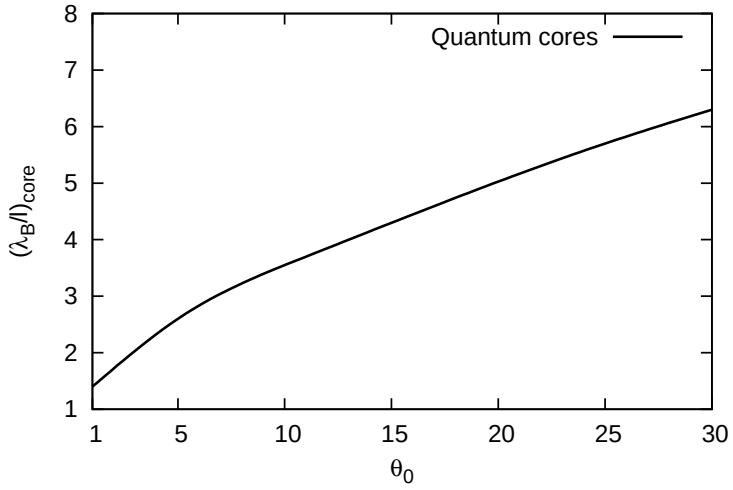

Figure I.2.: The less degenerate quantum cores in agreement with the halo observables (I.0.4) corresponds to $\theta_0 \approx 10$ ($\lambda_B \sim 3l_c$). These cores are the ones which achieve the largest sizes, of order $\sim$ kpc, and implying the lowest ino masses in the sub-keV region.

If we turn to the issue of an alternative interpretation to the black hole on SgrA*, we conclude that a compact degenerate core mass $M_c \sim 4 \times 10^6 M_\odot$ is definitely possible corresponding to an ino of $m \sim 10$ keV$/c^2$ (see Table K.1). However, the core radius of our configuration is larger by a factor $\sim 10^2$ than the one obtained with the closest observed star to Sgr A*, i.e. the S2 star Gillessen et al. (2009). We are currently studying how the introduction of additional interactions between the inos affects the mass and radius of the new dense quantum cores depending on the interaction adopted. This is analogous for instance to the case of neutron stars, where nuclear fermion interactions strongly influence the mass-radius relation (see, e.g., Lattimer and Prakash (2007)) . This may well make the mass and radius of this dark matter quantum core to fulfill the observational constraints imposed by the S2 star Argüelles et al. (2014).

We further compare and contrast in Fig. I.3 our theoretical curves in Fig. I.1 with observationally inferred ones. It is interesting that the quantum and relativistic treatment of the configurations considered here are characterized by the presence of central cored structures unlike the typical *cuspy* config-

urations obtained from a classic non-relativistic approximation, such as the ones of numerical N-body simulations in Navarro et al. (1997). This naturally leads to a solution to the well-known core-cusp discrepancy de Blok et al. (2001b). Such a difference between the ino's core and the cuspy NFW profile, as well as the possible black hole nature of the compact source in SgrA*, will certainly reactivate the development of observational campaigns in the near future. There the interesting possibility, in view of the BlackHoleCam Project based on the largest Very Long Baseline Interferometry (VLBI) array[1], to verify the general relativistic effects expected in the surroundings of the central compact source in SgrA*. Such effects depend on whether the source is modeled in terms of the RAR model presented here (with the possible inclusion of fermion interactions Argüelles et al. (2014)), or as a black hole. To compare and contrast these two alternatives is an observational challenge now clearly open.

Following the analysis developed here for a typical spiral, we have also considered two new different sets of physical dark matter halos: $r_h = 0.6$ kpc; $v_h = 13$ km/s; $M_h = 2 \times 10^7 M_\odot$ for typical dwarf spheroidal galaxies, e.g. Walker et al. (2009); and $r_h = 75$ kpc; $v_h = 345$ km/s; $M_h = 2 \times 10^{12} M_\odot$ for big spiral galaxies, as analyzed in Boyarsky et al. (2009a). For big spirals, $\lambda_B / l_c = 5.3$, while for typical dwarfs galaxies $\lambda_B / l_c = 4.1$, justifying the quantum treatment in both cases.

A remarkable outcome of the application of our model to such a wide range of representative dark halo galaxy types, from dwarfs to big spirals, is that *for the same* ino mass, $m \sim 10$ keV$/c^2$, we obtain respectively core masses $M_c \sim 10^4 M_\odot$ and radii $r_c \sim 10^{-1}$pc for dwarf galaxies, and core masses $M_c \sim 10^7 M_\odot$ and radii $r_c \sim 10^{-2}$pc for big spirals. This leads to a possible alternative to intermediate ($\sim 10^4 M_\odot$) and more massive ($\sim 10^{6-7} M_\odot$) black holes, thought to be hosted at the center of the galaxies.

We have obtained, out of first principles, a possible universal relation between the dark matter halos and the super massive dark central objects. For a fixed ino mass $m = 10$ keV$/c^2$, we found the M_c-M_h correlation law

$$\frac{M_c}{10^6 M_\odot} = 2.35 \left(\frac{M_h}{10^{11} M_\odot} \right)^{0.52}, \tag{I.0.5}$$

valid for core masses $\sim [10^4, 10^7]\, M_\odot$ (corresponding to dark matter halo

[1] http://horizon-magazine.eu/space

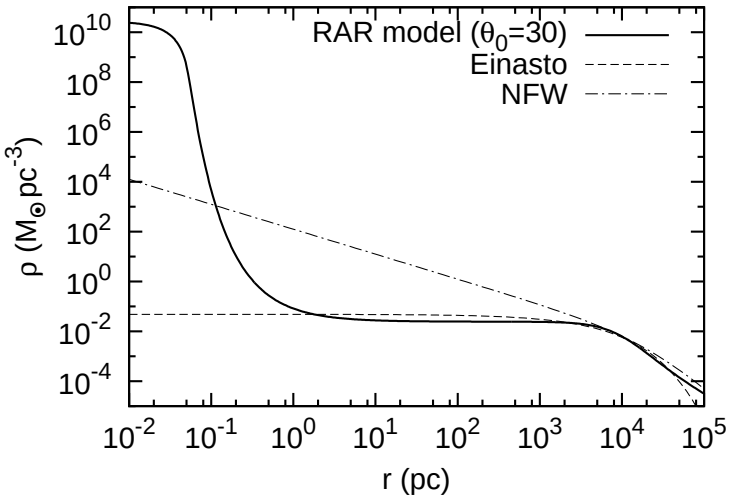

Figure I.3.: The cored behavior of the dark matter density profile from the Ruffini-Argüelles-Rueda (RAR) model is contrasted with the cuspy Navarro-Frenk-White (NFW) density profile Navarro et al. (1997), and with a cored-like Einasto profile Einasto (1965); Einasto and Haud (1989). The free parameters of the RAR model are fixed as $\beta_0 = 1.251 \times 10^{-7}$, $\theta_0 = 30$ and $m = 10.54$ keV$/c^2$. The corresponding free parameters in the NFW formula $\rho_{NFW}(r) = \rho_0 r_0/[r(1 + r/r_0)^2]$ are chosen as $\rho_0 = 5 \times 10^{-3} M_\odot$ pc^{-3} and $r_0 = 25$ kpc, and for the Einasto profile $\rho_E(r) = \rho_{-2} \exp\left[-2n(r/r_{-2})^{1/n} - 1\right]$, $\rho_{-2} = 2.4 \times 10^{-3} M_\odot$ pc^{-3}, $r_{-2} = 16.8$ kpc, and $n = 3/2$. In the last two models, the chosen free parameters are typical of spiral galaxies according to de Blok et al. (2008); Chemin et al. (2011).

masses $\sim [10^7, 10^{12}]\, M_\odot$). Regarding the observational relation between massive dark compact objects and bulge dispersion velocities in galaxies (the M_c-σ relation Ferrarese (2002b)), it can be combined with two observationally inferred relations such as the σ-V_c and the V_c-M_h correlations, where V_c is the observed halo circular velocity and M_h a typical halo mass. This was done in Ferrarese (2002a) to find, by transitivity, a new correlation between central mass concentrations and halo dark masses (M_c-M_h). Interestingly, such a correlation matches the one found above in Eq. (I.0.5) in the range $M_c = [10^6, 10^7]\, M_\odot$, without assuming the black hole hypothesis.

Such an approach of a core surrounded by a non-relativistic halo, is a key feature of the configurations presented in this Letter. It cannot however be extended to quantum cores with masses of $\sim 10^9 M_\odot$. Such core masses, observed in Active Galactic Nuclei (AGN), overcome the critical mass value for gravitational collapse $M_{cr} \sim M_{pl}^3/m^2$ for keV fermions, and therefore these cores have to be necessarily black holes Argüelles and Ruffini (2014). The characteristic signatures of such supermassive black-holes, including jets and X-ray emissions, are indeed missing from the observations of the much quiet SgrA* source, or the centers of dwarf galaxies.

In conclusion:

I) A consistent treatment of self-gravitating fermions within general relativity has been here introduced and solved with the boundary conditions appropriate to flat rotation curves observed in galactic halos of spiral and dwarf galaxies. A new structure has been identified: 1) a core governed by quantum statistics; 2) a velocity of rotation at the surface of this core which is bounded independently of the mass of the particle and remarkably close to the asymptotic rotation curve; 3) a semi-degenerate region leading to an asymptotic regime described by a pure Boltzmann distribution, consistent with the flat rotation curves observed in galaxies.

II) Our treatment is by construction different from the one of Tremaine and Gunn Tremaine and Gunn (1979). It is interesting to notice that their conclusions are reached by adopting the maximum phase-space density, $Q^h_{max} \sim \rho^h_0 m^{-4} \sigma_h^{-3}$, at the center of a halo described by a Maxwellian distribution, while in our model the maximum phase-space density is reached at the center of the dense quantum core described by Fermi-Dirac statistics, $Q^c_{max} \sim \rho^c_0 m^{-4} \sigma_c^{-3}$. An entire new family of solutions exists for larger values of central phase-space occupation numbers, always in agreement with the halo observables (see Fig. I.1). Now, since these phase-space values, by the

Liouville's theorem, can never exceed the maximum primordial phase-space density at decoupling, Q^d_{max}, we have $Q^{h,c}_{max} < Q^d_{max}$. Then, considering that all our quantum solutions satisfy $Q^c_{max} > Q^h_{max}$, it directly implies larger values of our ino mass with respect to the Tremaine and Gunn limit (I.0.1). As we have quantitatively shown, e.g. for the case of typical spiral galaxies, the two limits become comparable for our less degenerate ($\theta_0 \approx 10$) quantum cores in agreement with the used halo observables (I.0.4) .

III) For $m \sim 10\,\mathrm{keV}/c^2$ a universal relation between the mass of the core M_c and the mass of the halo M_h has been found. This universal relation applies in a vast region of galactic systems, ranging from dwarf to big spiral galaxies with core masses $\sim [10^4, 10^7]\, M_\odot$ (corresponding to dark matter halo masses $\sim [10^7, 10^{12}]\, M_\odot$).

IV) From the basic treatments here introduced, of bare self-gravitating fermions, we are currently examining the possibility to introduce new types of interactions Argüelles et al. (2014), including, for example, right-handed sterile neutrinos in the minimal standard model extension (see e.g. Boyarsky et al. (2009b)), as a viable candidate for the ino particles in our new scenario.

The inclusion of the interactions allows, for different central degeneracies, to reach higher compactness Argüelles et al. (2014). The relevance of the interactions in ultracold atomic collisions has been already shown in laboratory, for example, for (effective) Fermi gases, e.g. ^{6}Li, at temperatures of fractions of the Fermi energy. These systems can be studied in terms of a grand-canonical many-body Hamiltonian in second quantization, with a term accounting for fermion-fermion interaction Giorgini et al. (2008). This should allow to verify the possibility of the radius of the quantum core to become consistent with the observations of SgrA* Ghez et al. (2008); Gillessen et al. (2009).

J. Critical configurations for a system of semidegenerate fermions

J.1. INTRODUCTION

Systems of self-gravitating semidegenerate fermions in general relativity were studied in Ref. Gao et al. (1990) and more recently with applications to dark matter in galaxies in Ref. Argüelles et al. (2014). For a given central temperature parameter (β_0) in agreement with the corresponding observed halo circular velocity, lower bounds were shown to exist for the central degeneracy parameter (θ_0) and the particle mass ($m \gtrsim 0.4$ keV) above which the *observed* halo mass and radius are fulfilled. The solutions for the density profiles in this approach present a novel core-halo morphology composed of a quantum degenerate core followed by a low-degeneracy plateau until they reach the r^{-2} Boltzmannian region. This interesting overall morphology provides flat rotation curves in the outermost part of the galaxies, while the very dense degenerate cores arising at the center of the configurations provide a possible alternative to the central massive black holes paradigm (see Refs. Ruffini et al. (2013a) and Ruffini et al. (2014)).

The system of Einstein equations are written in a spherically-symmetric spacetime with the metric given by $g_{\mu\nu} = diag(e^{\nu}, -e^{\lambda}, -r^2, -r^2\sin^2\theta)$, where ν and λ depend only on the radial coordinate r, with the thermodynamic equilibrium conditions of Tolman (1930), and Klein (1949),

$$e^{\nu/2}T = const, \quad e^{\nu/2}(\mu + mc^2) = const,$$

where T is the temperature, μ the chemical potential, m the particle mass and c the speed of light. We then write the system of Einstein equations in the

following dimensionless way:

$$\frac{d\hat{M}}{d\hat{r}} = 4\pi\hat{r}^2\hat{\rho}\,, \tag{J.1.1}$$

$$\frac{d\theta}{d\hat{r}} = \frac{\beta_0(\theta-\theta_0)-1}{\beta_0}\,\frac{\hat{M}+4\pi\hat{P}\hat{r}^3}{\hat{r}^2(1-2\hat{M}/\hat{r})}\,, \tag{J.1.2}$$

$$\frac{d\nu}{d\hat{r}} = \frac{\hat{M}+4\pi\hat{P}\hat{r}^3}{\hat{r}^2(1-2\hat{M}/\hat{r})}\,, \tag{J.1.3}$$

$$\beta_0 = \beta(r)e^{\frac{\nu(r)-\nu_0}{2}}\,. \tag{J.1.4}$$

The variables of the system are the mass M, the metric factor ν , the temperature parameter $\beta = kT/(mc^2)$ and the degeneracy parameter $\theta = \mu/(kT)$. The dimensionless quantities are $\hat{r} = r/\chi$, $\hat{M} = GM/(c^2\chi)$, $\hat{\rho} = G\chi^2\rho/c^2$ and $\hat{P} = G\chi^2P/c^4$, with $\chi = 2\pi^{3/2}(\hbar/mc)(m_p/m)$ and $m_p = \sqrt{\hbar c/G}$ being the Planck mass. The mass density ρ and the pressure P are given by Fermi-Dirac statistics (see also Ref. Gao et al. (1990)).

This system is solved for a fixed particle mass m in the keV range with the initial conditions $M(0) = \nu(0) = 0$ for the given parameters $\theta_0 > 0$ (depending on the chosen central degeneracy) and β_0. We, thus, construct a sequence of different thermodynamic equilibrium configurations where each point in the sequence has a different central temperatures T_0 and central chemical potential μ_0, so that the given θ_0 condition is satisfied.

Defining the core radius r_c of each equilibrium system at the first maximum of its rotation curve or equivalently at the degeneracy transition point in which $\theta(r_c) = 0$, we represent the results obtained for each sequence in a central density (ρ_0) vs. core mass (M_c) diagram (see Fig. K.1). The critical core mass M_c^{cr} is shown to be reached at the maximum of each $M_c(\rho_0)$ curve.

It is important to emphasize that we are not interested in following the history of the equilibrium states of one specific system. Thus, the standard stability analysis done for compact stars or dense stellar cluster (see, e.g., Ref. Bisnovatyj-Kogan et al. (1993b)), which is based on the constancy of the entropy per nucleon (S/N) along the equilibrium sequence of a given configuration, does not apply here. Nonetheless, in computing the $M_c(\rho_0)$ curves in Fig. K.1, we have explored the full range of $\theta_0 > 1$ and $\beta_0 > 10^{-10}$ parameters (including the critical ones). Then, the equilibrium sequences with constant specific entropy (S/N), which differ from the ones with constant θ_0

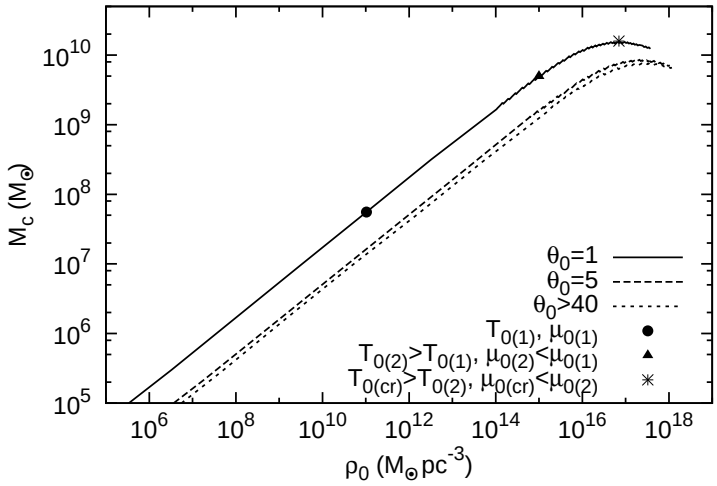

Figure J.1.: Different sequences of equilibrium configurations plotted in a central density (ρ_0) vs. core mass (M_c) diagram. The critical core mass is reached at the maximal value of M_c. Each sequence is built for selected values of $\theta_0 = \mu_0/kT_0$ and different values of T_0, with μ_0 varying accordingly.

considered here, necessarily must be contained within the full (T_0, μ_0) parameter space covered in Fig. K.1.

In Table 1, we show a set of central critical parameters of the model, together with the corresponding critical core masses, for a very wide range of fixed central degeneracy parameters θ_0 and $m = 8.5$ keV$/c^2$. Defining the halo radius of each configuration at the onset of the flat rotation curve, we show in Table 2 the critical halo magnitudes r_h^{cr}, M_h^{cr} and v_h^{cr} corresponding to the same set of critical parameters as given in Table 1. The results obtained in Tables 1 and 2 imply a marked division into two different families depending on the value of M_c^{cr}.

i) The first family: The critical mass has roughly a constant value $M_c^{cr} = 7.44 \times 10^9 M_\odot$. This family corresponds to large values of the central degeneracy ($\theta_0 \geq 40$), where the critical temperature parameter is always lower than $\beta_0^{cr} \lesssim 8 \times 10^{-3}$ and the critical chemical potential $\mu_0^{cr} \approx$ const. Physically, these highly-degenerate cores are entirely supported against gravitational collapse by the degeneracy pressure. In this case, the critical core mass is uniquely determined by the particle mass according the relation $M_c^{cr} \propto m_{pl}^3/m^2$ (see also Section III).

θ_0	β_0^{cr}	μ_0^{cr}/mc^2	$M_c^{cr}(M_\odot)$
1	6.45×10^{-2}	6.45×10^{-2}	1.59×10^{10}
5	2.23×10^{-2}	1.11×10^{-1}	7.91×10^{9}
40	8.33×10^{-3}	3.33×10^{-1}	7.44×10^{9}
55	6.06×10^{-3}	3.33×10^{-1}	7.44×10^{9}
100	3.33×10^{-3}	3.33×10^{-1}	7.44×10^{9}

Table J.1.: Critical temperature parameter and normalized chemical potential at the center of each different critical configuration for different fixed central degeneracies.

θ_0	$r_h^{cr}(pc)$	$M_h^{cr}/mc^2(M_\odot)$	$v_h^{cr}(km/s)$
1	4.4×10^{-1}	5.7×10^{11}	7.5×10^{4}
5	4.0×10^{-1}	4.3×10^{11}	6.2×10^{4}
40	4.3×10^{3}	1.1×10^{15}	3.3×10^{4}
55	2.9×10^{5}	6.0×10^{16}	2.9×10^{4}
100	2.0×10^{11}	2.3×10^{22}	2.2×10^{4}

Table J.2.: Critical halo magnitudes of different critical configurations for different fixed central degeneracies as given in Table 2.

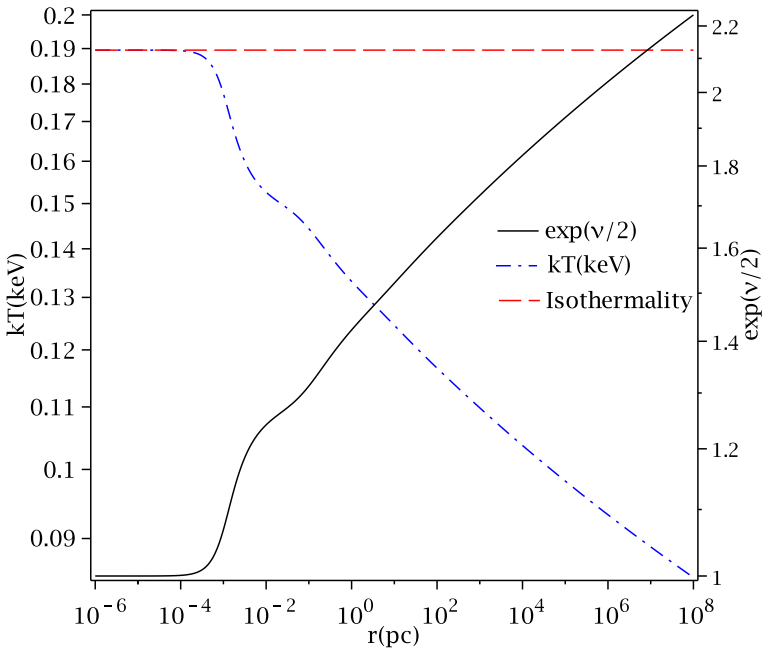

Figure J.2.: Critical temperature profile of the system (in keV) and critical metric for $\theta_0 = 5$ and $\beta_0^{cr} = 2.23 \times 10^{-2}$. The dashed line corresponds to the isothermality condition $Te^{\nu/2} = const$.

ii) The second family: The critical core mass increases from $M_c^{cr} = 7.44 \times 10^9 M_\odot$ to $M_c^{cr} \sim 10^{10} M_\odot$. This case corresponds to critical cores with a lower central degeneracy compared with the former family ($1 < \theta_0 < 40$). Here, the critical temperature parameter ($\beta_0 \sim 10^{-2}$) is closer to the relativistic region with respect to the first family. This result physically indicates that the thermal pressure term now makes an appreciable contribution to the total pressure, which supports the critical core against gravitational collapse. In this case, M_c^{cr} is completely determined by the particle mass m, the central temperature T_0^{cr} and the central chemical potential μ_0^{cr} (see Section III).
In Figs. (K.2) and (K.3), we show the critical metric factor $e^{\nu/2}$ and the critical temperature kT as function of the radius for the two different families mentioned above.

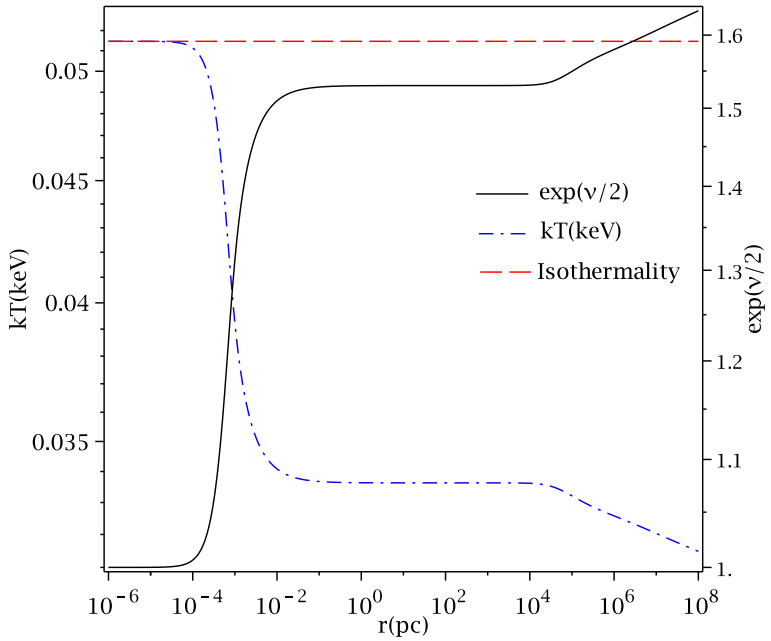

Figure J.3.: Critical temperature of the system (in keV) and critical metric for $\theta_0 = 55$ and $\beta_0^{cr} = 6.06 \times 10^{-3}$. The red line corresponds to the isothermality condition $Te^{\nu/2} = const$.

J.2. Astrophysical application

We will now attempt to use the critical configurations obtained before to explain the dark matter (DM) distribution in galactic halos and to provide an alternative candidate to the standard central-black-hole paradigm. From now on, we will use a fixed particle mass of m =8.5 keV$/c^2$, this choice being motivated by the fact that we want to deal with super-massive dark objects having critical core masses of the order $M_c^{cr} \propto m_{pl}^3/m^2 \sim 10^9 M_\odot$. In Figs. (K.4), (K.5) and (K.6), we show different critical density profiles, critical rotation curves and critical mass profiles, respectively, for a wide range of different central degeneracy parameters.

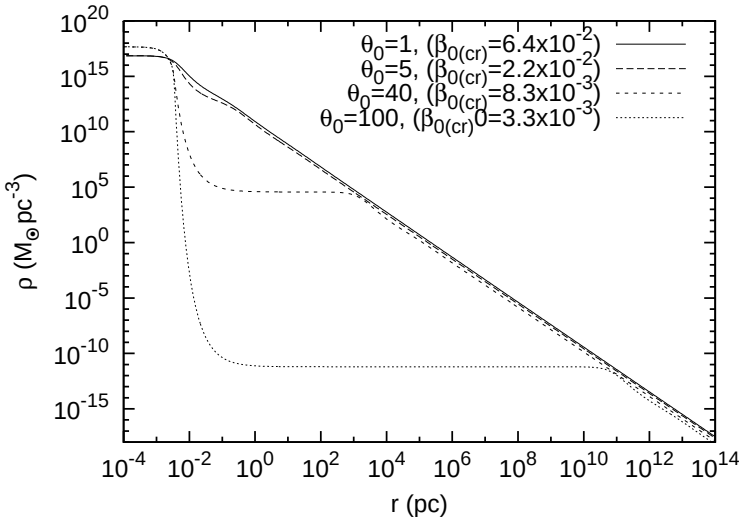

Figure J.4.: Critical density profiles for different values of θ_0 with the corresponding critical temperature parameters β_0^{cr}.

From Fig. K.5 and Table 2, we see that the critical configuration of self-gravitating fermions with central degeneracies ranging from $\theta_0 = 1$ (i.e., mainly thermal-pressure-supported cores) up to $\theta_0 = 100$ (i.e., mainly degeneracy-pressure-supported cores) have flat rotation velocities $v_h^{cr} \sim 10^4$ km/s. This value is well above any observed value. However, because larger values of θ_0 imply lower values for β_0^{cr}, as shown in Table 1, there is a point (at $\theta_0 \sim 10^6$ and so $\beta_0^{cr} \sim 10^{-7}$) where the *halo* rotation curves reach the typical observed value of $v_h^{cr} \sim 10^2$ km/s. Nonetheless, since even for $\theta_0 = 100$ we see (Fig. K.5) that the *halo* radius is larger than 10 Gpc for a total critical

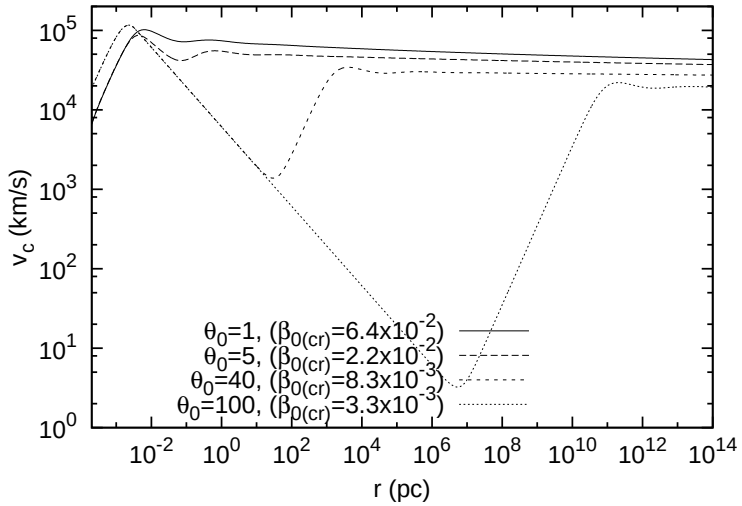

Figure J.5.: Critical rotation curves for different values of θ_0 as given in Fig. K.4. The high values of $v_c(r) \sim 10^4$ km/s in the flat parts of each curve are due to the high critical temperature parameter β_0^{cr}.

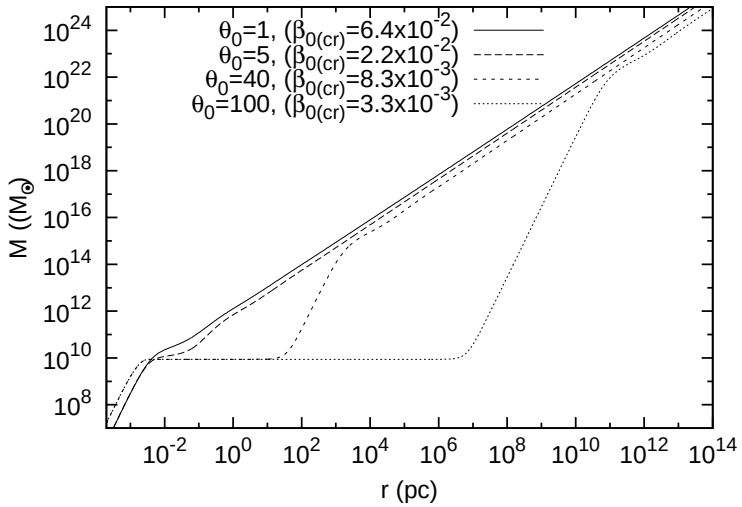

Figure J.6.: Critical mass profiles for different values of θ_0 as given in Figs. K.4–K.5.

mass larger than $10^{20}\ M_\odot$; this is again well above the value observed for any

galactic halo. We then conclude that any critical configuration belonging to this model is not able to reproduce the halo of galaxies.

Moving now to a completely different size scale, $r < 10^{-2}$ pc, even though at this scale the critical core masses are of the order of the more massive supermassive black holes in the center of Active Galactic Nuclei (AGN) (see Table 1), we find that the outer part of the system is either too large or has an extremely large velocity compared to observations, as explained before. Even inferred maser velocities for AGNs, with values up to 1000 km/s on a sub-parsec scale, are always below the critical velocity for any value of θ_0, as seen from Fig. K.5. We conclude, therefore, that critical configurations of semidegenerate self-gravitating fermions cannot be used to model AGNs.

J.3. An analytical expression for the critical mass

Finding an analytical formula for the critical mass to try to understand the physics behind it would be useful. For this, we will use the Newtonian hydrostatic equilibrium equation corresponding to the last stable configuration, where the pressure due to gravity is balanced by a highly relativistic semidegenerate Fermi gas:

$$\begin{aligned} P_g(r) &= P_T^{ur}(r), \\ \frac{GM(r)\rho(r)}{r} &\approx \frac{\mu^4}{12\pi^2(\hbar c)^3} + \frac{\mu^2(kT)^2}{6\sqrt{\pi}(\hbar c)^3}, \end{aligned} \tag{J.3.1}$$

where $P_T^{ur}(r)$ is an ultra-relativistic approximation of a highly-relativistic Fermi gas ($\mu \gg mc^2$), which has been expanded up to second order in the temperature around $\mu/kT \gg 1$ (see, e.g., Ref. Landau and Lifshitz (1980)). We have used in Eq. (K.4.1) the Fermi energy ($\epsilon_f = \mu$) with the rest energy substracted-off to be consistent with the theoretical formulation of our model. Considering that the density in the core is nearly constant (see Fig. K.4), i.e., $\rho = \rho_0^{cr} \approx const., \forall r \leq r_c^{cr}$, we can write the core radius as

$r_c^{cr} = (3M_c^{cr}/(4\pi\rho_0^{cr}))^{1/3}$. With this, we can rewrite Eq. (K.4.1) as follows:

$$\left(\frac{4\pi}{3}\right)^{1/3} G(M_c^{cr})^{2/3}(\rho_0^{cr})^{4/3} \approx \approx \frac{\mu^4}{12\pi^2(\hbar c)^3}\left(1+\frac{2\pi^2}{\theta_0^2}\right). \tag{J.3.2}$$

Finally, we write the central mass density as $\rho_0^{cr} \approx n^{ur}\, m$, where $n^{ur} = \mu^3/(3\pi^2(\hbar c)^3)$ is the number density of the ultra-relativistic particles. With this expression for ρ_0^{cr} in Eq. (J.3.2), we can directly give M_c^{cr} in terms of θ_0 as

$$M_c^{cr} \approx \frac{3\sqrt{\pi}}{16}\frac{M_{pl}^3}{m^2}\left(1+\frac{2\pi^2}{\theta_0^2}\right)^{3/2}. \tag{J.3.3}$$

From this equation, clearly for systems with high central degeneracy ($\theta_0 \gg \sqrt{2}\pi$), the critical core mass M_c^{cr} is independent of θ_0 and proportional to M_{pl}^3/m^2. However, for low values of the central degeneracy ($\theta_0 \sim \sqrt{2}\pi$), the second term in Eq. (K.4.2) starts to be relevant, showing finite temperature effects. In fact, using $\theta_0 = 40$, we have $M_c^{cr} = 7.62 \times 10^9\, M_\odot$, just a 2% difference with the numerical result of $7.44 \times 10^9\, M_\odot$. However, for $\theta_0 = 5$, we have $M_c^{cr} = 1.79 \times 10^{10}\, M_\odot$, almost a factor 2 above the numerical value of $7.91 \times 10^9\, M_\odot$ presented in Table 1. This shows that our approximation of an ultra-relativistic Fermi gas in Newtonian equilibrium breaks down, and that a fully relativistic treatment is needed.

K. Super massive black holes and dark matter halos in big elliptical galaxies

K.1. Introduction

The nature and role of the dark matter (DM) particle at galactic scales together with the intricate relation involving the spatial distribution of its density, mass-to-light ratios and the estimation of the very massive dark object mass, are yet unsolved issues of major importance in physics and astrophysics.

Observationally, the presence of DM halos is safely confirmed in the smallest and less luminous ($10^3 L_\odot \lesssim L \lesssim 10^7 L_\odot$) galactic systems, i.e.: dwarf galaxies, where DM contributes 90% or more to the total mass even much inside the half-light radius R_e. (see e.g. Strigari et al. (2008)). Instead, in the case of more luminous galaxies, both baryonic (i.e. stars) and dark matter contributes in comparable amounts to the total mass, being a big challenge to disentangle the gravitational effect of the DM component within $r \sim R_e$ (see e.g. Binney and Tremaine (2008) and refs. therein). In spiral galaxies the observation of extended HI regions in the disk structure provides an important and universal dynamical tracer which, through rotation curves analysis, has provided strong evidence for the existence of DM even up to several R_e (see e.g. de Blok et al. (2008)).

However, in the case of big elliptical and early-type galaxies, most of them containing super massive dark objects at their centers (see e.g. Gültekin et al. (2009)), there is no definitive evidence for the existence of DM halos. The low surface brightness beyond R_e makes it a hard task to obtain reliable spectra to determine dispersion velocities. Among the several methods available to prove the mass distribution beyond R_e in elliptical galaxies, such as integrated stellar light spectrum, globular cluster and planetary nebulae kinematics, diffuse X-ray observation or weak gravitational lensing; no evidence

for DM halos has been found even out to few R_e in many ellipticals by the use of kinematical methods (Gerhard et al. (2001); Romanowsky et al. (2003)). Meanwhile, by using X-ray observations in an small sample of nearby ellipticals, as for example in Humphrey et al. (2006) , a clear evidence for considerable amounts of DM at radii $r \sim 10R_e$ was given. In any case, the more interesting constraints on DM in early-type galaxies are restricted to the more massive systems, which are placed near the center of group or clusters. This implies to be a difficult task to confirm whether the existence of extensive halos are an inherent property of the galaxy itself, or whether corresponds to the group-scale (see e.g. Binney and Tremaine (2008) chapter 4.9.2).

On theoretical and numerical grounds, the paradigm regarding the nature and spatial distribution of the DM particle in large and small distance-scales is centered in Newtonian N-body simulations within Lambda Cold Dark Matter (ΛCDM) cosmologies Navarro et al. (1997, 2004b) , being the beyond Standard Model (SM) elementary particle WIMP (Weakly Interacting Massive Particles) the preferred DM candidate. Nonetheless, despite the good agreement of this model with the large scale structure of the Universe, some subtle problems remains at galactic scales such as the core-cusp discrepancy and the lost satellites problem (see e.g. Munshi et al. (2013)).

An alternative and very promising beyond SM particle which has received increasing attention in cosmology and structure formation in the last decade, is the right handed sterile neutrino with masses of $\sim$ keV (see e.g. Shi and Fuller (1999); Asaka et al. (2005); Stasielak et al. (2007)) . Moreover, in Lovell et al. (2012) (see also refs. therein), Warm Dark Matter (WDM) halos has been obtained from numerical simulations solving the discrepancies which arises at galactic scales in the CDM paradigm, being again the sterile neutrino a plausible DM candidate.

Continuing on theoretical grounds and from a different and complementary perspective, the problem of modeling the distribution of dark matter in galaxies in terms of equilibrium configurations of collisionless self-gravitating fermionic particles has already been considered in Ruffini and Stella (1983) . More recently in Argüelles et al. (2014); Siutsou et al. (2014); Ruffini et al. (2014) , this approach was developed in a fully relativistic treatment with applications to dark matter in normal galaxies being the spin $1/2$ fermion with masses $m \sim$few keV the preferred DM candidate in excellent agreement with halo observations (see e.g. Siutsou et al. (2014)). Again the sterile neutrino appears as an appealing candidate. An interesting characteristic in the density profile solutions of this kind of models

with $m \sim 10keV$, is that they present a novel core-halo morphology composed by: i) a compact degenerate core of constant density at sub-parsec scales governed by quantum statistics (i.e. Pauli principle); ii) an intermediate region with a sharply decreasing density distribution followed by an extended plateau; iii) a decreasing $\rho \propto r^{-2}$ leading to flat rotation curves fulfilling classical Boltzmann statistics. In Ruffini et al. (2014), and always for $m \sim 10keV$, using observations from typical dwarf galaxies up to typical big spirals allowing for DM halo characteristics, it is clearly shown how the compact core described above in i) may work as an alternative to intermediate ($M_c \sim 10^4 M_\odot$) and super massive Black Holes (BH) (up to $M_c \sim 10^7 M_\odot$) at their centers in simultaneous compatibility with each observed DM halo. It is then further shown in Ruffini et al. (2014) how, out of first principles, a possible universal correlation between the DM halos and the massive dark objects arises for $m = 10keV$. Interestingly, a very similar correlation law to the one theoretically found in Ruffini et al. (2014) in the range $M_c \in (10^6, 10^7) M_\odot$ (with correspondent halo masses M_h from $\sim 10^{11} M_\odot$ up to $\sim 10^{12} M_\odot$), has been found from observations in Ferrarese (2002a), relating the dark halo masses to central mass concentrations, these last however identified by Ferrarese as black hole masses.

In this essay we present a detailed analysis of the above sketched model involving full Fermi-Dirac statistics, in an extreme relativistic regime which will allow us to deal with the most massive central dark objects of $M_c \sim 10^9 M_\odot$ at miliparsec scales. In this context, we present the density profiles and rotation curves for a fermion mass $m \sim 10keV$, when the compact cores in all the solutions are very near Oppenheimer-Volkoff limit. Clearly, this approach makes the use of a General Relativistic treatment to be mandatory. In exploring the full range of the free model parameters such as temperature and degeneracy, we conclude that if a super massive dark object of $M_c \sim 10^9 M_\odot$ is formed at the center, no astrophysical DM halo structure should be present simultaneously in that system. A discussion to this respect in relation with observations and formation history is given in the third section.

K.2. Theoretical Framework

The system of Einstein equations are written in a spherically symmetric space-time metric $g_{\mu\nu} = diag(e^\nu, -e^\lambda, -r^2, -r^2 \sin^2\theta)$, where ν and λ depend only on the radial coordinate r, together with the thermodynamic equilibrium

conditions of Tolman (1930) , and Klein (1949) ,

$$e^{\nu/2}T = const., \quad e^{\nu/2}(\mu + mc^2) = const,$$

where T is the temperature, μ the chemical potential, m the particle mass and c the speed of light. We then write the system of Einstein equations in the following dimensionless way, following Gao et al. (1990) and Ruffini et al. (2013a) ,

$$\frac{d\hat{M}}{d\hat{r}} = 4\pi\hat{r}^2\hat{\rho} \tag{K.2.1}$$

$$\frac{d\theta}{d\hat{r}} = \frac{\beta_0(\theta-\theta_0)-1}{\beta_0}\frac{\hat{M}+4\pi\hat{P}\hat{r}^3}{\hat{r}^2(1-2\hat{M}/\hat{r})} \tag{K.2.2}$$

$$\frac{d\nu}{d\hat{r}} = \frac{\hat{M}+4\pi\hat{P}\hat{r}^3}{\hat{r}^2(1-2\hat{M}/\hat{r})} \tag{K.2.3}$$

$$\beta_0 = \beta(r)e^{\frac{\nu(r)-\nu_0}{2}}. \tag{K.2.4}$$

The variables of the system are the mass M, the metric factor ν , the temperature parameter $\beta = kT/(mc^2)$ and the degeneracy parameter $\theta = \mu/(kT)$. The dimensionless quantities are defined as: $\hat{r} = r/\chi$, $\hat{M} = GM/(c^2\chi)$, $\hat{\rho} = G\chi^2\rho/c^2$ and $\hat{P} = G\chi^2P/c^4$, with $\chi = 2\pi^{3/2}(\hbar/mc)(M_p/m)$ and $M_p = \sqrt{\hbar c/G}$ the Planck mass. The mass density ρ and pressure P are given by Fermi-Dirac statistics (with the particle helicity $g = 2$):

$$\rho = m\frac{2}{h^3}\int f(p)\left[1+\frac{\epsilon(p)}{mc^2}\right]d^3p, \tag{K.2.5}$$

$$P = \frac{1}{3}\frac{2}{h^3}\int f(p)\left[1+\frac{\epsilon(p)}{mc^2}\right]^{-1}\left[1+\frac{\epsilon(p)}{2mc^2}\right]\epsilon\, d^3p, \tag{K.2.6}$$

where the integration is extended over all the momentum space and $f(p) = (\exp[(\epsilon(p)-\mu)/(kT)]+1)^{-1}$. Here $\epsilon(p) = \sqrt{c^2p^2+m^2c^4}-mc^2$ is the particle kinetic energy, μ the chemical potential with the particle rest-energy subtracted off. We do not include the presence of anti-fermions, i.e. we consider temperatures that always satisfy $T < mc^2/k$.

We want to further emphasize the central role of the Fermionic quantum satistics in the model, by recalling the necessity of the Pauli principle to form

the central degenerate massive compact objects, mentioned above.

This system is solved for a fixed particle mass m in the keV range, with initial conditions $M(0) = \nu(0) = 0$, and given parameters $\theta_0 > 0$ (depending on the chosen central degeneracy), and β_0. We thus construct a sequence of different thermodynamic equilibrium configurations where each point in the sequence has different central temperatures T_0 and central chemical potential μ_0, so that satisfy the θ_0 fixed condition.

Defining the core radius r_c of each equilibrium system at the first maximum of its rotation curve, we represent the results obtained for each sequence in a central density (ρ_0) vs. core mass (M_c) diagram (see Fig.K.1). It is shown that the critical core mass M_c^{cr} is reached at the maximum of each $M_c(\rho_0)$ curve.

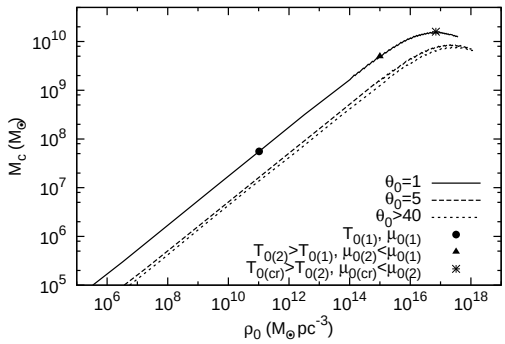

Figure K.1.: Different sequences of equilibrium configurations plotted in a central density (ρ_0) Vs. core mass (M_c) diagram. The critical core mass is reached at the maximal value of M_c. Each sequence is built for selected values of $\theta_0 = \mu_0/kT_0$ and different values of T_0, μ_0 varying accordingly.

It is important to emphasize that the method followed here to define the critical points along each family of thermodynamic equilibrium configurations, fulfills the *turning point* definition given in Schiffrin and Wald (2014) , which allows them to formally demonstrate Sorkin's theorem Sorkin (1981) showing the existence of a thermodynamic instability on one side of the turning point [1].

[1] In reality, to properly implement the formal concept of *turning point* as used for example in Schiffrin and Wald (2014) , the *total* mass of the system M_t (previous choice of a cut-off in the momentum space at i.e. $r_t \sim 10 r_h$ to define it) should be used in the central density (ρ_0) Vs. mass (M) diagram, instead of the core mass M_c. Nonetheless, considering that

In Table I we show a set of central critical parameters of the model together with the correspondent critical core masses, for a very wide range of fixed central degeneracy parameters θ_0 and particle mass $m = 8.5\ \mathrm{keV}/c^2$.

Table K.1.: Critical temperature parameter and normalized chemical potential at the center of each different critical configuration, for different fixed central degeneracies.

θ_0	β_0^{cr}	μ_0^{cr}/mc^2	$M_c^{cr}(M_\odot)$
1	6.45×10^{-2}	6.45×10^{-2}	1.59×10^{10}
5	2.23×10^{-2}	1.11×10^{-1}	7.91×10^{9}
40	8.33×10^{-3}	3.33×10^{-1}	7.44×10^{9}
55	6.06×10^{-3}	3.33×10^{-1}	7.44×10^{9}
100	3.33×10^{-3}	3.33×10^{-1}	7.44×10^{9}

Defining the halo radius of each configuration at the onset of the flat rotation curve, we show in Table II the critical halo magnitudes r_h^{cr}, M_h^{cr} and v_h^{cr} corresponding to the same set of critical parameters as given in Table I.

Table K.2.: Critical halo magnitudes of different critical configurations, for different fixed central degeneracies as given in Table I.

θ_0	r_h^{cr} (pc)	M_h^{cr}/mc^2 $(M_\odot)$	v_h^{cr} (km/s)
1	4.4×10^{-1}	5.7×10^{11}	7.5×10^{4}
5	4.0×10^{-1}	4.3×10^{11}	6.2×10^{4}
40	4.3×10^{3}	1.1×10^{15}	3.3×10^{4}
55	2.9×10^{5}	6.0×10^{16}	2.9×10^{4}
100	2.0×10^{11}	2.3×10^{22}	2.2×10^{4}

The results obtained in Tables I and II imply a marked division in two different families depending on the value of M_c^{cr}.

i) The first family: the critical mass has roughly a constant value $M_c^{cr} = 7.44 \times 10^9 M_\odot$. This family corresponds to large values of the central degeneracy ($\theta_0 \geq 40$), where the critical temperature parameter is always lower

in fully degenerate systems the critical masses M_c^{cr} are basically equal to the OV mass, it should imply that the extended and diluted halo plays no relevant role in the physics near the critical point, in some analogy to the case of Super-Nova core collapse where only the fully degenerate core is considered in the process.

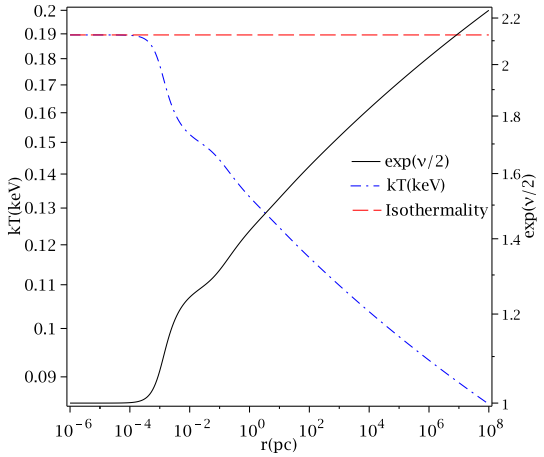

Figure K.2.: The critical temperature profile of the system (in keV) and the critical metric, for $\theta_0 = 5$ and $\beta_0^{cr} = 2.23 \times 10^{-2}$. The dashed line corresponds to the isothermality condition, $Te^{\nu/2} = const$.

than $\beta_0^{cr} \lesssim 8 \times 10^{-3}$ and the critical chemical potential $\mu_0^{cr} \approx$ const. Physically, these highly degenerate cores are entirely supported against gravitational collapse by the degeneracy pressure. In this case the critical core mass is uniquely determined by the particle mass according the relation $M_c^{cr} \propto M_{pl}^3/m^2$ (see also last section).

ii) The second family: the critical core mass increases from $M_c^{cr} = 7.44 \times 10^9 M_\odot$ up to $M_c^{cr} \sim 10^{10} M_\odot$. This case corresponds to critical cores with a lower central degeneracy compared with the former family ($1 < \theta_0 < 40$). Here the critical temperature parameter ($\beta_0 \sim 10^{-2}$), is closer to the relativistic regime with respect to the first family. This result physically indicates that the thermal pressure term has now an appreciable contribution to the total pressure, which supports the critical core against gravitational collapse. In this case M_c^{cr} is completely determined by the particle mass m, the central temperature T_0^{cr} and the central chemical potential μ_0^{cr} (see last section).

In Figs. (K.2) and (K.3) we show a critical metric factor $e^{\nu/2}$ and a critical temperature kT as a function of the radius for the two different families mentioned above.

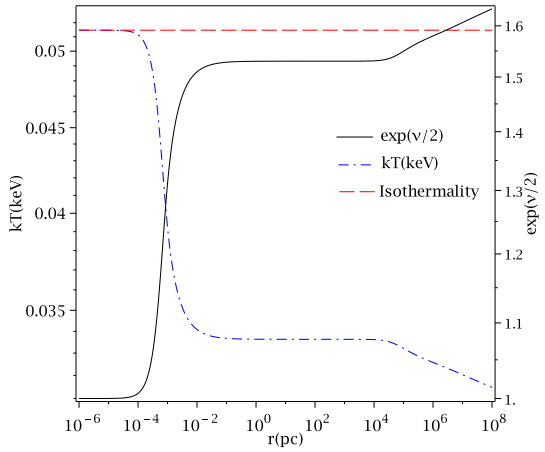

Figure K.3.: The critical temperature of the system (in keV) and the critical metric, for $\theta_0 = 55$ and $\beta_0^{cr} = 6.06 \times 10^{-3}$. The dashed line corresponds to the isothermality condition, $Te^{\nu/2} = const$.

K.3. Astrophysical Application and Discussion

We will now attempt to use the critical configurations obtained before to explain the DM distribution in big galactic halos, as well as providing an alternative candidate to the standard central black hole paradigm. From now on, we will use a fixed particle mass of m =8.5 keV$/c^2$, being this choice motivated by the fact we want to deal with super massive dark objects having critical core masses of the order $M_c^{cr} \propto m_{pl}^3/m^2 \sim 10^9 M_\odot$. Moreover, such a relativistic object would have an OV radius R_{OV} very near the Schwarschild radius R_s ($R_{OV} \sim 3R_s$), and then practically indistinguishable from a BH of the same mass.

In Figs. (K.4), (K.5) and (K.6) we show different critical density profiles, critical rotation curves and critical mass profiles respectively, for a wide range of different central degeneracy parameters.

From Fig. K.5 and Table II we see that critical configuration of self-gravitating fermions with central degeneracies ranging from $\theta_0 = 1$ (i.e. mainly thermal pressure supported cores) up to $\theta_0 = 100$ (i.e. mainly degeneracy pressure supported cores), have flat rotation velocities $v_h^{cr} \sim 10^4$ km/s. Even if for $\theta_0 \sim 50$ the halo sizes could match observations, the halo masses are well above any observed value and so the circular velocities; further implying that none of these mathematical solutions are compatible with

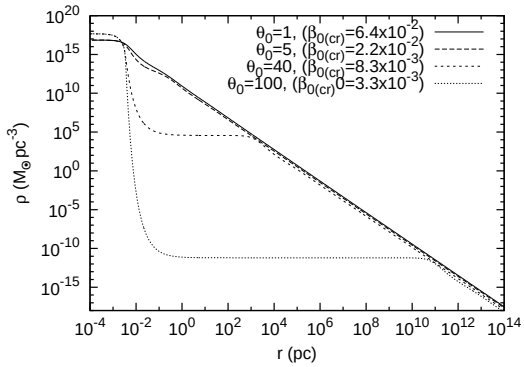

Figure K.4.: Critical density profiles for different values of θ_0 with the correspondent critical temperature parameters β_0^{cr}.

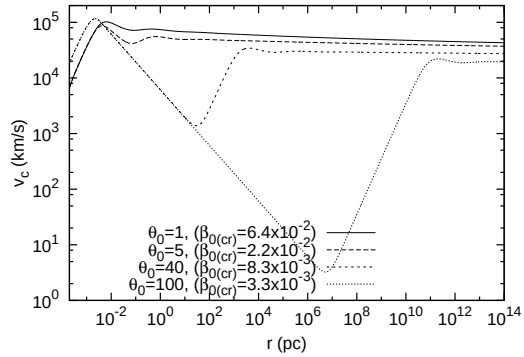

Figure K.5.: Critical rotation curves for different values of θ_0 as given in Fig. K.4. To note the high values of $v_c(r) \sim 10^4$ km/s in the flat parts of each curve due to the high critical temperature parameters β_0^{cr}.

any observable astrophysical systems. However, since larger values of θ_0 imply lower values for β_0^{cr}, as shown in Table I, there is a point (at $\theta_0 \sim 10^6$ and so $\beta_0^{cr} \sim 10^{-7}$) where the *halo* rotation curves reach the typical observed values as in spiral or elliptical galaxies of $v_h^{cr} \sim 10^2$ km/s [2]. Nonetheless, since already at $\theta_0 \gtrsim 80$ (see for example $\theta_0 = 100$ in Fig. K.4) the plateau region of the density profile is lower than the mean DM density of the Uni-

[2]These values of rotation curves were used in the very low (spetial) relativistic regime version of this model (i.e. $\theta_0 \sim 10^1$), as presented in Argüelles et al. (2014); Siutsou et al. (2014); Ruffini et al. (2014) , and in that case leading to the correct halo masses and sizes in galaxies.

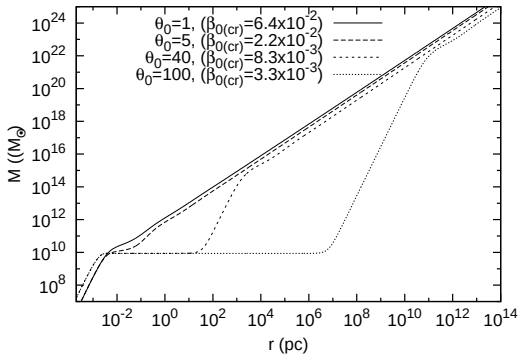

Figure K.6.: Critical mass profiles for different values of θ_0 as given in Figs. K.4–K.5.

verse ($\rho_{uni} \sim 3H_0^2/(4\pi G)$), then higher central degeneracies will imply even more diluted halos (i.e. already disappeared), never reaching typical flat rotation curves at 10^{1-2} Kpc halo distance-scales. Thus, the critical configurations here analyzed in the fully degenerate regime $\theta_0 \gg 1$, should only consist on a central super-massive compact objects of $M_c^{cr} \sim 10^9 M_\odot$ consisting on DM particles of $m \sim 10$keV.

In the light of the present analysis we then conclude that there is no critical core-halo configuration of self-gravitating DM fermions, able to explain both the most super-massive dark object at the center together with an outer DM halo simultaneously.

The concept of simultaneous co-existence of super-massive dark objects and DM halos at some cosmological epoch z is of central importance to better understand the structure growth, galaxy formation history and evolution. An important observational result aiming in these directions has been reported in Cassata et al. (2011) . In that work there is clear evidence for evolution of early-type galaxies evolving from $z \sim 2.5$ (consistently studied only in terms of light profiles) up to now ($z \sim 0$) enlarging their sizes and masses (lowering in density), which imply necessarily subsequent gathering of matter from larger-scale environments in their complex evolutionary history (probably in the form of dark and/or baryionic matter). Thus, contrasting the results obtained in this work with observational results for big ellipticals as the ones already recalled in Cassata et al. (2011) and Gerhard et al. (2001); Romanowsky et al. (2003); Humphrey et al. (2006) , but also in Gebhardt et al. (2011) for the more relevant case of the giant elliptical M87 with the detected

super-massive dark object of $M_c \sim 7 \times 10^9 M_\odot$; could well imply that even if there is clear evidence in some cases of co-existence of central dark massive objects and dark halos at $z \sim 0$, this could not be the case at early stages i.e.$z \sim 3$. The connection between the formation of super-massive compact dark objects at early epochs, the relation with the host halo and possible subsequent accretion form their larger-scale environments are still important open questions.

K.4. An Analytical Expression for the Critical Mass

What one may find very insightful is to derive an analytical (approximate) formula for the critical mass, so that one can then adventure to explore and understand the subjacent physics of it. For this we will use the Newtonian hydrostatic equilibrium equation corresponding to the last stable configuration, where the pressure due to gravity is balanced by a high relativistic semi-degenerate Fermi gas :

$$\begin{aligned} P_g(r) &= P_T^{ur}(r), \\ \frac{GM(r)\rho(r)}{r} &\approx \frac{\mu^4}{12\pi^2(\hbar c)^3} + \frac{\mu^2(kT)^2}{6\sqrt{\pi}(\hbar c)^3}, \end{aligned} \tag{K.4.1}$$

where $P_T^{ur}(r)$ is the ultra relativistic approximation of a highly relativistic Fermi gas ($\mu \gg mc^2$), which has been expanded up to second order in temperature around $\mu/kT \gg 1$ (see e.g. Landau and Lifshitz (1980)). We have used in K.4.1 the fermi energy ($\epsilon_f = \mu$) with the rest energy substracted-off in consistency with the theoretical formulation of our model.

Then, after constant density considerations for $r \lesssim r_c$ in the ultra-relativistic approximation here adopted, we get,

$$M_c^{cr} \approx \frac{3\sqrt{\pi}}{16} \frac{M_{pl}^3}{m^2} \left(1 + \frac{2\pi^2}{\theta_0^2}\right)^{3/2}. \tag{K.4.2}$$

It is clear from this equation that for high central degenerate systems ($\theta_0 \gg \sqrt{2}\pi$), the critical core mass M_c^{cr} is independent of θ_0 and then proportional to M_{pl}^3/m^2. However, for low values of the central degeneracy ($\theta_0 \sim \sqrt{2}\pi$) the second term in (K.4.2) starts to be relevant, showing the finite temperature effects. In fact, using $\theta_0 = 40$, we have $M_c^{cr} = 7.62 \times 10^9\, M_\odot$, just a 2%

difference with the numerical result of $7.44 \times 10^9\, M_\odot$. However, for $\theta_0 = 5$ we have $M_c^{cr} = 1.79 \times 10^{10}\, M_\odot$, almost a factor 2 above the numerical value of $7.91 \times 10^9\, M_\odot$ obtained in Table I. This shows that our approximation of an ultra-relativistic fermi gas in newtonian equilibrium breaks down and a fully relativistic treatment is needed.

L. Dark Einstein clusters within the S2 orbit in SgrA*

In 1939 Einstein [Einstein (1939)] provided a model of self-gravitating masses, each moving along geodesic circular orbits under the influence of the gravitational field of the rest of the particle in the system. This model allowed him to argue that 'Schwarzschild singularities' do not exist in physical reality because a cluster with a given number of masses cannot be arbitrarily concentrated. This is due to the fact that otherwise the particles constituting the cluster would reach the speed of light. Of course, this model can actually only be considered as an interesting possibility to try to provide a counterexample of a singularity within Einstein's theory of gravity, since Black Holes are a physical reality within the theory of General Relativity.

The aim of this paper is to model the central (sub-milliparsec) region of our galaxy in terms of a dark 'Einstein Cluster' (EC) in order to provide an alternative to the Super Massive Black Hole (SMBH) of mass $M = 4.4 \times 10^6 M_\odot$ thought to be hosted at very center [Ghez et al. (2008); Gillessen et al. (2009)]. A dark EC is understood as an EC composed by dark matter particles of mass m (regardless of its nature), and therefore no contribution to the pressure in form of radiation is assured as the cluster shrinks till relativistic regimes. The model is based on the assumption of a constant density distribution harbored inside the peri-center of the S2 star ($r_{p(S2)}$), the closest to SgrA* as observed in [Gillessen et al. (2009)]. We will first analyze the stability condition in the specific case of a regular and relativistic energy density EC, contained marginally inside the S2 peri-center. Secondly, and for an EC with fixed particle number $\mathcal{N}$, we will explicitly show through the R vs. M relation, and for particle velocities ranging from zero up to the speed of light, up to which point an EC can be shrank before loosing its global stability.

The full theoretical formalism of 'Einstein Clusters' and their different stability analysis has been extensively studied in [Zapolsky (1968); Gilbert (1954); Hogan (1973); Florides (1974); Comer and Katz (1993); Cocco and Ruffini (1997); Böhmer and Harko (2007); Geralico et al. (2012)].

We give in next a short summary of the most important outcomes of this theory, pointing out the principal formulas which will allow us to deal with the astrophysical application object of this work. Thus, consider a static spherically symmetric distribution of particles all with rest mass m which are moving along circular geodetic orbits about the center of symmetry. The associated line element ds^2 is written in terms of a Schwarzschild metric of the form $g_{\mu\nu} = diag(-e^{\nu}, e^{\lambda}, r^2, r^2 \sin^2\theta)$, where ν and λ depend only on the radial coordinate r. From now and on we will work in the geometric unit system ($G = c = 1$).

The stress-energy tensor in the laboratory frame is assumed to take the form

$$T^{\mu\nu} = m\, n_0\, U^{\mu} U^{\nu}\,, \qquad U = \gamma[e_{\hat{t}} + v^{\hat{\theta}} e_{\hat{\theta}} + v^{\hat{\phi}} e_{\hat{\phi}}]\,, \tag{L.0.1}$$

which is just the Einstein's ansatz [Einstein (1939)] (or a dust-like ansatz). n_0 is the proper particle number density (i.e. defined at rest w.r.t a coordinate system of special relativity), U is the particle 4-velocity satisfying the circular geodetic equations in the laboratory frame with $v^{\hat{\theta}}$ and $v^{\hat{\phi}}$ the linear velocities along the angular directions, $\gamma = (1 - v^2)^{-1/2}$ ($v^2 = \delta_{\theta\phi} v^{\theta} v^{\phi}$), and the unitary vectors introduced in U corresponds to the following orthonormal frame (adapted to the static observers)

$$e_{\hat{t}} = e^{-\nu/2}\partial_t\,, \qquad e_{\hat{r}} = e^{-\lambda/2}\partial_r\,, \qquad e_{\hat{\theta}} = \frac{1}{r}\partial_\theta\,, \qquad e_{\hat{\phi}} = \frac{1}{r^2 \sin\theta}\partial_\phi\,. \tag{L.0.2}$$

In the laboratory frame, and after applying the killing vector formalism to this specific spacetime (see also [Geralico et al. (2012)]) naturally appears the two constants of motion associated with each trajectory, the energy E and the angular momentum L which reads

$$E = m\gamma\, e^{\nu/2}, \qquad L^2 = L_{\theta}^2 + L_{\phi}^2/\sin^2\theta = m^2\gamma^2 r^2 v^2. \tag{L.0.3}$$

The angular momentum formula in (L.0.3) together with the definition of γ directly implies $\gamma = (1 + \tilde{L}^2/r^2)^{1/2}$ which will be very useful in what follows, with $\tilde{L} = L/m$.

By writing the conserved L^2 in terms of each angular component $L_{\theta} = m\gamma r v_{\theta}$ and $L_{\phi} = m\gamma r v_{\phi} \sin\theta$ as done in (L.0.3), implies the following relation $1 = (L_{\theta}/L)^2 + (L_{\phi}/(L\sin^2\theta))^2$. This last equation further implies that the possible values of L_{θ}/L and $L_{\phi}/(L\sin^2\theta)$ lie on a circle of unit radius, and

then each angular component can be written in terms of an angle α respect to the $e_{\hat{\theta}}$-axis. This decomposition allow us to make an average of the angular momentum components in the $e_{\hat{\theta}} - e_{\hat{\phi}}$ plane (i.e. around each orbit with $\alpha \in [0, 2\pi]$), as originally proposed by Einstein [Einstein (1939)]. The averaged variables reads[1].

$$\langle L_\theta \rangle = \langle L_\phi \rangle = 0, \qquad \langle L_\theta^2 \rangle = \langle L_\phi^2 / \sin^2\theta \rangle = L^2/2\,. \tag{L.0.4}$$

The above averaging allows to express the averaged stress-energy components without any angular dependence, and reads

$$\langle T^t{}_t \rangle = -mn_0 \left(1 + \frac{\tilde{L}^2}{r^2}\right) \equiv -\rho\,, \qquad \langle T^\theta{}_\theta \rangle = \langle T^\phi{}_\phi \rangle = \frac{mn_0}{2}\frac{\tilde{L}^2}{r^2} \equiv p_t\,, \tag{L.0.5}$$

where ρ is the energy density of the system and p_t the tangential pressure. It can be easily verified that the divergence of the stress-energy tensor vanishes identically.

The relevant Einstein equations are

$$\frac{1}{r^2}[r(1 - e^{-\lambda})]' = 8\pi\rho\,, \tag{L.0.6}$$

$$\nu' = \frac{1}{r}(e^\lambda - 1)\,, \tag{L.0.7}$$

$$\frac{e^{-\lambda}}{2}\left[\nu'' + \frac{\nu'^2}{2} + \frac{\nu' - \lambda'}{r} - \frac{\nu'\lambda'}{2}\right] = 8\pi p_t\,, \tag{L.0.8}$$

where a prime denotes differentiation with respect to r. By using the standard definition of the mass function in terms of λ, $e^\lambda = (1 - 2M(r)/r)^{-1}$, the system (L.0.6–L.0.8) is solved to give:

$$M(r) = 4\pi \int_0^r \rho r^2 dr, \qquad e^\nu = (1 - 2M/R)e^{-2\Phi(r)}\,, \tag{L.0.9}$$

where

$$\Phi(r) = \int_r^R \frac{v_k^2}{r} dr, \qquad v_k^2 = \frac{M(r)}{r - 2M(r)}, \qquad \tilde{L} = \gamma\, v_k\, r \tag{L.0.10}$$

[1]The average or mean value is defined by $2\pi\langle L_a(\alpha)\rangle = \int_0^{2\pi} L_a(\alpha)d\alpha$, with a either θ or ϕ.

where v_k is the Keplerian speed. Thus, in order to completely solve the problem we have to provide a the energy density $\rho(r)$ (or equivalently the mass profile).

Another needed relevant quantity is the total particle number $\mathcal{N}$. It can be easily shown that the averaged 4-current $\langle J^\mu \rangle = -n_0 \langle U^\mu \rangle$ is divergence-free. The associated conserved particle number is thus given byMisner and Sharp (1964)

$$\mathcal{N} = \int_\Sigma \langle J^\mu \rangle \, d\Sigma_\mu \, , \tag{L.0.11}$$

where Σ denotes a spacelike hypersurface with infinitesimal element $d\Sigma^\nu = n^\nu d\Sigma$ and unit timelike normal n. By choosing Σ to be a $t = \text{const}$ hypersurface with unit normal $n = e_{\hat{t}}$ and $d\Sigma = e^{\lambda/2} r^2 \sin\theta \, dr \, d\theta \, d\phi$, Eq. (L.0.11) gives

$$\mathcal{N} = 4\pi \int_0^R n_0(r) \gamma e^{\lambda/2} r^2 \, dr \, . \tag{L.0.12}$$

A constant energy density $\rho = 3M/(4\pi R^3)$ implies a radial distribution mass $M(r) = Mr^3/R^3$, and consequently through second and third Eqs. in (L.0.10), an angular momentum per unit mass $\tilde{L}$ with the corresponding number distribution of the particles mn_0 given by

$$\tilde{L} = \sqrt{\frac{M}{R}} \frac{r^2}{R} \left(1 - \frac{3Mr^2}{R^3} \right)^{-1/2} , \qquad mn_0 = \frac{3M}{4\pi R^3} \frac{R^3 - 3Mr^2}{R^3 - 2Mr^2} \, . \tag{L.0.13}$$

where $0 \leq r \leq R$. Thus, the full solution of the Einstein equations (L.0.6–L.0.8) gives for the metric functions

$$e^\nu = \left(1 - \frac{2M}{R} \right)^{3/2} \left(1 - \frac{2Mr^2}{R^3} \right)^{-1/2} , \qquad e^\lambda = \left(1 - \frac{2Mr^2}{R^3} \right)^{-1} , \tag{L.0.14}$$

The stability conditions for particles moving along a circular geodetic orbit on the equatorial plane is studied in next for the specific case of an EC of constant energy density, in terms of the effective potential $V_{eff} = e^{\nu/2}(1 + \tilde{L}^2/r^2)^{1/2}$ (see e.g. Ref. [Geralico et al. (2012)] for a general discussion of Stability). The existence of circular orbit at r_0 is calculated through the necessary condition $V'_{eff}(r_0) = 0$, while the the necessary condition for stability is $V''_{eff}(r_0) > 0$.

In general (for any given EC) both necessary conditions reads respectively

$$r > 3M(r), \qquad \frac{\mathrm{d}(\ln M(r))}{\mathrm{d}(\ln r)} + 1 - \frac{6M(r)}{r} > 0\,, \tag{L.0.15}$$

In particular, for $\rho = 3M/(4\pi R^3)$ =const, the stability analysis directly implies that stable circular orbits exist within the cluster in the range

$$r < R\sqrt{\frac{R}{3M}}. \tag{L.0.16}$$

Note that there is no upper limit on r if $R > 3M$, implying that circular orbits are stable all the way up to the boundary of the configuration.

For outer particles $r > R$, the stability conditions in (L.0.15) makes possible to distinguish the following classes: models with $R > 6M$ and models with $3M < R < 6M$. If $R > 6M$ the cluster is said to be globally stable, because circular orbits are always stable both inside and outside the configuration (see also Fig. L.3 (a)).

If $3M < R < 6M$ all particles constituting the cluster move on stable orbits, but in the adjacent exterior region of the configuration there is a region of instability ($R < r < 6M$), so that the cluster is meta-stable (see also Fig. L.3 (b)). This stability criterion was first applied in [Cocco and Ruffini (1997)].

Another formal criterion which will be also used in next to classify an EC regarding the stability, is the one adopted in [Zapolsky (1968)] based on the behaviour of the gravitational binding energy of the system. Where the fractional binding energy of the cluster is defined by

$$E_b^f = \frac{m\mathcal{N} - M}{m\mathcal{N}}. \tag{L.0.17}$$

A regular and relativistic EC marginally inside the pericenter of the S2 star, has to fulfill the following observational constraints for its boundary R and total mass M

$$R = r_{p(S2)} = 6 \times 10^{-4}\,\mathrm{pc}, \qquad M = 4.4 \times 10^6\, M_\odot, \tag{L.0.18}$$

where both values are subject to some $\sim$ few % of error due to propagated error in the distance from the sun to the galactic center $R_0 \approx 8.3$ kpc (see e.g. Ref. [Gillessen et al. (2009)]). These constraints implies (in geometrical units)

a ratio $R/M = 2840.9 \gg 6$, which safely indicates global stability, i.e. both inside and outside the cluster according with the criterion presented above with Ref. [Cocco and Ruffini (1997)].

In next we analyze, for an EC of constant number particles $\mathcal{N}$, up to which extent it can be shrank inside $r_{p(S2)}$ without becoming meta-stable, and moreover, what happens when the particles approach the ultra-relativistic regime. For this we first calculate the relation between M and R for fixed values of the rest mass $m\mathcal{N}$ of the system, taking the velocity $0 < v_k \leq 1$ as a parameter. By use of Eq. (L.0.12) we have

$$m\mathcal{N} = M\,[1/v_k^2 + 2]^{3/2} F(v_k)\,, \tag{L.0.19}$$

where $F(v_k) = -3/4[\arctan\,(x(v_k) - 3)^{-1/2} + (x(v_k) - 3)^{1/2}/x(v_k)] + (3/4)^{1/2} \arctan\,(3/(x(v_k) - 3))^{1/2}$, since $x(v_k) = R/M(v_k) = 1/v_k^2 + 2$. The direct relation between R/M and v_k is easily understood from the Keplerian velocity formula in (L.0.10) evaluated at $r = R$. Eq. (L.0.19) together with $x(v_k)$ automatically leads to the following total mass and radius normalized variables

$$\frac{R}{m\mathcal{N}} = \frac{1}{F(v_k)[1/v_k^2 + 2]^{1/2}}\,, \qquad \frac{M}{m\mathcal{N}} = \frac{1}{F(v_k)[1/v_k^2 + 2]^{3/2}}. \tag{L.0.20}$$

In Fig. (L.1) we explicitly show the R vs. M relation (normalized with the constant rest mass) with v_k taken as a free parameter. Regions of stability and meta-stability are differentiated depending on the value of the rotation velocity (v_k) at the boundary of the EC (see caption for details). Instead, in Fig. (L.2) we show the behaviour of the binding energy as a function of the velocity v_k, this is, showing the fraction of the total mass that turns into binding energy when the cluster is contracted from $R \gg 1$ to a given R. After the maximum a change of stability takes place and the cluster itself becomes unstable according to this criterion (see caption for details).

Even though these systems reach meta-stability (according to the classification given in [Cocco and Ruffini (1997)]) or become unstable (according the binding energy analysis), well before the velocity v_k reaches the ultra-relativistic regime; it is interesting to note that these tangential pressure supported self-gravitating systems, never reaches a critical mass as in the case of radial pressure supported self-gravitating systems, being neutron stars a typical example of this last case.

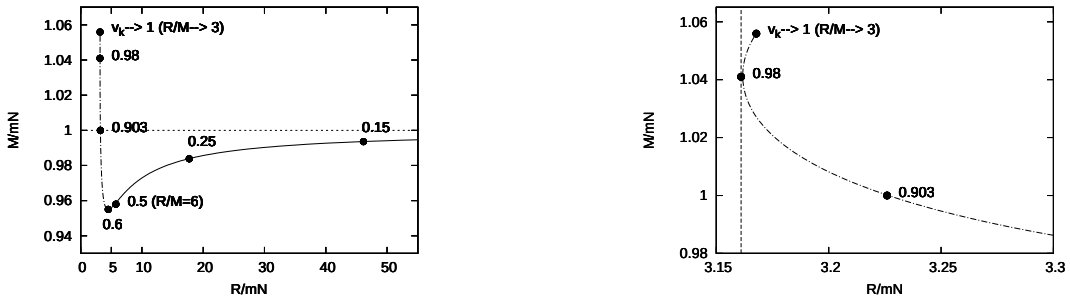

Figure L.1.: Gravitational mass vs. boundary radius relation (in units of rest mass) for an EC with constant energy density. The velocity at the boundary $0 < v_k < 1$ is taken as a parameter. In Fig. (a): for $v_k \to 0$ the total mass approaches the rest mass at $R/(mN) \to \infty$. At $v_k = 0.5$ the EC becomes meta-stable (i.e. $R/M = 6$), while $v_k = 0.6$ corresponds to the minimum in $M/(mN) = 0.955$ which further implies the maximum bounded state for the cluster (see Fig. L.2 for comparison). At $v_k = 0.903$ the gravitational mass equals the rest mass, and at $v_k = 0.98$ a turning point in the radius appears (see Fig. (b) for a zoom). Finally, the onset of instability $R/M = 3$ (according to the classification given in [Cocco and Ruffini (1997)]) is asymptotically approached when $v_k \to 1$.

In Fig. (L.3) we present two examples of constant energy density EC, the case of $R/M = 10$ (Fig. a) where circular stable orbits exist either for particles forming the EC but also for outside ones, and the case of $R/M = 3.1$ (Fig. b) where unstable orbits (i.e. a maximum in V_{eff}) appears for outer particles located in the outer vicinity of the border of the EC. In the second case the EC is called meta-stable according to the characterization given in [Cocco and Ruffini (1997)].

The fact of working with a fixed rest mass energy $m\mathcal{N}$ which can be calculated with the observational constraints (L.0.20), implies that the constant energy density $\rho = 3M/(4\pi R^3)$ increases more and more according the velocity v_k increases. From Eqs. (L.0.19) and $(R/M(v_k) = 1/v_k^2 + 2)$ it is possible to give an explicit expression for $\rho(v_k) = 3/(4\pi)(F(v_k)/(mN))^2$, from which we can give the uppermost limits for the density of a dark EC inside SgrA*. Changing units to $M_\odot/\mathrm{pc}^3$, the first upper limit corresponds to $\rho(v_k = 0.5) \approx 5.5 \times 10^{23} M_\odot/\mathrm{pc}^3$, below which the EC is always glob-

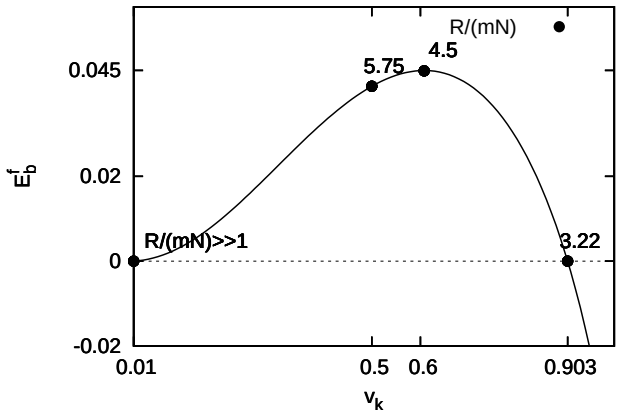

Figure L.2.: The behaviour of the fractional binding energy (L.0.17) as a function of v_k with fixed particle number. The maximum corresponds to an EC which has shrank to $R/(mN) = 4.5$ where $E_b^f \approx 0.045$. The latter vanishes at $R/(mN) = 3.22$ for a velocity $v_k = 0.903$ where the cluster is considered unstable according to this criterion. At $v_k = 0.5$ the radius of the cluster is $R/(mN) = 5.75$ implying $R/M = 6$ (see Fig. L.1 for comparison).

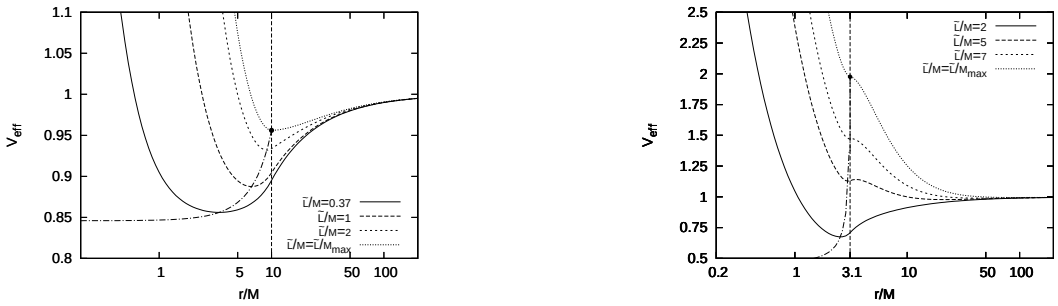

Figure L.3.: Behaviour of the effective potential as a function of r/M for an EC with constant energy density. In Fig. (a) we show a globally stable cluster with $R/M = 10$, and in Fig. (b) a meta-stable one with $R/M = 3.1$. Only in Fig. (b) and for relatively high values of $\tilde{L}$ an external maximum appears showing the existence of unstable orbits in the outer vicinity of the cluster. The dots corresponds to the point a maximum angular momentum at the border of the cluster.

ally stable. The second limit is given by $\rho(v_k = 0.6) \approx 1.1 \times 10^{24} M_\odot/\mathrm{pc}^3$, and will be considered as the uppermost limit for a regular and relativistic EC inside S2 and centered in SgrA*, due to the fact that above this velocity the value of the binding energy (L.0.17) starts to decrease from its maximum, undergoing a change of stability (see also Fig. L.2). These results are in consistency with the bound obtained in [Böhmer and Harko (2007)] from a different stability analysis, based on the lose of isotropy of the fluid due to non-radial perturbations; since anisotropy serves as a source of instability (see [Herrera and Santos (1997)] and refs. therein).

It is important to note that this specific EC model composed by dark matter particles with $\rho = const.$ provides a good alternative for the SMBH thought to be hosted in the center of SgrA*. This due to the fact that the upper limit for $\rho(v_k = 0.5)$ given above, is already about one order of magnitude higher than the lowest limit for the mass density of SgrA* as imposed in [Doeleman et al. (2008)] through the 1.3 mm Very Large Baseline Interferometry observations, but below the critical density required for a black hole of $4.4 \times 10^6 M_\odot$.

M. Dark matter and baryons in dwarf galaxies

M.1. Introduction

In the realm of galactic dynamics, baryonic and Dark Matter (DM) components are usually treated in the literature in terms of the Jeans equations (see e.g. Binney and Tremaine (2008) for a full development of the theory and next section for a brief introduction). When leading with dwarf galaxies it is usually assumed that the underlying gravitational potential $\Phi(r)$ in the halo regions is dominated by the DM component. This ansatz together with the assumptions of time-independent systems in spherical symmetry with no angular momentum dependence and constant line-of-sight velocity dispersions σ_{los} (LOSVD), allows to break the *Jeans degeneracy* appearing in anisotropic systems with $\sigma_\theta^2 \neq \sigma_r^2$ (see e.g. Binney and Tremaine (2008)). In this case it is possible to fully solve the Jeans equations to express the DM density profile in terms of the observables: σ_{los} and $\Sigma(R)$, the last being the surface brightness (see e.g. Evans et al. (2009) for a theoretical approach on this matter, and Walker et al. (2009) for a phenomenological approach).

The main motivation of this chapter is to establish a connection between the observations of the well resolved and nucleated dwarf galaxies as observed and studied in Kourkchi et al. (2012), with the model of semi-degenerate self-gravitating system of fermions introduced in Ruffini et al. (2014) and Argüelles et al. (2014). The fact that phase-space densities ($Q \sim \rho_0 m^{-4} \sigma^{-3}$) through the center of the configurations can rise to values much higher than its outer halo counterparts (see also conclusions in Chapter 2.2), suggests a natural way to explain the observed nucleated regions at the center of the dwarf galaxies. Indeed, this nucleated structure arising in the majority of dwarfs galaxies below pc scales is a non-well understood issue, many times associated with complex merging processes (see e.g. a discussion on this matter in Kourkchi et al. (2012)). Thus, the final objective of this more general

approach, even under the simplifying symmetries here adopted, is to give more light on this matter by providing an underlying fermionic phase-space distribution for the dark component which naturally condenses through the center due to the quantum pressure.

In next we provide a theoretical background based on the Jeans equations to deal, in a more consistent way, with the baryonic and DM components from the center up to the halo of well resolved dwarf galaxies. In this new picture, the assumption of considering an overall gravitational potential dominated by the DM component has to be relaxed to properly account for the gravitational effect of the baryons towards the center.

M.2. Standard Jeans equations & galactic DM

The Jeans equations corresponds to the theoretical framework of major importance when studying the problem of equilibrium distribution of matter in galaxies. These formalism, being written in terms of the collisionless Boltzmann equation, allow to study ideal systems of N collisionless identical point masses in dynamical equilibrium, which may represent stars or even dark matter particles. This treatment involves a smoothly distributed system's mass (or particle number, or even luminosity) in space, expressed in terms of an underlying phase-space distribution function $f(\mathbf{x}, \mathbf{v}, t)$. It has been shown that the assumption of a smooth, rather than discretized, distribution of matter in space is a very good approximation in order to give a complete description of the dynamics of the system. In fact, when N is a large number ($\gtrsim 10^4$), the possible deviation from the true trajectory of the particle in this idealized model, is very small even for times scales of the order of the age of the Universe (see e.g Binney and Tremaine (2008) chapter 7).

For time-independent systems, each of these spatial density distributions: of mass ($\rho(\mathbf{x})$), particle number ($n(\mathbf{x})$) or luminosity ($j(\mathbf{x})$), is obtained by simply multiplying the probability density of finding a particular component of the system at $\mathbf{x}$,

$$\nu(\mathbf{x}) \equiv g/h^3 \int \mathrm{d}^3\mathbf{v}\, f(\mathbf{x}, \mathbf{v})\,, \tag{M.2.1}$$

by M, N or L respectively, where M is the total mass, N the total number of particles and L the total luminosity. With g the particle state degeneracy, and h the Planck constant.

Since the astrophysical systems we are interested here are mainly isolated

dwarf spheroidal galaxies (dSph), we will work with the specific Jeans equations under the general assumptions of time-independent systems in spherical symmetry with no angular momentum dependence[1], which reads (see e.g Binney and Tremaine (2008) chapter 4):

$$\frac{\mathrm{d}}{\mathrm{d}r}(\nu\overline{v_r^2}) = -\nu\frac{\mathrm{d}}{\mathrm{d}r}\Phi(r)\,. \tag{M.2.2}$$

Where $\Phi(r)$ is the gravitational potential and $\overline{v_r^2}$ is the mean square radial velocity which, in this special symmetry, coincides with the radial dispersion velocity:

$$\overline{v_r^2} = \sigma_r^2 = 4\pi/(3\nu(r))\int dv v^4 f(r,v^2)\,. \tag{M.2.3}$$

The probability density (M.2.1) in this case is simply given by,

$$\nu(r) = 4\pi(g/h^3)\int_0^\infty dv\, v^2 f(r,v^2)\,. \tag{M.2.4}$$

The equation (M.2.2) is an hydrostatic equilibrium-like equation, and differs only in that $\nu(r)$ represents a probability density instead of a mass density, and that the mean particle velocity replaces the fluid velocity; being therefore $\nu(r)\overline{v_r^2}$ the pressure-like term.

The application of this Jeans analysis to the spatial distribution of matter in galaxies, depends on which kinds of matter components are pretended to be studied in relation with the observables. For example, in studying galactic halos of dSph galaxies, is usually assumed in the literature that $\nu(r)$ represents the distribution of luminous matter (i.e. stars), while the underlying gravitational potential $\Phi(r)$ is dominated by the dark matter component (see e.g. Walker et al. (2009); Evans et al. (2009)), allowing thus to write the Poisson equation uniquely in terms of the dark matter density ($\rho_{DM}(r)$), this is,

$$\nabla^2\Phi(r) = 4\pi G\rho_{DM}(r) \tag{M.2.5}$$

The observables are the surface brightness $\Sigma(R)$ (where R is the projected radius perpendicular to the line of sight), and the line-of-sight velocity dispersion $\sigma_{los}^2(R)$.

[1]This systems are characterized by a distribution function just depending on the total energy $f(H = 1/2v^2 + \Phi(r))$, and then having zero anisotropy (i.e. $\overline{v_r^2} = \overline{v_\theta^2} = \overline{v_\phi^2}$)

The connection between the observables and the theoretical functions in (M.2.2) are expressed in terms of the following formulas:

$$j(r) = -\frac{1}{\pi}\int_r^\infty \frac{\mathrm{d}}{\mathrm{d}R}\Sigma \frac{\mathrm{d}R}{\sqrt{R^2 - r^2}}, \qquad \rho_L(r) = \Upsilon_L j(r)\,, \tag{M.2.6}$$

where $j(r)$ is the three-dimensional luminosity density, related with the probability density by,

$$j(r) = L\nu(r)\,. \tag{M.2.7}$$

This function is related with the measured surface brightness $\Sigma(R)$ through the Abel de-projection formula as shown in (M.2.6). The factor which relates the mass density of the luminous material $\rho_L(r)$ and the luminous density $j(r)$ is the mass-to-light ratio of the given stellar population Υ_L, which in general is assumed to be a constant. The line-of-sight velocity dispersion $\sigma^2_{los}(R)$ relates with the radial velocity dispersion σ^2_r by the corresponding Abel de-projection formula (see e.g. Binney and Tremaine (1987)):

$$\sigma^2_r(r) = -\frac{1}{\pi j(r)}\int_r^\infty \frac{\mathrm{d}}{\mathrm{d}R}(\Sigma\sigma^2_{los})\frac{\mathrm{d}R}{\sqrt{R^2 - r^2}} \tag{M.2.8}$$

Once the link between the observables and the theoretical variables has been established, and using the simplifying assumption of constant dispersion velocity $\sigma^2_{los}(R) = const.$ (as suggested by obervations in most dSphs Walker et al. (2009)), it is possible to obtain an explicit expression for the dark matter density profile purely in terms of the observables. First of all, it is important to notice that if $\sigma^2_{los}(R)$ is a constant, then from (M.2.8) one directly obtains ($\sigma^2_r = \sigma^2_{los}$). Then, taking equation (M.2.2) in terms of the luminous mass density $\rho_L(r) = \Upsilon j(r)$ ($\Upsilon = const.$), and equation (M.2.5), we have the system:

$$\sigma^2_{los}\frac{\mathrm{d}}{\mathrm{d}r}j(r) = -j(r)\frac{\mathrm{d}}{\mathrm{d}r}\Phi(r)\,, \tag{M.2.9}$$

$$\nabla^2\Phi(r) = 4\pi G\rho_{DM}(r)\,. \tag{M.2.10}$$

These two equations can be easily combined to yield

$$\rho_{DM}(r) = -\frac{\sigma^2_{los}}{4\pi G}\nabla^2 \ln j(r)\,, \tag{M.2.11}$$

with $j(r)$ given by equation (M.2.6). Moreover, it is even possible to have analytic expressions for $\rho_{DM}(r)$ if standard light profiles as King, Plummer, Sérsic, etc. are obtained using parametric best fits from the observed surface brightness $\Sigma(R)$. The analysis presented above has been taken from Evans et al. (2009), and we have just shown here the part relevant to this work.

It is interesting to notice that with this kind of Jean analysis it is possible to make use of the observables (expressed in terms of the stellar density $\nu(\mathbf{x})$), without the need of knowing explicitly the underlying phase-space distribution function $f(\mathbf{x}, \mathbf{v})$.

M.3. Generalized formalism for a system of DM plus baryons

The objective of this section is to generalize the hydrostatic equilibrium-like equation (M.2.2) to the more general case of a multiple-component system of point masses in dynamical equilibrium. For definiteness, we will consider a self-gravitating system composed by N_1 identical collisionless dark matter particles and N_2 identical collisionless stars, neglecting any possible interaction (other than gravitational) between both kinds of matter. Therefore, within this more general effective treatment, we can write the analogous of Eq. (M.2.2) but in terms of the mass density and pressure terms as follows:

$$\frac{\mathrm{d}}{\mathrm{d}r}P_T = -\rho_T \frac{\mathrm{d}}{\mathrm{d}r}\Phi(r)\,, \tag{M.3.1}$$

where P_T and ρ_T are the total pressure and total mass density of the multi-component system composed by DM particles and stars.

There are many motivations for this generalization. In what follows we present three main important reasons:

1) We want to build a model to account in a more consistent way for the dynamical equilibrium of systems with two different matter components, luminous objects (i.e. stars), and dark matter particles.

2) Being interested in the overall distribution of matter in dSph galaxies, from sub-parsec up to kilo-parsec scales, we will relax the hypothesis of $\rho_{DM}(r) \gg \rho_L(r)$ [2] usually considered in the literature (see e.g. Evans et al.

[2] Even if in Strigari et al. (2008) has been demonstrated that the dSphs are the most dark

(2009); Walker et al. (2009)).

3) Have a formal approach to analyze the fundamental problem of understanding the detailed spatial distribution of dark matter relative to the baryonic one in relation with the observed central nucleated regions in dwarfs galaxies.

We will work here only under the simplifying assumptions of time-independent systems in spherical symmetry and with no angular momentum dependence.

The following step is to write Eq. (M.3.1) in terms of each pressure and density components. This is, by assuming the following decompositions $P_T = P_L + P_{DM}$ and $\rho_T = \rho_L + \rho_{DM}$, Eq. (M.3.1) reads

$$\frac{\mathrm{d}P_L}{\mathrm{d}r} + \frac{\mathrm{d}P_{DM}}{\mathrm{d}r} + \rho_L \frac{\mathrm{d}\Phi_T}{\mathrm{d}r} + \rho_{DM} \frac{\mathrm{d}\Phi_T}{\mathrm{d}r} = 0\,. \tag{M.3.2}$$

Because we are here assuming a possible linear independence between the gravitational effects of each component, plus the non-interacting (other than gravity) nature between the two matter components, we can write (M.3.2) as a coupled system of two ordinary differential equations as follows,

$$\frac{\mathrm{d}}{\mathrm{d}r}(j(r)\sigma_r^2) = -j(r)\frac{\mathrm{d}}{\mathrm{d}r}\Phi_T(r)\,, \tag{M.3.3}$$

$$\frac{\mathrm{d}}{\mathrm{d}r}P_{DM}(r) = -\rho_{DM}(r)\frac{\mathrm{d}}{\mathrm{d}r}\Phi_T(r)\,. \tag{M.3.4}$$

We have expressed the luminous pressure term above in terms of the luminosity density, which has been also introduced in the right side of the equation for compatibility. Notice moreover that this is possible because we are considering here constant (luminous) mass-to-light ratios.

The above system equations is considered together with the Poisson equation,

$$\nabla^2\Phi_T(r) = 4\pi G\rho_T(r)\,. \tag{M.3.5}$$

With the aim of obtaining an unique equation which contain the information of the coupled system (M.3.3–M.3.4), we divide both equations to eliminate the gravitational gradient, and separate each matter component func-

matter dominant galaxies in the Universe, this result corresponds only for halo regions.

tions at each side of the new equation, to obtain,

$$\frac{1}{\rho_{DM}(r)}\frac{\mathrm{d}}{\mathrm{d}r}P_{DM}(r) = \frac{1}{j(r)}\frac{\mathrm{d}}{\mathrm{d}r}j(r)\sigma_r^2\,. \tag{M.3.6}$$

Equation (M.3.6) will be considered from now on as a Jean *master* equation, containing the information of both kinds of matter which self-gravitates in an unique system.

We turn now to deal with the equation of state of the dark matter model. Here we will limit to deal with the parametric equation of state of a non-relativistic self-gravitating Fermi gas, being this physical regime more than sufficient when dealing with normal galaxies, and in particular as in this work, dwarf galaxies. Thus we have (the spin degeneracy has been taken $g = 2$),

$$\rho_{DM} = \frac{m^4}{\pi^2\hbar^3}\int_0^\infty v^2 f_{DM}(r, v^2)\, dv, \tag{M.3.7}$$

$$P_{DM} = \frac{1}{3}\frac{m^4}{\pi^2\hbar^3}\int_0^\infty v^4 f_{DM}(r, v^2)\, dv, \tag{M.3.8}$$

where $f_{DM}(r, v^2)$ is given by

$$f_{DM}(r, v^2) = \frac{1}{\exp\left[(mv^2/(2kT) - \theta(r)\right] + 1}\,. \tag{M.3.9}$$

with m the fermion mass, $T = constant$, the temperature of the isothermal dark matter component, $\theta(r) = \mu(r))/kT$ is the degeneracy parameter defined in terms of the gravitationally coupled chemical potential $\mu(r)$, and k the Boltzmann constant. The infinite integrals in (M.3.7–M.3.8) can be expressed in terms of the Polylogarithmic spetial functions $Li_s(z)$ of order s and argument z. Considering that $Li_s(-z) = -\Gamma(s)^{-1}\int_0^\infty dt\, t^{s-1}/[\exp(t)/z + 1]$, with $t = mv^2/(2kT)$, $z = \exp(\theta(r))$, and $s = 3/2$ or $s = 5/2$ in correspondence with (M.3.7) or (M.3.8) respectively. If the following property for the derivative of the Polylogarithm $d[Li_s(z(r))]/dr = z'(r)/z(r)\, Li_{s-1}(z(r))$ is used, we directly have for the left side in Eq. (M.3.6)

$$\frac{1}{\rho_{DM}(r)}\frac{\mathrm{d}P_{DM}(r)}{\mathrm{d}r} = \frac{kT}{m}\frac{\mathrm{d}}{\mathrm{d}r}\theta(r)\,. \tag{M.3.10}$$

Equation (M.3.10) will be considered from now on as a dark matter *master* equation, containing only information about the equation of state of the dark matter component.

Thus, we now combine the two *master* equations (M.3.6) and (M.3.10) in one unique equation given by,

$$\frac{1}{j(r)}\frac{\mathrm{d}}{\mathrm{d}r}(j(r)\sigma_r^2) = \frac{kT}{m}\frac{\mathrm{d}}{\mathrm{d}r}\theta_j(r)\,. \tag{M.3.11}$$

It is important to notice that equation (M.3.11) is an ordinary linear differential equation in $\theta_j(r)$, this last being interpreted as the degeneracy parameter affected by the gravitational effect of the baryonic distribution $j(r)$. Notice that on the left side of Eq. (M.3.11) we have the observables, and on the right side we have the parameters of the dark matter component (T,θ,m), with T the DM temperature which must be found to fully solve the equations.

Once the solution for the degeneracy parameter $\theta_j(r)$ is obtained from the observables $\sigma \equiv \sigma_r$ and $j(r)$, this must be replaced in the Polylogarithm variant of equation (M.3.7) to yield the following important expression for the dark matter density function,

$$\rho_{DM}(r) = -\frac{m^{5/2}(kT)^{3/2}}{\sqrt{2}\pi^{3/2}\hbar^3} Li_{3/2}[-\exp[\theta_j(r)]] \tag{M.3.12}$$

The importance of Eq. M.3.12 lays in the fact that if analytic expressions can be obtained for the luminosity density $j(r)$ and σ from observations, then we can have semi-analytic dark matter density profiles from it. This would further imply a valuable possibility to constraint the dark matter candidate mass m, when the observationally inferred magnitudes as core and halo mass are provided. In next section I proceed to apply this generalized treatment to a sample of well resolved nucleated dwarf galaxies, for which either spectrometric and photometric measurements has been obtained from parsec distance-scales up to $\sim 10^2$ pc.

M.4. Application to nucleated dwarf galaxies

The dwarf galaxies are an excellent astrophysical laboratory to study the distribution and nature of the dark matter particles because they belong to

the most dark matter-dominated objects in the Universe as demonstrated in Strigari et al. (2008). Recently, in Kourkchi et al. (2012) a big sample of about 70 dwarf galaxies in the Coma cluster (of distance $D = 100Mpc$) were analyzed from high-resolution spectroscopic and photometric data, evidencing a nucleated luminosity profile through the center in the majority of the cases. It is believed that this central light excess is an imprint of the formation history of these galaxies, but there is no closed explanation of the causes and processes which leads to this new structure at pc distance-scales or below. The application of the generalized approach here introduced pretends to give more light to this important issue.

The nucleated surface brightness profiles observed in dwarf galaxies Kourkchi et al. (2012), are typically modeled by a Sérsic+Gaussian model of the form[3] (see also Fig. M.1)

$$\frac{\Sigma(R)}{(L_\odot/pc^2)} = \Sigma_0\, e^{-0.5(R/R_c)^2} + \Sigma_e\, e^{-b(R/R_e-1)}. \tag{M.4.1}$$

where Σ_0 is the central observed value of the surface brightness and Σ_e the effective surface brightness, while R_c and R_e are the central core scale radius and the effective radius respectively. It is important to notice that the Sérsic index n in (M.4.1) has been taken equal to unity as it is representative of the majority of the sample considered in Kourkchi et al. (2012). The value of b depends on n (see e.g. Prugniel and Simien (1997)), and in the cases analyzed here (i.e. $n = 1$) it is $b \approx 1.66$. The three dimensional luminosity density profile $j(r)$ is obtained through the Abel de-projection formula to yield the following analytic expression,

$$\frac{j(r)}{(L_\odot/pc^3)} = \frac{1.25}{\pi}\frac{\Sigma_0}{R_c}e^{-0.5(r/R_c)^2} + \frac{7.92}{\pi}\frac{\Sigma_e}{R_e}K_0(1.6r/R_e) \tag{M.4.2}$$

where $K_0(x)$ is the modified Bessel function of second kind and of order 0. We adopt typical values of luminosity and scale-radii in dwarfs as shown in Kourkchi et al. (2012): $\Sigma_0 = 560$ $L_\odot/pc^2$, $\Sigma_e = 40$ $L_\odot/pc^2$, $R_c = 25$ pc, $R_e = 850$ pc. The constant line-of-sight velocity dispersion adopted here is $\sigma_{los} \equiv \sigma_r = 9$ km/s, according to Kourkchi et al. (2012), thus implying a total

[3] We take the nucleated dwarf GMP3080 as a prototype galaxy of the sample studied in Kourkchi et al. (2012), from which typical photometric and spectroscopic observed values are taken as a reference.

(integrated) mass-to-light ratio of $\Upsilon = 1.6$ as obtained from Kourkchi et al. (2012) (see Fig. 12 of that paper).

The DM temperature T needed to finally solve Eqtn. (M.3.11) is obtained by assuming DM predomination in the halo region, where clearly the Mawellian regime in the Fermi-Dirac distribution function is reached (i.e. $\mu(r)/kT << -1$). Therefore we must have necessarily $T \approx m\sigma_{DM}^2/k$, where σ_{DM} is the DM one-dimensional dispersion velocity. Now, σ_{DM} can be obtained from the flat part of the DM rotation curve proper of this classical regime, where the following relation holds (see e.g. Binney and Tremaine (2008)) $v_{circ} = \sqrt{2}\sigma_{DM}$. With this we have the desired DM temperature as $T = mv_{circ}^2/(2k)$. In what follows we adopt $v_{circ} = 13$ km/s, being a typical circular velocity in dwarf galaxies as shown in Walker et al. (2009); leading to $kT/m = v_{circ}^2/2$ (km/s)^2, most important in order to solve Eq. (M.3.11).

The function $\theta_j(r)$ is obtained by integration of the equation (M.3.11) between r_0 and r, with $\sigma_r^2 = 81$ (km/s)^2 and $kT/m = 84.5$ (km/s)^2, to yield $\theta_j(r) = 0.95 \ln[j(r)/j(r_0)] + \theta_j(r_0)$, with $j(r_0 = 4 \text{ pc}) = 12.3$ L$_\odot$/pc^3, being r_0 the innermost resolved radius for a typical dwarf galaxy as studied in Kourkchi et al. (2012).

Once with the solution for $\theta_j(r)$, and by using Eq. (M.3.12) together with the total mass density $\rho_T(r) = \Upsilon j(r)$, it is possible to obtain the ratio between them. This ratio is calculated in dimensionless units to obtain an expression only in terms of the free parameter θ_j^0 (i.e. independently of the fermion mass). For this, Eq. (M.3.12) is normalized dividing by $\rho_*^{DM} = m^4 v_{circ}^3/(4\pi^{3/2}\hbar^3)$, while $\rho^T(r)$ is normalized dividing by the central total mass density $\rho_0^T \approx 20 M_\odot/pc^3$. Therefore the new normalized formulas are

$$\rho_n^{DM} = -Li_{3/2}[-(j(r)/j_0)^{0.95} e^{\theta_j^0}]; \qquad \rho_n^T = \Upsilon j(r)/\rho_0^T \,. \tag{M.4.3}$$

In Fig. M.2 we show the (normalized) total mass density profile typical of a nucleated dwarf galaxy in the Coma cluster ρ_n^T together with two different ρ_n^{DM} for two different values of θ_j^0. The value of $\theta_j^0 = -0.4$ is selected assuming a dark matter dominance of $\sim 94\%$ at R_e (and a dominance of $\sim 55\%$ at r_0), while $\theta_j^0 = -0.7$ corresponds for a dark matter dominance of $\sim 70\%$ at R_e (with a $\sim 42\%$ at r_0). Values of $\theta_j^0 > 0$ are prohibited because otherwise the dark matter density would overcome the total mass density.

Once the precise DM dominance at the center of the configuration r_0 is known, the 'ino' mass m can be obtained from the DM density equation ρ_n^{DM}

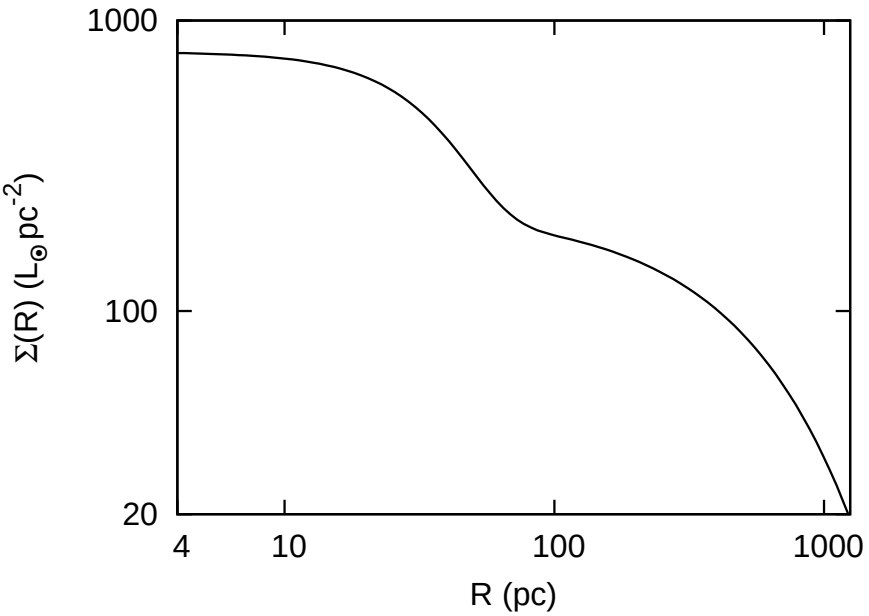

Figure M.1.: A double-component Sérsic-Gaussian model fit to a typical observed surface brightness $\Sigma(R)$ in $(L_{\odot}/\mathrm{pc}^2)$, as considered in Kourkchi et al. (2012).

together with the normalization factor ρ_*^{DM}. The calculations in the two cases here assumed $\theta_j^0 = -0.4$ and $\theta_j^0 = -0.7$ leads respectively, to rest fermion masses of $m = 1.15$ keV/c^2 and $m = 1.14$ keV/c^2; implying an small effect of few 10^1 eV/c^2 due to the different dark matter halo dominance adopted. These mass values has to be seriously considered only as order of magnitude due to the many different simplifying assumptions adopted such as spherical symmetry and constant σ_{los} and Y, being not necessarily the case in real dwarf galaxies.

M.5. Conclusions

In conclusion, from this two-component (DM plus stars) dynamic approach, and due to the semi-degenerate nature of the dark matter phase-space adopted here, it is possible to better understand the so-called central light excess observed in the light profiles of many dwarf galaxies. This is, the

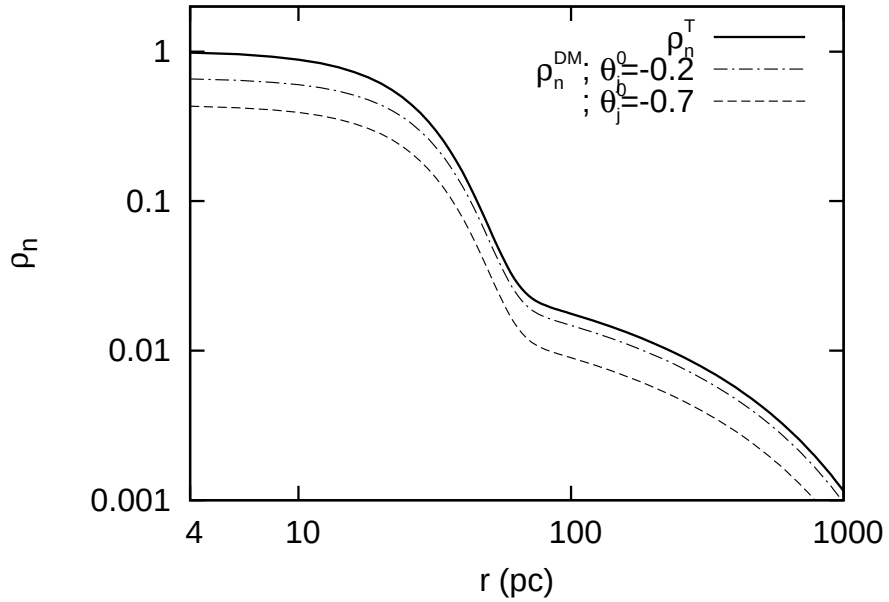

Figure M.2.: Two different dimensionless dark matter density profiles in correspondence with the free parameters $\theta_j^0 = -0.4$ and $\theta_j^0 = -0.7$ implying a dark matter dominance of $\sim 94\%$ and $\sim 70\%$ at R_e respectively. These dark profiles are obtained from the dynamical multi-component approach here developed and are contrasted against the total mass density profile as obtained directly from the observables, nicely showing how light follows dark matter all along the configuration.

fact that the dominating DM component condenses through the center due the (fermionic) quantum pressure, it generates a deepen in the gravitational potential well in which the baryonic component naturally falls in, generating as a response a nucleated behaviour in the light profile we observe at pc distance-scales or below. The second, and most important outcome of this approach, is that once the dark matter dominance is known at the effective radius R_e, the 'ino' mass value can be obtained from the equations, falling in the keV region. Nevertheless, a subtle point remains regarding the relation between the DM temperature and the observed dispersion velocity. It is important to notice that the DM density solution (see Eq. (M.4.3)) is very sensitive to the rate $\sigma_{los}^2/(kT/m)$, which enters as a power in the argument of the Polylogarythmic function $\mathrm{Li}_{3/2}$. The fact that the DM temperature is calcu-

lated through the observed circular velocity at halo scales (v_{circ}) as explained above, while σ_{los} cames from the distribution of light, makes crucial to obtain accurate data in both cases. In any case, if we center the attention in dwarf spheroidal galaxies (in better consistency with the symmetries adopted) as studied for example in Walker et al. (2009), we see that σ_{los} is always around 10 km/s, while typical v_{circ} are about 13 km/s for cored DM profiles, exactly as considered here.

Moreover, we want to emphasize the potential importance of this approach in views of future high-resolution observations through the center of nearby dwarfs which will reach sub-pc distance-scales; leading to a better understanding in the role of dark matter in connection with massive dark central objects generally interpreted as intermediate massive black holes.

Bibliography

ABRAMOWICZ, M.A., NOVIKOV, I.D. AND PACZYNSKI, B.
The appearance of highly relativistic, spherically symmetric stellar winds.
ApJ, **369**, pp. 175–178 (1991).
doi:10.1086/169748.

ACHTERBERG, A. AND WIERSMA, J.
The Weibel instability in relativistic plasmas. I. Linear theory.
A&A, **475**, pp. 1–18 (2007).
doi:10.1051/0004-6361:20065365.

AKSENOV, A.G., RUFFINI, R. AND VERESHCHAGIN, G.V.
Thermalization of Nonequilibrium Electron-Positron-Photon Plasmas.
Phys. Rev. Lett., **99(12)**, pp. 125003–+ (2007).
doi:10.1103/PhysRevLett.99.125003.

AKSENOV, A.G., RUFFINI, R. AND VERESHCHAGIN, G.V.
Thermalization of the mildly relativistic plasma.
Phys. Rev. D, **79(4)**, p. 043008 (2009).
doi:10.1103/PhysRevD.79.043008.

AKSENOV, A.G., RUFFINI, R. AND VERESHCHAGIN, G.V.
Pair plasma relaxation time scales.
Phys. Rev. E, **81**, p. 046401 (2010).

AKSENOV, A.G., RUFFINI, R. AND VERESHCHAGIN, G.V.
Comptonization of photons near the photosphere of relativistic outflows.
MNRAS, **436**, pp. L54–L58 (2013).
doi:10.1093/mnrasl/slt112.

ALCOCK, C., FARHI, E. AND OLINTO, A.
Strange stars.
ApJ, **310**, pp. 261–272 (1986).
doi:10.1086/164679.

ANDRÉASSON, H.
The Einstein-Vlasov System/Kinetic Theory.
Living Reviews in Relativity, **14**, p. 4 (2011).
doi:10.12942/lrr-2011-4.

ARBOLINO, M.V. AND RUFFINI, R.
The ratio between the mass of the halo and visible matter in spiral galaxies and limits on the neutrino mass.
A&A, **192**, pp. 107–116 (1988).

ARGÜELLES, C.R., MAVROMATOS, N., RUEDA, J.A. AND RUFFINI, R.
to be submitted (2014).

ARGÜELLES, C.R. AND RUFFINI, R.
Are the most super-massive dark compact objects harbored at the center of dark matter halos?
Honorable mention 2014 by the Gravity Research Foundation, arXiv:1405.7505 (2014).

ARGÜELLES, C.R., RUFFINI, R., SIUTSOU, I. AND FRAGA, B.
On the distribution of dark matter in galaxies: quantum treatments.
JKPS 65: 801, arXiv:astro-ph/1402.0700 (2014).

ARTSIMOVICH, L.A. AND SAGDEEV, R.Z.
Plasma physics for physicists.
Moscow Atomizdat (1979).

ASAKA, T., BLANCHET, S. AND SHAPOSHNIKOV, M.
The vMSM, dark matter and neutrino masses [rapid communication].
Physics Letters B, **631**, pp. 151–156 (2005).
doi:10.1016/j.physletb.2005.09.070.

BADJIN, D.A., BLINNIKOV, S.I. AND POSTNOV, K.A.
Thermal emission in gamma-ray burst afterglows.
Monthly Notices of the Royal Astronomical Society, **432(3)**, pp. 2454–2462 (2013).

BEGUE, D.
PhD thesis.
PhD thesis, University of Rome "Sapienza" (2014).

BÉGUÉ, D., SIUTSOU, I.A. AND VERESHCHAGIN, G.V.
Monte Carlo Simulations of the Photospheric Emission in Gamma-Ray Bursts.
ApJ, **767**, 139 (2013).
doi:10.1088/0004-637X/767/2/139.

BELIAEV, S.T. AND BUDKER, G.I.
The Relativistic Kinetic Equation.
Soviet Physics Doklady, **1**, p. 218 (1956).

BELOBORODOV, A.M.
Radiative Transfer in Ultrarelativistic Outflows.
ApJ, **737**, p. 68 (2011).
doi:10.1088/0004-637X/737/2/68.

BELVEDERE, R., PUGLIESE, D., RUEDA, J.A., RUFFINI, R. AND XUE, S.S.
Neutron star equilibrium configurations within a fully relativistic theory with strong, weak, electromagnetic, and gravitational interactions.
Nuclear Physics A, **883**, pp. 1–24 (2012).
doi:10.1016/j.nuclphysa.2012.02.018.

BENEDETTI, A., HAN, W.B., RUFFINI, R. AND VERESHCHAGIN, G.V.
On the frequency of oscillations in the pair plasma generated by a strong electric field.
Physics Letters B, **698**, pp. 75–79 (2011).
doi:10.1016/j.physletb.2011.02.050.

BENEDETTI, A., RUFFINI, R. AND VERESHCHAGIN, G.V.
Phase space evolution of pairs created in strong electric fields.
Physics Letters A, **377**, pp. 206–215 (2013).
doi:10.1016/j.physleta.2012.11.026.

BERESTETSKII, V.B., LIFSHITZ, E.M. AND PITAEVSKII, V.B.
Quantum Electrodynamics (Elsevier, 1982).

BERNARDINI, M.G., BIANCO, C.L., CAITO, L., DAINOTTI, M.G., GUIDA, R. AND RUFFINI, R.
GRB 970228 and a class of GRBs with an initial spikelike emission.
A&A, **474**, pp. L13–L16 (2007).
doi:10.1051/0004-6361:20078300.

BIANCO, C.L., RUFFINI, R. AND XUE, S.
The elementary spike produced by a pure e^+e^- pair-electromagnetic pulse from a Black Hole: The PEM Pulse.
A&A, **368**, pp. 377–390 (2001).
doi:10.1051/0004-6361:20000556.

BILIC, N., MUNYANEZA, F., TUPPER, G.B. AND VIOLLIER, R.D.
The dynamics of stars near Sgr A and dark matter at the center and in the halo of the galaxy*.
Progress in Particle and Nuclear Physics, **48**, pp. 291–300 (2002).
doi:10.1016/S0146-6410(02)00136-9.

BINNEY, J. AND TREMAINE, S.
Galactic dynamics (Princeton, NJ, Princeton University Press, 1987).

BINNEY, J. AND TREMAINE, S.
Galactic Dynamics: Second Edition (Princeton University Press, 2008).

BISNOVATYI-KOGAN, G.S., MERAFINA, M., RUFFINI, R. AND VESPERINI, E.
Stability of Dense Stellar Clusters against Relativistic Collapse. II. Maxwellian Distribution Functions with Different Cutoff Parameters.
ApJ, **500**, p. 217 (1998).
doi:10.1086/305689.

BISNOVATYI-KOGAN, G.S. AND MURZINA, M.V.A.
Early stages of relativistic fireball expansion.
Phys. Rev. D, **52**, pp. 4380–4392 (1995).

BISNOVATYI-KOGAN, G.S. AND ZEL'DOVICH, Y.B.
Growth of Perturbations in an Expanding Universe of Free Particles.
Soviet Ast., **14**, p. 758 (1971).

BISNOVATYI-KOGAN, G.S., ZEL'DOVICH, Y.B. AND SYUNYAEV, R.A.
Physical Processes in a Low-Density Relativistic Plasma.
Soviet Ast., **15**, pp. 17–+ (1971).

BISNOVATYJ-KOGAN, G.S., MERAFINA, M., RUFFINI, R. AND VESPERINI, E.
Stability of dense stellar clusters against relativistic collapse.
ApJ, **414**, pp. 187–199 (1993a).
doi:10.1086/173067.

BISNOVATYJ-KOGAN, G.S., MERAFINA, M., RUFFINI, R. AND VESPERINI, E.
Stability of dense stellar clusters against relativistic collapse.
ApJ, **414**, pp. 187–199 (1993b).
doi:10.1086/173067.

BLASCHKE, D.B., PROZORKEVICH, A.V., ROBERTS, C.D., SCHMIDT, S.M. AND SMOLYANSKY, S.A.
Pair Production and Optical Lasers.
Phys. Rev. Lett., **96(14)**, pp. 140402–+ (2006).
doi:10.1103/PhysRevLett.96.140402.

BOGOLIUBOV, N.N.
Problems of Dynamic Theory in Statistical Physics (Gostechizdat, 1946).
(in Russian).

BOGOLIUBOV, N.N.
Problems of Dynamic Theory in Statistical Physics (North Holland, Amsterdam, 1962).

BÖHMER, C.G. AND HARKO, T.
On Einstein clusters as galactic dark matter haloes.
MNRAS, **379**, pp. 393–398 (2007).
doi:10.1111/j.1365-2966.2007.11977.x.

BOLTZMANN, L.
Lectures on Gas Theory (Dover Publications, 2011).

BOND, J.R. AND SZALAY, A.S.
The collisionless damping of density fluctuations in an expanding universe.
ApJ, **274**, pp. 443–468 (1983).
doi:10.1086/161460.

BOYARSKY, A., RUCHAYSKIY, O., IAKUBOVSKYI, D., MACCIO', A.V. AND MALYSHEV, D.
New evidence for dark matter.
ArXiv e-prints (2009a).

BOYARSKY, A., RUCHAYSKIY, O. AND SHAPOSHNIKOV, M.
The Role of Sterile Neutrinos in Cosmology and Astrophysics.
Annual Review of Nuclear and Particle Science, **59**, pp. 191–214 (2009b).
doi:10.1146/annurev.nucl.010909.083654.

BRET, A., GREMILLET, L., BÉNISTI, D. AND LEFEBVRE, E.
Exact Relativistic Kinetic Theory of an Electron-Beam Plasma System: Hierarchy of the Competing Modes in the System-Parameter Space.
Physical Review Letters, **100(20)**, 205008 (2008).
doi:10.1103/PhysRevLett.100.205008.

BURKERT, A.
The Structure of Dark Matter Halos in Dwarf Galaxies.
ApJ, **447**, p. L25 (1995).
doi:10.1086/309560.

BUTI, B.
Plasma Oscillations and Landau Damping in a Relativistic Gas.
Physics of Fluids, **5**, pp. 1–5 (1962).
doi:10.1063/1.1706486.

CAITO, L., BERNARDINI, M.G., BIANCO, C.L., DAINOTTI, M.G., GUIDA, R. AND RUFFINI, R.
GRB060614: a "fake" short GRB from a merging binary system.
A&A, **498**, pp. 501–507 (2009).
doi:10.1051/0004-6361/200810676.

CALZETTI, D., GIAVALISCO, M. AND RUFFINI, R.
The normalization of the correlation functions for extragalactic structures.
A&A, **198**, pp. 1–2 (1988).

CALZETTI, D., GIAVALISCO, M., RUFFINI, R., EINASTO, J. AND SAAR, E.
The correlation function of galaxies in the direction of the Coma cluster.
Ap&SS, **137**, pp. 101–106 (1987).

CASSATA, P., GIAVALISCO, M., GUO, Y., RENZINI, A., FERGUSON, H., KOEKEMOER, A.M., SALIMBENI, S., SCARLATA, C., GROGIN, N.A., CONSELICE, C.J. ET AL.
The Relative Abundance of Compact and Normal Massive Early-type Galaxies and Its Evolution from Redshift z ˜ 2 to the Present.
ApJ, **743**, 96 (2011).
doi:10.1088/0004-637X/743/1/96.

CERCIGNANI, C. AND KREMER, G.M.

The relativistic Boltzmann equation: theory and applications (Boston: Birkhäuser, 2002).

CHEMIN, L., DE BLOK, W.J.G. AND MAMON, G.A.
Improved Modeling of the Mass Distribution of Disk Galaxies by the Einasto Halo Model.
AJ, **142**, 109 (2011).
doi:10.1088/0004-6256/142/4/109.

CHEN, F.F.
Introduction to Plasma Physics and Controlled Fusion Volume 1: Plasma Physics (Plenum press, 1984).

CHEN, H., WILKS, S.C., BONLIE, J.D., LIANG, E.P., MYATT, J., PRICE, D.F., MEYERHOFER, D.D. AND BEIERSDORFER, P.
Relativistic Positron Creation Using Ultraintense Short Pulse Lasers.
Phys. Rev. Lett., **102(10)**, pp. 105001–+ (2009).
doi:10.1103/PhysRevLett.102.105001.

CHERNIKOV, N.
Derivation of the equations of relativistic hydrodynamics from the relativistic transport equation.
Physics Letters, **5**, pp. 115–117 (1963a).
doi:10.1016/S0375-9601(63)91750-X.

CHERNIKOV, N.A.
Kinetic Equation for a Relativistic Gas in an Arbitrary Gravitational Field.
Soviet Physics Doklady, **7**, p. 397 (1962).

CHERNIKOV, N.
The relativistic gas in the gravitational field.
Acta Physica Polonica, **23**, pp. 629–645 (1963b).

CHERNIKOV, N.
Equilibrium distribution of the relativistic gas.
Acta Physica Polonica, **26**, pp. 1069–1091 (1964a).

CHERNIKOV, N.
Microscopic foundation of relativistic hydrodymanics.
Acta Physica Polonica, **27**, pp. 465–489 (1964b).

CHLUBA, J.
Spectral Distortions of the Cosmic Microwave Background.
Ph.D. thesis, Ludwig-Maximilians-Universität München (2005).

CHURAZOV, E., SUNYAEV, R., SAZONOV, S., REVNIVTSEV, M. AND VARSHALOVICH, D.
Positron annihilation spectrum from the Galactic Centre region observed by SPI/INTEGRAL.
MNRAS, **357**, pp. 1377–1386 (2005).
doi:10.1111/j.1365-2966.2005.08757.x.

COCCO, V. AND RUFFINI, R.
On metastable Einstein's clusters.
Nuovo Cimento B Serie, **112**, pp. 271–287 (1997).

COMER, G.L. AND KATZ, J.
Thick Einstein shells and their mechanical stability.
Classical and Quantum Gravity, **10**, pp. 1751–1765 (1993).
doi:10.1088/0264-9381/10/9/017.

COPPI, P.S. AND BLANDFORD, R.D.
Reaction rates and energy distributions for elementary processes in relativistic pair plasmas.
MNRAS, **245**, pp. 453–507 (1990).

COWSIK, R. AND MCCLELLAND, J.
An Upper Limit on the Neutrino Rest Mass.
Physical Review Letters, **29**, pp. 669–670 (1972).
doi:10.1103/PhysRevLett.29.669.

DAINOTTI, M.G., BERNARDINI, M.G., BIANCO, C.L., CAITO, L., GUIDA, R. AND RUFFINI, R.
GRB 060218 and GRBs associated with supernovae Ib/c.
A&A, **471**, pp. L29–L32 (2007).
doi:10.1051/0004-6361:20078068.

DAMOUR, T. AND RUFFINI, R.
Quantum electrodynamical effects in Kerr-Newman geometries.
Phys. Rev. Lett., **35**, pp. 463–466 (1975).

DE BLOK, W.J.G., MCGAUGH, S.S., BOSMA, A. AND RUBIN, V.C.
Mass Density Profiles of Low Surface Brightness Galaxies.
ApJ, **552**, pp. L23–L26 (2001a).
doi:10.1086/320262.

DE BLOK, W.J.G., MCGAUGH, S.S. AND RUBIN, V.C.
High-Resolution Rotation Curves of Low Surface Brightness Galaxies. II. Mass Models.
AJ, **122**, pp. 2396–2427 (2001b).
doi:10.1086/323450.

DE BLOK, W.J.G., WALTER, F., BRINKS, E., TRACHTERNACH, C., OH, S.H. AND KENNICUTT, JR., R.C.
High-Resolution Rotation Curves and Galaxy Mass Models from THINGS.
AJ, **136**, 2648 (2008).
doi:10.1088/0004-6256/136/6/2648.

DE JAGHER, P.C. AND SLUIJTER, F.W.
A covariant hierarchy of kinetic equations for classical particles and fields.
Contributions to Plasma Physics, **28**, pp. 169–183 (1988).
doi:10.1002/ctpp.2150280208.

DEBBASCH, F., RIVET, J.P. AND VAN LEEUWEN, W.A.
Invariance of the relativistic one-particle distribution function.
Physica A Statistical Mechanics and its Applications, **301**, pp. 181–195 (2001).
doi:10.1016/S0378-4371(01)00359-4.

DEBBASCH, F. AND VAN LEEUWEN, W.A.
General relativistic Boltzmann equation, I: Covariant treatment.
Physica A Statistical Mechanics and its Applications, **388**, pp. 1079–1104 (2009a).
doi:10.1016/j.physa.2008.12.023.

DEBBASCH, F. AND VAN LEEUWEN, W.A.
General relativistic Boltzmann equation, II: Manifestly covariant treatment.
Physica A Statistical Mechanics and its Applications, **388**, pp. 1818–1834 (2009b).
doi:10.1016/j.physa.2009.01.009.

DIECKMANN, M.E.

Particle Simulation of an Ultrarelativistic Two-Stream Instability.
Physical Review Letters, **94(15)**, 155001 (2005).
doi:10.1103/PhysRevLett.94.155001.

DOELEMAN, S.S., WEINTROUB, J., ROGERS, A.E.E., PLAMBECK, R., FREUND, R., TILANUS, R.P.J., FRIBERG, P., ZIURYS, L.M., MORAN, J.M., COREY, B. ET AL.
Event-horizon-scale structure in the supermassive black hole candidate at the Galactic Centre.
Nature, **455**, pp. 78–80 (2008).
doi:10.1038/nature07245.

DOLGOV, A.D.
Neutrinos in cosmology.
Phys. Rep., **370**, pp. 333–535 (2002).

DONATO, F., GENTILE, G., SALUCCI, P., FRIGERIO MARTINS, C., WILKINSON, M.I., GILMORE, G., GREBEL, E.K., KOCH, A. AND WYSE, R.
A constant dark matter halo surface density in galaxies.
MNRAS, **397**, pp. 1169–1176 (2009).
doi:10.1111/j.1365-2966.2009.15004.x.

ECKART, C.
The Thermodynamics of Irreversible Processes. III. Relativistic Theory of the Simple Fluid.
Physical Review, **58**, pp. 919–924 (1940).
doi:10.1103/PhysRev.58.919.

EHLERS, J.
Survey of general relativity theory.
In *Relativity, Astrophysics and Cosmology*, pp. 1–125 (1973).

EINASTO, J.
On the Construction of a Composite Model for the Galaxy and on the Determination of the System of Galactic Parameters.
Trudy Astrofizicheskogo Instituta Alma-Ata, **5**, pp. 87–100 (1965).

EINASTO, J. AND HAUD, U.
Galactic models with massive corona. I - Method. II - Galaxy.
A&A, **223**, pp. 89–106 (1989).

EINSTEIN, A.
Zur Elektrodynamik bewegter Körper.
Annalen der Physik, **322**, pp. 891–921 (1905).
doi:10.1002/andp.19053221004.

EINSTEIN, A.
On a Stationary System with Spherical Symmetry Consisting of Many Gravitating Masses.
Annals of Mathematics, **40**, p. 922 (1939).

EVANS, N.W., AN, J. AND WALKER, M.G.
Cores and cusps in the dwarf spheroidals.
MNRAS, **393**, pp. L50–L54 (2009).
doi:10.1111/j.1745-3933.2008.00596.x.

FAUCHER-GIGUÈRE, C.A. AND QUATAERT, E.
The physics of galactic winds driven by active galactic nuclei.
MNRAS, **425**, pp. 605–622 (2012).
doi:10.1111/j.1365-2966.2012.21512.x.

FERMI, E.
High Energy Nuclear Events.
Progress of Theoretical Physics, **5**, pp. 570–583 (1950).

FERRARESE, L.
Beyond the Bulge: A Fundamental Relation between Supermassive Black Holes and Dark Matter Halos.
ApJ, **578**, pp. 90–97 (2002a).
doi:10.1086/342308.

FERRARESE, L.
Black Hole Demographics.
In C.H. Lee and H.Y. Chang (eds.), *Current High-Energy Emission Around Black Holes*, pp. 3–24 (2002b).
doi:10.1142/9789812777959_0001.

FIUZA, F., FONSECA, R.A., TONGE, J., MORI, W.B. AND SILVA, L.O.
Weibel-Instability-Mediated Collisionless Shocks in the Laboratory with Ultraintense Lasers.
Physical Review Letters, **108(23)**, 235004 (2012).

doi:10.1103/PhysRevLett.108.235004.

FLORIDES, P.S.
A New Interior Schwarzschild Solution.
Royal Society of London Proceedings Series A, **337**, pp. 529–535 (1974).
doi:10.1098/rspa.1974.0065.

FREDERIKSEN, J.T., HEDEDAL, C.B., HAUGBØLLE, T. AND NORDLUND, Å.
Magnetic Field Generation in Collisionless Shocks: Pattern Growth and Transport.
ApJ, **608**, pp. L13–L16 (2004).
doi:10.1086/421262.

FRIIS, M. AND WATSON, D.
Thermal Emission in the Early X-Ray Afterglows of Gamma-Ray Bursts: Following the Prompt Phase to Late Times.
The Astrophysical Journal, **771(1)**, p. 15 (2013).

FRYER, C.L., RUEDA, J.A. AND RUFFINI, R.
Hypercritical Accretion, Induced Gravitational Collapse, and Binary-Driven Hypernovae.
Accepted for publication in ApJL, p. 1473 (2014).

GAO, J.G., MERAFINA, M. AND RUFFINI, R.
The semidegenerate configurations of a selfgravitating system of fermions.
A&A, **235**, pp. 1–7 (1990).

GAO, J.G. AND RUFFINI, R.
Relativistic limits on the masses of self-gravitating systems of degenerate neutrinos.
Physics Letters B, **97**, pp. 388–390 (1980).

GEBHARDT, K., ADAMS, J., RICHSTONE, D., LAUER, T.R., FABER, S.M., GÜLTEKIN, K., MURPHY, J. AND TREMAINE, S.
The Black Hole Mass in M87 from Gemini/NIFS Adaptive Optics Observations.
ApJ, **729**, 119 (2011).
doi:10.1088/0004-637X/729/2/119.

GERALICO, A., POMPI, F. AND RUFFINI, R.
On Einstein Clusters.

International Journal of Modern Physics Conference Series, **12**, pp. 146–173 (2012).
doi:10.1142/S2010194512006356.

GERHARD, O., KRONAWITTER, A., SAGLIA, R.P. AND BENDER, R.
Dynamical Family Properties and Dark Halo Scaling Relations of Giant Elliptical Galaxies.
AJ, **121**, pp. 1936–1951 (2001).
doi:10.1086/319940.

GERSTNER, E.
Laser physics: Lasing at the limit.
Nature Physics, **6**, pp. 638–+ (2010).
doi:10.1038/nphys1785.

GHEZ, A.M., SALIM, S., WEINBERG, N.N., LU, J.R., DO, T., DUNN, J.K., MATTHEWS, K., MORRIS, M.R., YELDA, S., BECKLIN, E.E. ET AL.
Measuring Distance and Properties of the Milky Way's Central Supermassive Black Hole with Stellar Orbits.
ApJ, **689**, pp. 1044–1062 (2008).
doi:10.1086/592738.

GHISELLINI, G., GHIRLANDA, G. AND TAVECCHIO, F.
Did we observe the supernova shock breakout in GRB 060218?
Monthly Notices of the Royal Astronomical Society: Letters, **382(1)**, pp. L77–L81 (2007).

GIAVALISCO, M.
The gravitational formation of cosmological structures.
Ph.D. thesis, University of Rome "La Sapienza" (1992).

GILBERT, C.
Stellar Clusters, Nebulae, Milky Way: The stability of a spherically symmetric cluster of stars describing circular orbits.
MNRAS, **114**, p. 628 (1954).

GILLESSEN, S., EISENHAUER, F., FRITZ, T.K., BARTKO, H., DODDS-EDEN, K., PFUHL, O., OTT, T. AND GENZEL, R.
The Orbit of the Star S2 Around SGR A from Very Large Telescope and Keck Data*.

ApJ, **707**, pp. L114–L117 (2009).
doi:10.1088/0004-637X/707/2/L114.

GIORGINI, S., PITAEVSKII, L.P. AND STRINGARI, S.
Theory of ultracold atomic Fermi gases.
Reviews of Modern Physics, **80**, pp. 1215–1274 (2008).
doi:10.1103/RevModPhys.80.1215.

GOODMAN, J.
Are gamma-ray bursts optically thick?
ApJ, **308**, pp. L47–L50 (1986).
doi:10.1086/184741.

GOTT, III, J.R., GUNN, J.E., SCHRAMM, D.N. AND TINSLEY, B.M.
An unbound universe.
ApJ, **194**, pp. 543–553 (1974).
doi:10.1086/153273.

GOULD, R.J.
Thermal bremsstrahlung from high-temperature plasmas.
ApJ, **238**, pp. 1026–1033 (1980).
doi:10.1086/158068.

GOULD, R.J.
Kinetic theory of relativistic plasmas.
Physics of Fluids, **24**, pp. 102–107 (1981).

GOULD, R.J.
Processes in relativistic plasmas.
ApJ, **254**, pp. 755–766 (1982).
doi:10.1086/159787.

GOULD, R.J.
The cross section for double Compton scattering.
ApJ, **285**, pp. 275–278 (1984).
doi:10.1086/162503.

GRIMSRUD, O.M. AND WASSERMAN, I.
Non-equilibrium effects in steady relativistic $e^+ + e^-$-gamma winds.
MNRAS, **300**, pp. 1158–1180 (1998).

GROOT, S., LEEUWEN, W. AND WEERT, C.
Relativistic kinetic theory: principles and applications (North-Holland Pub. Co., 1980).
ISBN 9780444854537.

GUILBERT, P.W. AND STEPNEY, S.
Pair production, Comptonization and dynamics in astrophysical plasmas.
MNRAS, **212**, pp. 523–544 (1985).

GÜLTEKIN, K., RICHSTONE, D.O., GEBHARDT, K., LAUER, T.R., TREMAINE, S., ALLER, M.C., BENDER, R., DRESSLER, A., FABER, S.M., FILIPPENKO, A.V. ET AL.
The M-σ and M-L Relations in Galactic Bulges, and Determinations of Their Intrinsic Scatter.
ApJ, **698**, pp. 198–221 (2009).
doi:10.1088/0004-637X/698/1/198.

HAKIM, R.
Introduction to Relativistic Statistical Mechanics: Classical and Quantum (World Scientific Publishing Company, 2011).

HALL, G. AND WATT, J.M.
Modern Numerical Methods for Ordinary Differential Equations (New York, Oxford University Press, 1976).

HAUG, E.
Electron-positron bremsstrahlung in mildly relativistic thermal plasmas.
A&A, **148**, pp. 386–390 (1985).

HAUG, E. AND NAKEL, W.
The Elementary Process of Bremsstrahlung (World Scientific Publishing Co., Singapore, 2004).

HERRERA, L. AND SANTOS, N.O.
Local anisotropy in self-gravitating systems.
Phys. Rep., **286**, pp. 53–130 (1997).
doi:10.1016/S0370-1573(96)00042-7.

HOGAN, P.
.
Proc. R. Irish Acad., **73**, p. 91 (1973).

HUMPHREY, P.J., BUOTE, D.A., GASTALDELLO, F., ZAPPACOSTA, L., BULLOCK, J.S., BRIGHENTI, F. AND MATHEWS, W.G.
A Chandra View of Dark Matter in Early-Type Galaxies.
ApJ, **646**, pp. 899–918 (2006).
doi:10.1086/505019.

INGROSSO, G., MERAFINA, M., RUFFINI, R. AND STRAFELLA, F.
System of self-gravitating semidegenerate fermions with a cutoff of energy and angular momentum in their distribution function.
A&A, **258**, pp. 223–233 (1992).

IZZO, L., RUFFINI, R., PENACCHIONI, A.V., BIANCO, C.L., CAITO, L., CHAKRABARTI, S.K., RUEDA, J.A., NANDI, A. AND PATRICELLI, B.
A double component in GRB 090618: a proto-black hole and a genuinely long gamma-ray burst.
Astronomy and Astrophysics, **543**, p. A10 (2012).

JAUCH, J.M. AND ROHRLICH, F.
The theory of photons and electrons. The relativistic quantum field theory of charged particles with spin one-half (Springer, New York, 1976).

JEANS, J.H.
The Stability of a Spherical Nebula.
Royal Society of London Philosophical Transactions Series A, **199**, pp. 1–53 (1902).
doi:10.1098/rsta.1902.0012.

JÜTTNER, F.
Das Maxwellsche Gesetz der Geschwindigkeitsverteilung in der Relativtheorie.
Annalen der Physik, **339**, pp. 856–882 (1911).
doi:10.1002/andp.19113390503.

KHALATNIKOV, I.M.
Sov. Phys. JETP, **27**, p. 29 (1954).

KHATRI, R. AND SUNYAEV, R.A.
Creation of the CMB spectrum: precise analytic solutions for the blackbody photosphere.
J. Cosmology Astropart. Phys., **6**, 038 (2012).
doi:10.1088/1475-7516/2012/06/038.

KHATRI, R., SUNYAEV, R.A. AND CHLUBA, J.
Does Bose-Einstein condensation of CMB photons cancel μ distortions created by dissipation of sound waves in the early Universe?
A&A, **540**, A124 (2012).
doi:10.1051/0004-6361/201118194.

KIRK, J.G., LYUBARSKY, Y. AND PETRI, J.
Neutron Stars and Pulsars, volume 357 of *Astrophysics and Space Science Library*, chapter The Theory of Pulsar Winds and Nebulae, p. 421 (Springer, 2009).
doi:10.1007/978-3-540-76965-1_16.

KLEIN, O.
On the Thermodynamical Equilibrium of Fluids in Gravitational Fields.
Reviews of Modern Physics, **21**, pp. 531–533 (1949).
doi:10.1103/RevModPhys.21.531.

KLIMONTOVICH, I.L.
The kinetic theory of electromagnetic processes.
Springer Verlag Springer Series on Synergetics, **10** (1983).

KLIMONTOVICH, Y.L.
REVIEWS OF TOPICAL PROBLEMS: Physics of collisionless plasma.
Physics Uspekhi, **40**, pp. 21–51 (1997).
doi:10.1070/PU1997v040n01ABEH000200.

KLIMONTOVICH, Y.L.
Relativistic transport equations for a plasma i.
Sov. Phys. JETP, **37**, pp. 524–530 (1960a).

KLIMONTOVICH, Y.L.
Relativistic transport equations for a plasma ii.
Sov. Phys. JETP, **37**, pp. 876–882 (1960b).

KOURKCHI, E., KHOSROSHAHI, H.G., CARTER, D. AND MOBASHER, B.
Dwarf galaxies in the Coma cluster - II. Spectroscopic and photometric fundamental planes.
MNRAS, **420**, pp. 2835–2850 (2012).
doi:10.1111/j.1365-2966.2011.19980.x.

KUZ'MENKOV, L.S.
The Bogolyubov hierarchy of equations for relativistic systems. Radiation damping of waves in a plasma.
Soviet Physics Doklady, **23**, pp. 469–471 (1978).

LAING, E.W. AND DIVER, D.A.
Relativistic Landau damping of longitudinal waves in isotropic pair plasmas.
Physics of Plasmas, **13(9)**, p. 092115 (2006).
doi:10.1063/1.2353901.

LAMERS, H.J.G.L.M. AND CASSINELLI, J.P.
Introduction to Stellar Winds (Cambridge University Press, 1999).

LANDAU, L.D.
On the vibration of the electronic plasma.
Journal of Physics (USSR), **10**, p. 25 (1946).

LANDAU, L.D.
Ann. Sov. Acad. Sci. Phys., **17(51)** (1953).

LANDAU, L.D. AND LIFSHITS, E.M.
The Classical Theory of Fields (Butterworth-Heinemann, 1994), 4th edition.
ISBN 9780750627689.

LANDAU, L.D. AND LIFSHITZ, E.M.
Fluid mechanics (Oxford: Pergamon Press, 1959).

LANDAU, L.D. AND LIFSHITZ, E.M.
Statistical physics. Pt.1, Pt.2 (Oxford: PergamonPress, 1980).

LANDAU, L.D. AND LIFSHITZ, E.M.
Physical Kinetics (Elsevier, 1981).

LANDAU, L.
Die kinetische gleichung fur den fall coulombscher wechselwirkung.
Phys. Z. Sowjetunion, **10**, pp. 154–164 (1936).

LANDAU, L.
The kinetic equation in the case of coulomb interaction.
ZhETF, **7**, pp. 203–209 (1937).

LATTANZI, M., RUFFINI, R. AND VERESHCHAGIN, G.
On the possible role of massive neutrinos in cosmological structure formation.
In M. Novello and S.E. Perez Bergliaffa (eds.), *Cosmology and Gravitation*, volume 668 of *American Institute of Physics Conference Series*, pp. 263–287 (2003).

LATTANZI, M., RUFFINI, R. AND VERESHCHAGIN, G.V.
Joint constraints on the lepton asymmetry of the Universe and neutrino mass from the Wilkinson Microwave Anisotropy Probe.
Phys. Rev. D, **72(6)**, pp. 063003–+ (2005).
doi:10.1103/PhysRevD.72.063003.

LATTANZI, M., RUFFINI, R. AND VERESHCHAGIN, G.V.
Do WMAP data constraint the lepton asymmetry of the Universe to be zero?
In *Albert Einstein Century International Conference*, volume 861 of *American Institute of Physics Conference Series*, pp. 912–919 (2006).
doi:10.1063/1.2399677.

LATTIMER, J.M. AND PRAKASH, M.
Neutron star observations: Prognosis for equation of state constraints.
Physics Reports, **442**, pp. 109–165 (2007).
doi:10.1016/j.physrep.2007.02.003.

LAZZATI, D.
Precursor activity in bright, long BATSE gamma-ray bursts.
MNRAS, **357**, pp. 722–731 (2005).
doi:10.1111/j.1365-2966.2005.08687.x.

LAZZATI, D., GHISELLINI, G., CELOTTI, A. AND REES, M.J.
Compton-dragged Gamma-Ray Bursts Associated with Supernovae.
ApJ, **529**, pp. L17–L20 (2000).
doi:10.1086/312452.

LEE, B.W. AND WEINBERG, S.
Cosmological lower bound on heavy-neutrino masses.
Physical Review Letters, **39**, pp. 165–168 (1977).
doi:10.1103/PhysRevLett.39.165.

LIBOFF, R.L.

Kinetic theory : classical, quantum, and relativistic descriptions (New York : Springer, 2003).

LIFSHITZ, E.M. AND PITAEVSKII, L.P.
Physical kinetics (Oxford: Pergamon Press, 1981).

LIGHTMAN, A.P.
Double Compton emission in radiation dominated thermal plasmas.
ApJ, **244**, pp. 392–405 (1981).
doi:10.1086/158716.

LIGHTMAN, A.P.
Relativistic thermal plasmas - Pair processes and equilibria.
ApJ, **253**, pp. 842–858 (1982).
doi:10.1086/159686.

LIGHTMAN, A.P. AND BAND, D.L.
Relativistic thermal plasmas - Radiation mechanisms.
ApJ, **251**, pp. 713–726 (1981).
doi:10.1086/159516.

LOVELL, M.R., EKE, V., FRENK, C.S., GAO, L., JENKINS, A., THEUNS, T., WANG, J., WHITE, S.D.M., BOYARSKY, A. AND RUCHAYSKIY, O.
The haloes of bright satellite galaxies in a warm dark matter universe.
MNRAS, **420**, pp. 2318–2324 (2012).
doi:10.1111/j.1365-2966.2011.20200.x.

LYNDEN-BELL, D.
Statistical mechanics of violent relaxation in stellar systems.
MNRAS, **136**, p. 101 (1967).

MANDELSTAM, S.
Determination of the Pion-Nucleon Scattering Amplitude from Dispersion Relations and Unitarity. General Theory.
Physical Review, **112**, pp. 1344–1360 (1958).
doi:10.1103/PhysRev.112.1344.

MANDL, F. AND SKYRME, T.H.R.
The Theory of the Double Compton Effect.
Royal Society of London Proceedings Series A, **215**, pp. 497–507 (1952).
doi:10.1098/rspa.1952.0227.

MERAFINA, M. AND RUFFINI, R.
Systems of selfgravitating classical particles with a cutoff in their distribution function.
A&A, **221**, pp. 4–19 (1989).

MESZAROS, P.
Gamma-ray bursts.
Reports of Progress in Physics, **69**, pp. 2259–2322 (2006).

MÉSZÁROS, P., LAGUNA, P. AND REES, M.J.
Gasdynamics of relativistically expanding gamma-ray burst sources - Kinematics, energetics, magnetic fields, and efficiency.
ApJ, **415**, pp. 181–190 (1993).

MIHALAS, D. AND MIHALAS, B.W.
Foundations of Radiation Hydrodynamics (New York, Oxford University Press, 1984).

MIKHAILOVSKII, A.B.
Plasma instability theory. Volume 1 - Instabilities in a homogeneous plasma /2nd revised and enlarged edition/.
Moscow Atomizdat (1975).

MISNER, C.W. AND SHARP, D.H.
Relativistic Equations for Adiabatic, Spherically Symmetric Gravitational Collapse.
Physical Review, **136**, pp. 571–576 (1964).
doi:10.1103/PhysRev.136.B571.

MOUHOT, C. AND VILLANI, C.
On Landau damping.
Acta Mathematica, **207**, pp. 29–201 (2011).
ISSN 0001-5962.
doi:10.1007/s11511-011-0068-9.

MUCCINO, M., RUFFINI, R., BIANCO, C.L., IZZO, L. AND PENACCHIONI, A.V.
GRB 090227B: The Missing Link between the Genuine Short and Long Gamma-Ray Bursts.
ApJ, **763**, 125 (2013).

doi:10.1088/0004-637X/763/2/125.

MUNSHI, F., GOVERNATO, F., BROOKS, A.M., CHRISTENSEN, C., SHEN, S., LOEBMAN, S., MOSTER, B., QUINN, T. AND WADSLEY, J.
Reproducing the Stellar Mass/Halo Mass Relation in Simulated ΛCDM Galaxies: Theory versus Observational Estimates.
ApJ, **766**, 56 (2013).
doi:10.1088/0004-637X/766/1/56.

MUSTAFA, M.G. AND KÄMPFER, B.
Gamma flashes from relativistic electron-positron plasma droplets.
Phys. Rev. A, **79(2)**, pp. 020103–+ (2009).
doi:10.1103/PhysRevA.79.020103.

NAUMOV, N.D.
Kinetic theory of a relativistic plasma.
Soviet Physics Journal, **24**, pp. 270–274 (1981).
doi:10.1007/BF00891606.

NAVARRO, J.F., FRENK, C.S. AND WHITE, S.D.M.
The Structure of Cold Dark Matter Halos.
ApJ, **462**, p. 563 (1996).
doi:10.1086/177173.

NAVARRO, J.F., FRENK, C.S. AND WHITE, S.D.M.
A Universal Density Profile from Hierarchical Clustering.
ApJ, **490**, p. 493 (1997).
doi:10.1086/304888.

NAVARRO, J.F., HAYASHI, E., POWER, C., JENKINS, A.R., FRENK, C.S., WHITE, S.D.M., SPRINGEL, V., STADEL, J. AND QUINN, T.R.
The inner structure of ΛCDM haloes - III. Universality and asymptotic slopes.
MNRAS, **349**, pp. 1039–1051 (2004a).
doi:10.1111/j.1365-2966.2004.07586.x.

NAVARRO, J.F., HAYASHI, E., POWER, C., JENKINS, A.R., FRENK, C.S., WHITE, S.D.M., SPRINGEL, V., STADEL, J. AND QUINN, T.R.
The inner structure of ΛCDM haloes - III. Universality and asymptotic slopes.
MNRAS, **349**, pp. 1039–1051 (2004b).
doi:10.1111/j.1365-2966.2004.07586.x.

OCHELKOV, I.P., PRILUTSKII, O.F., ROZENTAL, I.L. AND USOV, V.V.
Relativistic kinetics and hydrodynamics.
Moscow Atomizdat (1979).

PACZYNSKI, B.
Super-Eddington winds from neutron stars.
ApJ, **363**, pp. 218–226 (1990).
doi:10.1086/169332.

PADMANABHAN, T.
Structure Formation in the Universe (Structure Formation in the Universe, by T. Padmanabhan, pp. 499. ISBN 0521424860. Cambridge, UK: Cambridge University Press, June 1993., 1993).

PAGE, K.L., STARLING, R.L.C., FITZPATRICK, G., PANDEY, S.B., OSBORNE, J.P., SCHADY, P., MCBREEN, S., CAMPANA, S., UKWATTA, T.N., PAGANI, C. ET AL.
GRB 090618: detection of thermal X-ray emission from a bright gamma-ray burst.
Monthly Notices of the Royal Astronomical Society, **416(3)**, pp. 2078–2089 (2011).

PATRICELLI, B., BERNARDINI, M.G., BIANCO, C.L., CAITO, L., DE BARROS, G., IZZO, L., RUFFINI, R. AND VERESHCHAGIN, G.V.
Analysis of GRB 080319B and GRB 050904 within the Fireshell Model: Evidence for a Broader Spectral Energy Distribution.
ApJ, **756**, 16 (2012).
doi:10.1088/0004-637X/756/1/16.

PE'ER, A.
Temporal Evolution of Thermal Emission from Relativistically Expanding Plasma.
ApJ, **682**, pp. 463–473 (2008).
doi:10.1086/588136.

PE'ER, A., MESZAROS, P. AND REES, M.J.
Radiation from an Expanding Cocoon as an Explanation of the Steep Decay Observed in GRB Early Afterglow Light Curves.
The Astrophysical Journal, **652(1)**, pp. 482–489 (2006).

PENACCHIONI, A.V., RUFFINI, R., BIANCO, C.L., IZZO, L., MUCCINO, M., PISANI, G.B. AND RUEDA, J.A.

GRB 110709B in the induced gravitational collapse paradigm.
A&A, **551**, A133 (2013).
doi:10.1051/0004-6361/201220679.

PENACCHIONI, A.V., RUFFINI, R., IZZO, L., MUCCINO, M., BIANCO, C.L., CAITO, L., PATRICELLI, B. AND AMATI, L.
Evidence for a proto-black hole and a double astrophysical component in GRB 101023.
A&A, **538**, A58 (2012).
doi:10.1051/0004-6361/201118403.

PILLA, R.P. AND SHAHAM, J.
Kinetics of Electron-Positron Pair Plasmas Using an Adaptive Monte Carlo Method.
ApJ, **486**, pp. 903–+ (1997).
doi:10.1086/304534.

PIRAN, T.
Gamma-ray bursts and the fireball model.
Phys. Rep., **314**, pp. 575–667 (1999).

PIRAN, T.
The physics of gamma-ray bursts.
Reviews of Modern Physics, **76**, pp. 1143–1210 (2005).
doi:10.1103/RevModPhys.76.1143.

PIRAN, T., SHEMI, A. AND NARAYAN, R.
Hydrodynamics of Relativistic Fireballs.
MNRAS, **263**, pp. 861–867 (1993).

POLYAKOV, P.A.
Bogolyubov (BBGKY) hierarchy in classical relativistic electrodynamics.
Theoretical and Mathematical Physics, **76**, pp. 939–944 (1988).
doi:10.1007/BF01016857.

PRUGNIEL, P. AND SIMIEN, F.
The fundamental plane of early-type galaxies: non-homology of the spatial structure.
A&A, **321**, pp. 111–122 (1997).

REES, M.J. AND MESZAROS, P.
Relativistic fireballs - Energy conversion and time-scales.
MNRAS, **258**, pp. 41P–43P (1992).

ROMANOWSKY, A.J., DOUGLAS, N.G., ARNABOLDI, M., KUIJKEN, K., MERRIFIELD, M.R., NAPOLITANO, N.R., CAPACCIOLI, M. AND FREEMAN, K.C.
A Dearth of Dark Matter in Ordinary Elliptical Galaxies.
Science, **301**, pp. 1696–1698 (2003).
doi:10.1126/science.1087441.

RUFFINI, R.
On the de Vaucouleurs density-radius relation and the cellular intermediate large-scale structure of the universe.
In H.G. Corwin Jr. and L. Bottinelli (eds.), *World of Galaxies (Le Monde des Galaxies)*, pp. 461–472 (1989).

RUFFINI, R., AKSENOV, A.G., BERNARDINI, M.G., BIANCO, C.L., CAITO, L., CHARDONNET, P., DAINOTTI, M.G., DE BARROS, G., GUIDA, R., IZZO, L. ET AL.
The Blackholic energy and the canonical Gamma-Ray Burst IV: the "long," "genuine short" and "fake-disguised short" GRBs.
In M. Novello and S. Perez (eds.), *American Institute of Physics Conference Series*, volume 1132 of *American Institute of Physics Conference Series*, pp. 199–266 (2009).
doi:10.1063/1.3151839.

RUFFINI, R., ARGÜELLES, C.R., FRAGA, B.M.O., GERALICO, A., QUEVEDO, H., RUEDA, J.A. AND SIUTSOU, I.
Black Holes in Gamma Ray Bursts and Galactic Nuclei.
International Journal of Modern Physics D, **22**, 1360008 (2013a).
doi:10.1142/S0218271813600080.

RUFFINI, R., ARGÜELLES, C.R. AND RUEDA, J.A.
On the core-halo distribution of dark matter in galaxies.
Submitted to PRL, arXiv:astro-ph/1409.7365 (2014).

RUFFINI, R., BERNARDINI, M.G., BIANCO, C.L., CAITO, L., CHARDONNET, P., DAINOTTI, M.G., FRASCHETTI, F., GUIDA, R., ROTONDO, M., VERESHCHAGIN, G. ET AL.

The Blackholic energy and the canonical Gamma-Ray Burst.
In *American Institute of Physics Conference Series*, volume 910 of *American Institute of Physics Conference Series*, pp. 55–217 (2007).
doi:10.1063/1.2752480.

RUFFINI, R., BIANCO, C.L., CHARDONNET, P., FRASCHETTI, F. AND XUE, S.
On the Structures in the Afterglow Peak Emission of Gamma-Ray Bursts.
ApJ, **581**, pp. L19–L22 (2002).
doi:10.1086/345804.

RUFFINI, R., BIANCO, C.L., FRASCHETTI, F., XUE, S. AND CHARDONNET, P.
On the Interpretation of the Burst Structure of Gamma-Ray Bursts.
ApJ, **555**, pp. L113–L116 (2001).
doi:10.1086/323176.

RUFFINI, R., BIANCO, C.L., XUE, S.S., CHARDONNET, P., FRASCHETTI, F. AND GURZADYAN, V.
Emergence of a Filamentary Structure in the Fireball from GRB Spectra.
International Journal of Modern Physics D, **14**, pp. 97–105 (2005a).
doi:10.1142/S0218271805006201.

RUFFINI, R., FRASCHETTI, F., VITAGLIANO, L. AND XUE, S.
Observational Signatures of AN Electromagnetic Overcritical Gravitational Collapse.
International Journal of Modern Physics D, **14**, pp. 131–141 (2005b).
doi:10.1142/S0218271805006146.

RUFFINI, R., MUCCINO, M., BIANCO, C.L., ENDERLI, M., IZZO, L., KOVACEVIC, M., PENACCHIONI, A.V., PISANI, G.B., RUEDA, J.A. AND WANG, Y.
On binary-driven hypernovae and their nested late X-ray emission.
Astronomy and Astrophysics, **565**, p. L10 (2014a).

RUFFINI, R., SALMONSON, J.D., WILSON, J.R. AND XUE, S.S.
On the pair electromagnetic pulse of a black hole with electromagnetic structure.
A&A, **350**, pp. 334–343 (1999).

RUFFINI, R., SALMONSON, J.D., WILSON, J.R. AND XUE, S.S.
On the pair-electromagnetic pulse from an electromagnetic black hole surrounded by a baryonic remnant.

A&A, **359**, pp. 855–864 (2000).

RUFFINI, R., SIUTSOU, I.A. AND VERESHCHAGIN, G.V.
A Theory of Photospheric Emission from Relativistic Outflows.
ApJ, **772**, 11 (2013b).
doi:10.1088/0004-637X/772/1/11.

RUFFINI, R., SONG, D.J. AND STELLA, L.
On the statistical distribution off massive fermions and bosons in a Friedmann universe.
A&A, **125**, pp. 265–270 (1983).

RUFFINI, R., SONG, D.J. AND TARAGLIO, S.
The 'ino' mass and the cellular large-scale structure of the universe.
A&A, **190**, pp. 1–9 (1988).

RUFFINI, R. AND STELLA, L.
On semi-degenerate equilibrium configurations of a collisionless self-gravitating Fermi gas.
A&A, **119**, pp. 35–41 (1983).

RUFFINI, R. AND VERESHCHAGIN, G.
Electron-positron plasma in GRBs and in cosmology.
Il Nuovo Cimento C, **36**, pp. 255–266 (2013).

RUFFINI, R., VERESHCHAGIN, G. AND XUE, S.S.
Electron-positron pairs in physics and astrophysics.
Physics Reports, **487**, pp. 1–140 (2010).

RUFFINI, R., WANG, Y., KOVACEVIC, M., BIANCO, C.L., ENDERLI, M., MUCCINO, M., PENACCHIONI, A.V., PISANI, G.B. AND RUEDA, J.A.
GRB 130427A and SN 2013cq: A Multi-wavelength Analysis of An Induced Gravitational Collapse Event.
Accepted for publication in ApJ, p. 5723 (2014b).

RUFFINI, R., VERESHCHAGIN, G. AND XUE, S.S.
Electron-positron pairs in physics and astrophysics: From heavy nuclei to black holes.
Physics Reports, **487(1)**, pp. 1–140 (2010).

RYBICKI, G.B. AND LIGHTMAN, A.P.
Radiative processes in astrophysics (New York, Wiley-Interscience, 1979).

SAMPSON, D.H.
Electron-Positron Pairs at Very High Temperatures.
ApJ, **135**, p. 261 (1962).
doi:10.1086/147263.

SCHIFFRIN, J.S. AND WALD, R.M.
Turning point instabilities for relativistic stars and black holes.
Classical and Quantum Gravity, **31(3)**, 035024 (2014).
doi:10.1088/0264-9381/31/3/035024.

SCHWINGER, J.
On Gauge Invariance and Vacuum Polarization.
Phys. Rev., **82**, pp. 664–679 (1951).

SHEMI, A. AND PIRAN, T.
The appearance of cosmic fireballs.
ApJ, **365**, pp. L55–L58 (1990).

SHI, X. AND FULLER, G.M.
New Dark Matter Candidate: Nonthermal Sterile Neutrinos.
Physical Review Letters, **82**, pp. 2832–2835 (1999).
doi:10.1103/PhysRevLett.82.2832.

SIGOV, Y.S.
Computing Experiment: a Bridge between the Past and Future of Plasma Physics. Selected Works (Moscow: Fizmatlit, 2001).

SILIN, V.P.
Introduction in kinetic theory of gases (Lebedev institute press, 1998).
(in Russian).

SILVA, L.O.
Physical Problems (Microphysics) in Relativistic Plasma Flows.
In P.A. Hughes and J.N. Bregman (eds.), *Relativistic Jets: The Common Physics of AGN, Microquasars, and Gamma-Ray Bursts*, volume 856 of *American Institute of Physics Conference Series*, pp. 109–128 (2006).
doi:10.1063/1.2356387.

SIUTSOU, I., ARGÜELLES, C.R. AND RUFFINI, R.
Dark Matter Massive Fermions and Einasto Profiles in Galactic Haloes.
arXiv:astro-ph/1402.0695 (2014).

SMOLYANSKY, S.A.
Comments on the principle of attenuation of correlation.
Acta Physica Academiae Scientiarum Hungaricae, **25**, pp. 147–151 (1968).
doi:doi={10.1007/BF03157119}.

SOFUE, Y., HONMA, M. AND OMODAKA, T.
Unified Rotation Curve of the Galaxy – Decomposition into de Vaucouleurs Bulge, Disk, Dark Halo, and the 9-kpc Rotation Dip –.
PASJ, **61**, pp. 227– (2009).

SORKIN, R.
A Criterion for the Onset of Instability at a Turning Point.
ApJ, **249**, p. 254 (1981).
doi:10.1086/159282.

SPARRE, M. AND STARLING, R.L.C.
A search for thermal X-ray signatures in gamma-ray bursts - II. The Swift sample.
Monthly Notices of the Royal Astronomical Society, **427(4)**, pp. 2965–2974 (2012).

SPITKOVSKY, A.
On the Structure of Relativistic Collisionless Shocks in Electron-Ion Plasmas.
ApJ, **673**, pp. L39–L42 (2008a).
doi:10.1086/527374.

SPITKOVSKY, A.
Particle Acceleration in Relativistic Collisionless Shocks: Fermi Process at Last?
ApJ, **682**, pp. L5–L8 (2008b).
doi:10.1086/590248.

STARLING, R.L.C., PAGE, K.L., PE'ER, A., BEARDMORE, A.P. AND OSBORNE, J.P.
A search for thermal X-ray signatures in gamma-ray bursts - I. Swift bursts with optical supernovae.
Monthly Notices of the Royal Astronomical Society, **427(4)**, pp. 2950–2964 (2012).

STASIELAK, J., BIERMANN, P.L. AND KUSENKO, A.
Sterile Neutrinos and Structure Formation.
Acta Physica Polonica B, **38**, p. 3869 (2007).

STEPNEY, S.
Two-body relaxation in relativistic thermal plasmas.
MNRAS, **202**, pp. 467–481 (1983).

STEPNEY, S. AND GUILBERT, P.W.
Numerical FITS to important rates in high temperature astrophysical plasmas.
MNRAS, **204**, pp. 1269–1277 (1983).

STRIGARI, L.E., BULLOCK, J.S., KAPLINGHAT, M., SIMON, J.D., GEHA, M., WILLMAN, B. AND WALKER, M.G.
A common mass scale for satellite galaxies of the Milky Way.
Nature, **454**, pp. 1096–1097 (2008).
doi:10.1038/nature07222.

SVENSSON, R.
Electron-Positron Pair Equilibria in Relativistic Plasmas.
ApJ, **258**, pp. 335–+ (1982a).
doi:10.1086/160082.

SVENSSON, R.
The pair annihilation process in relativistic plasmas.
ApJ, **258**, pp. 321–334 (1982b).
doi:10.1086/160081.

SVENSSON, R.
Steady mildly relativistic thermal plasmas - Processes and properties.
MNRAS, **209**, pp. 175–208 (1984).

SYNGE, J.L.
The Relativistic Gas (North-Holland, 1957).

THORNE, K.S.
Relativistic radiative transfer - Moment formalisms.
MNRAS, **194**, pp. 439–473 (1981).

TOLMAN, R.C.
On the Weight of Heat and Thermal Equilibrium in General Relativity.

Physical Review, **35**, pp. 904–924 (1930).
doi:10.1103/PhysRev.35.904.

TREMAINE, S. AND GUNN, J.E.
Dynamical role of light neutral leptons in cosmology.
Physical Review Letters, **42**, pp. 407–410 (1979).
doi:10.1103/PhysRevLett.42.407.

UEHLING, E.A.
Transport Phenomena in Einstein-Bose and Fermi-Dirac Gases. II.
Physical Review, **46**, pp. 917–929 (1934).
doi:10.1103/PhysRev.46.917.

UEHLING, E.A. AND UHLENBECK, G.E.
Transport Phenomena in Einstein-Bose and Fermi-Dirac Gases. I.
Physical Review, **43**, pp. 552–561 (1933).
doi:10.1103/PhysRev.43.552.

USOV, V.V.
Bare Quark Matter Surfaces of Strange Stars and e^+e^- Emission.
Phys. Rev. Lett., **80**, pp. 230–233 (1998).

VERESHCHAGIN, G.V.
Physics of Nondissipative Ultrarelativistic Photospheres.
International Journal of Modern Physics D, **23**, 1430003 (2014).
doi:10.1142/S0218271814300031.

VLASOV, A.
On vibration properties of electron gas.
Journal of Experimental and Theoretical Physics, **8 (3)**, p. 291 (1938).
(in Russian).

WALKER, M.G., MATEO, M., OLSZEWSKI, E.W., PEÑARRUBIA, J., WYN EVANS, N. AND GILMORE, G.
A Universal Mass Profile for Dwarf Spheroidal Galaxies?
ApJ, **704**, pp. 1274–1287 (2009).
doi:10.1088/0004-637X/704/2/1274.

WARDLE, J.F.C., HOMAN, D.C., OJHA, R. AND ROBERTS, D.H.
Electron-positron jets associated with the quasar 3C279.

Nature, **395**, pp. 457–461 (1998).
doi:10.1038/26675.

WEAVER, T.A.
Reaction rates in a relativistic plasma.
Phys. Rev. A, **13**, pp. 1563–1569 (1976).

WEIBEL, E.S.
Spontaneously Growing Transverse Waves in a Plasma Due to an Anisotropic Velocity Distribution.
Physical Review Letters, **2**, pp. 83–84 (1959).
doi:10.1103/PhysRevLett.2.83.

WEINBERG, S.
Gravitation and Cosmology: Principles and Applications of the General Theory of Relativity (1972).

WEINBERG, S.
Cosmology (Oxford University Press, April 2008., 2008).

WHITE, S.D.M., FRENK, C.S. AND DAVIS, M.
Clustering in a neutrino-dominated universe.
ApJ, **274**, pp. L1–L5 (1983).
doi:10.1086/184139.

ZAKHAROV, A.
Macroscopic gravitation (Yanus-K, Moscow, 2000).
(in Russian).

ZAPOLSKY, H.S.
Can the Redshifts of Quasi-Stellar Objects BE Gravitational?
ApJ, **153**, p. L163 (1968).
doi:10.1086/180244.

ZDZIARSKI, A.A.
Spectra from pair-equilibrium plasmas.
ApJ, **283**, pp. 842–847 (1984).
doi:10.1086/162370.